INTERNATIONAL DOCTORAL
SCHOOL OF THE USC

Sandra
Robla Álvarez

PhD Thesis

Biomimetic systems for transmucosal drug delivery

Santiago de Compostela, 2023

Doctoral Programme in Drug Research and Development

DOCTORAL THESIS

BIOMIMETIC SYSTEMS FOR TRANSMUCOSAL DRUG DELIVERY

Sandra Robla Álvarez

IINTERNATIONAL PHD SCHOOL OF THE UNIVERSITY OF SANTIAGO DE COMPOSTELA

PHD PROGRAMM IN DRUG RESEARCH AND DEVELOPMENT

SANTIAGO DE COMPOSTELA

2023

TESIS DE DOCTORADO

SISTEMAS BIOMIMÉTICOS PARA LA ADMINISTRACIÓN TRANSMUCOSA DE FÁRMACOS

Sandra Robla Álvarez

ESCUELA DE DOCTORADO INTERNACIONAL DE LA UNIVERSIDAD DE SANTIAGO DE COMPOSTELA

PROGRAMA DE DOCTORADO EN INVESTIGACIÓN Y DESARROLLO DE MEDICAMENTOS

SANTIAGO DE COMPOSTELA

2023

DECLARACIÓN DEL AUTOR/A DE LA TESIS

D./Dña. **Sandra Robla Álvarez**

Título de la tesis: **Biomimetic systems for transmucosal drug delivery**

Presento mi tesis, siguiendo el procedimiento adecuado al Reglamento y declaro que:

1) La tesis abarca los resultados de la elaboración de mi trabajo.
2) De ser el caso, en la tesis se hace referencia a las colaboraciones que tuvo este trabajo.
3) Confirmo que la tesis no incurre en ningún tipo de plagio de otros autores ni de trabajos presentados por mí para la obtención de otros títulos.
4) La tesis es la versión definitiva presentada para su defensa y coincide la versión impresa con la presentada en formato electrónico.

Y me comprometo a presentar el Compromiso Documental de Supervisión en el caso que el original no esté depositado en la Escuela.

En **Santiago de Compostela**, **8 de Mayo de 2023**.

Firma electrónica

AUTORIZACIÓN DE LAS DIRECTORAS DE LA TESIS

Sistemas biomiméticos para la administración transmucosa de fármacos

Dra. **Noémi Csaba**, Profesora Titular del Departamento de Farmacología, Farmacia y Tecnología Farmacéutica de la Universidad de Santiago de Compostela, España.
Dra. **Rita Ambrus**, Profesora Asociada del Instituto de Tecnología Farmacéutica y Asuntos Regulatorios de la Universidad de Szeged, Hungría.

INFORMAN:

Que la presente tesis, se corresponde con el trabajo realizado por **Sandra Robla Álvarez**, bajo nuestra dirección, y autorizamos su presentación, considerando que reúne los requisitos exigidos en el Reglamento de Estudios de Doctorado de la USC, y que como directoras de esta no incurre en las causas de abstención establecidas en la Ley 40/2015.

De acuerdo con lo indicado en el Reglamento de Estudios de Doctorado, declaramos también que la presente tesis doctoral es idónea para ser defendida en base a la modalidad monográfica con reproducción de publicaciones, en los que la participación de la doctoranda fue decisiva para su elaboración, y las publicaciones se ajustan al Plan de Investigación.

En Santiago de Compostela, 18 de Mayo de 2023

Noémi Csaba **Rita Ambrus**

THESIS DIRECTORS AUTORIZATION

Biomimetic systems for transmucosal drug delivery

Dra. **Noémi Csaba**, Full Professor in the Department of Pharmacology, Pharmacy and Pharmaceutical Technology of the University of Santiago de Compostela, Spain.
Dra. **Rita Ambrus**, Associate Professor of the Institute of Pharmaceutical Technology and Regulatory Affairs of the University of Szeged, Hungary.

REPORT:

That the following thesis corresponds to the work carried out by **Sandra Robla Álvarez**, under our supervision, and we authorize its submission, considering It meets the requirements established by the Doctoral Studies Regulations of the USC. As the thesis directors, we confirm they are no grounds for abstention as set forth in Law 40/2015.

In accordance with the provisions of the Doctoral Studies Regulations, we also declare that this doctoral thesis is suitable to be defended under the monographic modality with reproduction of publications, in which the involvement of the doctoral candidate was decisive in its preparation, and the publications comply with the Research Plan.

In Santiago de Compostela, 18th May 2023

Noémi Csaba **Rita Ambrus**

AUTORIZACIÓN DE LA TUTORA DE LA TESIS

Sistemas biomiméticos para la administración transmucosa de fármacos

Dra. Noemi Csaba

INFORMA:

Que la presente tesis, se corresponde con el trabajo realizado por **Sandra Robla Álvarez**, bajo mi tutorización, y autorizo su presentación, considerando que reúne los requisitos exigidos en el Reglamento de Estudios de Doctorado de la USC, y que como director de esta no incurre en las causas de abstención establecidas en la Ley 40/2015.

De acuerdo con lo indicado en el Reglamento de Estudios de Doctorado, declara también que la presente tesis doctoral es idónea para ser defendida en base a la modalidad de Monográfica con reproducción de publicaciones, en los que la participación de la doctoranda fue decisiva para su elaboración y las publicaciones se ajustan al Plan de Investigación.

En Santiago de Compostela, 18 de Mayo de 2023

A mi familia

"Memoria selectiva para recordar lo bueno,
prudencia lógica para no arruinar el presente,
y optimismo desafiante para encarar el futuro"

Isabel Allende

TABLE OF CONTENTS

TABLE OF CONTENTS

ABSTRACT/RESUMEN

ABSTRACT

The use of mucosal delivery routes such as oral, pulmonary, and ocular is becoming increasingly popular due to its convenience, non-invasive nature, and safety. To improve the efficacy of mucosal delivery, nanocarriers have been extensively investigated as delivery tools allowing the maximization of pharmacological efficacy by reducing side effects and improving the stability and bioavailability of drugs. However, despite the capacity of nanocarriers to deliver high drug payloads and interact efficiently with mucosal tissues, the attempts to demonstrate consistently high and reproducible efficacy *in vivo* have failed so far due to their premature removal from the mucosa, resulting in limited bioavailability.

Considering this information, the main objective of this thesis has been the design of a multi-stage delivery platform able to integrate and protect the nanocarriers in their inner core and transport them to the target region where they deliver their therapeutic cargo with higher efficiency. Within this context, plant pollen grains are natural, needle-like biological microstructures with attractive properties, such as high resistance and excellent bioadhesion. A protocol to produce hollow pollen microcapsules from *Helianthus annuus* and *Matricaria chamomilla* was developed, and the obtained vehicles were associated with model polystyrene nanoparticles of different sizes and surface functionalizations, to unravel their loading and release mechanisms. Based on these results, biodegradable polymeric nanocapsules were designed and loaded into pollen platforms to evaluate their mucointeraction and biodistribution after oral administration.
Likewise, the developed protamine nanocapsules were evaluated for the pulmonary release of rifabutin, aiming to overcome the limitations and resistance associated with current systemic treatment of tuberculosis. These nanocapsules were characterized and optimized for their subsequent atomization to obtain a dry powder formulation and their aerodynamic properties were evaluated.

-Párrafo afectado por la protección de derechos-

Finally, pollen microcapsules were evaluated to enhance the mucointeraction and residence time of protamine nanocapsules loaded with bilastine, an antihistamine drug, for the topical treatment of allergic rhinoconjunctivitis. The developed platforms gave rise to a highly tolerable bifunctional strategy that increased residence time and epithelial penetration with reduced drug loss, preserving the integrity of the corneal epithelial barrier.

Globally, these results highlight the versatility and potential of the produced pollen-based platforms, which combine the benefits of nanotechnology and the capacity of pollen grains to be anchored to the mucosa for obtaining a multi-step delivery system that can be tailor-made for diverse biomedical applications, by different administration routes and for the delivery of different nanoencapsulated therapeutics.

RESUMEN

La administración de fármacos por vías como la oral, pulmonar y ocular, está ganando popularidad debido a su conveniencia, su naturaleza no invasiva y su seguridad. Con el fin de mejorar la eficacia de la administración mucosa de fármacos, se ha investigado el uso de nanosistemas como sistemas de liberación, ya que permiten maximizar la eficacia farmacológica, reducir los efectos secundarios y mejorar la estabilidad y biodisponibilidad de los medicamentos. Sin embargo, a pesar de la capacidad de los nanosistemas para transportar fármacos e interactuar eficientemente con las mucosas, hasta ahora los intentos de demostrar su eficacia y reproducibilidad *in vivo* han fracasado debido a su eliminación prematura, lo que limita su biodisponibilidad.

El objetivo principal de esta tesis ha sido el diseño de una plataforma de entrega en varias etapas con capacidad de integrar y proteger los nanosistemas en su núcleo interno y transportarlos al lugar de acción de manera eficiente. En este contexto, los granos de polen son microestructuras biológicas naturales en forma de aguja con una elevada resistencia y excelentes propiedades de bioadhesión. En esta tesis, se desarrolló un protocolo para producir microcápsulas de polen huecas a partir del polen de *Helianthus annuus* y *Matricaria chamomilla*, y estas plataformas se asociaron con nanopartículas modelo de poliestireno de diferentes tamaños y carga superficial, para evaluar sus mecanismos de carga y liberación. Basándose en estos resultados, se diseñaron nanocápsulas poliméricas biodegradables y se cargaron en plataformas de polen para estudiar su mucointeracción y biodistribución tras su administración por vía oral.
Asimismo, las nanocápsulas de protamina se analizaron para la liberación pulmonar de rifabutina, con el fin de superar las limitaciones y resistencia asociadas con el tratamiento sistémico actual de la tuberculosis. Estas nanocápsulas se caracterizaron y optimizaron para su posterior atomización y se obtuvo una formulación de polvo seco, que se evaluó aerodinámicamente.

-Párrafo afectado por la protección de derechos-

Finalmente, las microcápsulas de polen fueron evaluadas en términos de mucointeracción y aumento del tiempo de residencia de nanocápsulas de protamina cargadas con bilastina, un medicamento antihistamínico, para el tratamiento tópico de la rinoconjuntivitis alérgica. Esta estrategia bifuncional aumentó la penetración epitelial, disminuyendo la pérdida de fármaco y preservando la integridad corneal.

En general, estos resultados resaltan la versatilidad y el potencial de las microcápsulas basadas en polen, en una plataforma que combina los beneficios de la nanotecnología y la capacidad de los granos de polen de anclarse a la mucosa, dando lugar a un sistema de liberación con diversas aplicaciones biomédicas y con posibilidad de uso en diferentes vías de administración.

RESUMEN *IN EXTENSO*

RESUMEN *IN EXTENSO*

La administración de fármacos a través de las mucosas ofrece una alternativa atractiva para superar los problemas relacionados con formas de dosificación inyectables, ya que permite un mejor acceso al tejido diana, imitando la vía de liberación natural de biomacromoléculas endógenas de forma no invasiva [1]. Su facilidad de uso permite una mejor adherencia y cumplimiento por parte del paciente, y supone un menor coste de producción, al no requerir de condiciones de esterilidad. En este contexto, la nanotecnología permite un incremento de la eficacia farmacológica al reducir los efectos secundarios, mejorando la estabilidad y la biodisponibilidad de los fármacos [2]. El desarrollo de nanosistemas poliméricos ha suscitado gran interés en la liberación de fármacos debido a su seguridad, biocompatibilidad y estabilidad física y biológica mejoradas [3]. Sin embargo, hasta la fecha, los intentos de demostrar una eficacia alta y reproducible *in vivo* han fallado [4] debido a su eliminación prematura de la mucosa, lo que resulta en una biodisponibilidad limitada en comparación con otras vías [5]. Con el fin de abordar este problema, se ha investigado la integración de nanosistemas en plataformas funcionales como una estrategia de liberación multietapa, demostrando resultados prometedores en la administración mucosa de fármacos, protegiendo los nanosistemas y transportándolos a su diana de una manera más eficiente [6, 7].

Los granos de polen son microcápsulas naturales derivadas de los gametofitos masculinos del ciclo reproductivo de las plantas con semillas [8]. Están constituidos principalmente por esporopolenina, un biopolímero con una arquitectura tridimensional especial que les otorga propiedades atractivas como una alta resistencia y una adherencia biológica [9]. El polen se compone de tres capas principales (**Figura 1**): un revestimiento externo llamado pollenkitt; seguido por una pared de múltiples capas (exina e intina), y un esporoplasma interno, donde se encuentra el gameto celular [10, 11].

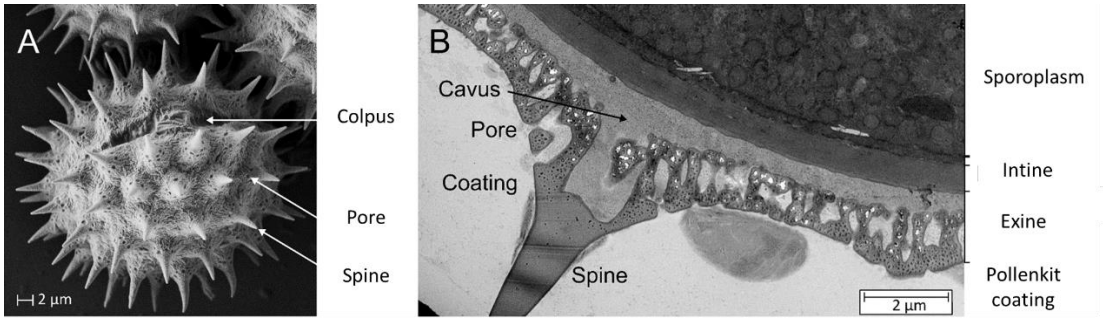

Figura 1. (A) Micrografías de microscopía electrónica de barrido (SEM) de exina de *Helianthus annuus* y (B) sección de micrótomo que muestra las diferentes capas desde el pollenkitt externo hasta la cavidad interna (barra = 2 µm).

Debido a su diseño natural, se han desarrollado diversos procesos químicos con el fin de eliminar los compuestos presentes tanto en el exterior como interior del polen, así como proteínas y alérgenos que constituyen un riesgo potencial para la salud humana, dando lugar a una estructura hueca de esporopolenina [12, 13]. Son muchas las especies de esporas y polen que se han empleado para la producción de microcápsulas de esporopolenina y que se han utilizado para diversas aplicaciones, ya sea como catalizadores, para el enmascaramiento de sabores o la microencapsulación y liberación de fármacos y proteínas, entre otros [14, 15]. En la naturaleza, las plantas producen miles de tipos diferentes de polen, y cada polen puede exhibir variaciones en cuanto a su tamaño, morfología y estructura fisicoquímica. Además, la superficie del polen puede presentar ornamentaciones insulares, elementos en forma de clava o puntiagudos, granulaciones, crestas, agujeros o una superficie lisa según la especie, así como

una o varias aperturas elongadas (colpus) o circulares (poros), con diferentes denominaciones según su número y ubicación [16].
El reino Plantae incluye tanto las plantas no vasculares (briofitas) como las plantas vasculares, las cuales se dividen en plantas sin semilla (pteridofitas) o con semilla, que pueden presentar óvulos no protegidos (gimnospermas, división Magnoliophyta) o protegidos (angiospermas, división Pinophyta). Dentro de las gimnospermas, las dicotiledóneas constituyen el grupo de mayor evolución y complejidad, con gran diversidad de pólenes que presentan un mayor número y diversidad de aperturas, generalmente ecuatoriales, con prevalencia de polen triaperturado, con una intina simple y una exina bien desarrollada [17, 18]. En este grupo, la familia Asteraceae, engloba especies como el girasol (*Helianthus annuus*) con un polen de tamaño entre 26-50 µm y la manzanilla (*Matricaria chamomilla*), con granos de polen entre 13-25 µm. Ambos presentan una distintiva morfología superficial con espinas, que permite su fijación a los insectos durante la polinización y que potencialmente podría favorecer su adherencia a las mucosas, lo que aumentaría el contacto con las superficies biológicas, mejorando la absorción y biodisponibilidad de fármacos [19].
Nuestro grupo ha desarrollado un protocolo simplificado para obtener microcápsulas huecas de polen utilizando el polen de girasol como modelo y evaluando su eficacia también para la purificación del polen de manzanilla [20].

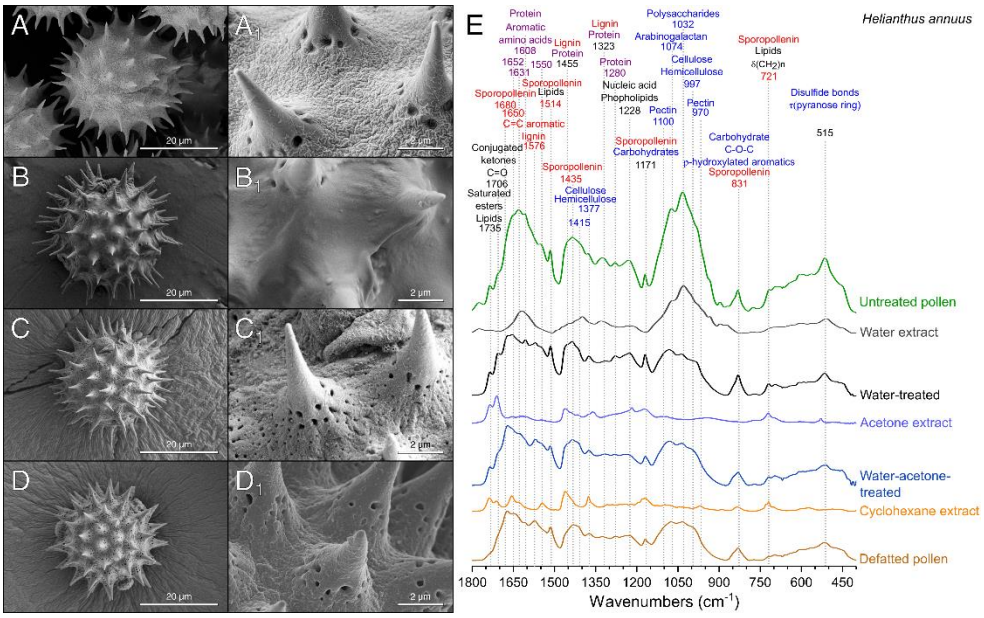

Figura 2. Micrografías electrónicas de barrido de muestras de polen de girasol procesados (A-D). (A). Polen sin tratar. (B). Polen tratado con agua. (C). Polen tratado con agua después del tratamiento con acetona. (D). Polen de girasol desgrasado. (E). Espectros ATR-FTIR de muestras de polen de girasol y extractos obtenidos durante la purificación.

En este proceso, el polen de *H. annuus* fue sometido a un lavado secuencial con agua, acetona y cicloheaxano, para eliminar los compuestos que recubren la esporopolenina (**Figura 2**), dando lugar a un polen desgrasado. El tratamiento con agua permitió la extracción de carbohidratos y proteínas [21, 22], mientras que la acetona eliminó ácidos grasos como α-linolénico, láurico, esteárico y otros lípidos [23] y el ciclohexano permitió la extracción de componentes superficiales, como la pectina. La obtención de plataformas huecas de polen tuvo lugar tras la incubación del polen desgrasado con ácido ortofosfórico (85%, H_3PO_4) a 70ºC durante 5 horas,

eliminando proteínas y carbohidratos presentes en el esporoplasma interno. A partir de los resultados obtenidos, se empleó este método para la obtención de polen hueco de *M. chamomilla* a partir de flores secas, prescindiéndo del uso de ciclohexano al obtenerse una eliminación eficiente de los polisacáridos tras el tratamiento del polen solo con el empleo de acetona y agua.

Aunque no son abundantes en *H. annuus*, las proteínas y glicoproteínas son los principales compuestos alergénicos del polen [24], por lo que su eliminación es un punto crítico para su uso con fines farmacéuticos. El contenido de proteína (**Figura 3**) del polen de girasol se redujo de un 33% en peso a un 4,4% tras el proceso de purificación y obtención de las plataformas huecas, mientras que en el caso del polen de camomila, la reducción fue de un 16% a un 4%.

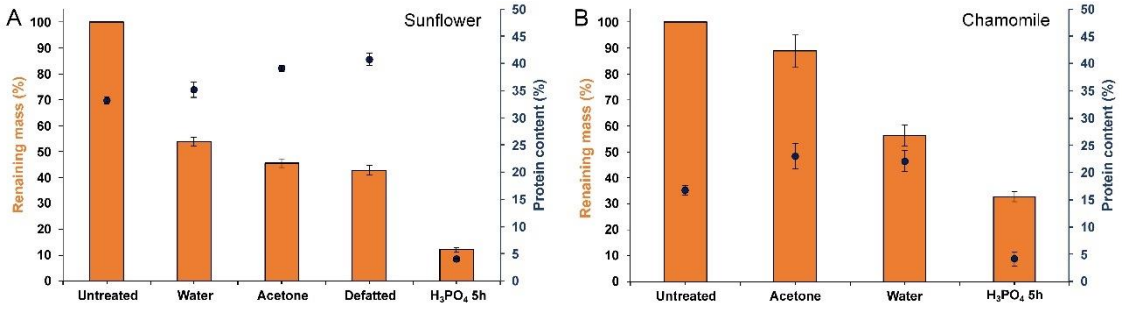

Figura 3. Masa restante (barras) y contenido de proteína (% de la masa restante, puntos) de las muestras de polen durante el proceso de purificación de (A) Girasol y (B) Manzanilla. Los datos representan la media ± desviación estándar, n=3 medidas independientes.

Con el fin de desarrollar un sistema multietapa a partir de estas microcápsulas huecas de polen, se llevó a cabo la asociación de nanopartículas (NPs) de poliestireno no degradables de diferentes tamaños (100, 200 y 500 nm) y funcionalización superficial (aminadas, no modificadas y carboxiladas) empleando liofilización y vacío, y determinando los parámetros críticos de la asociación y liberación.

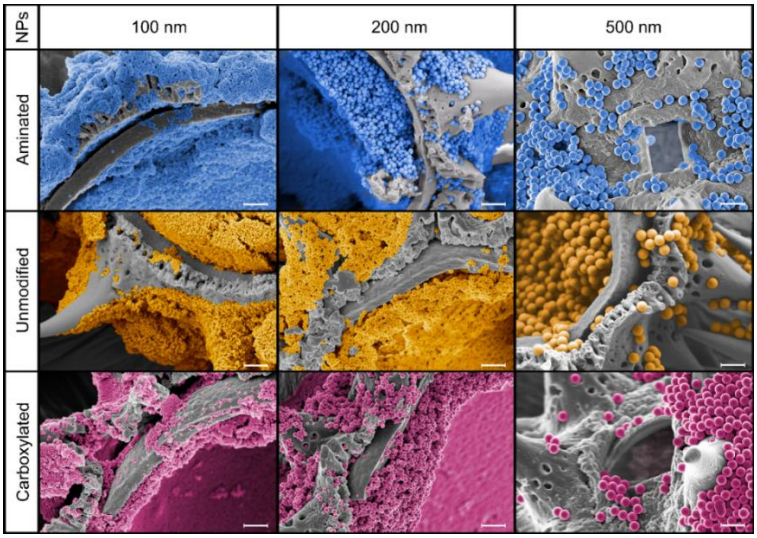

Figura 4. Imágenes de microscopía electrónica de barrido (SEM) de microcápsulas huecas de polen cargadas al vacío con nanopartículas comerciales (NPs; 100, 200 y 500 nm) con diferente funcionalización. Las barras representan 1 µm. Las NPs se colorearon artificialmente para aumentar el contraste con la esporopolenina.

Se observó (**Figura 4**) que las NPs de 100 y 200 nm recubrieron completamente las microcápsulas incluyendo las espinas y las áreas internas de la exina y que las NPs de mayor tamaño se unieron principalmente a la superficie del polen. Asimismo, las NPs no modificadas y carboxiladas se acumularon internamente en función del método de carga, mientras que, en las NPs aminadas, la acumulación tenía lugar en las superficies externa e interna del polen, independientemente del método de carga.

El perfil de liberación de las NPs de las microcápsulas huecas de polen mostró una liberación rápida durante las primeras 8 h (**Figura 5**). La carga por liofilización produjo una mayor liberación en los primeros 15 min, logrando una estabilización después de 24 h. En cambio, las NPs cargadas en el polen mediante vacío dieron lugar a una liberación continua tras 8 h hasta 120 h, similar a lo descrito en estudios previos de la liberación de eritromicina [25] y paracetamol [26] de microcápsulas de polen. Esto podría deberse a una mayor asociación de las NPs a la superficie externa de las plataformas de polen empleando la liofilización como método de carga, lo que produciría su liberación más rápida que mediante la carga mediante vacío, donde las NPs se localizaron predominantemente en la cavidad interior. Si bien el método de carga influyó en la liberación inicial, el tamaño y la funcionalización superficial de las NPs fueron determinantes en su liberación a lo largo del tiempo, siendo menor para las partículas más pequeñas. Considerando la funcionalización superficial, la carga mediante liofilización resultó en una liberación de NPs entre 40-60%, lo que se aproxima a una difusión Fickiana, mientras que la carga mediante vacío produjo una liberación con valores por debajo del 40% para todos los tamaños, siguiendo un modelo de difusión cuasi-Fickiana.

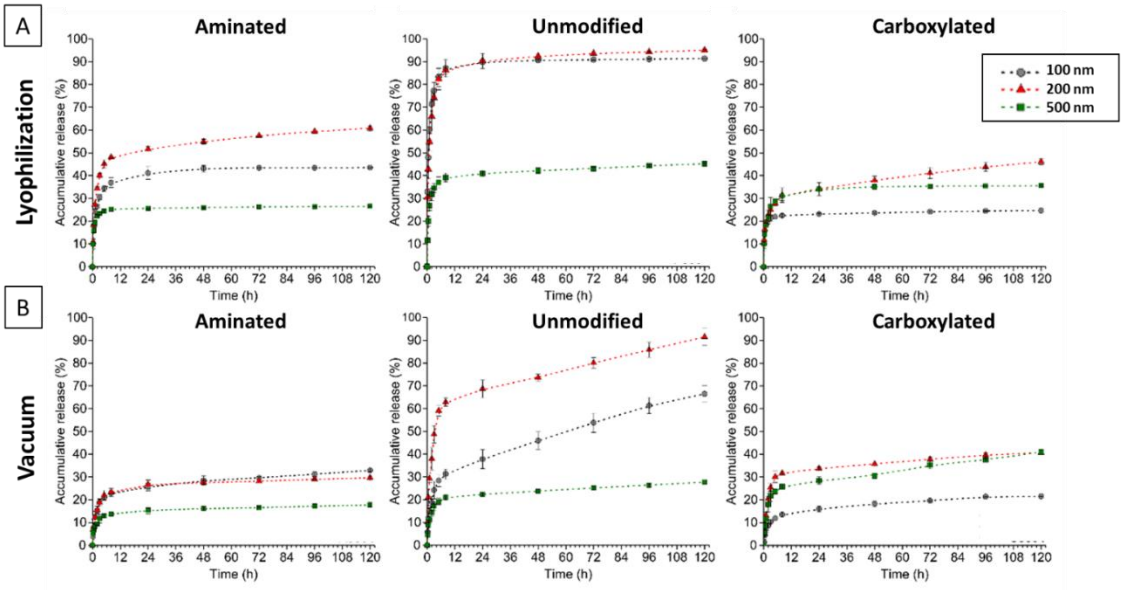

Figura 5. Estudio de liberación de nanopartículas (NPs) con diferentes tamaños, cargadas en microcápsulas huecas de polen mediante (A) liofilización y (B) carga asistida por vacío. ● 100 nm. ▲ 200 nm. ■ 500 nm. Los datos representan la media ± desviación estándar, n=9 medidas independientes.

Las NPs con un tamaño de 200 nm presentaron una mayor eficiencia de carga y una mayor liberación, independientemente de la funcionalización superficial o el método de carga utilizado. Teniendo en cuenta estos resultados, se desarrolló un prototipo biodegradable de nanocápsulas poliméricas (NCs) con un tamaño cercano a los 200 nm que se encapsuló en plataformas de polen, tanto de *H. annuus* como de *M. chamomilla* y se investigó su potencial interés como sistemas de liberación para vía oral (Capítulo II) y ocular (Capítulo V). Para la cubierta polimérica de las NCs se seleccionó la protamina, un polipéptido natural rico en

arginina, ampliamente utilizado en el diseño de sistemas poliméricos [27], y para el núcleo oleoso se empleó Miglyol, en combinación con surfactantes no iónicos como el polietilenglicol (PEGst-40), y glicocolato de sodio que, en conjunto, mejoran la estabilidad y penetración de las formulaciones [28]**.** Las NCs de protamina se prepararon mediante la técnica de desplazamiento de solvente siguiendo el procedimiento descrito por nuestro grupo [29] y se llevó a cabo su caracterización físicoquímica, su estabilidad en medio biológico y su evaluación para su aplicación en diferentes vías de administración.

En primer lugar, para su evaluación en los sistemas de vía oral, las NCs de protamina fueron cargadas en microcápsulas huecas de polen de *H. annuus* mediante vacío, empleando una ratio de carga 1:1 (p/p). Se obtuvieron valores de asociación inferiores a las NPs de poliestireno (66% vs 73%) con una liberación acumulativa de alrededor del 40% tras 48 h en fluido intestinal simulado. Las microcápsulas de polen cargadas con NCs de protamina presentaron elevada adhesión a la superficie de la mucosa en un modelo *ex vivo* de saco intestinal no evertido de rata (**Figura 6**), con una intensidad de fluorescencia significativamente mayor que las NCs administradas en forma libre tras 3 h de incubación. Asimismo, la evaluación de su distribución intestinal *in vivo* tras su administración oral confirmó una menor acumulación de las NCs de protamina cuando fueron administradas en forma libre en comparación con las NCs cargadas en microcápsulas de polen, lo que sugiere su liberación progresiva desde la cavidad interior del polen.

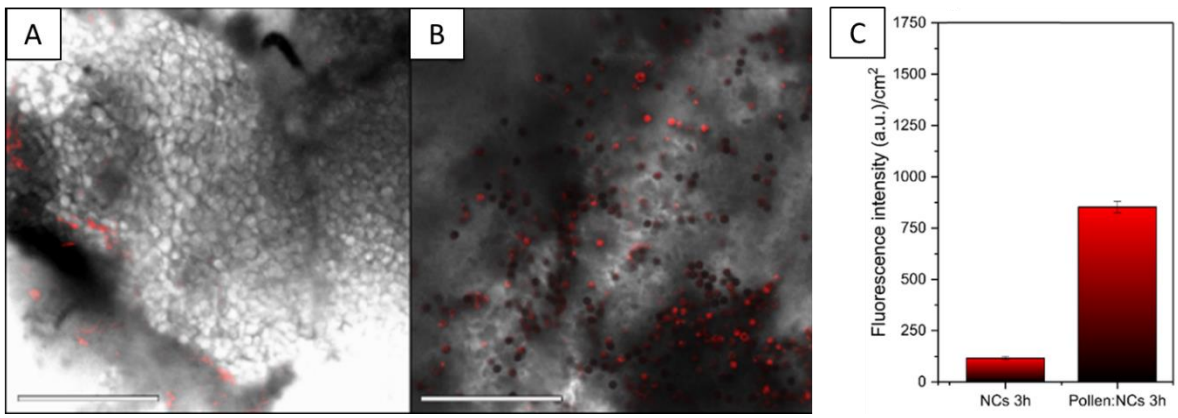

Figura 6. Microscopía confocal de la mucosa de sacos intestinales de rata no evertidos, tras 3 horas de incubación con: (A) Nanocápsulas de protamina (NCs) y (B) Microcápsulas huecas de esporopolenina cargadas con NCs de protamina. Canal rojo: NCs. DIC: Contraste de interferencia diferencial. Las barras blancas representan 500 µm. (C) Cuantificación de la fluorescencia en el tejido expresada como densidad integrada por área de tejido. Los datos representan la media ± error estándar, n=3 medidas independientes.

En segundo lugar, en el capítulo III de esta tesis, con el fin de evitar las limitaciones y resistencia al tratamiento sistémico actual de la tuberculosis, donde el elevado metabolismo de primer paso y degradación de fármacos dan lugar a unos niveles subterapéuticos [30, 31], se desarrollaron NCs de protamina para la liberación de rifabutina por vía pulmonar. Estas NCs se caracterizaron y atomizaron para su administración mediante inhaladores de polvo seco (DPIs) en un estudio publicado recientemente en el *European Journal of Pharmaceutical Sciences* (Abril de 2023 doi: 10.1016/j.ejps.2023.106442) [32]. Por otra parte, estas NCs se encapsularon en microcápsulas de polen para su uso como DPIs, tras un proceso de optimización de las propiedades aerodinámicas del polen.

Las NCs de protamina encapsularon la rifabutina en el núcleo oleoso empleando cargas teóricas de 1, 2,5 y 5 % (p/p) y presentaron un tamaño nanométrico, de alrededor de 200 nm y una carga superficial positiva, apropiada para lograr una mayor interacción e internalización con los macrófagos alveolares, de carga superficial negativa [33]. La encapsulación del fármaco fue satisfactoria, entre el 42-54%, y presentaron estabilidad tras 30 días a 4ºC, tras su liofilización en presencia de manitol, así como en medio de cultivo celular y medio pulmonar simulado hasta 24 h. La liberación de rifabutina de las NCs siguió un patrón lineal (**Figura 7**) en medio pulmonar simulado, con una liberación dependiente de la concentración de fármaco (cinética de primer orden), con una difusión del fármaco desde la matriz polimérica (Korsmeyer-Peppas > Higuchi), similar a otras formulaciones que emplearon polímeros como quitosano de bajo peso molecular o fucoidan [34]. La permeabilidad de rifabutina se evaluó en un modelo de difusión horizontal modificado (tipo "side-by-side") [35]. Los resultados indicaron mayor permeabilidad del fármaco tras su incorporación en las NCs en comparación con el fármaco libre tras 1 h.

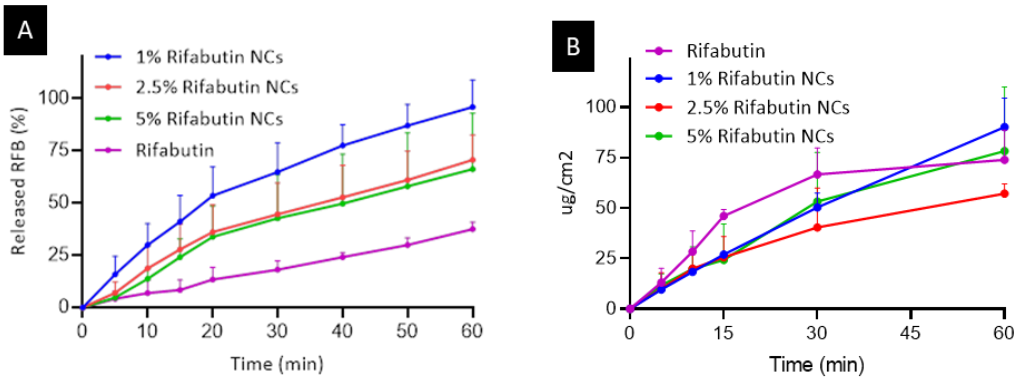

Figura 7. (A) Disolución y (B) permeabilidad del fármaco de las NCs de protamina cargadas con rifabutina al 1%, 2.5% y 5%. Los datos representan la media ± desviación estándar, n=3 medidas independientes.

Las NCs de rifabutina mostraron una viabilidad concentración-dependiente, superior al 75% para concentraciones de 0,1 mg/mL, en células epiteliales alveolares humanas A549 y macrófagos Raw 264.7 tras 24 h, con una elevada internalización (> 90 %) y una intensidad media de fluorescencia superior al control para ambos tipos de células.

Estas NCs cargadas con rifabutina fueron atomizadas en presencia de manitol, carbohidrato degradable aprobado por la FDA para su uso como excipiente en inhaladores de polvo seco [36], y se llevó a cabo su evaluación aerodinámica empleando un inhalador de baja resistencia Breezhaler® con un flujo de 60 L/min mediante el Impactador de Cascada de Andersen (ACI). Tras su administración mediante DPI (**Tabla 1**), la dosis emitida (ED) obtenida fue notablemente alta para todas las formulaciones (69-80%), obteniéndose una fracción de partículas finas (FPF, partículas <5 µm) de 19 a 32%, similares al producto referencia comercial Onbreez Breezhaler®, (FPF< 36% para 90 L/min) [37]. El diámetro aerodinámico medio (MMAD), entre 4,2-5,8 µm, fue óptimo para su distribución en la región bronquial y alveolar. Las NCs de rifabutina atomizadas se distribuyeron a través de la región extratorácica (63-79%), especialmente en la tráquea (25-30%), seguidas de la región bronquial (15-18%) y alveolar (1-9%), constituyendo un sistema prometedor para la terapia inhalable de la tuberculosis pulmonar.

Tabla 1. Propiedades aerodinámicas *in vitro* de los polvos de manitol atomizados (SPD) en una proporción de 80/20. FPD: Dosis de partículas finas; FPF: Fracción de partículas finas (<5 µm); ED: Dosis emitida; MMAD: Diámetro aerodinámico medio. Los datos representan la media ± desviación estándar, n=3 medidas independientes.

Producto atomizado	Andersen Cascade Impactor				Dynamic Light Scattering		
	FPF (%)	FPD (mg)	ED (%)	MMAD (µm)	Tamaño (nm)	PDI	Carga (mV)
NCs blancas	32 ± 10	1.8 ± 1	77 ± 8	4.2 ± 0.8	290 ± 34	<0.4	19 ± 6
NCs 1% Rifabutina	26 ± 6	1.1 ± 0.4	75 ± 11	5.8 ± 1.4	259 ± 32	<0.3	18 ± 7
NCs 2.5% Rifabutina	19 ± 8	0.8 ± 0.6	69 ± 25	5.8 ± 1.3	564 ± 104	<0.6	19 ± 2
NCs 5% Rifabutina	26 ± 8	1.2 ± 0.6	80 ± 9	5.5 ± 1.8	487 ± 96	<0.7	14 ± 3

-Párrafos afectados por la protección de derechos-

Por último, en el capítulo V de esta tesis se evaluó por primera vez el uso de las microcápsulas de polen para la administración tópica ocular de fármacos, utilizando como modelo la bilastina, un fármaco utilizado en el tratamiento tópico de la rinitis alérgica y llevando a cabo su encapsulación en NCs de protamina y microcápsulas de polen de *H. annuus* con el fin de mejorar su mucointeracción y tiempo de residencia en el ojo.

En primer lugar, se extrajo bilastina pura a partir de comprimidos orales comercializados, utilizando cloroformo como solvente de aislamiento. La bilastina se encapsuló en el núcleo oleoso de las NCs de protamina anteriormente descritas, que presentaron un tamaño medio de 200 nm y una asociación del fármaco de hasta el 12%, una carga superficial neutra y un pH (6.9 ± 0.4) considerado óptimo para su administración ocular. Estas NCs presentaron una estabilidad adecuada tras 30 días a 4ºC en suspensión, tras su liofilización en presencia de trehalosa al 5% (p/v), así como en fluido lacrimal simulado hasta 8 h. Las NCs se cargaron en microcápsulas huecas de polen de *H. annuus* mediante vacío, empleando una ratio de carga 1:1 (p/p), con una eficiencia de encapsulación del 71% y un patrón de liberación bifásico de bilastina en medio simulado lacrimal, con una liberación del 64% tras 24 h.

Tanto las NCs de bilastina como las NCs de bilastina cargadas en las microcápsulas de polen mostraron biocompatibilidad en la línea celular promonocítica THP-1 a concentraciones de 0,1 mg/mL, con valores entre 80-90% y 60-80%, respectivamente. Asimismo, presentaron buena adherencia e internalización en estas células, siendo más uniforme (96% de internalización) para las NCs de bilastina, y más localizada (6,6% de internalización) para las NCs cargadas en las microcápsulas de polen. Además, estas microcápsulas de polen presentaron una baja expresión de marcadores de activación de procesos inflamatorios (CD80 y CD83) en la superficie ocular, responsables de la activación de células inmunitarias innatas en la periferia de la córnea y la conjuntiva, en comparación con la estimulación por el lipopolisacárido.

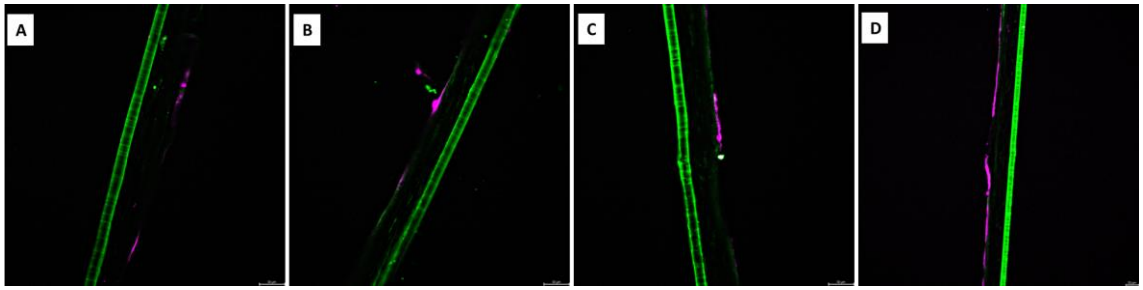

Figura 10. Imágenes de microscopía del modelo corneal 3D tras la administración tópica de NCs de protamina marcadas con DiD (A y B) y de NCs cargadas en microcápsulas de polen *H. annuus* (C y D). Las barras de escala representan 30 µm. Verde: ß-catenina. Rosa: NCs de protamina.

La evaluación de la compatibilidad celular y la internalización de NCs se realizó *in vitro* en un modelo tridimensional de tejido de córnea humana (QobuR) [38], desarrollado a partir de cultivos primarios humanos de células epiteliales corneales (**Figura 10**). La intensa expresión de β-catenina confirmó la ausencia de daño celular, así como la distribución de las NCs en la capa externa del tejido. Finalmente, ni las NCs ni las NCs encapsuladas en plataformas de polen mostraron expresión de proteínas y citoquinas mediadoras de procesos alérgicos e inflamatorios a nivel corneal (TNFα, CamKII, S100A o CD4+) tras su administración *in vivo*. Esta plataforma desarrollada da lugar, por una parte, a un aumento de la penetración del fármaco debido a su incorporación en nanocápsulas de protamina, mientras que, por otra, promueve su adhesión y permanencia prolongada y segura en la córnea al asociarse a microcápsulas de polen, constituyendo una estrategia prometedora en el tratamiento de alergias a nivel ocular.

Como conclusión general, en esta tesis se investigó la versatilidad y el potencial de las plataformas de polen y su combinación con nanosistemas, obteniéndose una plataforma de liberación multietapa de gran interés para la administración transmucosa de fármacos. Estas plataformas se enfocan en mejorar la biodisponibilidad de los fármacos al prolongar su tiempo de permanencia en la mucosa, aumentando su absorción y, como resultado, disminuyendo tanto su dosis como su frecuencia de administración y la aparición de efectos secundarios. La liberación transmucosa de medicamentos a través de su encapsulación en microcápsulas de polen es un área que está experimentando una evolución y progreso continuo y se espera que continúe brindando nuevos avances y posibilidades en el campo de la medicina.

RESUMO *IN EXTENSO*

RESUMO *IN EXTENSO*

A administración de fármacos a través das mucosas ofrece unha alternativa atractiva para superar os problemas relacionados coas formas de dosificación inxectables, xa que permite un mellor acceso ao tecido diana, imitando a vía de liberación natural de biomacromoléculas endóxenas de xeito non invasivo [1]. A súa facilidade de uso permite unha mellor adhesión e cumprimento por parte do paciente, e supón un menor custo de produción, ao non precisar de condicións de esterilidade. Neste contexto, a nanotecnoloxía permite un incremento da eficacia farmacolóxica ao reducir os efectos secundarios, mellorando a estabilidade e a dispoñibilidade dos fármacos [2]. O desenvolvemento de nanosistemas poliméricos espertou gran interese na liberación de fármacos debido á súa seguridade, biocompatibilidade e estabilidade física e biolóxica melloradas [3]. Con todo, ata a data, os intentos de demostrar unha eficacia alta e reproducible *in vivo* fracasaron [4] debido á súa eliminación prematura da mucosa, o que resulta nunha biodispoñibilidade limitada en comparación con outras vías [5]. Co fin de abordar este problema, investigouse a integración de nanosistemas en plataformas funcionais como unha estratexia de liberación multi-etapa, demostrando resultados prometedores na administración mucosa de fármacos, protexendo os nanosistemas e transportándoos á súa diana dun xeito más eficiente [6, 7].

Os grans de pole son microcápsulas naturais derivadas dos gametofitos masculinos do ciclo reprodutivo das plantas con sementes [8]. Están constituidos principalmente por esporopolenina, un biopolímero cunha arquitectura tridimensional especial que lles dá propiedades atractivas como unha alta resistencia e unha adhesión biolóxica [9]. O pole componse de tres capas principais (Figura 1): un revestimento externo chamado “pollenkitt”; seguido por unha parede de múltiples capas (exina e intina), e un esporoplasma interno, onde se atopa o gameto celular [10, 11].

Debido ao seu deseño natural, desenvolvéronse diversos procesos químicos co fin de eliminar os compostos presentes tanto no exterior como interior o pole, así como proteínas e alérxenos que constitúen un risco potencial para a saúde humana, dando lugar a unha estrutura oca de esporopolenina [12, 13]. Son moitas as especies de esporas y pole que se empregaron para la produción de microcápsulas de esporopolenina e que se utilizaron para diversas aplicacións, xa sexa como catalizadores, para enmascaramento de sabores ou a microencapsulación e liberación de fármacos e proteínas, entre outros [14, 15]. Na natureza, as plantas producen miles de tipos diferentes de pole, e cada pole pode mostrar variacións en canto ao seu tamaño, morfoloxía e estrutura fisicoquímica. Ademais, a superficie do pole pode presentar ornamentacións insulares, elementos en forma de clava ou puntiagudos, granulacións, crestes, buratos ou unha superficie lisa segundo a especie, así como unha ou varias aperturas alongadas (colpus) ou circulares (poros), con diferentes denominacións segundo o seu número e localización [16].

O reino Plantae inclúe tanto as plantas non vasculares (briofitas) como as plantas vasculares, as cales se dividen en plantas sen semente (pteridofitas) ou con semente, que poden presentar óvulos non protexidos (gimnospermas, división Magnoliophyta) ou protexidos (angiospermas, división Pinophyta). Dentro das gimnospermas, as dicotiledóneas constitúen o grupo de maior evolución y complexidade, con gran diversidade de grans de pole que presentan un maior número e diversidade de aperturas, xeralmente ecuatoriais, con prevalencia do pole triaperturado, con unha intina sinxela e unha exina ben desenvolvida [17, 18]. Neste grupo, a familia Asteraceae, engloba especies coma o xirasol (*Helianthus annuus*) cun pole de tamaño entre 26-50 μm e a camomila (*Matricaria chamomilla*), con grans de pole entre 13-25 μm. Ambos os dous presentan unha distintiva morfoloxía superficial con espiñas, que permite a súa

adhesión aos insectos durante a polinización e que potencialmente podería favorecer a súa adherencia ás mucosas, o que aumentaría o contacto coas superficies biolóxicas, mellorando a absorción e biodispoñibilidade de fármacos [19].

O noso grupo desenvolveu un protocolo simplificado para obter microcápsulas ocas de pole utilizando o pole de xirasol como modelo e avaliando a súa eficacia tamén para a purificación do pole de camomila [20].
Neste proceso, o pole de *H. annuus* foi sometido a un lavado secuencial con auga, acetona e cicloheaxano, para eliminar os compostos que recubren a esporopolenina, dando lugar a un pole desgraxado. O tratamento con auga permitiu a extracción de carbohidratos e proteínas [21], [22], mentres que a acetona eliminou ácidos grasos como α-linolénico, láurico, esteárico e outros lípidos [23] e o ciclohexano permitiu a extracción de compoñentes superficiais, como a pectina. A obtención de plataformas ocas de pole tivo lugar tras a incubación do pole desgraxado con ácido ortofosfórico (85%, H_3PO_4) a 70ºC durante 5 h, eliminando proteínas e carbohidratos presentes no esporoplasma interno. A partir dos resultados obtidos, empregouse este método para a obtención de pole de *M. chamomilla* a partir de flores secas, prescindindo do uso de ciclohexano ao obterse unha eliminación eficiente dos polisacáridos tras o tratamento do pole só co emprego de acetona e auga.

Aínda que non son abundantes en *H. annuus*, as proteínas e glicoproteínas son os principais compostos alerxénicos do pole [24], polo que a súa eliminación é un punto crítico para o seu uso con fins farmacéuticos. O contido de proteína do pole de xirasol diminuíu de un 33% en peso a un 4,4% tralo proceso de purificación e obtención das plataformas ocas, mentres que no caso do pole de camomila, a redución foi dun 16% a un 4%.

Co fin de desenvolver un sistema multietapa a partir destas microcápsulas ocas de pole, levouse a cabo a asociación de nanopartículas (NPs) de poliestireno non degradables de diferentes tamaños (100, 200 y 500 nm) e funcionalización superficial (aminadas, non modificadas e carboxiladas) empregando liofilización e baleiro, e determinando os parámetros críticos da asociación e liberación. Observouse que as NPs de 100 y 200 nm recubriron completamente as microcápsulas incluíndo as espiñas e as áreas internas da exina e que as NPs de maior tamaño se uniron principalmente á superficie do pole. Ademais, as NPs non modificadas e carboxiladas acumuláronse internamente en función do método de carga, mentres que, nas NPs aminadas, a acumulación tiña lugar nas superficies externa e interna do pole, independentemente do método de carga.

O perfil de liberación das NPs das microcápsulas de pole mostrou unha liberación rápida durante as primeiras 8 h. A carga por liofilización produciu unha maior liberación nos primeiros 15 min, conseguindo a estabilización despois de 24 h. Pola contra, as NPs cargados ao baleiro no pole deron lugar a unha liberación continua despois de 8 h ata 120 h, semellante ao descrito en estudos anteriores sobre a liberación de eritromicina [25] e paracetamol [26] das microcápsulas de pole. Isto podería deberse a unha maior asociación das NPs á superficie externa das plataformas de pole usando a liofilización como método de carga, o que produciría a súa liberación máis rápida que mediante a carga ao baleiro, onde as NPs estaban predominantemente situados na cavidade interior. Aínda que o método de carga influíu na liberación inicial, o tamaño e a funcionalización superficial das NPs foron determinantes na súa liberación co paso do tempo, sendo menor para as partículas máis pequenas. Tendo en conta a funcionalización superficial, a carga por liofilización deu lugar a unha liberación de NPs entre o 40-60%, o que se aproxima a unha difusión Fickiana, mentres que a carga por baleiro produciu

unha liberación con valores inferiores ao 40% para todos os tamaños, seguindo un modelo de difusión cuasi-Fickiano.

As NPs cun tamaño de 200 nm presentaron unha maior eficiencia de carga e maior liberación, independentemente da funcionalización da superficie ou do método de carga utilizado. Tendo en conta estes resultados, desenvolveuse un prototipo biodegradable de nanocápsulas poliméricas (NCs) cun tamaño próximo aos 200 nm que foi encapsulado en plataformas de pole, tanto de *H. annuus* como de *M. chamomilla*, e investigouse o seu potencial interese como sistemas de liberación para a vía oral (capítulo II), pulmonar (capítulo III e IV) e ocular (capítulo V). Para a capa polimérica das NCs, seleccionouse a protamina, un polipéptido natural rico en arginina, moi utilizado no deseño de sistemas poliméricos [27], e o Miglyol utilizouse para o núcleo oleoso, en combinación con surfactantes non iónicos como o polietilenglicol (PEGst-40) e glicocolato de sodio que, xuntos, melloran a estabilidade e penetración das formulacións [28]. As NCs de protamina preparáronse mediante a técnica de desprazamento de disolventes seguindo o procedemento descrito polo noso grupo [29] e realizouse a súa caracterización fisicoquímica, a súa estabilidade en medio biolóxico e a súa avaliación para a súa aplicación en diferentes vías de administración.

En primeiro lugar, para a avaliación en sistemas orais, cargáronse NCs de protamina en microcápsulas ocas de pole de *H. annuus* ao baleiro, utilizando unha relación de carga de 1:1 (p/p). Obtivéronse valores de asociación máis baixos que as NP de poliestireno (66% vs 73%) cunha liberación acumulada de arredor do 40% despois de 48 h en líquido intestinal simulado. As microcápsulas de pole cargadas con NCs de protamina mostraron unha alta adhesión á superficie da mucosa nun modelo de saco intestinal non evertido de rata *ex vivo*, cunha intensidade de fluorescencia significativamente maior que as NCs administradas libremente despois de 3 h de incubación. Así mesmo, a avaliación da súa distribución intestinal *in vivo* tras a súa administración oral confirmou unha menor acumulación de NCs de protamina cando se administraron en forma libre en comparación coas NCs cargados en microcápsulas de pole, o que suxire a súa liberación progresiva dende a cavidade interior de pole.

En segundo lugar, no capítulo III desta tese, co fin de evitar as limitacións e resistencias ao tratamento sistémico actual da tuberculose, onde un alto metabolismo de primeiro paso e a degradación do fármaco conducen a niveis subterapéuticos [30, 31], desenvolvéronse NCs de protamina. para a liberación pulmonar de rifabutina. Estas NCs caracterizáronse e atomizáronse para a súa administración mediante inhaladores de po seco (DPIs) nun estudo publicado recentemente no *European Journal of Pharmaceutical Sciences* (abril de 2023 doi: 10.1016/j.ejps.2023.106442) [32]. Por outra banda, estas NCs foron encapsulados en microcápsulas de pole para o seu uso como DPIs, tras un proceso de optimización das propiedades aerodinámicas do pole.

As NCs de protamina encapsularon a rifabutina no núcleo oleoso utilizando cargas teóricas do 1, 2,5 e 5% (p/p) e amosaron un tamaño nanométrico de arredor de 200 nm e unha carga superficial positiva, axeitada para lograr unha maior interacción e interiorización cos macrófagos alveolares, cunha carga superficial negativa [33]. A encapsulación do fármaco foi satisfactoria, entre un 42-54%, e mostraron estabilidade aos 30 días a 4ºC, tras a liofilización en presenza de manitol, así como no medio de cultivo celular e medio pulmonar simulado durante ata 24 h. A liberación de rifabutina das NCs seguiu un patrón lineal nun ambiente pulmonar simulado, con liberación dependente da concentración do fármaco (cinética de primeira orde), con difusión do fármaco desde a matriz polimérica (Korsmeyer-Peppas > Higuchi), similar á outras formulacións que usaban polímeros como o quitosano de baixo peso

molecular ou o fucoidan [34]. A permeabilidade da rifabutina foi avaliada nun modelo de difusión lado a lado modificado [35] Os resultados indicaron unha maior permeabilidade do fármaco despois da incorporación das NCs en comparación co fármaco libre despois de 1 h.

As NCs de rifabutina mostraron unha viabilidade dependente da concentración, superior ao 75% para concentracións de 0,1 mg/mL, en células epiteliais alveolares humanas A549 e macrófagos Raw 264.7 despois de 24 h, cunha alta internalización (>90%) e unha intensidade media de fluorescencia superior ao control para ambos tipos celulares.

Estas NCs cargados con rifabutina atomizáronse en presenza de manitol, un carbohidrato aprobado pola FDA para o seu uso como excipiente en inhaladores de po seco [36], e a avaliación aerodinámica realizouse mediante un inhalador de baixa resistencia Breezhaler® cun caudal de 60 L/min empregando o Impactador de Cascada de Andersen (ACI). Despois da administración por DPI, a dose emitida (DE) obtida foi notablemente alta para todas as formulacións (69-80%), obtendo unha fracción de partículas finas (FPF, partículas <5 µm) de 19 a 32%, similar ao produto comercial de referencia Onbreez Breezhaler®, (FPF <36%, 90 L/min) [37]. O diámetro aerodinámico medio (MMAD), entre 4,2-5,8 µm, foi óptimo para a súa distribución na rexión bronquial e alveolar. As NCs de rifabutina atomizados distribuíronse por toda a rexión extratorácica (63-79%), especialmente na tráquea (25-30%), seguida da rexión bronquial (15-18%) e alveolar (1-9%). constituíndo sistema prometedor para la terapia de inhalación de tuberculosis pulmonar.

-Párrafos afectados por la protección de derechos-

Finalmente, no capítulo V desta tese, avaliouse por primeira vez o uso de microcápsulas de pole para a administración tópica ocular de fármacos, tomando como modelo bilastina, fármaco empregado no tratamento tópico da rinitis alérxica e levando a cabo a súa encapsulación en NCs de protamina e microcápsulas de pole de *H. annuus* co fin de mellorar a súa mucointeracción e tempo de residencia na superficie ocular.

En primeiro lugar, a bilastina pura foi extraída de comprimidos orais dispoñibles comercialmente usando cloroformo como disolvente illante. A bilastina encapsulouse no núcleo oleoso das NCs de protamina anteriormente descritos, que teñan un tamaño medio de 200 nm, e cunha eficazia de asociación do fármaco de ata un 12%, con unha carga superficial neutra e un pH (6,9 ± 0,4) considerado óptimo para a súa administración ocular. Estas NCs mostraron unha estabilidade adecuada despois de 30 días a 4ºC en suspensión, despois da liofilización en presenza de trehalosa ao 5% (p/v), así como en líquido lacrimóxeno simulado durante ata 8 h. As NC cargáronse en microcápsulas ocas de pole de *H. annuus* empregando baleiro, cunha relación de carga de 1:1 (p/p) e cunha eficiencia de encapsulación do 71% e un patrón de liberación bifásica de bilastina . do 64% en medio lacrimal simulado despois de 24 h.

Tanto as NCs de bilastina como as NCs de bilastina cargados nas microcápsulas de pole mostraron boa biocompatibilidade na liña celular promonocítica THP-1 a concentracións de 0,1 mg/ml, con valores entre 80-90% e 60-80%, respectivamente. Así mesmo, presentaron boa adherencia e interiorización nestas células, sendo os resultados máis uniformes (96% de internalización) para as NCs de bilastina, e máis localizadas (6,6% de internalización) para as NCs cargadas nas microcápsulas de pole. Ademais, estas microcápsulas de pole mostraron unha baixa expresión de marcadores de activación de procesos inflamatorios (CD80 e CD83) na superficie ocular, responsables da activación das células inmunes innatas na periferia da córnea e da conxuntiva, en comparación coa estimulación dos lipopolisacáridos.

A avaliación da compatibilidade celular e a internalización das NCs realizouse *in vitro* nun modelo tridimensional de tecido corneal humano (QobuR) [40], desenvolvido a partir de cultivos humanos primarios de células epiteliais da córnea. A intensa expresión da β-catenina confirmou a ausencia de dano celular, así como a distribución das NCs na capa externa do tecido. Finalmente, nin as NCs nin as NCs encapsulados nos vehículos de pole mostraron expresión de proteínas e citocinas que median procesos alérxicos e inflamatorios a nivel corneal (TNFα, CamKII, S100A ou CD4+) despois da súa administración *in vivo*. Esta plataforma desenvolvida conduce, por unha banda, a un aumento da penetración do fármaco pola súa incorporación a nanocápsulas de protamina, mentres que, por outra banda, favorece a súa adhesión e permanencia prolongada e segura na córnea cando se asocia con microcápsulas de pole, constituíndo unha estratexia prometedora no tratamento das alerxias a nivel ocular.

Como conclusión xeral, nesta tese investigouse a versatilidade e potencialidade das microcápsulas derivadas de grans de pole e a súa combinación con nanosistemas, obtendo unha plataforma de liberación multietapa de gran interese para a administración transmucosa de fármacos. Estas plataformas céntranse en mellorar a biodispoñibilidade dos fármacos ao prolongar o seu tempo de residencia na mucosa, aumentar a súa absorción e, como consecuencia, diminuír tanto a súa dose e frecuencia de administración como a aparición de efectos secundarios. A liberación transmucosa de fármacos a través da súa encapsulación en microcápsulas de pole é un ámbito que está en continua evolución e progreso e que se espera que siga aportando novos avances e posibilidades no campo da medicina.

REFERENCIAS

[1] Lakkireddy, H. R.; Urmann, M.; Besenius, M.; Werner, U.; Haack, T.; Brun, P.; Alié, J.; Illel, B.; Hortala, L.; Vogel, R.; et al. Oral Delivery of Diabetes Peptides - Comparing Standard Formulations Incorporating Functional Excipients and Nanotechnologies in the Translational Context. *Adv. Drug Deliv. Rev.*, **2016**, *106* (Pt B), 196–222. https://doi.org/10.1016/j.addr.2016.02.011.

[2] Ageitos, J. M.; Garcia-Fuentes, M. Advances in Drug Delivery Strategies for Microbial Healthcare Products. In *Pharmaceuticals from Microbes. The Bioengineering Perspective*; Arora, D., Sharma, C., Jaglan, S., Lichtfouse, E., Eds.; Springer International Publishing, 2019; pp 1–38. https://doi.org/10.1007/978-3-030-01881-8_1.

[3] Fosgerau, K.; Hoffmann, T. Peptide Therapeutics: Current Status and Future Directions. *Drug Discov. Today*, **2015**, *20* (1), 122–128. https://doi.org/10.1016/j.drudis.2014.10.003.

[4] Ensign, L. M.; Cone, R.; Hanes, J. Oral Drug Delivery with Polymeric Nanoparticles: The Gastrointestinal Mucus Barriers. *Adv. Drug Deliv. Rev.*, **2012**, *64* (6), 557–570. https://doi.org/10.1016/j.addr.2011.12.009.

[5] Wu, L.; Shan, W.; Zhang, Z.; Huang, Y. Engineering Nanomaterials to Overcome the Mucosal Barrier by Modulating Surface Properties. *Adv. Drug Deliv. Rev.*, **2018**, *124*, 150–163. https://doi.org/10.1016/j.addr.2017.10.001.

[6] Yu, F.; Li, Y.; Liu, C. S.; Chen, Q.; Wang, G. H.; Guo, W.; Wu, X. E.; Li, D. H.; Wu, W. D.; Chen, X. D. Enteric-Coated Capsules Filled with Mono-Disperse Micro-Particles Containing PLGA-Lipid-PEG Nanoparticles for Oral Delivery of Insulin. *Int. J. Pharm.*, **2015**, *484* (1–2), 181–191. https://doi.org/10.1016/j.ijpharm.2015.02.055.

[7] Gaspar, D. P.; Gaspar, M. M.; Eleutério, C. V.; Grenha, A.; Blanco, M.; Gonçalves, L. M. D.; Taboada, P.; Almeida, A. J.; Remuñán-López, C. Microencapsulated Solid Lipid Nanoparticles as a Hybrid Platform for Pulmonary Antibiotic Delivery. *Mol. Pharm.*, **2017**, *14* (9), 2977–2990. https://doi.org/10.1021/acs.molpharmaceut.7b00169.

[8] Knox, R. B. The Pollen Grain. In *Embryology of Angiosperms*; Johri, B. M., Ed.; Springer Berlin Heidelberg: Berlin, Heidelberg, 1984; pp 197–271. https://doi.org/10.1007/978-3-642-69302-1_5.

[9] Mackenzie, G.; Boa, A. N.; Diego-Taboada, A.; Atkin, S. L.; Sathyapalan, T. Sporopollenin, The Least Known Yet Toughest Natural Biopolymer. *Front. Mater.*, **2015**, *2* (October), 1–5. https://doi.org/10.3389/fmats.2015.00066.

[10] Wiermann, R.; Gubatz, S. Pollen Wall and Sporopollenin. *Int. Rev. Cytol.*, **1992**, *140* (C), 35–72. https://doi.org/10.1016/S0074-7696(08)61093-1.

[11] Jiang, J.; Zhang, Z.; Cao, J. Pollen Wall Development: The Associated Enzymes and Metabolic Pathways. *Plant Biol.*, **2013**, *15* (2), 249–263. https://doi.org/10.1111/j.1438-8677.2012.00706.x.

[12] Gonzalez-Cruz, P.; Uddin, M. J.; Atwe, S. U.; Abidi, N.; Gill, H. S. Chemical Treatment Method for Obtaining Clean and Intact Pollen Shells of Different Species. *ACS Biomater. Sci. Eng.*, **2018**, *4* (7), 2319–2329. https://doi.org/10.1021/acsbiomaterials.8b00304.

[13] Mackenzie, G.; Beckett, S.; Atkin, S.; Diego-Taboada, A. *Pollen and Spore Shells—Nature's Microcapsules*; Elsevier Inc., 2014. https://doi.org/10.1016/B978-0-12-404568-2.00024-8.

[14] Alshehri, S. M.; Al-Lohedan, H. A.; Chaudhary, A. A.; Al-Farraj, E.; Alhokbany, N.; Issa, Z.; Alhousine, S.; Ahamad, T. Delivery of Ibuprofen by Natural Macroporous Sporopollenin Exine Capsules Extracted from *Phoenix Dactylifera* L. *Eur. J. Pharm. Sci.*, **2016**, *88*, 158–165. https://doi.org/10.1016/j.ejps.2016.02.004.

[15] Ma, H.; Zhang, P.; Wang, J.; Xu, X.; Zhang, H.; Zhang, Z.; Zhang, Y.; Ning, Y. Preparation of a Novel Rape Pollen Shell Microencapsulation and Its Use for Protein Adsorption and PH-Controlled Release. *J. Microencapsul.*, **2014**, *31* (7), 667–673. https://doi.org/10.3109/02652048.2014.913723.

[16] Halbritter, H.; Ulrich, S.; Grímsson, F.; Weber, M.; Zetter, R.; Hesse, M.; Buchner, R.; Svojtka, M.; Frosch-Radivo, A. *Illustrated Pollen Terminology*; 2018. https://doi.org/10.1007/978-3-319-71365-6.

[17] Kuprianova, L. A. Apertures of Pollen Grains and Their Evolution in Angiosperms. *Rev. Palaeobot. Palynol.*, **1967**, *3* (1–4), 73–80. https://doi.org/10.1016/0034-6667(67)90041-3.

[18] Structures, W. Comparative Morphology of Monocot Pollen and and Wall Structures. *Bot. Rev.*, **1983**, *4* (4), 331–379.

[19] Diego-Taboada, A.; Beckett, S. T.; Atkin, S. L.; Mackenzie, G. Hollow Pollen Shells to Enhance Drug Delivery. *Pharmaceutics*, **2014**, *6* (1), 80–96. https://doi.org/10.3390/pharmaceutics6010080.

[20] Ageitos, J. M.; Robla, S.; Valverde-Fraga, L.; Garcia-Fuentes, M.; Csaba, N. Purification of Hollow Sporopollenin Microcapsules from Sunflower and Chamomile Pollen Grains. *Polymers (Basel).*, **2021**, *13* (13), 2094. https://doi.org/10.3390/polym13132094.

[21] Grube, M.; Bekers, M.; Upite, D.; Kaminska, E. Infrared Spectra of Some Fructans. *Spectroscopy*, **2002**, *16* (3–4), 289–296. https://doi.org/10.1155/2002/637587.

[22] Schulte, F.; Lingott, J.; Panne, U.; Kneipp, J. Chemical Characterization and Classification of Pollen. *Anal. Chem.*, **2008**, *80* (24), 9551–9556. https://doi.org/10.1021/ac801791a.

[23] Schulz, H.; Baranska, M. Identification and Quantification of Valuable Plant Substances by IR and Raman Spectroscopy. *Vib. Spectrosc.*, **2007**, *43* (1), 13–25. https://doi.org/10.1016/j.vibspec.2006.06.001.

[24] Ghosh, N.; Sircar, G.; Saha, B.; Pandey, N.; Bhattacharya, S. G. Search for Allergens from the Pollen Proteome of Sunflower (Helianthus Annuus L): A Major Sensitizer for Respiratory Allergy Patients. *PLoS One*, **2015**, *10* (9), 1–20. https://doi.org/10.1371/journal.pone.0138992.

[25] Dyab, A. K. F.; Mohamed, M. A.; Meligi, N. M.; Mohamed, S. K. Encapsulation of Erythromycin and Bacitracin Antibiotics into Natural Sporopollenin Microcapsules: Antibacterial, Cytotoxicity, in Vitro and in Vivo Release Studies for Enhanced Bioavailability. *RSC Adv.*, **2018**, *8* (58), 33432–33444. https://doi.org/10.1039/C8RA05499A.

[26] Mujtaba, M.; Sargin, I.; Akyuz, L.; Ceter, T.; Kaya, M. Newly Isolated Sporopollenin Microcages from *Platanus Orientalis* Pollens as a Vehicle for Controlled Drug Delivery. *Mater. Sci. Eng. C*, **2017**, *77*, 263–270. https://doi.org/10.1016/j.msec.2017.02.176.

[27] Jakubiak, P.; Thwala, L. N.; Cadete, A.; Préat, V.; Alonso, M. J.; Beloqui, A.; Csaba, N. Solvent-Free Protamine Nanocapsules as Carriers for Mucosal Delivery of Therapeutics. *Eur. Polym. J.*, **2017**, *93* (March), 695–705. https://doi.org/10.1016/j.eurpolymj.2017.03.049.

[28] Thwala, L. N.; Delgado, D. P.; Leone, K.; Marigo, I.; Benetti, F.; Chenlo, M.; Alvarez, C. V.; Tovar, S.; Dieguez, C.; Csaba, N. S.; et al. Protamine Nanocapsules as Carriers for Oral Peptide Delivery. *J. Control. Release*, **2018**, *291* (October), 157–168. https://doi.org/10.1016/j.jconrel.2018.10.022.

[29] Thwala, L. N.; Beloqui, A.; Csaba, N. S.; González-Touceda, D.; Tovar, S.; Dieguez, C.; Alonso, M. J.; Préat, V. The Interaction of Protamine Nanocapsules with the Intestinal Epithelium: A Mechanistic Approach. *J. Control. Release*, **2016**, *243*, 109–120. https://doi.org/10.1016/j.jconrel.2016.10.002.

[30] Chae, J.; Choi, Y.; Tanaka, M.; Choi, J. Inhalable Nanoparticles Delivery Targeting Alveolar Macrophages for the Treatment of Pulmonary Tuberculosis. *J. Biosci. Bioeng.*, **2021**, *132* (6), 543–551. https://doi.org/10.1016/j.jbiosc.2021.08.009.

[31] Sosnik, A.; Carcaboso, Á. M.; Glisoni, R. J.; Moretton, M. A.; Chiappetta, D. A. New Old Challenges in Tuberculosis: Potentially Effective Nanotechnologies in Drug Delivery. *Adv. Drug Deliv. Rev.*, **2010**, *62* (4–5), 547–559. https://doi.org/10.1016/j.addr.2009.11.023.

[32] Robla, S.; Varela Calviño, R.; Ambrus, R.; Csaba, N. A Ready-to-Use Dry Powder Formulation Based on Protamine Nanocarriers for Pulmonary Drug Delivery. *Eur. J. Pharm. Sci.*, **2023**, *185* (April), 106442. https://doi.org/10.1016/j.ejps.2023.106442.

[33] Lee, W. H.; Loo, C. Y.; Traini, D.; Young, P. M. Nano- and Micro-Based Inhaled Drug Delivery Systems for Targeting Alveolar Macrophages. *Expert Opin. Drug Deliv.*, **2015**, *12* (6), 1009–1026. https://doi.org/10.1517/17425247.2015.1039509.

[34] Rodrigues, S.; da Costa, A. M. R.; Flórez-Fernández, N.; Torres, M. D.; Faleiro, M. L.; Buttini, F.; Grenha, A. Inhalable Spray-Dried Chondroitin Sulphate Microparticles: Effect of Different Solvents on Particle Properties and Drug Activity. *Polymers (Basel).*, **2020**, *12* (2), 1–13. https://doi.org/10.3390/polym12020425.

[35] Gieszinger, P.; Kiss, T.; Szabó-Révész, P.; Ambrus, R. The Development of an In Vitro Horizontal Diffusion Cell to Monitor Nasal Powder Penetration Inline. *Pharmaceutics*, **2021**, *13* (6), 809. https://doi.org/10.3390/pharmaceutics13060809.

[36] Sham, J. O. H.; Zhang, Y.; Finlay, W. H.; Roa, W. H.; Löbenberg, R. Formulation and Characterization of Spray-Dried Powders Containing Nanoparticles for Aerosol Delivery to the Lung. *Int. J. Pharm.*, **2004**, *269* (2), 457–467. https://doi.org/10.1016/j.ijpharm.2003.09.041.

[37] Horváth, A.; Farkas, Á.; Szipőcs, A.; Tomisa, G.; Szalai, Z.; Gálffy, G. Numerical Simulation of the Effect of Inhalation Parameters, Gender, Age and Disease Severity on the Lung Deposition of Dry Powder Aerosol Drugs Emitted by Turbuhaler®, Breezhaler® and Genuair® in COPD Patients. *Eur. J. Pharm. Sci.*, **2020**, *154* (March). https://doi.org/10.1016/j.ejps.2020.105508.

[38] Chacón, M.; Vázquez, N.; Persinal-Medina, M.; Alonso-Alonso, S.; Alcalde, I.; Merayo-Lloves, J.; Meana, Á. In-House Performance Assessment of 3D QobuR-Reconstructed Human Cornea-Like Epithelium (RhCE) for the Evaluation of Eye Hazard. *Toxicol. Vitr.*, **2022**, *82* (January). https://doi.org/10.1016/j.tiv.2022.105390.

INTRODUCTION

Natural sporopollenin microcapsules: state-of-the-art and application perspectives

INTRODUCTION

Natural sporopollenin microcapsules: state-of-the-art and application perspectives

Abstract

Natural microstructures, such as diatoms, pollen, or spores are generating considerable interest for encapsulation, protection, and delivery of actives in the food and pharmaceutical industry due to their abundance, low cost, and their uniform shape, size, and structure. Part of the secret of pollen and spores lies in the composition of their external layer, the sporopollenin, a complex biopolymer resistant to chemicals, enzymes, and radiation. Due to their smart natural design, pollen grains and spores have been employed to produce hollow sporopollenin structures, via chemical processes designed to solubilize the different additional compounds present in their structures. Hollow sporopollenin microcapsules have been used for the microencapsulation of drugs, proteins or oils, employed as microreactors, molecular sieves, templates for metallic replicas, and even as smart self-propelled devices. In this review, we summarize the different strategies to produce such sporopollenin capsules from pollen and spores, the methods for their characterization, and the purification processes, highlighting their most promising applications for the delivery of active pharmaceutical ingredients.

1. INTRODUCTION

Pollen grains are the microscopic capsules of male gametophytes in the reproductive cycle of seed plants [1, 2]. Their structure is adapted to perform its biological activity of fertilizing female gametophytes of higher plants. Due to their lack of mobility, they must be dispersed by several means, such as wind, water, rain, animals, or insects [3], which drastically affects the adaptation of pollen size, shape, density, and composition in different plant species. The pollen wall of seed plants consists of a multilayered heterogeneous wall of three main domains: pollen coat, exine, and intine, with a different structure and chemical composition which act as physical barriers, protecting male sperm from harsh environmental conditions [4, 5].

Pollen grains are surrounded by various types of adhesive materials that facilitate transportation. These agents differ in their composition, origin, development, and partly in their function. Regarding their solubility, these can be divided as aqueous soluble materials (carbohydrates, glycoproteins, and proteins) [4], and the pollenkitt, a common adhesive material composed of saturated and unsaturated lipids, carotenoids, flavonoids, and proteins [6, 7]. Pollenkitt contributes to the adhesion of the pollen grains through the formation of capillary bridges establishing non-polar van der Waals interactions [7]. Under this surface coating, the protective sculpted shell of the pollen wall is mainly composed of a stable non-soluble polymer named sporopollenin, a highly cross-linked polymer with extraordinary resistance to acidic and enzymatic treatments [8]. This structure, known as exine presents multiple nanometric pores and elongated apertures or colpus, where the pollen tube emerges during germination [1]. In the case of echinate pollen (**Figure 1**), the exine presents prominent spines which vary in size and distribution between pollen species. The cavities inside the exine are known as cavi (cavus), and they can be filled with a granular content mainly composed of pectins [5]. In some pollen species, the exine is stratified into ectexine (the external ornamented part of the exine and comprised of the tectum, columella, and foot layer [9]) and endexine (the internal part that can be formed as a granular or laminar layer). The endexine is related to the transport of nutrients and solvents as well as in harmomegathy [10], the process by which pollen grains fold and unfold depending on the humidity and desiccation [11]. The endexine is composed of sporopollenin, polysaccharides, lipids, and proteins, and it can be present in different forms

such as a continuous, spongy, or laminar layer, also depending on the plant species [10]. The layer bordering the surface of the pollen cytoplasm is known as internal intine, and it is mainly composed of hemicellulose, pectins, and microfibrillar cellulose. This inner layer is usually considered labile to acid treatments, and it is absent in some treated pollen samples [2]. Lastly, the inner cavity of the pollen grain (sporoplasm) comprises a large vegetative and a smaller generative cell, enclosed in the cytoplasm of the vegetative cell and responsible for the production of sperm cells [1, 12].

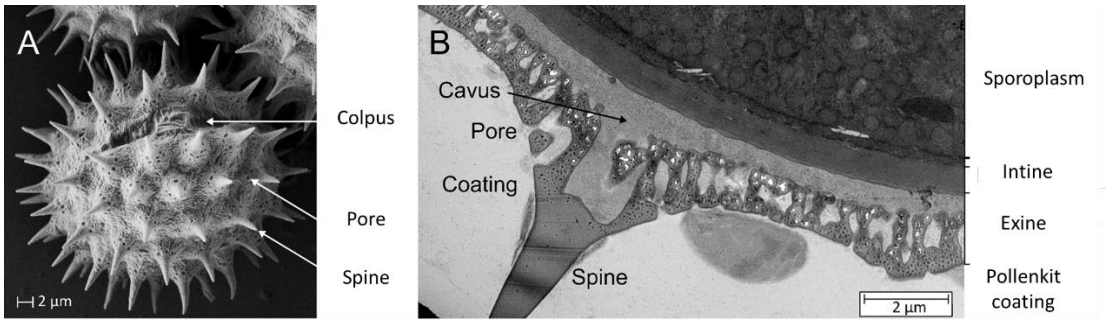

Figure 1. (A) Scanning electron microscopy (SEM) micrographs of *Helianthus annuus* exine and (B) microtome section showing the different layers from the external pollenkitt up to the internal cavity (bar=2 µm). Figure provided by the authors.

In contrast to pollen grains, spores are less complex haploid cells derived from sporangium (in avascular, seedless vascular plants, fungi, and algae) [1] and are the main dispersal agent, essential for reproduction. Spores are produced by the diploid phase or sporophyte by meiosis and germinate into a haploid plant with sex organs that produce microgametophytes (male) and megagametophytes (female) [1]. When mobile microgametophytes reach the megagametophytes, fertilization occurs, and the sporophyte grows to continue the cell cycle [13]. The wall of the spore or sporoderm is constituted by a main layer, the exospore. In the literature related to spore microcapsules, this layer is also usually termed as exine, and is mainly composed of sporopollenin [14].

1.1. Sporopollenin

Sporopollenin is the main component of spores and pollen exines, initially described in the early 19th century, and detailed one hundred years later, in *Lycopodium* spores [15, 16]. Sporopollenin is an extremely resistant biopolymer with a cross-linked structure composed of carbon, oxygen, and hydrogen [8, 17]. Despite 200 years of research in the elucidation of its composition and structure, this aspect is still controversial. The main problems in the study of sporopollenin are due to its extraordinary resistance which requires the use of aggressive chemical treatments for solubilization that can alter its native chemical composition. Two recent studies have shed light on pollen and spore sporopollenin with more precision than previous studies. Li and collaborators have elucidated the structure of pine sporopollenin by solid-state NMR, showing that it is mainly composed of aliphatic-polyketide-derived polyvinyl alcohol units and 7-*O*-*p*-coumaroylated C_{16} aliphatic units [18]. On the other hand, Michael and collaborators, employing mass spectrometry and high-resolution X-ray photoelectron spectroscopy techniques, found that *L. clavatum* sporopollenin was composed of two different building units of polyhydroxylated tetraketide-like monomeric units cross-linked with poly(hydroxy acid) networks [17]. The main difference between these studies is the presence/absence of aromatic residues in the sporopollenin structure, such as *p*-coumaric acid [18]. The presence of aromatic phenylpropanoid compounds as ferulic and coumaric acids have been reported in the main part

of the studies carried out in the elucidation of sporopollenin structure based on UV, infrared, or gas chromatography-mass spectrometry [19–25].

2. PROCESSING OF PLANT SPORES AND POLLEN TO PRODUCE SPOROPOLLENIN MICROCAPSULES

2.1. Elimination of pollenkitt

Many of the studies performed in the production of sporopollenin microcapsules use commercially defatted pollen as starting material, but in other cases, raw natural pollen and spores were the preferred option. The lipidic layer of spores or the pollenkitt [6] is extracted using organic solvents, by heating or at room temperature. Acetone is one of the most universally used solvents, however, other reagents are often preferable for extraction since acetone tends to precipitate proteins [26]. For instance, mixtures of chloroform/methanol [7, 27], cyclohexane [26, 28] ethyl ether [29, 30], diethyl ether [26, 31], or combined treatments with acetone followed with diethyl ether [32, 33] or petroleum ether [34] are commonly used alternatives. The washing and defatting process is more intensive in the studies which use bee pollen granules [33], since these granules/pellets contain multifloral pollen blended with bee secretions, enzymes, wax, and nectar or honey [35].

2.2. Purification of sporopollenin

Using defatted spores or pollen as the starting material, hollow sporopollenin microcapsules are obtained by the elimination of the internal components (sporoplasm), and in most cases, the intine layer. Several techniques have been developed for plant spores and pollen grains involving procedures such as alkaline lysis, acidolysis, or enzymatic treatments, with specific reflux conditions and fixed temperature to minimize damage to the exine surface, thus preserving its structure.

Zetzsche and Huggler [15] were pioneers in proposing a method to extract sporopollenin, which is still in use with several modifications. After an initial treatment with organic solvents for the removal of lipids from the outer layer, the defatted pollen undergoes an alkali treatment to remove the genetic materials (sporoplasm), and a final aqueous acid treatment to extract the polysaccharide intine [36]. Follow-up investigations modified the initial technique, which entailed the introduction of distinct acids or bases. The most common alkali employed is potassium hydroxide (KOH), and for acidolysis, orthophosphoric acid (H_3PO_4) is used. Recent methods have also changed the order of the treatment, performing first the acidolysis in H_3PO_4 followed by an alkali treatment in KOH, allowing a reduction of the process temperature [37].

Another method widely employed in palynology is Erdman's acidolysis in a (9:1) acetic anhydride: sulfuric acid mixture [38, 39]. This harsh method removes the cellular content and the intine while preserving pollen size, although it can cause swelling and change the morphology of pollen. For these reasons, other acids, such as hydrochloric acid (HCl) or H_3PO_4, are often preferred to perform acidolysis [40]. Enzymatic digestion by using trypsin has been also performed to isolate sporopollenin after an acidolysis procedure [41].

Depending on the nature and composition of each pollen, the methods need to be optimized to achieve intact sporopollenin microcapsules. Their outstanding physicochemical properties have led to their use as a microparticulate system for the encapsulation of biomacromolecules [8]. The detailed process of each pollen type and pharmacological applications are schematized in **Figure 2** and are described in detail in the section 4**.**

3. ANALYTICAL TECHNIQUES FOR THE CHARACTERIZATION OF SPOROPOLLENIN MICROCAPSULES CHARACTERIZATION

3.1. Fourier transform Infrared Spectroscopy (FTIR)

FTIR is a widely used technique for the characterization of pollen and sporopollenin microcapsules production. It requires a small amount of sample and allows the detection of characteristic chemical bonds. Nevertheless, although FTIR is a non-destructive technique, some authors grind the pollen for the uniform measurement of internal and external compounds, especially when large pollen grains are studied [23]. This technique can be performed by several methods, such as total attenuated reflectance (ATR), which works with native samples [42], or using potassium bromide (KBr) [43]. ATR technique is more appropriate for the study of the compounds of the pollen wall since the penetration of infrared light is limited to 0.5-5 µm [43], and it depends on the wavenumber employed. In addition, the high signal-to-noise ratio, simplicity, and fast measurement of ATR-FTIR make it the most viable option for the study of the biodegradation mechanisms of sporopollenin microcapsules in simulated gastrointestinal fluid or human plasma [44, 45]. **Table 1** summarizes some of the characteristic FTIR bands of pollen and sporopollenin microcapsules, depicting the corresponding vibration and associated chemical bonds. The bands corresponding to sporopollenin are considered a fingerprint region for the quality of sporopollenin microcapsules production.

Table 1. Values of wavenumbers with the corresponding vibration and compound assignation in pollen samples.

Wavenumbers (cm^{-1})	Assignation	Compounds	References
721	v(C=C), v(CH_n)	Lipids, Sporopollenin	[46–48]
831	v(Aromatic ring) (Ar.)	Sporopollenin, aromatic	[47, 49, 50]
970	vAr.	Sporopollenin	[51]
1032	v(C-O), (C-C)	Polysaccharides	[52, 53]
1074	v(CO), v(CC), ß(COH)	Arabinogalactan, ribose, glucose	[49, 54, 55]
1100	v(C–O–C), v(s)C–OH	Pectin, polysaccharides, polygalacturonic acid (PGA)	[46, 47, 54]
1171	Ar., v(as)CO-O-C	Sporopollenin, glycomaterials	[46, 47]
1243	v(C-O) from acetyl	Sporopollenin	[56]
1280	v(s)C-O	Amide III (protein)	[37]
1377	v(b)[CH_2], v(b)(O–H), Ar.	Lignin, cellulose, hemicellulose Sporopollenin	[48, 57]
1415	v(s) (C–O) [COO^-]	Hemicellulose, PGA	[58]
1435	CH_3 δ, v(CO), δOH	Sporopollenin	[59]
1455	v(as)[CH_3, CH_2]	Proteins, lignin	[46]
1514	Ar.	Sporopollenin	[46, 47]
1550	v(s)C-N, v(b)N-H	Amide II (protein)	[46]
1576	v(δ)C–H [CH_3, CH_2], Ar.	Lignin	[60]
1608	Ar.	Sporopollenin, aromatic amino acids	[46, 50]
1631	v(s)C=O	Amide I (Proteins) ß-sheet	[46]
1680	v(s)C=O [-CO_2H], Ar.	Sporopollenin, lignin	[21]
1706	v(s)C=O	Lipids	[46]
1735 1743	v(s)C=O	Saturated esters (lipids)	[54, 61]
2854 2925	v(s)[CH_2]	Lipids	[37, 62] [33, 63]
3300	v(s)O-H	H_2O	[33, 51]

v: vibration; v(s): stretching; v(as): asymmetric stretching; v(b): blending; δ: deformation.

3.2. Thermogravimetric analysis

Thermogravimetric analysis (TGA) is employed for the characterization of polymers and biomaterials by measuring the weight loss of samples as a function of temperature or time in a controlled atmosphere. The degradation and decomposition patterns and the amount and rate of mass change are often characteristic of the different materials [64]. TGA curves are especially useful in the analysis of polymer blends and composite materials since several decomposition steps can be observed, allowing the identification of the main components, as well as their weight percentage in the sample. The first derivate of TGA curves (derivative thermogram, DTG) enables more precise identification of inflection points for the interpretation of the thermogram [64] in complex samples such as pollen or spores. The comparison of TGA/DTG curves of raw, defatted, and hollow sporopollenin microcapsules allows the characterization of the composition or the purification degree of sporopollenin, due to the different thermal stability of the pollen constituents (polysaccharides, proteins, and lipids) with different degradation behavior and contribution to the mass change. In general, an initial thermal decomposition of pollen at 30 and 150ºC leads to mass change produced by the evaporation of absorbed water and the breakdown of hydrogen bonds, leading to the elimination of water and other volatile components with a low molecular weight [65]. Then, the degradation stage from 130 to 270ºC can be attributed to the decomposition of carbohydrates, proteins, and fibers [66]. For instance, the temperature of the maximum rate of pectin decomposition is 234ºC [65], and hemicelluloses degrade at temperatures from 200 to 260ºC. A degradation stage between 270-370ºC is attributed to the decomposition of cellulosic compounds (300 and 355ºC) or proteins (320-330ºC) [65–67], while the thermal degradation of lipids, in the case of bee pollen samples occurs at 440-450ºC, and for triglycerides, it depends on their saturation degree, being lower for poly- (200-380ºC) and mono-unsaturated fatty acids (300-480ºC) than saturated ones [66]. Sporopollenin shows a remarkable thermal resistance, and its thermal decomposition varies among the different species, and has been reported at 431ºC in *P. deltoides* [68], 437ºC for *L. clavatum* [69], ~480ºC for *P. orientalis* [67] or between 580-630ºC for coconut, coriander, rapeseed or multifloral pollens [66].

3.3. Elemental analysis (CHN)

Elemental analysis is often employed for the study of the exine purification in pollen and spore microcapsules. Sporopollenin is free of nitrogen [70] and therefore, the protein content of purified pollen and spores is often inferred from the nitrogen content of the samples, using a multiplication factor of 5.6 [41, 71] or 6.25, following the recommendation of the Association of Analytical Communities (AOAC) [11]. Nevertheless, some authors suggested that the exine indeed contains nitrogen in its structure [72, 73], while others reported that 30% of the detected nitrogen was not of proteic origin but from free amino acids [35]. Thus, it appears that the detection of nitrogen by elemental analysis can be either explained by the presence of residual proteins, or amino acids in the exine or contamination of the solvents [70].

3.4. Confocal laser scanning microscopy (CLSM)

Pollen and spores have natural autofluorescence and the pattern and intensity of fluorescence, as well as the characteristic fluorescence excitation (λ_{Ex}) and emission (λ_{Em}) wavelengths, can change depending on the species and state of maturation [74, 75]. Some of the fluorescent compounds found in pollen and spores are polyphenolic compounds (flavonoids as anthocyanins, flavons or isoflavons) lipofuscin and ceroid, sporopollenin or terpene compounds (carotenoids as carotenes, xanthophylls or retinoids) [76, 77]. **Table 2** summarizes some of

these characteristic fluorescent compounds in pollen and spores as well as the different wavelengths according to the variation in the fluorescence levels among various types of species. Before processing, defatted pollen grains display autofluorescence attributed to the existence of terpenoid, phenolic, and carotenoid molecules in the sporoplasm [40]. Its elimination can be studied by fluorescence microscopy, and confocal laser scanning microscopy (CLSM). CLSM is the preferred technique as plane separation can reduce the background fluorescence of exine, allowing the tridimensional reconstruction of the structure. In purified hollow sporopollenin microcapsules, the inner part of pollen has lost the fluorescence and the clean exine is visible, while in loaded microcapsules, it is possible to identify the loading of the active compounds or dye-labelled active compounds (as FITC-conjugated BSA, eosin Y-eritromycin) and their internal distribution.

Table 2. Values of the wavelength of the different pollen and spores' fluorescent compounds.

Fluorescent compounds in pollen and spores	λ_{Ex} (nm)	λ_{Em} (nm)
Flavonoids	365	440-610
Lipofuscin and ceroid	260-280 340-390	430-670
Carotenoids	400-500	520-560
Sporopollenin	300-550	400-650
- *Zea mays* [11]	405	410-516
	488	493-556
	561	566-686
- *Pinus massoniana* [31], *Camelia sinensis* [33], *Helianthus annuus* [40, 78-80], *Taraxacum Officinale* [41], *Typha angustifolia* [81], *Lycopodium clavatum* [82], *Pinus taeda* [83]	405	416-477
	488	498-550
	561	572-620
- *Lycopodium clavatum* [84, 85]	405	410-481
	488	491-541
	543	595-735

3.5. Scanning and transmission electron microscopy (SEM/TEM)

Observation by electron microscopy is a well-established and reliable technique for studying the purification process of spore and pollen exine microcapsules. Scanning electron microscopy (SEM) is often employed for the study of pollen shape, polarity, surface, or apertures, while sections or fractured grains are employed for the study of the inner parts of the exine, such as the structure of pores and endexine as well as for the verification of presence/absence of the sporoplasmatic compounds. Pollen surface can present insular ornamentations (areolate), club-shaped elements (clavate), pointed elements (echinate), <1µm ornaments (granulate), exine ridges (lophate), holes (perforate), smooth surface (psilate) or network-like pattern (reticulate) according to the species, as well as elongated (colpus) or circular (porus) aperture/s, with different designations according to their number and location (sulcate, ulcerate..) [39]. SEM methodology is also employed for loaded exine microcapsules to investigate the location of the cargo. In addition, sporopollenin microcapsules can be damaged during excessive purification and SEM allows ensuring that the morphology of microcapsules is preserved, or, on the contrary, the hollow microcapsules collapse and become "deflated" [22, 81]. On the other hand, transmission electron microscopy (TEM) is employed to study the ultrastructure of the spores and pollen grains, being more employed in palynology [1, 4, 10, 86] than in the study of the herein reviewed sporopollenin microcapsules [87].

4. REPRESENTATIVE EXAMPLES OF SPORE AND POLLEN SPECIES TO PRODUCE SPOROPOLLENIN MICROCAPSULES

Pollen morphological data have been widely used in taxonomic, systematic, and phylogenetic studies. As is known, in nature, plants produce thousands of different pollens, and each single pollen type can exhibit subtle variations in its morphology and physicochemical structure. This section describes the main families of pollen and spores used to obtain hollow sporopollenin microcapsules, the procedures carried out, as well as their application for drug delivery. They have been divided according to their taxonomy, following the scheme shown below (**Figure 3**).

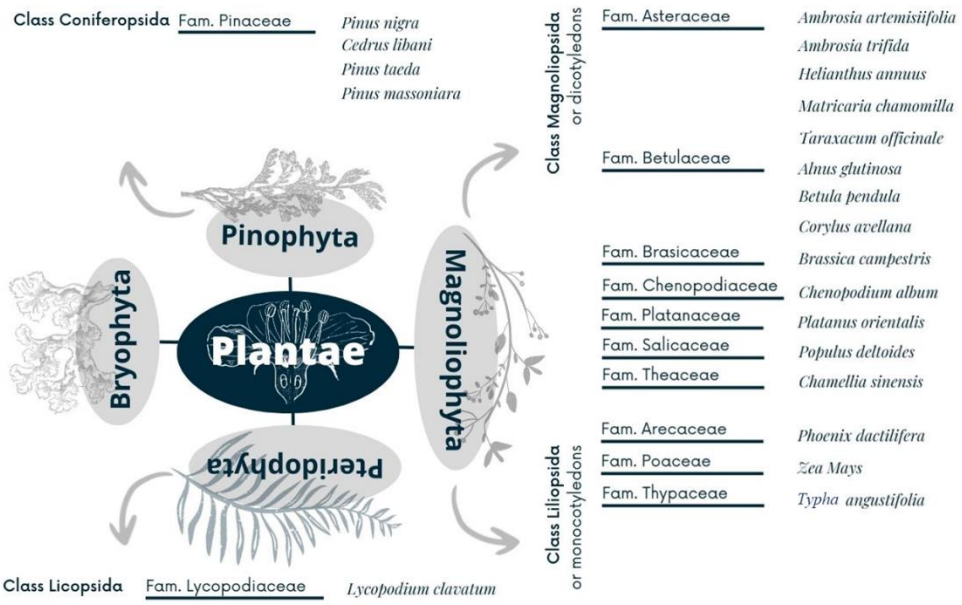

Figure 3. Scheme of the different kingdom Plantae and its four main groups: Bryophyta, Pteridophyta, gymnosperms (Pinophyta), and angiosperms (Magnoliophyta), and the selected spores and pollens that have been the subject of this review.

The plant kingdom is divided into four main divisions: Bryophyta or non-vascular plants, and vascular plants, which are further divided into seedless (division Pteridophyta) or seed-bearing plants, with unprotected ovules (gymnosperm, division Magnoliophyta) or protected ovules (angiosperm, division pinophyte).

4.1. Division Pteridophyta

4.1.1. Class Licopsida

Fam. Lycopodiaceae

In general, spore wall from the Lycopodiaceae family shows an inner endospore and an outer exospore with a diffuse sporopollenin texture, a foveolate or rugate/reticulate ornamentation, a subtriangular-spheroidal shape with trilete apertures [14]. ***Lycopodium clavatum*** spore (common clubmoss, medium-sized spore: 25-33 µm) is among the most studied sources for obtaining sporopollenin microcapsules. Multiple methods have been developed for the removal of the sporoplasm and external components from these pteridophyte spores, the first one reported in 1928 by Zetzsche and Huggler [15]. One classical method has been described by Atkin *et al* [22], consisting of initial reflux with acetone to remove the lipidic coating (4 h), followed by treatment with KOH for 6 h. Then, the base-treated spores were subjected to an acid treatment with H_3PO_4 for 7 days to obtain hollow sporopollenin microcapsules. Other

procedures employed a modified method indicating that base treatment was carried out at 80ºC [88] or 120ºC [37, 89] for a prolonged time (12 h) and were followed by acid treatment with H_3PO_4 at 60ºC for 5 days or 160 and 180ºC for 7 days, respectively.
The research group of Cho developed a method, eliminating the initial base treatment, for the obtention of sporopollenin microcapsules that drastically reduced the duration of the treatment [82]. *L. clavatum* spores were defatted by acetone reflux at 50ºC (6 h), followed by reflux with 85% H_3PO_4 at 70ºC (30 h), and a fifteen-step washing with water, acetone, HCl, NaOH, water, and ethanol. The obtained microcapsules kept the initial morphology of raw *L. clavatum* spores, but without sporoplasmic content and presented a residual nitrogen content of 0.15%.

The developed hollow sporopollenin microcapsules were suitable for the encapsulation of compounds, such as oils, melted cocoa butter, enzymes, resins, dyes, and ascorbic acid and have been used to shield and mask their flavors. For example, the encapsulation of cod liver and sunflower oil confirmed the efficacy of sporopollenin microcapsules for taste masking [90]. *L. clavatum* hollow sporopollenin microcapsules were able to encapsulate cod ω-3 oil up to a 1:2 mass ratio, protecting the oil from oxidation in a similar way to food additives such as butylated hydroxytoluene or ferulic acid [88], while the encapsulation of polyunsaturated oils and enzymes as streptavidin-horseradish peroxidase and alkaline phosphatase helped to preserve their bioactivity [91]. Photoprotective properties were also reported for encapsulated folic acid (vitamin B_9), which showed a sustained delivery with a pH-dependent release profile [92]. The same group reported eicosapentaenoic acid-loaded microcapsules with efficient taste masking and improved serum bioavailability as compared with free eicosapentaenoic acid esters [93].

On the other hand, these hollow sporopollenin microcapsules have also been used for the release of proteins, vitamins, and active pharmaceutical ingredients. For example, sporopollenin microcapsules were filled with several molecules such as sulforhodamine, dextran, bovine serum albumin, or ovalbumin [89]. Hollow sporopollenin microcapsules loaded with ovalbumin were able to produce an immune response in BALB/c mice after translocation into the mouse intestinal wall upon oral administration.
L. clavatum sporopollenin microcapsules were also used in the encapsulation of ibuprofen (loading efficiency of 97%) showing fast drug release and retention in simulated gastric fluid and taste masking after oral dosing [94]. In another study, natural *L. clavatum* spores were evaluated for loading of BSA [95] and 5-FU (5-Fluoruracil) [96] with several filling methods (passive, compression, and vacuum). BSA loading efficiency ranged from 42 to 59%, and vacuum-assisted loading was the most efficient method. However, the BSA release had a burst of ~90% in the first 5 min regardless of the loading method. To achieve a controlled release, the authors incorporated BSA-vacuum-loaded *L. clavatum* spores in alginate microbeads, however, the release was similar to BSA-loaded plain alginate microcapsules [97]. In the case of 5-FU, the vacuum was the most efficient loading method, achieving an association efficiency of 49%. As in the case of BSA [95], 5-FU had a burst release of ~90% in the first 5 min. Authors coated 5-FU-vacuum-loaded *L. clavatum* spores in Eudragit RS 100 to achieve a controlled release, slower (of 70% for 2.5% Eudragit RS 100 and 50% to 10% Eudragit RS 100 after 2 h) than previously reported uncoated 5-FU loaded microcapsules (complete release in 1 h) [96]. The potential of different types of Eudragit was evaluated to target 5-FU release in the colon, taking advantage of its insolubility in water and its pH-independent release profile. The presence of higher quaternary ammonium groups in Eudragit RL resulted in a faster release (between 5-11 h) while the use of RS and RSPO showed a complete release of the drug between 8-12 h, depending on their concentration [98].

L. clavatum microcapsules have been employed for the encapsulation of erythromycin by vacuum, with an entrapping efficiency of 32.4%, and improved antibacterial activity as compared with free antibiotics. Erythromycin-loaded sporopollenin microcapsules showed an *in vitro* accumulative release profile with an initial burst of ~30% in the first 5 min, followed by a more sustained phase attributed to a diffusion mechanism of porous materials. These erythromycin-loaded sporopollenin microcapsules were able to increase the apparent half-life of the drug as compared with unencapsulated erythromycin [84].
In another work carried out by the group of El-Mageed, the encapsulation of aspirin (ASA) in *L. clavatum* sporopollenin microcapsules by passive diffusion followed by vacuum loading showed a loading capacity of 26.7% (w/w) and an encapsulation efficiency of 53.4%. The ASA release in simulated gastric and intestinal fluid fitted a pH dependent Fickian diffusion mechanism, with an initial release of 43-62% of the ASA in the first hour, followed by a sustained release up to 9 h. In the case of gastric fluid, release was more limited due to the lower solubility of ASA at this pH [99]. More recently, enhanced oral bioavailability was reported for the lipophilic vitamin D_2 encapsulated into *L. clavatum* sporopollenin microcapsules (loading efficiency of 90%), Authors indicated enhancement of the mucoadhesion as a possible explanation [100]. Similar findings were reported for alginate-coated sporopollenin microcapsules for the oral delivery of metformin [101].
Even though slightly out of the scope of this review, it is worth briefly mentioning the interest of these platforms for other applications, such as loading of contrast agents [102] or encapsulation of living baker's yeast (*Saccharomyces cerevisiae*) cells [103]. By using microwave chemistry, *L. clavatum* sporopollenin microcapsules could be used as reusable catalysts for the dehydration of D-xylose and xylan into furfural [104], synthesis of cinnoline derivatives [85] or for Hg^{2+} [32], Rhodamine B [105] or heavy metal removal [106]. *L. clavatum* spores can also be converted into magnetic biocomposites with robust bioelectronic and conductive interfaces by its functionalization with graphene oxide [107]. Finally, *L. clavatum* microcapsules have been explored for the in-situ synthesis of magnetite nanoparticles (Fe_3O_4) for directed drug delivery by using a magnetic field [108].

4.2. Division of Phynophita/Coniferophyta

4.2.1. Class Coniferopsida

Coniferophyta are wind-pollinated species and therefore, have received significant attention in terms of their aerodynamic properties. Here, the gametophytic cells are enclosed within a spherical pollen wall consisting of an inner intine layer of cellulose, surrounded by an exine of sporopollenin, which extends outward from the central structure, forming one to three sac-like structures filled with air, in general, with a verrucate/scabrate surface ornamentation [109].

Fam. Pinaceae
Pinus nigra as well as ***Cedrus libani*** (pollen class: saccate, aperture: 1, large-sized pollen: 51-100 μm) sporopollenin microcapsules were developed by an acid-base (HCl-NaOH) and chloroform: methanol treatment for the delivery of the anticancer drug oxaliplatin. The encapsulation efficiency after passive drug-loading was around 10% for *C. libani* and 38% for *P. nigra*, and both drug-loaded sporopollenin microcapsules showed a slower release rate than the unloaded/free drug, of 15.72% and 28.97%, respectively. These differences could be attributed to structural modifications, such as the formation of sporopollenin plaques, providing a larger surface area for drug interaction, during the acid treatment of *P. nigra* [110].

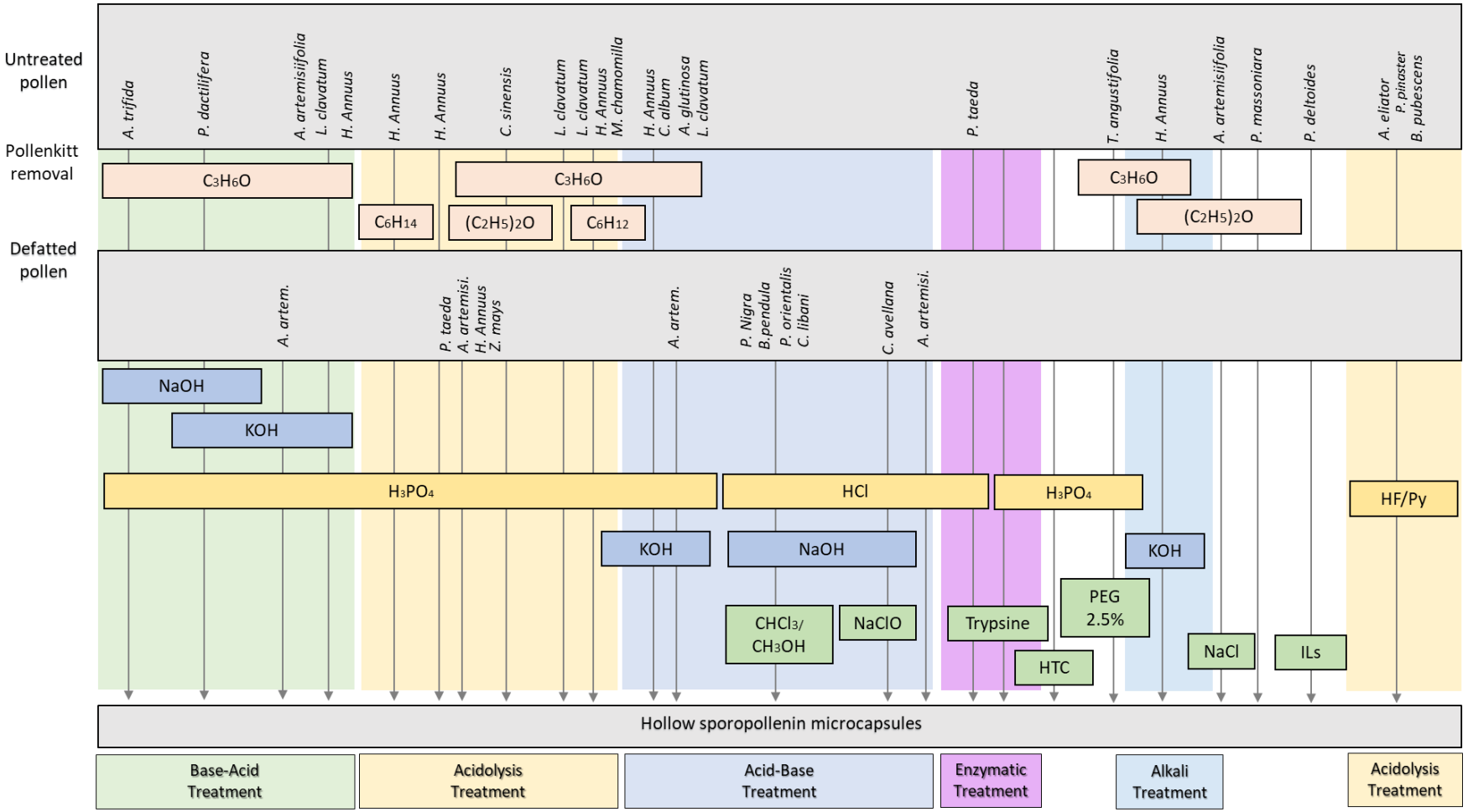

Figure 2. Schematic diagram of conventional and modified treatments and the main plant families used to produce hollow sporopollenin microcapsules: diethyl ether ($(C_2H_5)_2O$), hydrogen fluoride in pyridine (HF/Py), chloroform/methanol ($CHCl_3/CH_3OH$), sodium hypochlorite solution (NaClO), hydrothermal carbonization (HTC), polyethylene glycol (PEG), sodium chloride (NaCl), Ionic Liquids (ILs).

Pinus taeda (loblolly pine, pollen class: saccate, aperture: 1, large-sized pollen: 45–75 µm, tripartite) sporopollenin microcapsules were obtained after incubating defatted pollen with H_3PO_4 or other acids (HCl, H_2SO_4). Due to the thinness of *P. taeda* exine, sporopollenin microcapsules tended to collapse or fragment after aggressive treatments and storage. Therefore, the authors adapted a treatment at 25 ºC and wet storage conditions that were more suitable for this type of pollen. A two-step process, with 18% HCl (5 h at 70 ºC) and a subsequent trypsin treatment also allowed a high percentage of intact sporopollenin microcapsules and low residual protein content. Both treatments allowed the loading of BSA by vacuum with a loading efficiency in the range of 23-26% for hollow pollen grains, while defatted pollen only reached 8% loading efficiency [83].

Defatted ***Pinus massoniana*** (Chinese red pine, pollen class: saccate, aperture: 1, large-sized pollen: 45–75 µm, tripartite) has also been employed for the encapsulation of BSA, taking advantage of their natural air sacs [111]. Double-defatted pollen was obtained after treatment with diethyl ether (3.5 h) and was loaded with BSA (ratio 1:1) by vacuum, achieving a moderate encapsulation efficiency of 10% and a burst release after 5 min in intestinal and gastric fluids. BSA release was slower after forming tablets with the pollen, producing a linear release of up to 80% during 3 h in gastric fluid, however, tablets still produced a fast release in intestinal fluids. The authors further coated the tablets with xanthan gum or alginate at different concentrations. These coated tablets were able to control the amount of BSA released and reduce the initial release in gastric fluid. Defatted pine pollen has also recently been converted into micromotors by encapsulation of magnetic particles (Fe_3O_4) in their hollow air sacs. These micromotors could load drugs such as doxorubicin (vacuum loading, 1:1:2 magnetic NCs:drug: pollen ratio), and operate like a magnetic rotor by generating a flow field that could transport doxorubicin through the outer wall of the pollen air sac, producing its release [112].

4.3. Division of Magnoliophyta

4.3.1. Class Liliopsida or monocotyledons

Monocotyledons exhibit monoporate pollen where exine is absent or reduced to a thin layer and a thick and intricate intine [113, 114].

Fam. Poaceae

Pollen grains of the Poaceae family exhibit a remarkable range of diversity in their morphology. They are typically monoporate, of the monad type, and spheroidal in shape. Some species have small opercula/annulate pores and insular sculptured elements <1µm (scabrate) [115]. ***Zea mays*** (maize, pollen class: ulcerate, aperture: 1, large-sized pollen: 70-100 µm) pollen is characterized by a thin exine (~1 µm), which ultimately converts it into a delicate structure when internal components are eliminated. Conventional acidolysis treatments resulted in exine capsules with cracks and morphology alterations [116], while treatments with anhydrous hydrogen fluoride in pyrimidine (5 h 40ºC under vacuum conditions) [117] can produce sporopollenin microcapsules with other pollens, resulting in collapsed structures. Cho et. al. performed a complete study regarding the optimal parameters for the development of maize sporopollenin microcapsules by optimizing a one-pot acidolysis in 85% H_3PO_4 at 70ºC during 2.5 h, avoiding the dehydration step, employing defatted *Z. mays* pollen. The resulting sporopollenin microcapsules were 91% intact and had a nitrogen content of 0.76% (a reduction of 82%) [11] and were able to preserve the delicate particle morphology, positioning them as attractive candidates for aerosol drug delivery.

Fam. Arecaceae

The Arecaceae family exhibits an exceptionally wide range of pollen characteristics, including aperture number, orientation, and surface exine ornamentation. While most species in this family have monosulcate pollen, there have been descriptions of 17 different aperture types and 13 exine types [118]. ***Phoenix dactylifera*** (date palm, pollen class: sulcate, aperture: 1, small-sized pollen: 10-25 µm) sporopollenin microcapsules were produced with a base-acid treatment after defatting with acetone (6 h). Then, defatted pollen was washed with NaOH and KOH for 10 h followed by a final incubation with H_3PO_4 for 6 days. Date palm sporopollenin microcapsules were coated with chitosan-glutaraldehyde-based polymers (SMC@poly) for ibuprofen delivery, with maximum adsorption of 88% of ibuprofen after 25 h of contact time between the drug and the SMC@poly-coated sporopollenin microcapsules. Ibuprofen-loaded sporopollenin microcapsules showed a pH-sensitive behaviour, achieving a 94% release in PBS while the total release in the simulated gastric fluid was 42% after 10 h, being appropriate for the controlled release of the drug within the basic environment of the large intestine, colon, and rectal mucosa [119]. The same research group also developed date palm sporopollenin microcapsules coated with carboxymethyl cellulose (CMC) crosslinked with epichlorohydrin by using a reverse-dispersion cross-linking technique for the loading and release of paracetamol. Similar to ibuprofen, the maximum loading percentage (97%) was achieved at pH 6. Carboxymethyl cellulose/epichlorohydrin coated sporopollenin microcapsules showed a similar release to chitosan-coated sporopollenin microcapsules, with a 96% after 8 h in intestinal fluid and 39% in gastric fluid [120]. *P. dactylifera* was also loaded with 5-FU by vacuum using different drug: microcapsules ratios (1:4, 1:2, and 3:4) for their use in the oral treatment of colon cancer. The encapsulation efficiency was found in the range of 47 - 59% with a final drug load of up to 25%. The sporopollenin microcapsules were coated with Eudragit RS 100 and showed a prolonged and controlled release of 80% of 5-FU in SIF (pH 6.8) and around 40% in SGF (pH 1.2) due to the slower solubilization of the Eudragit RS 100 coating at pH 1.2 [121]. Finally, *P. dactylifera* microcapsules were recently evaluated for the microencapsulation of the type 2 diabetes drug metformin (1:1, w/w), taking advantage of their elliptical shape, which changes by harmomegathy to a spherical one upon hydration, allowing the entrance of liquid and modulates the release of the drug. This phenomenon is involved in the controlled release pattern with a super case II transport mechanism, controlled by polymer swelling and relaxation. These metformin loaded-microcapsules showed a loading capacity of 15% and encapsulation efficiency of 30%, with 76% of the metformin released within 9.5 h in simulated intestinal fluids [101].

4.3.2. Class of Magnoliopsida or dicotyledons

A notable characteristic of the evolution of dicotyledons is the increase in the number and diversity of apertures, displaying generally equatorial apertures and with a prevalence of triaperturate pollen grains. Contrary to monocotyledons, dicotyledons intine is simple, and endexine is usually present and well-developed [113, 114].

Fam. Asteraceae

Ambrosia artemisiifolia (sym. *A. elatior*, common ragweed, pollen classification: colporate, apertures: 3, small-sized pollen: 10-25 µm) ragweed pollen grains are among the most hazardous ones due to their facility to remain airborne for long distances. The allergens of this pollen are the causative agents of severe respiratory allergies and are considered a threat to public health, and great efforts are directed toward the prohibition and eradication of this invasive plant species in many countries [122]. However, its small size and high porosity, as

well as its ubiquity and high production [123], make ragweed an interesting candidate for the development of sporopollenin microcapsules. For all the above, several protocols have been developed to achieve structures without the presence of allergens. One of the first reports can be found in the patent application of Amber and Tawashi, who described the obtention of defatted pollen after organic acid (preferably ethyl ether) extraction. This defatted ragweed pollen was treated with continuous extraction in isotonic saline solution (0.9% NaCl) for protein removal, and the authors claimed that it can be employed for drug loading, using insulin as a model drug [29]. The same authors described an acidic treatment to produce ragweed sporopollenin microcapsules by incubating defatted pollen in 6N HCl at 110 ºC for 24 h. As summarized in **Table 3**, ragweed sporopollenin microcapsules were loaded with bovine insulin and angiotensin either by vacuum or using a passive loading method, and the developed microcapsules were subsequently coated with several polymers as hydroxypropyl cellulose, hydroxypropyl methyl cellulose, methacrylic acid or dimethyl aminoethyl methacrylate to achieve sustained or pulsed release patterns [124].

Production of ragweed sporopollenin microcapsules has also been reported employing a base-acid treatment by 6% KOH incubation followed by an 85% H_3PO_4 for 7 days. The sporopollenin microcapsules showed a weight loss of ~80% when compared with defatted pollen, and they were employed for *in-situ* polymerization to produce a reinforcing filler for poly (vinyl acetate)[61].

Uddin and Gill described the obtention of ragweed sporopollenin microcapsules using a high-temperature base-acid treatment. Raw ragweed pollen was defatted with acetone reflux at 70 ºC (18 h); and after that, was twice incubated in 2M KOH at 120 ºC (6 h + 6 h), and the base-treated pollen was then washed and incubated with H_3PO_4 at 180 ºC for 7 days. Ragweed sporopollenin microcapsules obtained by this method had an intact structure and a final nitrogen content of 0.2%. Moreover, they did not show cell toxicity or the capacity to impair Caco-2 cells' functionality *in vitro* and were suitable for the loading of large molecules such as dextran or ovalbumin [72]. As ragweed sporopollenin microcapsules induced the production of proinflammatory cytokines and were phagocyted by macrophages, the same authors proposed ragweed sporopollenin microcapsules as an oral vaccine carrier employing a milder treatment, eliminating the base-treatment step, and performing the acidolysis at 60 ºC (7 days). They found that ovalbumin-loaded sporopollenin microcapsules were able to produce systemic and mucosal immune responses for a prolonged period upon oral administration (3 months). Interestingly, they did not find any immune response to ragweed-specific proteins [73]. Gill and collaborators have also produced stable ragweed sporopollenin microcapsules with a reduced nitrogen content of 0.1% (reduction of 97.6%), changing the order between acid and base treatment in the same manner as described for *A. glutinosa*, *C. album*, or *H. annuus* pollen. The authors followed a switched low-temperature protocol, reducing the acid temperature to 60 ºC and that of the base to 80 ºC, maintaining incubation times (12 h for KOH and 7 days for H_3PO_4). Results showed that similar sporopollenin microcapsules could be obtained regardless of the employed temperature, with a higher percentage of carbohydrates. They concluded that the switched protocol could aid in releasing the turgor pressure generated during the orthophosphoric acid treatment [37].

Hollow ragweed pollen microcapsules have been studied for BSA release, showing a limited capacity to load proteins (protein loading of 1% and encapsulation efficiency of 7%). The authors slightly improved the protein loading by employing a matrix of Eudragit L100-55 as a coating (protein loading: 2.45% and encapsulation efficiency of 12.23%). This moderate loading and release were similar to formulations only with Eudragit particles, with a slower release in simulated intestinal fluid [125].

For the obtention of microcapsules from ***Ambrosia trifida*** (giant ragweed, pollen class: colporate, apertures: 3, small-sized pollen: 17-21 µm), pollen was suspended in acetone and the defatted pollen was incubated in 1% (w/v) NaOH for 1 h. The solution was neutralized with hydrochloric acid diluted in ethanol and the resultant base-hydrolyzed sporopollenin was suspended in 85% (v/v) ortho-phosphoric acid for 1 h. The aim of this study was to assess the light-blocking and shielding capabilities of the 3 µm thick sporopollenin microcapsules for their use as encapsulation and protection material against UV radiation-induced chemical degradation by analyzing the reduction in UV transmission through the exine wall [22].

Helianthus annuus (common sunflower, pollen class: colporate, aperture: 3, medium-sized pollen: 26-50 µm) echinate pollen was treated by several methods for the obtention of sporopollenin microcapsules. *H. annuus* pollen structure was reported to be incompatible with alkaline lysis treatment (KOH 60ºC, 12 h) or an acidolysis (HCl 70ºC, 24 h) followed by trypsin (0.25%) or Tween-20 (2%) treatment. Alkaline lysis resulted in fully destroyed sporopollenin microcapsules while HCl treatment led to residual compounds within the cavity. The use of trypsin to eliminate adhered proteinaceous substances, caused damage to the spikes, even though the inner cavity remained clean, while pollen debris was still visible on the surface after the use of Tween-20. Although the initial acidolysis studies were performed with HCl and H_3PO_4, at different time points, H_3PO_4 showed to be more efficient for the production of *H. annuus* sporopollenin microcapsules after 10 [40] or even 5 h [79]. Hollow sunflower sporopollenin microcapsules were studied for BSA loading, resulting in a lower encapsulation efficiency (40%) than defatted sunflower pollen (65%) [78], and a similarly high burst release of 90% in the first 5 min. After forming tablets with BSA-loaded *H. annuus* sporopollenin microcapsules, the release was slower, and when sporopollenin microcapsules tablets were coated with Eudragit L100, it allowed a pH-controlled release. The BSA release profile of Eudragit L100-coated sporopollenin tablets was different from BSA-loaded Eudragit L100 tablets, producing 100% release in 8 h compared with less than 40% in the control tablet without sporopollenin microcapsules [79]. The use of Eudragit as coating-material was previously reported, as Eudragit RS 100-coated *L. clavatum* and *Phoenix dactylifera* microcapsules or Eudragit L100-55-coated ragweed pollen microcapsules to enhance 5-FU and BSA release in simulated gastrointestinal media.

Recently, Cho and collaborators have described a new protocol to produce flexible sunflower sporopollenin structures from natural pollen grains, after defatting with acetone and diethyl ether. Subsequent cytoplasmic removal was performed by employing an initial alkaline treatment with 10% KOH at 80 ºC for 2 h and a secondary treatment with KOH (80ºC for different periods up to 12 h). This treatment eliminates sporoplasmic content and chemically de-esterifies the pectin of the intine, which converts hard pollen grains into soft microparticles. This de-esterification of pectin to form pectane is the natural process by which pollen can control the swelling during germination. Flexible hollow pollen particles were able to swell by a pH-controlled process, and de-swell by the interaction with divalent cations. Due to this behavior, these pollen-based microparticles were able to form gels. Even though the pollen processed with this method lost part of its natural toughness and structure [126], pollen microgels were able to form films after water evaporation, producing a semitransparent flexible paper with a sensitive and reversible response to humidity or water [127]. These films showed humidity-driven motility, allowing to control the flexion by changing their thickness as well as the base processing of sunflower pollen. This group also performed the coating of defatted *H. annuus* pollen with graphene for its use as a flexible biosensor [128]. At present, the future of

Table 1: Applications of different hollow sporopollenin microcapsules in drug delivery. HPC: hydroxypropyl cellulose, HPC: hydroxypropyl methyl cellulose, DMAEM: dimethyl aminoethyl. OVA: Ovalbumin. BSA: Bovine Serum Albumin. SGF: Simulated Gastric Fluid. SIF: Simulated Intestinal Fluid. CMP: Carboxymethylpachymaran. SMC@poly: chitosan-glutaraldehyde-based polymers. CMC-E: carboxymethyl cellulose with epichlorohydrin. NP: Nanoparticle. $CaHPO_4$: Calcium hydrogen phosphate

Plant species	Encapsulated material	Coating	Ratio pollen: drug (w/w)	Method loading	Drug Loading (%)	Encapsulation efficiency (%)	Cumulative release (%)	Ref.
L. clavatum	Ibuprofen		1:1	Vacuum		97	88 pH 1.2 (45 min) 85 pH 7.4 (5 min)	[94]
	Erythromycin			Vacuum		32.4		[84]
	BSA		1:1	Vacuum	17 ± 1	16.62		[82]
	BSA		2:1	Passive Compression Vacuum	21.3 ± 1.8 21.4 ± 0.5 29.6 ± 1.1	42.7 ± 3.7 42.8 ± 1.1 59.2 ± 2.2	90 (5 min) 100 (30-60 min) pH 1.2 and 7.4	[95]
	5-Fluoruracil		3:1	Passive Compression Vacuum	5.2 ± 0.7 9.2 ± 2.0 16.3 ± 0.6	15.5 ± 2.1 32.0 ± 5.6 49.0 ± 1.8	90 (10 min) 100 (60 min) pH 1.2 and 7.4	[96]
	5-Fluoruracil	Eudragit RS 100						[98]
	BSA	Alginate microbeads						[97]
	Aspirin			Passive and vacuum	26.7	53.4		[99]
	Vitamin D2				90			[100]
	Metformin				14.9 ± 0.7	29.8 ± 0.8		[101]
P. nigra and C. libani	Oxaliplatin			Passive	PN CL	38.2 10.06	28.97 15.72	[110]
P. taeda	BSA			Vacuum	23- 26 (hollow) 8 (defatted)			[83]
P. dactylifera	Ibuprofen	SMC@poly	4:1; 2:1; 4:3		88.4		42.4 SGF 94.2 SIF	[119]
	Paracetamol	CMC-E			97.2		38.8 (8h) SGF 96.4 (8h) SIF	[120]
	5- Fluorouracil	- Eudragit® RS-100	2:1		25	47-59	- 79.9 SIF and 40 SGF	[121]
	Metformin		1:1		15.2 ± 0.7	30.3 ± 1.0	76 (9.5H) SIF	[101]
A. artemisiifolia	Bovine insulin Angiotensin	HPC, HPMC, DMAEM	2:1	Vacuum Passive				[124]
	OVA/Dextran		10:1	Vacuum				[72]
	OVA		50:1	Vacuum				[73]

	BSA	- Eudragit L100-55	5:1 to 1:1	Vacuum	1 2.45	7 12.23	64 vs 24 (2h) SGF 87 vs 76 (6h) SIF	[125]
H. annuus	BSA		2:1 1:1.2	Passive Compression Vacuum	18.6 ± 2.2 18.8 ± 1.5 32.8 ± 0.9	37.2 ± 4.4 37.8 ± 3.2 65.7 ± 1.8	80 (5 min) 100 (30–60 min) pH 1.2 and 7.4	[78]
	BSA	Eudragit						[79]
	BSA	Graphene Alginate				65.7	90 (5 min)	[128]
	B-Galactosidase	CMP-zein	50:1	Vacuum			70 (24h)	[34]
	B-Galactosidase	CMP-($AlCl_3$)					70 (24h)	[129]
	BSA		1:1.5	Vacuum	32.23 ± 0.33	53.7 (hollow) 21.1 (defatted)		[41]
B.pendula	Imatinib mesylate		2:1	Passive		21.46	100 (24h) PBS 65 (24h) acidic pH	[130]
C. avellana	Pantoprazole		1.4:1	Passive	-	29.81	61 (5 min) pH 7.4 100 (6h) pH 7.4	[131]
B. campestris	BSA		25:1	Dispersion and shook	HHCP-I 15.86 mg/g HHCP-II 3.59 mg/g		HHCP-I (9 days) 10 pH 4 52.2 pH 7 99.0 pH 10	[132]
P. orientalis	Paracetamol		2:1	Passive Evaporation	8.2 23.7		56.0 pH 7.4 (24h) 88.8 pH 7.4 (5 min)	[67]

these sporopollenin microcapsules is promising, however, they have not yet been investigated for biomedical purposes.

As described above for *A. glutinosa*, sunflower sporopollenin microcapsules could be obtained with a low-temperature switched acid-base treatment. This allowed the production of microcapsules with the lowest nitrogen content reported in the literature (0.19 %) [37]. Production of hollow sunflower sporopollenin microcapsules was also performed by employing an acidolysis process to remove proteinaceous components. Sunflower pollen grains were washed with petroleum ether to obtain defatted pollen and were subsequently treated with phosphoric acid for 5 h. These microcapsules were used for the vacuum-assisted encapsulation of β-galactosidase (β-gal) and were post-coated with carboxymethylpachymaran (CMP)-zein (an alcohol soluble protein) [34] or CMP-metal ion ($AlCl_3$) combinations [129] to improve their oral delivery. These coatings were carried out to address the leakage of charged β-gal, by sealing the pores on the surface of the microcapsules by a thicker layer that originates a lattice structure by the interaction between the microcapsules, zein or metal ions, respectively, and CMP. While uncoated β-gal loaded microcapsules lost enzyme activity in simulated gastric fluid, the coated pollen grains were able to protect β-gal from acidic pH and showed an improved release profile than β-gal carboxymethyl (1-3)- β-D-glucan and zein without pollen, achieving a 70% accumulative release after 24 h [34], similar to those reported for CMP 3% $AlCl_3$ [129] in simulated gastric conditions.
The groups of Pumera and Cho have functionalized *H. annuus* sporopollenin microcapsules [80] and defatted pollen [32] with a partial platinum coating after acidolysis, using phosphoric acid or diethyl ether treatment, respectively, for the development of micromotors. Pt-coated sporopollenin microcapsules were able to load BSA or absorb heavy metals, such as Pb(II) [80] or Hg^{2+} [32], confirming their high decontamination efficiency.

In a more recent variant of producing hollow *H. annuus* microcapsules, Ageitos et. al., pre-treated the pollen with water and acetone followed by cyclohexane to obtain defatted pollen. The acidolysis process was optimized by a systematic screening of different acids (HCl, $HClO_4$, H_3PO_4, CF_3COOH, H_2SO_4, or HNO_3), incubation times (1 to 14 h) and temperatures (25 and 70 °C) to maximize solubilization and removal of internal components. Treatment with H_3PO_4 for 5h at 70ºC allowed the most efficient and simple production of fully intact, hollow pollen without the requirement of additional neutralization steps [133]. In addition, these studies also indicated the feasibility of applying enzymatic purification protocols for the purification of previously defatted sunflower pollen grains.

The same group produced hollow sporopollenin microcapsules from ***Matricaria chamomilla*** (sym *Matricaria recutita*, pollen class: colporate, aperture: 3, small-sized pollen: 10-25 µm) after their direct extraction of the dried medicinal plants, using a similar protocol to the above. In this case, the final protein content was 4%, similar to that obtained for sunflower [133], ***Taraxacum officinale*** (common dandelion, pollen class: lophate, aperture: 3, medium-sized pollen: 26-40 µm) sporopollenin microcapsules were produced after acidolysis with H_3PO_4 or HCl as previously described by Cho et al. Similar to sunflower, dandelion pollen did not resist prolonged alkaline treatments. On the other hand, dandelion, together with *Lycopodium* sporopollenin platforms was found to be the most robust in a comparative study evaluating the biodegradation profile of sporopollenin microcapsules from different species in simulated gastrointestinal fluid [44]. *T. officinale* pollen treatment with trypsin after 5 h acidolysis with H_3PO_4 was able to reduce its protein content. These microcapsules were assayed for BSA encapsulation employing a vacuum-assisted method (microcapsules: BSA ratio of 1:1.5). The

loading efficiency of sporopollenin microcapsules was higher than the defatted dandelion pollen (53.7% vs. 21.1%) [41]. Using the same methodology as for sunflower pollen, defatted dandelion pollen was functionalized as microrobots by the group of Pumera [32]. Dandelion microrobots were faster than sunflower ones, being able to produce a more efficient absorption of Hg^{2+}.

Fam. Betulaceae

Alnus glutinosa (black alder, pollen classification: stephanoporate, apertures: 5, medium-sized pollen: 26-50 µm) clean and intact sporopollenin microcapsules were obtained employing a combined high or low-temperature switched acid-base treatment, as also reported for *Chenopodium album*, *H. annuus*, and *A. artemisiifolia*, with acetone, H_3PO_4 (7 days at 60 ºC) and KOH (12 h at 80ºC), renewing the KOH solution after 6 h. This method resulted in the production of clean and intact protein-free pollen microcapsules with a reduction of 92.5% of the nitrogen content [37].

Betula pendula (European white birch, pollen classification: porate, aperture: 3, small-sized pollen: 14-23 µm [134]) sporopollenin microcapsules were obtained after a combined acid (6N HCl at 50 ºC for 1 h) and base (4N NaOH 100ºC for 6 h) treatment followed by a chloroform-methanol solution wash. *B. pendula* sporopollenin microcapsules were loaded with imatinib mesylate by a passive loading method, achieving an encapsulation efficiency of 21% (microcapsules: drug ratio of 2:1). Imatinib mesylate-loaded sporopollenin microcapsules showed an initial burst release (30 min) of 36.95% and a pH-dependent release profile, and a total release at acidic pH after 120 h, while the free drug was completely released in 1 h at both pH values [130].

Corylus avellana (European hazelnut, pollen classification: porate, aperture: 3, medium-sized pollen: 26-50 µm) hollow sporopollenin microcapsules were obtained following a double combined treatment with acid (HCl at 60 ºC for 2 h) and basic (NaOH at 70 ºC for 10 h) solutions, with final bleaching with 4% (w/w) sodium hypochlorite (NaClO) at 50 ºC for 10 min. The microcapsules were loaded with pantoprazole following a passive method with an encapsulation efficiency of 30%. Drug release followed a Fickian diffusion with a total release after 6 h with a burst release of 60% in the first 5 min [131].

Fam Brassicaceae

Brassicaceae or Cruciferae is one of the largest angiosperm families with subprolate or prolate-spheroidal pollen shape, three apertures, and reticulate ornamentation [135]. In this family, ***Brassica campestris*** (sym. *B. rapa*, rapeseed, pollen classification: colpate, aperture: 3, medium-sized pollen: 23-28 µm) porous hollow carbon microspheres were produced by hydrothermal carbonization of the pollen, consisting of acid treatment with 40% H_3PO_4 at room temperature (1 h) and carbonization at 200 ºC (6 h). Hollow pollen structures were able to load and release protein with a pH-dependent pattern [132]. This rapeseed pollen has been used as a biotemplate for the production of monodisperse iron phosphate-coated pollen grains [136] and silica microspheres [137] as candidates for drug delivery systems.

Fam. Chenopodiaceae

Chenopodiaceae pollen grains are spheroidal in shape with a regular distribution pores pattern (pantoporate) and a surface covered with small spinules [138]. In this family, ***Chenopodium album*** (lamb's quarters, pollen class: porate, aperture >6, medium-sized pollen: 26-50 µm) sporopollenin microcapsules were obtained after a high and low-temperature acid-base

treatment, as described above for *A. glutinosa*. *C. album* sporopollenin microcapsules had a final nitrogen content of 0.22% and a 93.4% reduction as compared with unprocessed pollen, of interest in oral delivery [37].

Fam. Platanaceae

The pollen of the Platanus family shows remarkable variability, with a tricolpate aperture structure, a prolate to spheroidal shape, and fine to coarse reticulated exine ornamentation [139]**.** ***Platanus orientalis*** (Old World sycamore, pollen class: colpate, aperture: 3, small-sized pollen: 16-20 µm) sporopollenin microcapsules were obtained after a double acid-base treatment with HCl solution at 50°C for 1 h and 4M NaOH at 90°C for 12 h. Then, pollen grains were kept in chloroform-methanol solution 1:1, (v:v) at room temperature for 1 h. *P. orientalis* sporopollenin microcapsules were loaded with paracetamol (ratio sporopollenin microcapsules: drug 2:1) and employed a passive-loading as well as a less frequently used evaporation method. By this evaporation method, a suspension of sporopollenin microcapsules and paracetamol was initially vortexed (10 min) and then rotaevaporated (4 h) at 22ºC. The paracetamol-loaded sporopollenin microcapsules were filtrated and incubated in a freezer at −80ºC (30 min) and air-drying at room temperature for 24 h. The passive method achieved a loading efficiency of 8.2%, and a cumulative pH-independent release profile of 56% after 24 h, while the evaporation method achieved a loading efficiency of 23.7% and a release of 100% after 4 h in PBS and 6 h in HCl solution [67].

Fam. Salicaceae

Populus deltoides (eastern cottonwood, pollen classification: inaperturate, aperture: 0, medium-sized pollen: 25-40 µm) pollen was treated with ionic liquids (ILs), able to solubilize cellulose under mild conditions, to achieve a one-pot extraction method. Treatment with ILs as tetra-n-butylphosphonium hydroxide, [Bu4P]OH, 1-butyl-3-methylimidazolium chloride, [BMIM]Cl or 1,3-dimethylimidazolium methylphosphosphonate, [DMIM][(MeO)(H)PO_2 [51] or 1-(4-sulfonic acid)butyl- 3-methyl-imidazolium hydrogen sulfate [HSO_3C_4mim][HSO4] [68] for 80-90 min at 160 ºC was able to obtain clean IL-functionalized sporopollenin microcapsules to act as catalysts.

Fam. Theaceae

Camellia sinensis (tea plant, pollen classification: colporate, apertures: 3, medium-sized pollen: 26-50 µm) sporopollenin microcapsules were produced from raw pollen, which required a conscientious defatting process with an initial incubation in hot acetone and water (50 ºC) for 3 and 1 h, respectively, followed by sieving for retaining the pollen. Acetone-treated pollen was then incubated in diethyl ether for 2 h and with 85% H_3PO_4 for 5 h. These *C. sinensis* sporopollenin microcapsules suffered chemical and physical alterations after incubation in physiological buffers (gastric and intestinal) [44] or human plasma [45].

In other uses of sporopollenin microcapsules beyond the realm of medicine, the partial coating of defatted *C. sinensis* microcapsules with platinum was used to produce microrobots, able to have autonomous movement in H_2O_2 [32]. Finally, the surface of defatted *C. sinensis* pollen has also been modified by an ultraviolet-ozone treatment, opening the aromatic rings of sporopollenin increasing the proportion of surface elemental oxygen and ketones, which ultimately increased their hydrophilicity, colloidal dispersibility, ease of emulsification, and of interest in promoting improved cell adhesion [33].

5. FINAL REMARKS AND FUTURE PERSPECTIVES

The use of natural sporopollenin microcapsules extracted from plant spores and pollens has emerged as a promising tool for drug delivery. There is a huge variety of spores and pollen grains, all characterized by highly reproducible and extraordinarily resistant chemical structures, but with distinct, plant-specific properties (i.e., size, shape, surface morphology), which can give them unique features, depending on the application sought. Pollen and spores' geometry and their uniform size distribution allow for improved adherence to the mucosal surfaces, providing greater bioavailability of the active ingredient in the desired location. A wide variety of procedures have been developed and optimized to obtain these hollow sporopollenin platforms for the controlled loading and release of active substances, ranging from the use of mild chemical or enzymatic treatments to more aggressive and prolonged non-oxidizing reactive treatments. Taken together, the use of sporopollenin as a biomaterial has become an attractive and green alternative and the development of robust, low-cost, and scalable protocols are of great interest for future applications in the field of controlled drug release.

REFERENCES

[1] Knox, R. B. The Pollen Grain. In *Embryology of Angiosperms*; Johri, B. M., Ed.; Springer Berlin Heidelberg: Berlin, Heidelberg, 1984; pp 197–271. https://doi.org/10.1007/978-3-642-69302-1_5.

[2] Punt, W.; Hoen, P. P.; Blackmore, S.; Nilsson, S.; Le Thomas, A. Glossary of Pollen and Spore Terminology. *Rev. Palaeobot. Palynol.*, **2007**, *143* (1–2), 1–81. https://doi.org/10.1016/j.revpalbo.2006.06.008.

[3] McCartney, H. A. Dispersal of Spores and Pollen from Crops. *Grana*, **1994**, *33* (2), 76–80. https://doi.org/10.1080/00173139409427835.

[4] Wiermann, R.; Gubatz, S. Pollen Wall and Sporopollenin. *Int. Rev. Cytol.*, **1992**, *140* (C), 35–72. https://doi.org/10.1016/S0074-7696(08)61093-1.

[5] Jiang, J.; Zhang, Z.; Cao, J. Pollen Wall Development: The Associated Enzymes and Metabolic Pathways. *Plant Biol.*, **2013**, *15* (2), 249–263. https://doi.org/10.1111/j.1438-8677.2012.00706.x.

[6] Pacini, E.; Hesse, M. Pollenkitt - Its Composition, Forms and Functions. *Flora Morphol. Distrib. Funct. Ecol. Plants*, **2005**, *200* (5), 399–415. https://doi.org/10.1016/j.flora.2005.02.006.

[7] Lin, H.; Gomez, I.; Meredith, J. C. Pollenkitt Wetting Mechanism Enables Species-Specific Tunable Pollen Adhesion. *Langmuir*, **2013**, *29* (9), 3012–3023. https://doi.org/10.1021/la305144z.

[8] Mackenzie, G.; Boa, A. N.; Diego-Taboada, A.; Atkin, S. L.; Sathyapalan, T. Sporopollenin, The Least Known Yet Toughest Natural Biopolymer. *Front. Mater.*, **2015**, *2* (October), 1–5. https://doi.org/10.3389/fmats.2015.00066.

[9] Blackmore, S.; Wortley, A. H.; Skvarla, J. J.; Rowley, J. R. Pollen Wall Development in Flowering Plants. *New Phytol.*, **2007**, *174* (3), 483–498. https://doi.org/10.1111/j.1469-8137.2007.02060.x.

[10] Weber, M.; Ulrich, S. The Endexine: A Frequently Overlooked Pollen Wall Layer and a Simple Method for Detection. *Grana*, **2010**, *49* (2), 83–90. https://doi.org/10.1080/00173131003743949.

[11] Park, J. H.; Seo, J.; Jackman, J. A.; Cho, N.-J. Inflated Sporopollenin Exine Capsules Obtained from Thin-Walled Pollen. *Sci. Rep.*, **2016**, *6* (1), 28017. https://doi.org/10.1038/srep28017.

[12] McCue, A. D.; Cresti, M.; Feijó, J. A.; Slotkin, R. K. Cytoplasmic Connection of Sperm Cells to the Pollen Vegetative Cell Nucleus: Potential Roles of the Male Germ Unit Revisited. *J. Exp. Bot.*, **2011**, *62* (5), 1621–1631. https://doi.org/10.1093/jxb/err032.

[13] Rodríguez de la Cruz, D.; Sánchez-Reyes, E.; Sánchez-Sánchez, J.; Sánchez-Agudo, J. Á. New Insights on Atmospheric Fern Spore Dynamics. In *Current Advances in Fern Research*; Springer International Publishing: Cham, 2018; pp 427–452. https://doi.org/10.1007/978-3-319-75103-0_20.

[14] Tryon, A. F.; Lugardon, B. *Spores of the Pteridophyta*; Springer-Verlag New York: New York, NY, 1991. https://doi.org/10.1007/978-1-4613-8991-0.

[15] Zetzsche, F.; Huggler, K. Untersuchungen Über Die Membran Der Sporen Und Pollen. I. 1. *Lycopodium Clavatum* L. *Justus Liebig's Ann. der Chemie*, **1928**, *461* (1), 89–109. https://doi.org/10.1002/jlac.19284610105.

[16] Brooks, J.; Shaw, G. Sporopollenin: A Review of Its Chemistry, Palaeochemistry and Geochemistry. *Grana*, **1978**, *17* (2), 91–97. https://doi.org/10.1080/00173137809428858.

[17] Mikhael, A.; Jurcic, K.; Schneider, C.; Karr, D.; Fisher, G. L.; Fridgen, T. D.; Diego-Taboada, A.; Georghiou, P. E.; Mackenzie, G.; Banoub, J. Demystifying and Unravelling the Molecular Structure of the Biopolymer Sporopollenin. *Rapid Commun. Mass Spectrom.*, **2020**, *34* (10). https://doi.org/10.1002/rcm.8740.

[18] Li, F.; Phyo, P.; Jacobowitz, J.; Hong, M.; Weng, J. The Molecular Structure of Plant Sporopollenin. *Nat. Plants*, **2019**, *5*, 41–46. https://doi.org/10.1038/s41477-018-0330-7.

[19] Shaw, G.; Yeadon, A. Chemical Studies on the Constitution of Some Pollen and Spore Membranes. *Grana Palynol.*, **1964**, *5* (2), 247–252. https://doi.org/10.1080/00173136409430017.

[20] Schulze Osthoff, K.; Wiermann, R. Phenols as Integrated Compounds of Sporopollenin from Pinus Pollen. *J. Plant Physiol.*, **1987**, *131* (1–2), 5–15. https://doi.org/10.1016/S0176-1617(87)80262-6.

[21] Domínguez, E.; Mercado, J. A.; Quesada, M. A.; Heredia, A. Pollen Sporopollenin: Degradation and Structural Elucidation. *Sex. Plant Reprod.*, **1999**, *12* (3), 171–178. https://doi.org/10.1007/s004970050189.

[22] Atkin, S. L.; Barrier, S.; Cui, Z.; Fletcher, P. D. I.; MacKenzie, G.; Panel, V.; Sol, V.; Zhang, X. UV and Visible Light Screening by Individual Sporopollenin Exines Derived from Lycopodium Clavatum (Club Moss) and *Ambrosia Trifida* (Giant Ragweed). *J. Photochem. Photobiol. B Biol.*, **2011**, *102* (3), 209–217. https://doi.org/10.1016/j.jphotobiol.2010.12.005.

[23] Bağcıoğlu, M.; Zimmermann, B.; Kohler, A.; Baʇcioʇlu, M.; Zimmermann, B.; Kohler, A. A Multiscale Vibrational Spectroscopic Approach for Identification and Biochemical Characterization of Pollen. *PLoS One*, **2015**, *10* (9), 1–19. https://doi.org/10.1371/journal.pone.0137899.

[24] Zimmermann, B.; Bağcıoğlu, M.; Sandt, C.; Kohler, A. Vibrational Microspectroscopy Enables Chemical Characterization of Single Pollen Grains as Well as Comparative Analysis of Plant Species Based on Pollen Ultrastructure. *Planta*, **2015**, *242* (5), 1237–1250. https://doi.org/10.1007/s00425-015-2380-7.

[25] Zimmermann, B.; Bağcıoğlu, M.; Tafinstseva, V.; Kohler, A.; Ohlson, M.; Fjellheim, S. A High-Throughput FTIR Spectroscopy Approach to Assess Adaptive Variation in the Chemical Composition of Pollen. *Ecol. Evol.*, **2017**, *7* (24), 10839–10849. https://doi.org/10.1002/ece3.3619.

[26] Rejón, J.; Delalande, F.; Schaeffer-Reiss, C.; Alché, J.; Rodríguez-García, M.; Van Dorsselaer, A.; Castro, A. The Pollen Coat Proteome: At the Cutting Edge of Plant Reproduction. *Proteomes*, **2016**, *4* (1), 5. https://doi.org/10.3390/proteomes4010005.

[27] Qu, Z.; Meredith, J. C. The Atypically High Modulus of Pollen Exine. *J. R. Soc. Interface*, **2018**, *15* (146). https://doi.org/10.1098/rsif.2018.0533.

[28] Bashir, M. E. H.; Ward, J. M.; Cummings, M.; Karrar, E. E.; Root, M.; Mohamed, A. B. A.; Naclerio, R. M.; Preuss, D. Dual Function of Novel Pollen Coat (Surface) Proteins: IgE-Binding Capacity and Proteolytic Activity Disrupting the Airway Epithelial Barrier. *PLoS One*, **2013**, *8* (1), e53337. https://doi.org/10.1371/journal.pone.0053337.

[29] Amber, M. S.; Tawashi, R. Modified Pollen Grains for Delivering Biologically Active Substances to Plants and Animals. US5013552A, 1991.

[30] Seo, J.; Wang, L.; Ng, W. B.; Ch, N. J.; Cho, N.-J. Preparation of Highly Monodisperse Electroactive Pollen Biocomposites. *ChemNanoMat*, **2016**, *2* (5), 414–418. https://doi.org/10.1002/cnma.201600004.

[31] Prabhakar, A. K.; Potroz, M. G.; Tan, E. L.; Jung, H.; Park, J. H.; Cho, N. J. Macromolecular Microencapsulation Using Pine Pollen: Loading Optimization and Controlled Release with Natural Materials. *ACS Appl. Mater. Interfaces*, **2018**, *10* (34), 28428–28439. https://doi.org/10.1021/acsami.8b09952.

[32] Maric, T.; Nasir, M. Z. M.; Rosli, N. F.; Budanović, M.; Webster, R. D.; Cho, N.-J.; Pumera, M. Microrobots Derived from Variety Plant Pollen Grains for Efficient Environmental Clean Up and as an Anti-Cancer Drug Carrier. *Adv. Funct. Mater.*, **2020**, *2000112*, 1–13. https://doi.org/10.1002/adfm.202000112.

[33] Tan, E. L.; Potroz, M. G.; Ferracci, G.; Jackman, J. A.; Jung, H.; Wang, L.; Cho, N.-J. Light-Induced Surface Modification of Natural Plant Microparticles: Toward Colloidal Science and Cellular Adhesion Applications. *Adv. Funct. Mater.*, **2018**, *28* (18), 1–13. https://doi.org/10.1002/adfm.201707568.

[34] Deng, Z.; Wang, S.; Zhou, B.; Li, J.; Zhou, P.; Li, B.; Liang, H. Carboxymethylpachymaran-Zein Coated Plant Microcapsules-Based β-Galactosidase Encapsulation System for Long-Term Effective Delivery. *Food Res. Int.*, **2020**, *128*, 108867. https://doi.org/10.1016/j.foodres.2019.108867.

[35] Ares, A. M.; Valverde, S.; Bernal, J. L.; Nozal, M. J.; Bernal, J. Extraction and Determination of Bioactive Compounds from Bee Pollen. *J. Pharm. Biomed. Anal.*, **2018**, *147*, 110–124. https://doi.org/10.1016/j.jpba.2017.08.009.

[36] Diego-Taboada, A.; Beckett, S. T.; Atkin, S. L.; Mackenzie, G. Hollow Pollen Shells to Enhance Drug Delivery. *Pharmaceutics*, **2014**, *6* (1), 80–96. https://doi.org/10.3390/pharmaceutics6010080.

[37] Gonzalez-Cruz, P.; Uddin, M. J.; Atwe, S. U.; Abidi, N.; Gill, H. S. Chemical Treatment Method for Obtaining Clean and Intact Pollen Shells of Different Species. *ACS Biomater. Sci. Eng.*, **2018**, *4* (7), 2319–2329. https://doi.org/10.1021/acsbiomaterials.8b00304.

[38] Cain, S. A. Pollen Analysis as a Paleo-Ecological Research Method. *Bot. Rev.*, **1939**, *5* (12), 627–654. https://doi.org/10.1007/BF02871650.

[39] Halbritter, H.; Ulrich, S.; Grímsson, F.; Weber, M.; Zetter, R.; Hesse, M.; Buchner, R.; Svojtka, M.; Frosch-Radivo, A. *Illustrated Pollen Terminology*; 2018. https://doi.org/10.1007/978-3-319-71365-6.

[40] Mundargi, R. C.; Potroz, M. G.; Park, J. H.; Seo, J.; Lee, J. H.; Cho, N.-J. Extraction of Sporopollenin Exine Capsules from Sunflower Pollen Grains. *RSC Adv.*, **2016**, *6* (20), 16533–16539. https://doi.org/10.1039/C5RA27207F.

[41] Fan, T.; Park, J. H.; Pham, Q. A.; Tan, E.-L.; Mundargi, R. C.; Potroz, M. G.; Jung, H.; Cho, N.-J. Extraction of Cage-like Sporopollenin Exine Capsules from Dandelion Pollen Grains. *Sci. Rep.*, **2018**, *8* (1), 6565. https://doi.org/10.1038/s41598-018-24336-9.

[42] Anjos, O.; Santos, A. J. A.; Dias, T.; Estevinho, L. M. Application of FTIR-ATR Spectroscopy on the Bee Pollen Characterization. *J. Apic. Res.*, **2017**, *8839* (March), 1–9. https://doi.org/10.1080/00218839.2017.1289657.

[43] Zimmermann, B.; Kohler, A.; B. Zimmermann; Kohler, A. Infrared Spectroscopy of Pollen Identifies Plant Species and Genus as Well as Environmental Conditions. *PLoS One*, **2014**, *9* (4), 1–12. https://doi.org/10.1371/journal.pone.0095417.

[44] Fan, T. F.; Potroz, M. G.; Tan, E. L.; Ibrahim, M. S.; Miyako, E.; Cho, N.-J. Species-Specific Biodegradation of Sporopollenin-Based Microcapsules. *Sci. Rep.*, **2019**, *9* (1), 1–13. https://doi.org/10.1038/s41598-019-46131-w.

[45] Fan, T. F.; Hwang, Y.; Potroz, M. G.; Lau, K. L.; Tan, E. L.; Shahrudin Ibrahim, M.; Miyako, E.; Cho, N.-J. Degradation of the Sporopollenin Exine Capsules (SECs) in Human Plasma. *Appl. Mater. Today*, **2020**, *19* (xxxx), 100594. https://doi.org/10.1016/j.apmt.2020.100594.

[46] Bağcıoğlu, M.; Zimmermann, B.; Kohler, A. A Multiscale Vibrational Spectroscopic Approach for Identification and Biochemical Characterization of Pollen. *PLoS One*, **2015**, *10* (9), 1–19. https://doi.org/10.1371/journal.pone.0137899.

[47] Zhao, F.; Elkelish, A.; Durner, J.; Lindermayr, C.; Winkler, J. B.; Ruioff, F.; Behrendt, H.; Traidl-Hoffmann, C.; Holzinger, A.; Kofler, W.; et al. Common Ragweed (Ambrosia Artemisiifolia L.): Allergenicity and Molecular Characterization of Pollen after Plant Exposure to Elevated NO2. *Plant Cell Environ.*, **2016**, *39* (1), 147–164.

https://doi.org/10.1111/pce.12601.

[48] Julier, A. C. M.; Jardine, P. E.; Coe, A. L.; Gosling, W. D.; Lomax, B. H.; Fraser, W. T. Chemotaxonomy as a Tool for Interpreting the Cryptic Diversity of Poaceae Pollen. *Rev. Palaeobot. Palynol.*, **2016**, *235*, 140–147. https://doi.org/10.1016/j.revpalbo.2016.08.004.

[49] Wiercigroch, E.; Szafraniec, E.; Czamara, K.; Pacia, M. Z.; Majzner, K.; Kochan, K.; Kaczor, A.; Baranska, M.; Malek, K. Raman and Infrared Spectroscopy of Carbohydrates: A Review. *Spectrochim. Acta - Part A Mol. Biomol. Spectrosc.*, **2017**, *185*, 317–335. https://doi.org/10.1016/j.saa.2017.05.045.

[50] Schulte, F.; Lingott, J.; Panne, U.; Kneipp, J. Chemical Characterization and Classification of Pollen. *Anal. Chem.*, **2008**, *80* (24), 9551–9556. https://doi.org/10.1021/ac801791a.

[51] Chiappe, C.; Demontis, G. C.; Di Bussolo, V.; Rodriguez Douton, M. J.; Rossella, F.; Pomelli, C. S.; Sartini, S.; Caporali, S. From Pollen Grains to Functionalized Microcapsules: A Facile Chemical Route Using Ionic Liquids. *Green Chem.*, **2017**, *19* (4), 1028–1033. https://doi.org/10.1039/c6gc02892f.

[52] Kędzierska-Matysek, M.; Matwijczuk, A.; Florek, M.; Barłowska, J.; Wolanciuk, A.; Matwijczuk, A.; Chruściel, E.; Walkowiak, R.; Karcz, D.; Gładyszewska, B. Application of FTIR Spectroscopy for Analysis of the Quality of Honey. *BIO Web Conf.*, **2018**, *10* (January), 02008. https://doi.org/10.1051/bioconf/20181002008.

[53] Depciuch, J.; Kasprzyk, I.; Roga, E.; Parlinska-Wojtan, M. Analysis of Morphological and Molecular Composition Changes in Allergenic Artemisia Vulgaris L. Pollen under Traffic Pollution Using SEM and FTIR Spectroscopy. *Environ. Sci. Pollut. Res.*, **2016**, *23* (22), 23203–23214. https://doi.org/10.1007/s11356-016-7554-8.

[54] Fang, K.; Wang, Y.; Jinxing, L.; Yu, T.; Zhang, L.; Baluška, F.; Šamaj, J.; Lin, J. Isolation of De-Exined Pollen and Cytological Studies of the Pollen Intines of Pinus Bungeana Zucc. Ex Endl. and Picea Wilsonii Mast. *Flora Morphol. Distrib. Funct. Ecol. Plants*, **2008**, *203* (4), 332–340. https://doi.org/10.1016/j.flora.2007.04.007.

[55] Zhou, X. L.; Sun, P. N.; Bucheli, P.; Huang, T. H.; Wang, D. FT-IR Methodology for Quality Control of Arabinogalactan Protein (AGP) Extracted from Green Tea (Camellia Sinensis). *J. Agric. Food Chem.*, **2009**, *57* (12), 5121–5128. https://doi.org/10.1021/jf803707a.

[56] Ahlers, F.; Bubert, H.; Steuernagel, S.; Wiermann, R. The Nature of Oxygen in Sporopollenin from the Pollen of Typha Angustifolia L. *Zeitschrift fur Naturforsch. - Sect. C J. Biosci.*, **2000**, *55* (3–4), 129–136.

[57] Carballo-Meilan, A.; Goodman, A. M.; Baron, M. G.; Gonzalez-Rodriguez, J. A Specific Case in the Classification of Woods by FTIR and Chemometric: Discrimination of Fagales from Malpighiales. *Cellulose*, **2014**, *21* (1), 261–273. https://doi.org/10.1007/s10570-013-0093-2.

[58] Buta, E.; Cantor, M.; Tefan, R.; Pop, R.; Mitre, I.; Buta, M.; Sestra, R. E. FT-IR Characterization of Pollen Biochemistry, Viability, and Germination Capacity in Saintpaulia H. Wendl. Genotypes. *J. Spectrosc.*, **2015**, *2015*, 1–7.

https://doi.org/10.1155/2015/706370.

[59] Gubbuk, I. H.; Gürfidan, L.; Erdemir, S.; Yilmaz, M. Surface Modification of Sporopollenin with Calixarene Derivative: Characterization and Application for Metal Removal. *Water. Air. Soil Pollut.*, **2012**, *223* (5), 2623–2632. https://doi.org/10.1007/s11270-011-1054-8.

[60] Rahman, O. S. A.; Chellasamy, V.; Ponpandian, N.; Amirthapandian, S.; Panigrahi, B. K.; Thangadurai, P. A Facile Green Synthesis of Reduced Graphene Oxide by Using Pollen Grains of Peltophorum Pterocarpum and Study of Its Electrochemical Behavior. *Rsc Adv.*, **2014**, *4* (100), 56910–56917. https://doi.org/10.1039/C4RA06203E.

[61] Fadiran, O. O.; Meredith, J. C. Surface Treated Pollen Performance as a Renewable Reinforcing Filler for Poly(Vinyl Acetate). *J. Mater. Chem. A*, **2014**, *2* (40), 17031–17040. https://doi.org/10.1039/C4TA03219E.

[62] Depciuch, J.; Kasprzyk, I.; Sadik, O.; Parlińska-Wojtan, M. FTIR Analysis of Molecular Composition Changes in Hazel Pollen from Unpolluted and Urbanized Areas. *Aerobiologia (Bologna).*, **2017**, *33* (1), 1–12. https://doi.org/10.1007/s10453-016-9445-3.

[63] Kaya, M.; Akyuz, L.; Sargin, I.; Mujtaba, M.; Salaberria, A. M.; Labidi, J.; Cakmak, Y. S.; Koc, B.; Baran, T.; Ceter, T. Incorporation of Sporopollenin Enhances Acid–Base Durability, Hydrophobicity, and Mechanical, Antifungal and Antioxidant Properties of Chitosan Films. *J. Ind. Eng. Chem.*, **2017**, *47*, 236–245. https://doi.org/10.1016/j.jiec.2016.11.038.

[64] Ng, H. M.; Saidi, N. M.; Omar, F. S.; Ramesh, K.; Ramesh, S.; Bashir, S. Thermogravimetric Analysis of Polymers. *Encycl. Polym. Sci. Technol.*, **2018**, No. 13, 1–29. https://doi.org/10.1002/0471440264.pst667.

[65] Uddin, M. J.; Liyanage, S.; Abidi, N.; Gill, H. S. Physical and Biochemical Characterization of Chemically Treated Pollen Shells for Potential Use in Oral Delivery of Therapeutics. *J. Pharm. Sci.*, **2018**, *107* (12), 3047–3059. https://doi.org/10.1016/j.xphs.2018.07.028.

[66] Thakur, M.; Nanda, V. Exploring the Physical, Functional, Thermal, and Textural Properties of Bee Pollen from Different Botanical Origins of India. *J. Food Process Eng.*, **2020**, *43* (1), 1–14. https://doi.org/10.1111/jfpe.12935.

[67] Mujtaba, M.; Sargin, I.; Akyuz, L.; Ceter, T.; Kaya, M. Newly Isolated Sporopollenin Microcages from *Platanus Orientalis* Pollens as a Vehicle for Controlled Drug Delivery. *Mater. Sci. Eng. C*, **2017**, *77*, 263–270. https://doi.org/10.1016/j.msec.2017.02.176.

[68] Palazzo, I.; Mezzetta, A.; Guazzelli, L.; Sartini, S.; Pomelli, C. S.; Parker, W. O.; Chiappe, C. Chiral Ionic Liquids Supported on Natural Sporopollenin Microcapsules. *RSC Adv.*, **2018**, *8* (38), 21174–21183. https://doi.org/10.1039/c8ra03455a.

[69] Pomelli, C. S.; D'Andrea, F.; Mezzetta, A.; Guazzelli, L. Exploiting Pollen and Sporopollenin for the Sustainable Production of Microstructures. *New J. Chem.*, **2020**, *44* (3), 647–652. https://doi.org/10.1039/c9nj05082e.

[70] Descolas-Gros, C.; Schölzel, C. Stable Isotope Ratios of Carbon and Nitrogen in Pollen

Grains in Order to Characterize Plant Functional Groups and Photosynthetic Pathway Types. *New Phytol.*, **2007**, *176* (2), 390–401. https://doi.org/10.1111/j.1469-8137.2007.02176.x.

[71] Rabie, A. L.; Wells, J. D.; Dent, L. K. The Nitrogen Content of Pollen Protein. *J. Apic. Res.*, **1983**, *22* (2), 119–123. https://doi.org/10.1080/00218839.1983.11100572.

[72] Uddin, M. J.; Gill, H. S. Ragweed Pollen as an Oral Vaccine Delivery System: Mechanistic Insights. *J. Control. Release*, **2017**, *268* (October), 416–426. https://doi.org/10.1016/j.jconrel.2017.10.019.

[73] Uddin, M. J.; Gill, H. S. From Allergen to Oral Vaccine Carrier: A New Face of Ragweed Pollen. *Int. J. Pharm.*, **2018**, *545* (1–2), 286–294. https://doi.org/10.1016/j.ijpharm.2018.05.003.

[74] Willemse, M. T. M. Changes in the Autofluorescence of the Pollen Wall during Microsporogenesis and Chemical Treatments. *Acta Bot. Neerl.*, **1972**, *21* (1), 1–16. https://doi.org/10.1111/j.1438-8677.1972.tb00742.x.

[75] Urbanczyk, J.; Fernandez Casado, M. A.; Díaz, T. E.; Heras, P.; Infante, M.; Borrego, A. G. Spectral Fluorescence Variation of Pollen and Spores from Recent Peat-Forming Plants. *Int. J. Coal Geol.*, **2014**, *131*, 263–273. https://doi.org/10.1016/j.coal.2014.06.024.

[76] Pöhlker, C.; Huffman, J. A.; Pöschl, U. Autofluorescence of Atmospheric Bioaerosols - Fluorescent Biomolecules and Potential Interferences. *Atmos. Meas. Tech.*, **2012**, *5* (1), 37–71. https://doi.org/10.5194/amt-5-37-2012.

[77] Park, S.; Chin, H.; Hwang, Y.; Fan, T. F.; Cho, N. J. A Facile Approach to Patterning Pollen Microparticles for in Situ Imaging. *Appl. Mater. Today*, **2020**, *20*, 100702. https://doi.org/10.1016/j.apmt.2020.100702.

[78] Mundargi, R. C.; Potroz, M. G.; Park, S.; Shirahama, H.; Lee, J. H.; Seo, J.; Cho, N.-J. Natural Sunflower Pollen as a Drug Delivery Vehicle. *Small*, **2016**, *12* (9), 1167–1173. https://doi.org/10.1002/smll.201500860.

[79] Potroz, M. G.; Mundargi, R. C.; Gillissen, J. J.; Tan, E.-L.; Meker, S.; Park, J. H.; Jung, H.; Park, S.; Cho, D.; Bang, S.-I.; et al. Plant-Based Hollow Microcapsules for Oral Delivery Applications: Toward Optimized Loading and Controlled Release. *Adv. Funct. Mater.*, **2017**, *27* (31), 1700270. https://doi.org/10.1002/adfm.201700270.

[80] Wang, H.; Potroz, M. G.; Jackman, J. A.; Khezri, B.; Marić, T.; Cho, N.-J.; Pumera, M. Bioinspired Spiky Micromotors Based on Sporopollenin Exine Capsules. *Adv. Funct. Mater.*, **2017**, *27* (32), 1–9. https://doi.org/10.1002/adfm.201702338.

[81] Corliss, M. K.; Bok, C. K.; Gillissen, J.; Potroz, M. G.; Jung, H.; Tan, E. L.; Mundargi, R. C.; Cho, N.-J. Preserving the Inflated Structure of Lyophilized Sporopollenin Exine Capsules with Polyethylene Glycol Osmolyte. *J. Ind. Eng. Chem.*, **2018**, *61*, 255–264. https://doi.org/10.1016/j.jiec.2017.12.023.

[82] Mundargi, R. C.; Potroz, M. G.; Park, J. H.; Seo, J.; Tan, E.-L.; Lee, J. H.; Cho, N.-J. Eco-Friendly Streamlined Process for Sporopollenin Exine Capsule Extraction. *Sci. Rep.*, **2016**, *6* (1), 1–14. https://doi.org/10.1038/srep19960.

[83] Prabhakar, A. K.; Lai, H. Y.; Potroz, M. G.; Corliss, M. K.; Park, J. H.; Mundargi, R. C.; Cho, D.; Bang, S. I.; Cho, N.-J. Chemical Processing Strategies to Obtain Sporopollenin Exine Capsules from Multi-Compartmental Pine Pollen. *J. Ind. Eng. Chem.*, **2017**, *53*, 375–385. https://doi.org/10.1016/j.jiec.2017.05.009.

[84] Dyab, A. K. F.; Mohamed, M. A.; Meligi, N. M.; Mohamed, S. K. Encapsulation of Erythromycin and Bacitracin Antibiotics into Natural Sporopollenin Microcapsules: Antibacterial, Cytotoxicity, in Vitro and in Vivo Release Studies for Enhanced Bioavailability. *RSC Adv.*, **2018**, *8* (58), 33432–33444. https://doi.org/10.1039/C8RA05499A.

[85] Dyab, A. K. F.; Sadek, K. U. Microwave Assisted One-Pot Green Synthesis of Cinnoline Derivatives inside Natural Sporopollenin Microcapsules. *RSC Adv.*, **2018**, *8* (41), 23241–23251. https://doi.org/10.1039/C8RA04195D.

[86] Halbritter, H.; Ulrich, S.; Grímsson, F.; Weber, M.; Zetter, R.; Hesse, M.; Buchner, R.; Svojtka, M.; Frosch-Radivo, A. Palynology: History and Systematic Aspects. In *Illustrated Pollen Terminology*; Springer International Publishing: Cham, 2018; pp 3–21. https://doi.org/10.1007/978-3-319-71365-6_1.

[87] Uddin, M. J.; Gonzalez-Cruz, P.; Warzywoda, J.; Gill, H. S. Sporopollenin Spikes Augment Antigen-Specific Immune Response and Generate Long-Lived Humoral Immunity. *Adv. Ther.*, **2020**, *2000102*, 2000102. https://doi.org/10.1002/adtp.202000102.

[88] Thomasson, M. J.; Diego-Taboada, A.; Barrier, S.; Martin-Guyout, J.; Amedjou, E.; Atkin, S. L.; Queneau, Y.; Boa, A. N.; Mackenzie, G. Sporopollenin Exine Capsules (SpECs) Derived from *Lycopodium Clavatum* Provide Practical Antioxidant Properties by Retarding Rancidification of an ω-3 Oil. *Ind. Crops Prod.*, **2020**, *154*, 112714. https://doi.org/10.1016/j.indcrop.2020.112714.

[89] Atwe, S. U.; Ma, Y.; Gill, H. S. Pollen Grains for Oral Vaccination. *J Control Release*, **2015**, *194*, 45–52. https://doi.org/10.1016/j.jconrel.2014.08.010.Pollen.

[90] Barrier, S.; Rigby, A. S.; Diego-Taboada, A.; Thomasson, M. J.; Mackenzie, G.; Atkin, S. L. Sporopollenin Exines: A Novel Natural Taste Masking Material. *LWT - Food Sci. Technol.*, **2010**, *43* (1), 73–76. https://doi.org/10.1016/j.lwt.2009.07.001.

[91] Barrier, S.; Diego-Taboada, A.; Thomasson, M. J.; Madden, L.; Pointon, J. C.; Wadhawan, J. D.; Beckett, S. T.; Atkin, S. L.; Mackenzie, G. Viability of Plant Spore Exine Capsules for Microencapsulation. *J. Mater. Chem.*, **2011**, *21* (4), 975–981. https://doi.org/10.1039/C0JM02246B.

[92] Mohammed, A. S. Y.; Dyab, A. K. F.; Taha, F.; Abd El-Mageed, A. I. A. Encapsulation of Folic Acid (Vitamin B9) into Sporopollenin Microcapsules: Physico-Chemical Characterisation, in Vitro Controlled Release and Photoprotection Study. *Mater. Sci. Eng. C*, **2021**, *128* (March), 112271. https://doi.org/10.1016/j.msec.2021.112271.

[93] Wakil, A.; MacKenzie, G.; Diego-Taboada, A.; Bell, J. G.; Atkin, S. L. Enhanced Bioavailability of Eicosapentaenoic Acid from Fish Oil after Encapsulation within Plant Spore Exines as Microcapsules. *Lipids*, **2010**, *45* (7), 645–649. https://doi.org/10.1007/s11745-010-3427-y.

[94] Diego-Taboada, A.; Maillet, L.; Banoub, J. H.; Lorch, M.; Rigby, A. S.; Boa, A. N.; Atkin, S. L.; Mackenzie, G. Protein Free Microcapsules Obtained from Plant Spores as a Model for Drug Delivery: Ibuprofen Encapsulation, Release and Taste Masking. *J. Mater. Chem. B*, **2013**, *1* (5), 707–713. https://doi.org/10.1039/c2tb00228k.

[95] Mundargi, R. C.; Potroz, M. G.; Park, S.; Park, J. H.; Shirahama, H.; Lee, J. H.; Seo, J.; Cho, N.-J. Lycopodium Spores: A Naturally Manufactured, Superrobust Biomaterial for Drug Delivery. *Adv. Funct. Mater.*, **2016**, *26* (4), 487–497. https://doi.org/10.1002/adfm.201502322.

[96] Mundargi, R. C.; Tan, E. L.; Seo, J.; Cho, N.-J. Encapsulation and Controlled Release Formulations of 5-Fluorouracil from Natural *Lycopodium Clavatum* Spores. *J. Ind. Eng. Chem.*, **2016**, *36*, 102–108. https://doi.org/10.1016/j.jiec.2016.01.022.

[97] Benchabane, S.; Subirade, M.; Vandenberg, G. W. Production of BSA-Loaded Alginate Microcapsules: Influence of Spray Dryer Parameters on the Microcapsule Characteristics and BSA Release. *J. Microencapsul.*, **2007**, *24* (6), 565–576. https://doi.org/10.1080/02652040701452917.

[98] Vaghani, S.; Vasanti, S.; Chaturvedi, K.; Satish, C. S.; Shankar, S. J. Formulation and Evaluation of 5-FU Loaded Eudragit Microspheres: Effect of Various Eudragit on Micromeretic Properties of Microspheres. *J. Macromol. Sci. Part A Pure Appl. Chem.*, **2008**, *45* (12), 1015–1027. https://doi.org/10.1080/10601320802454540.

[99] Mohammed, A.-S. Y.; Dyab, A. K. F.; Taha, F.; Abd El-Mageed, A. I. A. Pollen-Derived Microcapsules for Aspirin Microencapsulation: In Vitro Release and Physico-Chemical Studies. *RSC Adv.*, **2022**, *12* (34), 22139–22149. https://doi.org/10.1039/D2RA02888C.

[100] Diego-taboada, A.; Sathyapalan, T.; Courts, F.; Lorch, M.; Walther, T.; Almutairi, F.; Burke, B. P.; Harris, K.; Kruusm, M.; Booth, J.; et al. Spore Exines Increase Vitamin D Clinical Bioavailability by Mucoadhesion and Bile Triggered Release ☆. **2022**, *350* (January), 244–255. https://doi.org/10.1016/j.jconrel.2022.08.017.

[101] Meligi, N. M.; Dyab, A. K. F.; Paunov, V. N. Sustained in Vitro and in Vivo Delivery of Metformin from Plant Pollen-Derived Composite Microcapsules. *Pharmaceutics*, **2021**, *13* (7), 9–12. https://doi.org/10.3390/pharmaceutics13071048.

[102] Lorch, M.; Thomasson, M. J.; Diego-taboada, A.; Barrier, S.; Atkin, S. L.; Mackenzie, G.; Archibald, S. J. MRI Contrast Agent Delivery Using Spore Capsules : Controlled Release in Blood Plasma. *Chem. Commun.*, **2009**, No. 42, 6442–6444. https://doi.org/10.1039/b909551a.

[103] Hamad, S. A.; Dyab, A. F. K.; Stoyanov, S. D.; Paunov, V. N. Encapsulation of Living Cells into Sporopollenin Microcapsules. *J. Mater. Chem.*, **2011**, *21* (44), 18018–18023. https://doi.org/10.1039/c1jm13719k.

[104] Wang, Y.; Len, T.; Huang, Y.; Diego Taboada, A.; Boa, A. N.; Ceballos, C.; Delbecq, F.; Mackenzie, G.; Len, C. Sulfonated Sporopollenin as an Efficient and Recyclable Heterogeneous Catalyst for Dehydration of D-Xylose and Xylan into Furfural. *ACS Sustain. Chem. Eng.*, **2017**, *5* (1), 392–398. https://doi.org/10.1021/acssuschemeng.6b01780.

[105] Elmacı, G. Magnetic Hollow Biocomposites Prepared from *Lycopodium Clavatum*

Pollens as Efficient Recyclable Catalyst. *ChemistrySelect*, **2020**, *5* (7), 2225–2231. https://doi.org/10.1002/slct.201904152.

[106] Dyab, A. K. F.; Abdallah, E. M.; Ahmed, S. A.; Rabee, M. M. Fabrication and Characterisation of Novel Natural Lycopodium Clavatum Sporopollenin Microcapsules Loaded In-Situ with Nano-Magnetic Humic Acid-Metal Complexes. *J. Encapsulation Adsorpt. Sci.*, **2016**, *06* (04), 109–131. https://doi.org/10.4236/jeas.2016.64009.

[107] Wang, L. L.; Ng, W. B. B.; Jackman, J. A.; Cho, N. J. Graphene-Functionalized Natural Microcapsules: Modular Building Blocks for Ultrahigh Sensitivity Bioelectronic Platforms. *Adv. Funct. Mater.*, **2016**, *26* (13), 2097–2103. https://doi.org/10.1002/adfm.201504940.

[108] Paunov, V. N.; Mackenzie, G.; Stoyanov, S. D. Sporopollenin Micro-Reactors for in-Situ Preparation, Encapsulation and Targeted Delivery of Active Components. *J. Mater. Chem.*, **2007**, *17* (7), 609. https://doi.org/10.1039/b615865j.

[109] Schwendemann, A. B.; Wang, G.; Mertz, M. L.; McWilliams, R. T.; Thatcher, S. L.; Osborn, J. M. Aerodynamics of Saccate Pollen and Its Implications for Wind Pollination. *Am. J. Bot.*, **2007**, *94* (8), 1371–1381. https://doi.org/10.3732/ajb.94.8.1371.

[110] Mujtaba, M.; Yilmaz, B. A.; Cansaran-Duman, D.; Akyuz, L.; Yangın, S.; Kaya, M.; Çeter, T.; Khawar, K. M. Newly Isolated Sporopollenin Microcages from Cedrus Libani and Pinus Nigra as Carrier for Oxaliplatin; XCELLigence RTCA-Based Release Assay. *Polym. Bull.*, **2021**. https://doi.org/10.1007/s00289-020-03531-7.

[111] Prabhakar, A. K.; Potroz, M. G.; Tan, E. L.; Jung, H.; Park, J. H.; Cho, N.-J. Macromolecular Microencapsulation Using Pine Pollen: Loading Optimization and Controlled Release with Natural Materials. *ACS Appl. Mater. Interfaces*, **2018**, *10* (34), 28428–28439. https://doi.org/10.1021/acsami.8b09952.

[112] Sun, M.; Fan, X.; Meng, X.; Song, J.; Chen, W.; Sun, L.; Xie, H. Magnetic Biohybrid Micromotors with High Maneuverability for Efficient Drug Loading and Targeted Drug Delivery. *Nanoscale*, **2019**, *11* (39), 18382–18392. https://doi.org/10.1039/c9nr06221a.

[113] Structures, W. Comparative Morphology of Monocot Pollen and and Wall Structures. *Bot. Rev.*, **1983**, *4* (4), 331–379.

[114] Kuprianova, L. A. Apertures of Pollen Grains and Their Evolution in Angiosperms. *Rev. Palaeobot. Palynol.*, **1967**, *3* (1–4), 73–80. https://doi.org/10.1016/0034-6667(67)90041-3.

[115] Nazish, M.; Althobaiti, A. T. Palyno-Morphological Characteristics as a Systematic Approach in the Identification of Halophytic Poaceae Species from a Saline Environment. *Plants*, **2022**, *11* (19). https://doi.org/10.3390/plants11192618.

[116] Rowley, J.; Skvarla, J. The Elasticity of the Exine. *Grana*, **2000**, *39* (1), 1–7. https://doi.org/10.1080/00173130150503759.

[117] Domínguez, E.; Heredia, A.; Mercado, J. A.; Quesada, M. A. Isolation of Intact Pollen Exine Using Anhydrous Hydrogen Fluoride. *Grana*, **1998**, *37* (2), 93–96. https://doi.org/10.1080/00173139809362649.

[118] Harley, M. M.; Baker, W. J. *Pollen Aperture Morphology in Arecaceae: Application*

within Phylogenetic Analyses, and a Summary of the Fossil Record of Palm-like Pollen; 2001; Vol. 40. https://doi.org/10.1080/00173130152591877.

[119] Alshehri, S. M.; Al-Lohedan, H. A.; Chaudhary, A. A.; Al-Farraj, E.; Alhokbany, N.; Issa, Z.; Alhousine, S.; Ahamad, T. Delivery of Ibuprofen by Natural Macroporous Sporopollenin Exine Capsules Extracted from *Phoenix Dactylifera* L. *Eur. J. Pharm. Sci.*, **2016**, *88*, 158–165. https://doi.org/10.1016/j.ejps.2016.02.004.

[120] Alshehri, S. M.; Al-Lohedan, H. A.; Al-Farraj, E.; Alhokbany, N.; Chaudhary, A. A.; Ahamad, T. Macroporous Natural Capsules Extracted from Phoenix Dactylifera L. Spore and Their Application in Oral Drugs Delivery. *Int. J. Pharm.*, **2016**, *504* (1–2), 39–47. https://doi.org/10.1016/j.ijpharm.2016.02.049.

[121] Raish, M.; Kalam, M. A.; Ahmad, A.; Shahid, M.; Ansari, M. A.; Ahad, A.; Ali, R.; Jardan, Y. A. B.; Alshamsan, A.; Alkholief, M.; et al. Eudragit-Coated Sporopollenin Exine Microcapsules (Semc) of Phoenix Dactylifera l. of 5-Fluorouracil for Colon-Specific Drug Delivery. *Pharmaceutics*, **2021**, *13* (11). https://doi.org/10.3390/pharmaceutics13111921.

[122] Bordas-Le Floch, V.; Groeme, R.; Chabre, H.; Baron-Bodo, V.; Nony, E.; Mascarell, L.; Moingeon, P. New Insights into Ragweed Pollen Allergens. *Curr. Allergy Asthma Rep.*, **2015**, *15* (11). https://doi.org/10.1007/s11882-015-0565-6.

[123] Grater, W. C.; Stemen, T. R. The Plant, the Pollen and the Patient. *Rev. Palaeobot. Palynol.*, **1967**, *4* (1–4), 187–192. https://doi.org/10.1016/0034-6667(67)90185-6.

[124] Amber, M. S.; Tawashi, R. Drug Loaded Pollen Grains with an Outer Coating for Pulsed Delivery. US5275819A, 1994.

[125] Lale, S. V.; Gill, H. S. Pollen Grains as a Novel Microcarrier for Oral Delivery of Proteins. *Int. J. Pharm.*, **2018**, *552* (1–2), 352–359. https://doi.org/10.1016/j.ijpharm.2018.10.016.

[126] Fan, T.; Park, S.; Shi, Q.; Zhang, X.; Liu, Q.; Song, Y.; Chin, H.; Shahrudin, M.; Ibrahim, B.; Mokrzecka, N.; et al. Transformation of Hard Pollen into Soft Matter. *Nat. Commun.*, **2020**, *11* (1), 1449. https://doi.org/10.1038/s41467-020-15294-w.

[127] Zhao, Z.; Hwang, Y.; Yang, Y.; Fan, T.; Song, J.; Suresh, S.; Cho, N.-J. Actuation and Locomotion Driven by Moisture in Paper Made with Natural Pollen. *Proc. Natl. Acad. Sci. U. S. A.*, **2020**, *117* (16), 8711–8718. https://doi.org/10.1073/pnas.1922560117.

[128] Wang, L.; Jackman, J. A.; Ng, W. B.; Cho, N.-J. Flexible, Graphene-Coated Biocomposite for Highly Sensitive, Real-Time Molecular Detection. *Adv. Funct. Mater.*, **2016**, *26* (47), 8623–8630. https://doi.org/10.1002/adfm.201603550.

[129] Deng, Z.; Pei, Y.; Wang, S.; Zhou, B.; Hou, X.; Li, J.; Li, B.; Liang, H. Designable Carboxymethylpachymaran/Metal Ion Architecture on Sunflower Sporopollenin Exine Capsules as Delivery Vehicles for Bioactive Macromolecules. *J. Agric. Food Chem.*, **2020**, *68* (47), 13990–14000. https://doi.org/10.1021/acs.jafc.0c05169.

[130] Sargin, I.; Akyuz, L.; Kaya, M.; Tan, G.; Ceter, T.; Yildirim, K.; Ertosun, S.; Aydin, G. H.; Topal, M. Controlled Release and Anti-Proliferative Effect of Imatinib Mesylate Loaded Sporopollenin Microcapsules Extracted from Pollens of *Betula Pendula*. *Int. J.*

Biol. Macromol., **2017**, *105*, 749–756. https://doi.org/10.1016/j.ijbiomac.2017.07.093.

[131] Akyuz, L.; Sargin, I.; Kaya, M.; Ceter, T.; Akata, I. A New Pollen-Derived Microcarrier for Pantoprazole Delivery. *Mater. Sci. Eng. C*, **2017**, *71*, 937–942. https://doi.org/10.1016/j.msec.2016.11.009.

[132] Ma, H.; Zhang, P.; Wang, J.; Xu, X.; Zhang, H.; Zhang, Z.; Zhang, Y.; Ning, Y. Preparation of a Novel Rape Pollen Shell Microencapsulation and Its Use for Protein Adsorption and PH-Controlled Release. *J. Microencapsul.*, **2014**, *31* (7), 667–673. https://doi.org/10.3109/02652048.2014.913723.

[133] Ageitos, J. M.; Robla, S.; Valverde-Fraga, L.; Garcia-Fuentes, M.; Csaba, N. Purification of Hollow Sporopollenin Microcapsules from Sunflower and Chamomile Pollen Grains. *Polymers (Basel).*, **2021**, *13* (13), 2094. https://doi.org/10.3390/polym13132094.

[134] Mäkelä, E. M. Size Distinctions between Betula Pollen Types — a Review. *Grana*, **1996**, *35* (4), 248–256. https://doi.org/10.1080/00173139609430011.

[135] Gabr, D. G. I. Taxonomic Importance of Pollen Morphology for Some Species of Brassicaceae. *Pakistan J. Biol. Sci.*, **2018**, *21* (5), 215–223. https://doi.org/10.3923/pjbs.2018.215.223.

[136] Cao, F.; Li, D. Biotemplate Synthesis of Monodispersed Iron Phosphate Hollow Microspheres. *Bioinspiration and Biomimetics*, **2010**, *5* (1). https://doi.org/10.1088/1748-3182/5/1/016005.

[137] Cao, F.; Li, D. X. Morphology-Controlled Synthesis of SiO2 Hollow Microspheres Using Pollen Grain as a Biotemplate. *Biomed. Mater.*, **2009**, *4* (2). https://doi.org/10.1088/1748-6041/4/2/025009.

[138] Dehghani, M.; Akhani, H. Pollen Morphological Studies in Inffamily Suaedoideae (Chenopodiaceae). *Grana*, **2009**, *48* (2), 79–101. https://doi.org/10.1080/00173130902842968.

[139] Denk, T.; Tekleva, M. V. Comparative Pollen Morphology and Ultrastructure of Platanus: Implications for Phylogeny and Evaluation of the Fossil Record. *Grana*, **2006**, *45* (3), 195–221. https://doi.org/10.1080/00173130600873901.

HYPOTHESIS

Background:

Transmucosal drug delivery offers an attractive alternative to overcome problems related to injectable dosage forms, as it allows better access to the target tissue, mimicking the natural release pathway of endogenous biomacromolecules in a non-invasive approach. Its ease of use promotes better patient adherence and compliance, and it involves lower production costs since it does not require sterile conditions. In this context, nanotechnology enables an increase in pharmacological efficacy by reducing side effects and improving the stability and bioavailability of drugs and the development of polymeric nanosystems has generated significant interest in drug delivery due to their enhanced safety, biocompatibility, and physical and biological stability.

HYPOTHESIS

1. Despite the widely reported, efficient interaction of nanosystems with mucosal tissue and their ability to deliver high drug payloads, their *in vivo* efficacy has not been consistent due to their premature elimination from the mucosa, leading to a limited bioavailability.

2. The echinate surface morphology of pollen grains from *Helianthus annuus* and *Matricaria chamomilla* could promote adhesion to mucosal surfaces, leading to extended contact with biological surfaces, thereby enhancing drug absorption and bioavailability.

3. The combination of sporopollenin microcapsules obtained from echinate pollen grains and drug-loaded nanocarriers could be a new multi-stage delivery strategy to enhance transmucosal drug delivery, allowing for improved mucointeraction and enhanced residence times.

OBJECTIVES

OBJECTIVES

Taking into consideration the background information and the outlined hypothesis, the main goal of this thesis was the development of hollow pollen microcapsules from *Helianthus annuus* and *Matricaria chamomilla* and their evaluation as potential transmucosal delivery systems, in combination with nanocarriers. To accomplish this goal, different technological approaches were adopted, and the following experimental activities were undertaken.

- **Sub-objective 1.** The development of a suitable treatment protocol that allows the production of hollow sporopollenin vehicles, with preserved surface morphology, shape and stability using sunflower (*Helianthus annuus*) and chamomile (*Matricaria chamomilla*) pollen. The results are collected in Chapter I of this doctoral thesis.

- **Sub-objective 2.** The association of the developed pollen microcapsules with model polystyrene nanoparticles of different sizes and surface functionalization to unravel their loading and release mechanisms. Based on the results, the secondary objective has been the rational design of protamine nanocapsules and their loading into pollen platforms in order to evaluate their mucointeraction and biodistribution after oral administration. The results are collected in Chapter II of this doctoral thesis.

- **Sub-objective 3**. *-Párrafo afectado por la protección de derechos-*

- **Sub-objective 4.** The design of an allergen-free ocular delivery system based on bilastine nanocapsules, loaded into *H.annuus* hollow pollen microcapsules for the treatment of allergic rhinoconjunctivitis. The results are collected in Chapter V of this doctoral thesis.

CAPÍTULO I/ CHAPTER I

Purification of hollow sporopollenin microcapsules from sunflower and chamomile pollen grains

Jose Manuel Ageitos, **Sandra Robla**, Lorena Valverde-Fraga, Marcos García-Fuentes and Noemi Csaba

Centre for Research in Molecular Medicine and Chronic Diseases (CiMUS), Department Pharmacology, Pharmacy and Pharmaceutical Technology, School of Pharmacy, Universidade de Santiago de Compostela, Spain

Publication: *Jose Manuel Ageitos, Sandra Robla, Lorena Valverde-Fraga, Marcos Garcia-Fuentes & Noemi Csaba (2021). "Purification of Hollow Sporopollenin Microcapsules from Sunflower and Chamomile Pollen Grains, "Polymers"13, no. 13: 2094.*

DOI*:* *https://doi.org/10.3390/polym13132094*

Author Contributions: Investigation & writing

CHAPTER I/ CAPÍTULO I

Purification of hollow sporopollenin microcapsules from sunflower and chamomile pollen grains

Abstract

Pollen grains are natural microcapsules comprised of the biopolymer sporopollenin. The uniformity and special tridimensional architecture of these sporopollenin structures confer them attractive properties such as high resistance and improved bioadhesion. However, natural pollen can be a source of allergens, hindering its biomedical applicability. Several methods have been developed to remove internal components and allergenic compounds, usually involving long and laborious processes, which often cannot be extended to other pollen types. In this work, we propose an abridged protocol to produce stable and pristine hollow pollen microcapsules, together with a complete physicochemical and morphological characterization of the intermediate and final products. The optimized procedure has been validated for different pollen samples, also producing sporopollenin microcapsules from *Matricaria* species for the first time. Pollen microcapsules obtained through this protocol presented low protein content (4.4%), preserved ornamented morphology with a nanoporous surface, and low product density (0.14 g/cm3). These features make them interesting candidates from a pharmaceutical perspective due to the versatility of this biomaterial as a drug delivery platform.

Keywords

Sporopollenin; microcapsules; pollen; sunflower; chamomile; FTIR; SEM

1. INTRODUCCION

Pollen grains are protective microcapsules of the male gametes of seed plants, involved in dispersion and adhesion, as well as recognition, during pollination and fertilization processes [1]. These natural microcapsules are composed by several layers of different lipidic and polymeric materials that confer them unique, plant-specific morphologies [2]. The terminology of pollen wall layers is heterogeneous in the literature and is usually based on the different staining affinity of the biomaterials [3]. Basically, three main layers can be distinguished: first, the external coating, named pollenkitt; followed by the multi-layered pollen-wall (exine and intine); and finally, the inner sporoplasm, where the cell gamete is located [4]. The exine is mainly composed by sporopollenin, one of the most resistant biopolymers found in nature, still part of 500-million-year-old sedimentary rocks [5,6]. This biomaterial is considered a keystone in the adaptation of early aquatic plant gametes to terrestrial life [7]. Sporopollenin is composed of carbon, oxygen, and hydrogen and is constituted of long, highly cross-linked biopolymer chains [7]. In addition to its unique chemical composition, pollen exine has a complex tridimensional structure with ornaments and nanopores, naturally designed for interacting with different biological surfaces, such as insect cuticula, animals, and plant tissues. Synthetic microcapsules often present variability in size and morphology during their production. In contrast, pollen grains can be considered natural, monodisperse nanostructured microcapsules with highly resistant and specific three-dimensional morphologies that, so far, are difficult to replicate with current methods [8]. Pollen structure and composition are dependent on the dispersal pathway of the species (wind, water, insects, animals) in order to protect the male gametophyte best from external environmental conditions. These unique properties have already drawn researchers' attention [2]; notwithstanding, it is well known that most pollens contain allergens that constitute a

potential risk to human health [1,9]. A few protocols have already been established for the elimination of such components and/or the chemical extraction of sporopollenin from fern spores and pollen grains [10–12] to encapsulate drugs [13,14], lipids [15], cells [16], proteins [17,18], or chemical catalysts [19,20]. Such procedures usually involve laborious processes using harsh reagents (e.g., strong acids and/or bases) and prolonged incubation times that can alter the ultrastructure of the pollen grain [10,12].

In addition, the above-mentioned pollen species are generally characterized by simple morphology and produce thin microcapsules with limited applicability. Looking for alternatives, sunflower (*Helianthus annuus*) pollen has been recently drawing attention due to its widespread cultivation, flower size, and high pollen production with low allergenicity [10–12]. Chamomile (*Matricaria chamomilla*, sym. *M. recutita*) belongs to the same family as sunflower and is one of the most important medicinal plants [21,22]. Chamomile pollen is smaller than that of sunflower (13–25 μm vs. 26–50 μm) [23,24] and has a highly porous surface. Despite its interesting size and structure, which make it an ideal candidate for producing sporopollenin microcapsules, this pollen has not yet been explored for this purpose.

Taken together, the aim of our study has been the establishment of a simplified protocol for the obtention of hollow pollen microcapsules, employing sunflower pollen as reference (Figure 1), and the evaluation of its the suitability for chamomile pollen purification. Each step of the process has been studied in detail by several independent techniques to characterize the pollen, as well as the extracted products. To the best of the authors' knowledge, this is the first comparative morphological and physicochemical characterization of sporopollenin microcapsules throughout their sequential chemical purification steps, as well as the first report on the production of hollow sporopollenin micro-capsules from chamomile pollen.

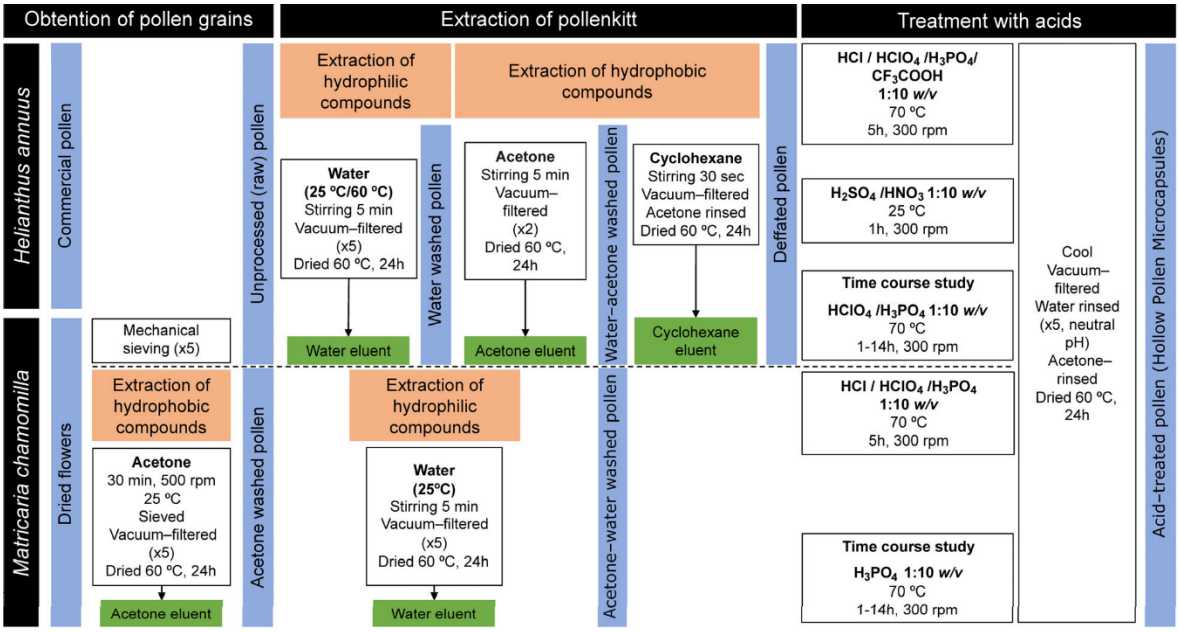

Figure 1. Processing scheme for the different pollen samples.

2. MATERIALS AND METHODS

2.1. Materials

Sunflower pollen (H. annuus) was obtained from Control Bio (El Alquián, Spain) and Pharmallerga (Lisov, Czech Republic). Chamomile (M. chamomilla) dried plant and flower

were purchased from Soria Natural (Soria, Spain). Cyclohexane, orthophosphoric acid (H_3PO_4, 85%), perchloric acid ($HClO_4$, 70%), hydrochloric acid (HCl, 37%), and sulfuric acid (HCl, 98%) were purchased from Merck KGaA (Darmstadt, Germany). Trifluoroacetic acid (CF_3COOH, 99%), nitric acid (HNO_3, 65%), and further standard chemicals were obtained from Sigma-Aldrich (Madrid, Spain). Organic solvents were HPLC grade, and all other products used were of reagent grade purity or higher. All chemicals were used as received without further purification.

2.2. Treatment of Sunflower Pollen

Pollen of *H. annuus* was treated in several consecutive washing steps to remove the external pollenkitt coating of the sporopollenin (**Figure 1**), as well as internal cellular components.

2.2.1. Extraction of the pollenkitt of sunflower pollen

Sunflowe r pollen was treated with water at different temperatures (25 or 60 °C) to extract hydrophilic compounds from pollenkitt. For this purpose, 2 g of pollen were mixed with 40 mL of water and vortexed for 5 min. Afterwards, the suspension was vacuum filtered. First, filtration eluant was recovered, frozen, and lyophilized. Pollen was subsequently resuspended in 40 mL of water and filtered in the same conditions. Water extraction process was repeated in a total of five washes. Water-washed pollen was recovered by filtration and dried at 60 °C for 24 h or until no weight variation was observed.

Water-treated pollen was resuspended in 20 mL of acetone, homogenized for 5 min by vortex, and vacuum filtered (two times). Acetone-treated pollen was recovered by filtration and dried again at 60 °C for 24 h. For the obtention of defatted sunflower pollen, acetone-treated pollen was resuspended in 20 mL of cyclohexane [25] and vortexed for 30s. Cyclohexane-treated pollen was recovered by filtration, rinsed with acetone, and left overnight in a fume hood. Afterwards, it was dried at 60 °C for 24 h and stored in a desiccant chamber. Acetone and cyclohexane eluents were concentrated by rotary evaporation for further analysis.

2.2.2. Elimination of Sporoplasm, Production of Hollow Sunflower Pollen with Acids

For the obtention of hollow sunflower pollen [10], several acids were assayed as follows. On one hand, sunflower pollen was incubated with concentrated acid (HCl, $HClO_4$, H_3PO_4, CF_3COOH) at 1:10 ratio (*w*/*v*) in a bath at 70 °C with gentle stirring at 300 rpm. For the time course study, defatted sunflower pollen was incubated with $HClO_4$ and H_3PO_4 from 1 to 14 h under the same conditions as above. The same pollen to acid ratio (1:10 *w*/*v*) was employed with H_2SO_4 or HNO_3 at 25 °C for 1h under gentle stirring (300 rpm). Afterwards, solutions were cooled, and acid-treated pollen was recovered by filtration in each case. The filtrate was rinsed with water until the pH of the pollen grains became neutral (five washes with 50 mL of water) and rinsed with acetone. Finally, acid-treated (hollow) pollen was dried at 60 °C for 24 h and stored in a desiccant chamber until use.

2.3.Treatment of Chamomile Dried Plant and Flower

A protocol for the purification of chamomile pollen was designed using dried flowers as starting material, since no available commercial source was found for this specific pollen.

2.3.1. Purification of Pollen from Dried Chamomile

Several strategies were assayed for the extraction of pollen from dried chamomile with the purpose of achieving optimal conditions. For physical extraction of unprocessed pollen, 1 g of dried chamomile was sieved through 50 μm and 30 μm mesh fitted stainless steel sieves of 8 cm diameter. Five cycles of sieving were performed, recovering the unprocessed pollen from

the lower reservoir. Process was repeated for a total of 15 g of dried plant and flowers.

As another strategy, the pollen was extracted from 15 g of dried chamomile flowers by infusion with 500 mL of acetone during 30 min at 500 rpm and 25 °C. Acetonic infusion was filtered through 50 μm and 30 μm mesh fitted stainless steel sieves followed by a paper filter, employing vacuum. Acetone eluant was recovered and added to the acetone- treated chamomile. Incubation and filtering process were repeated until no visible pollen was recovered from the acetonic infusion (i.e., five extractions). Pollen was then rinsed with fresh acetone, dried at 60 °C for 24 h and stored in a desiccant chamber until use. Acetone eluant was concentrated by rotary evaporation and the concentrated extract was recovered for analysis.

2.3.2. Extraction of Pollenkitt of Chamomile Pollen

Unprocessed chamomile pollen obtained by mechanical sieving, was treated as described for sunflower pollen (Section 2.2), maintaining the 1:10 ratio (*w*/*v*). In the case of pollen already extracted with acetone, only the extraction process of hydrophilic compounds was performed, as described above.

2.3.3. Elimination of Sporoplasm, Production of Hollow Chamomile Pollen with Acids

Acetone–water-treated pollen was incubated with concentrated acid (HCl, $HClO_4$, H_3PO_4) at 1:10 ratio (*w*/*v*) in a bath at 70 °C for 5 h under gentle stirring at 300 rpm. For the time course study, acetone–water-treated pollen was incubated with H_3PO_4 at 1:10 ratio (*w*/*v*) for 1 to 14 h under the same conditions. Filtering and washing processes wereperformed as described in Section 2.2.2.

2.4. Analytical Measurements

All analytical measurements were performed at the analytical facilities of the University of Santiago de Compostela (RIAIDT).

2.4.1. Fourier Transform Infrared Spectroscopy (FTIR)

FITR technique was employed to explore the different functional groups present in the pollen samples [26] after each purification step as well as in the obtained eluates. FTIR spectra were recorded in a VARIAN FT-IR 670 (Varian Inc. Scientific Instr., Palo Alto, CA, USA) equipped with an attenuated total reflectance (ATR) accessory (GladiATR, PIKE technologies, Madison, WI, USA) from 400 to 4000 cm^{-1} at 4 cm^{-1} resolution using 64 scans.

2.4.2. Elemental CHN Analysis

The CHN analyses were carried out using an EA1108 CHNS-O Elemental Analyzer (Fisons Instrument, Mt Pleasant, NJ, USA). Protein content of samples was estimated using the percent of nitrogen content with a conversion factor of 6.25 [10].

2.4.3. Scanning Electron Microscopy (SEM) Analysis

Pollen grains were analyzed in a field emission scanning electron microscopy (Fesem Ultra Plus, Zeiss, Jena, Germany). Samples were deposited in a carbon tape and covered with iridium. Micrographs were recorded with an acceleration voltage of 3.00 kV at different magnifications (5000×, 20,000× or 30,000×).

2.4.4. Confocal Laser Scanning Microscopy (CLSM)

Internal and external structures of treated pollen grains were studied by CLSM (SP5 Leica

AOBS-SP5, Leica Biosystems Nussloch GmbH, Wetzlar, Germany) employing the natural autofluorescence of pollen (λex: 405 nm, λem: 414–479 nm; λex: 492 nm, λem: 505–554;λex: 561 nm, λem: 571–635 nm) [27].

2.4.5. Determination of Pollen Density and Number of Grains per Unit of Mass

Tapped density of pollen samples was determined by gravimetry of five different volumes of pollen with a graduated cylinder. Pollen was manually tapped for 5 min until no variations in the volume were observed. Tapped density was measured with three different batches per group. Number of grains per unit of mass was calculated using a haemocytometer (Neubauer chamber, Paul Marienfeld GmbH & Co. KG, Lauda-Königshofen, Germany) [28], where 1 mg of pollen sample was resuspended in 1 mL of water and immediately counted by optical microscopy. Number of grains per unit of mass was measured in triplicate employing three batches for each sample.

2.4.6. Thermal Gravimetric Analysis (TGA)

The thermal properties of the different pollen samples were investigated using TGA analyses (TGA/DSC 1–Thermogravimetric Analyzer; Mettler Toledo GmbH, Schwarzen bach, Switzerland) performed in N_2 atmosphere. Samples were analyzed in an alumina pan at 10 °C/min as heating rate. Differential thermal gravimetry analysis was calculated employing the OriginPro 2017 software (Origin Lab Corporation, Northampton, MA, USA).

Statistical Analysis

Statistical significance of the difference between the means was determined by analysis of variance (ANOVA) followed by pairwise multiple comparison using Tukey's HSD method. Pair comparisons were evaluated by Student t-tests. All tests were performed with Statgraphics centurion XVIII software (Statgraphics Technologies, Inc. The Plains, VA, USA). Differences were considered significant at $p < 0.05$.

3. RESULTS AND DISCUSSION

3.1. Extraction of the Pollenkitt: Sunflower Pollen

Sunflower pollen (**Figure 2**) was selected for the optimization and validation of the purification method because of its echinate and tricolporate structure, which makes it an interesting candidate from a technological standpoint. Sunflower pollen grains are composed by a multilayer structure covered by an external layer named pollenkitt. This layer fills the nanopores on the surface (Figure 2A) and is prone to contain environmental contaminants and allergens, such as coat proteins [25]. To remove the pollenkitt, a sequential treatment was designed based on the different solubility of coating materials and sporopollenin [29]. To study the components removed on each step, both the purification extracts and pollen were studied by SEM and FTIR analyses (Figure 2E), techniques widely employed for the identification of pollen species and biomaterials [30–32].

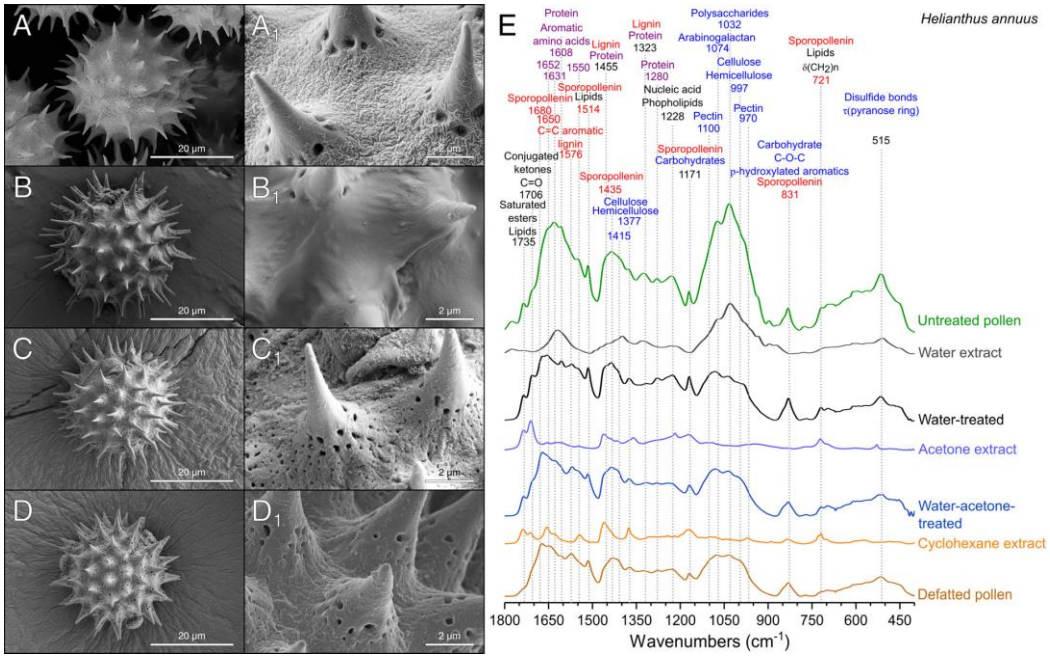

Figure 2. Scanning electron micrographs of sunflower pollen samples (**A**–**D**). (**A**). Untreated pollen. (**B**). Water-treated pollen. (**C**). Water-treated pollen after treatment with acetone. (**D**). Defatted sunflower pollen. (**E**). ATR-FTIR spectra of sunflower pollen samples and extracts obtained during the purification depicting characteristic bands.

Untreated samples presented the typical morphology of raw sunflower pollen with the surface completely coated with pollenkitt (Figure 2A), as well as their characteristic FTIR spectrum [26] (Figure 2E). We analyzed sunflower pollen from two different origins: Spain, and Czech Republic. Both samples presented the same FTIR bands but with varia-tions in their relative intensities, particularly for the signals assignable to proteins and polysaccharides (Figure S1A). Water-soluble and debris materials from the exterior of raw pollen (Figure 2A) were more efficiently extracted with purified water at 25°C than at 60°C, possibly due to the denaturalization of proteins at temperatures over 55°C. After this step, the spectra of sunflower pollen from both origins were similar (Figure S1A). The water-washing treatment mainly extracted carbohydrates [33,34] and proteins [35,36] (Figure 2E), which represented 46% of the raw pollen mass (**Figure 3A**).

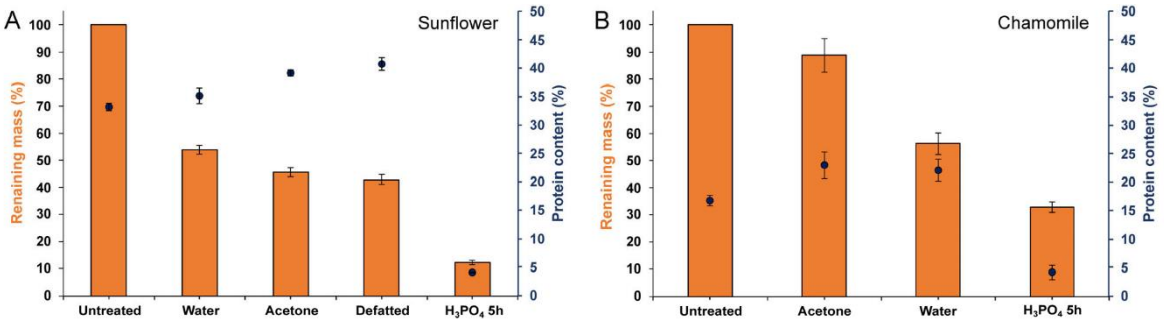

Figure 3. Remaining mass (bars) and protein content (% of remaining mass, dots) of pollen samples during purification process. (**A**). Sunflower. (**B**). Chamomile. Error bars represent the standard deviation of the mean (n = 3).

As expected, this treatment did not fully eliminate coating materials, and therefore, nanopores of the pollen wall were still not clearly uncovered (Figure 2B). This preliminary water-washing

step is unfrequently used in the literature, where it is more common to treat pollen directly with organic solvents. However, polysaccharides and proteins are poorly soluble in organic solvents [37], which leads to suboptimal purification of the samples. Once water-soluble subproducts were removed, the extraction of the lipophilic compounds of pollenkitt was assayed using a combined sequential treatment of acetone and cyclohexane. Prolonged incubation in hot acetone is another widely employed method to produce defatted pollen [27,38,39], but similar results could be obtained with shorter extractions processes [40]. In this study, the short washing with acetone at 25 °C (Figure 2C) extracted α-linolenic acid (3008, 1220, 721, 606, 486 cm^{-1}), lauric acid (2922 and 2852 cm^{-1}), stearic acid (1113 cm^{-1}), and other lipids (1711, 1462, 1415 cm^{-1}) [41,42]. The bands of compounds such as aliphatic esters (1173 cm^{-1}) [43], carboxylic groups (970 and 948 cm^{-1}) [34,44], and phenols (1620 cm^{-1}) [45] were also present in the spectra of the acetone extract. As compared to hot acetone extraction, our low temperature process could be advantageous as it should reduce any thermal alteration of the product. After this step, sunflower pollen became white, indicative of the removal of flavonoids and carotenoid pigments [26], and product mass was reduced by approximately 8% (Figure 3A). Acetone washing was unable to eliminate saturated lipids and proteins, as shown by FTIR bands at 1735 cm^{-1} (Figure 2E). To improve the extraction of these insoluble compounds [25], an additional cyclohexane washing step was performed. This allowed the elimination of surface components without causing morphological changes in the exine (Figure 2D). Lipid and protein extraction (Figure 2E) [25] was confirmed by the disappearance of the bands at 1735 cm^{-1} (saturated esters [45]), 1655, 1627, 1608, 1547, and 1455 cm^{-1} (proteins [35,36]), and 1455, 720 cm^{-1} (lipids [41]). The analysis of the cyclohexane extract (Figure 2E) showed the presence of additional compounds, such as pectin, with a signal at 970 cm^{-1} [46]. Cyclohexane extraction represented a further mass reduction of 2.6% from the raw pollen mass (Figure 3A). The accumulated percent of mass corresponding to the lipid phase of the pollenkitt (~10%, Figure 3A) was in line with the lipid content previously reported for sunflower pollen [26,47]. After treatment with cyclohexane, the bands assigned to sporopollenin [48] became evident in the spectra (Figure 2E), indicating the successful cleaning of the pollen surface.

Albeit not abundant in *H. annuus*, proteins and glycoproteins are the principal allergenic compounds found in pollen [49]. Therefore, protein elimination is a critical point for pollen purification when considering pharmaceutical applications. The protein content of the samples was calculated from the nitrogen content determined by CHN elemental analysis (Figure 3A). Protein percent of raw sunflower pollen was initially ~33 wt%, and this fraction rose to ~40 wt% after pollenkitt elimination. This value was higher than that previously reported for commercial defatted sunflower pollen grains (~32 wt% of proteins) [10,17]. The relative increase in the protein content of defatted sunflower pollen, as compared with the untreated one, can be explained by the elimination of lipids and polysaccharides, rich in C and H but without N, and by the reduction of the relative mass by dehydration. Protein removal from this product, leading to hollow sporopollenin microcapsules, was undertaken in a subsequent step (Section 3.3).

3.2.Extraction of Pollenkitt: Chamomile Pollen

Considering the results obtained after the treatment of sunflower pollen, the applicability of the method was also tested for *M. chamomilla*, a widely studied medicinal plant, with an echinate pollen grain of smaller size (13–25 μm vs. 26–50 μm [23,24]). In contrast to sunflower, it is unusual to find commercially available *M. chamomilla* pollen. However, their dried flowers are universally available, and thus, we devised a cleaning protocol starting from this source (Figure 1).

The isolation of pollen by mechanical sieving from dried flowers was only feasible for small

batches, yielding a 0.2 ± 0.1% of pollen. This indicated an extraction below 10% since it is estimated that pollen represents the 2.5% of the weight of dried *Matricaria* sp. flowers [50]. Although still suboptimal, this extraction technique was the only one that allowed the obtention of pollen with intact pollenkitt coating (Figure 4A). Due to the low productivity of mechanical sieving, several alternative methods for pollen recovery were assayed, such as initial pollen extraction with water or acetone. Water extraction of chamomile pollen from dried flowers produced the release of mucilage [21] that obturated the paper filters and hindered recovery, being eventually discarded as a pollen extraction method. On the other hand, when acetone was employed (Figure 1), pollen was easily recovered by filtration, allowing for scaling-up the process and achieving a pollen mass yield of 2.3 ± 0.1% with respect to the dried flowers (88.9 ± 6.2% *w/w* recovery, Figure 3B), close to the above-mentioned theoretical value [50]. This difference in the extraction efficacy can be attributed to the poor solubility of mucilage in acetone.

As compared to sunflower pollen grains (Figure 2A), chamomile pollen is smaller, and its exine layer is less covered with pollenkitt (**Figure 4A$_1$**). Due to these inherent differences, the protein content of raw chamomile pollen was found to be significantly lower (16.6 ± 0.9 wt%, Figure 3B) than that of raw sunflower pollen (Figure 3A). The FTIR spectra of unprocessed chamomile pollen (Figure 4D) was similar to sunflower (Figure 2E) except for changes in relative band intensities attributed to lipids, polysaccharides, cellulose, and the presence of minerals in chamomile. This similarity could be expected as both plants belong to the Asteraceae family [51]. The main differences were the absence of a 1774 cm^{-1} band of esterified pectin [52] present in sunflower (Figure 2E) and the presence of several bands corresponding to minerals in chamomile pollen (Figure 5B) [53], which were probably debris derived from flower harvesting.

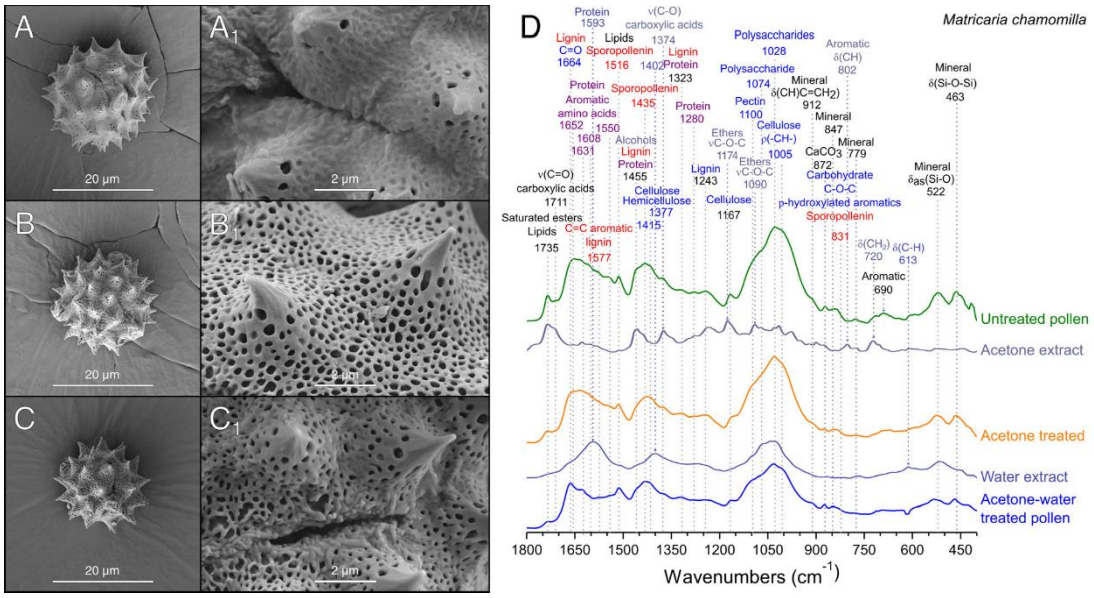

Figure 4. Scanning electron micrographs of chamomile pollen samples (**A**–**D**). (**A**). Untreated pollen. (**B**). Pollen treated with acetone. (**C**). Acetone–water-treated pollen. (**D**). ATR-FTIR spectra of pollen samples and extracts obtained during the elimination of pollenkitt.

After filtration and recovery of the pollen, the yellow eluant was concentrated in a rotavapor, and the recovered acetone was recycled for further pollen extraction. The extract was analyzed by FTIR (Figure 4D), and the presence of bands previously described for chamomile oil, such as ethers (1174, 1090 cm^{-1}) and carboxylic acids (1374 cm^{-1}), was found [54,55]. Therefore, we expect that this subproduct could be a starting point for the purification of therapeutically

significant bioactive compounds [21] in the future.
Untreated chamomile pollen had its exine pores filled with pollenkitt (Figure 4A), but these became clearly visible after acetone extraction (Figure 4B). The protein content of chamomile pollen treated with acetone was 22.9 ± 2.3 wt%, significantly higher than that of raw pollen (Figure 3B). This can be attributed to the elimination of hydrocarbon-rich compounds, as previously discussed for sunflower pollen in Section 3.1. Acetone extracted pollen was washed with water as described above, resulting in a slight reduction in average size (16 ± 3%) (Figure 4C). The water extract exhibited FTIR bands assignable to polysaccharides and proteins, and accordingly, the pollen spectrum showed a decrease in their corresponding bands (Figure 4E). The protein content remained similar (22.0 ± 1.9 wt%, no significant difference), although pollen mass was reduced by ~33% (Figure 3B). FTIR analysis showed that the main components extracted with water treatment consisted of proteins and polysaccharides (Figure 4E). The spectra of the defatted chamomile pollen (Figure S1B), treated with the protocol developed for sunflower (Figure 1), showed a less efficient removal of polysaccharides than the pollen only treated with acetone and water, suggesting that the use of cyclohexane is not required in this case. Hence, the following experiments were performed with acetone-water-treated pollen.

3.3. Comparison of Different Acid Treatments on the Purification of Pollen

Sporopollenin is generally described as a biopolymer highly resistant to acidolysis [6]; however, harsh acidic treatment can affect its ultrastructure [10]. Therefore, acidolysis processes were optimized herein to maximize solubilization and removal of internal components (proteins, polysaccharides, and lipids) while preserving the sporopollenin and pollen structure. Sunflower pollen presented different sensibility depending on the acid treatment used. For instance, CF_3COOH was unable to penetrate the pollen wall after 5 h at 70 °C while H_2SO_4 and HNO_3 completely destroyed their structure, even after 1 h incubation at room temperature. Among the assayed acids, HCl, $HClO_4$, and H_3PO_4 were the most effective removing the cellular content without affecting sporopollenin morphology and chemical composition (**Figure 5**). Treatment with HCl was unable to produce homogeneous hollow pollen grains (Figure 5A) but decreased protein and polysaccharide content (Figure 5D). The intense band at 1705 cm^{-1} suggests the formation of hydrochloride salts [56] and an increase in the formation of conjugated ketones (C=O stretching) after the degradation of lignin [57], which might indicate that HCl produced chemical modifications to the pollen structure and the degradation of the intine.
$HClO_4$ is a strong acid with oxidizing properties at high temperatures that has not been previously applied for sporopollenin purification. However, it has been used in the extraction and digestion of polysaccharides [39], polyamines [58], and proteins [59] in bee pollen and plant tissues. To study the suitability of this acid for pollen purification, a time course study was carried out with sunflower pollen using FTIR analysis and SEM images to evaluate the process (Figure S2). Results indicated that 5 h of treatment (Figure 5B) produced a cleaner intine as compared with shorter treatments (Figure S2). The percent of protein of $HClO_4$-treated samples decreased up to 9 wt% at 5 h, a similar value to that reported for samples treated for 20 h in HCl (~10 wt%) [10]. SEM images evidenced that $HClO_4$ treatment left residues on the exine surface (Figure $5B_1$), probably perchlorates that could also be detected through their FTIR band at 623 cm^{-1} [60] (Figure 5D and S3B). Although $HClO_4$ can be considered an alternative for the acid treatment of pollen, it produces chemical modifications in the pollen.

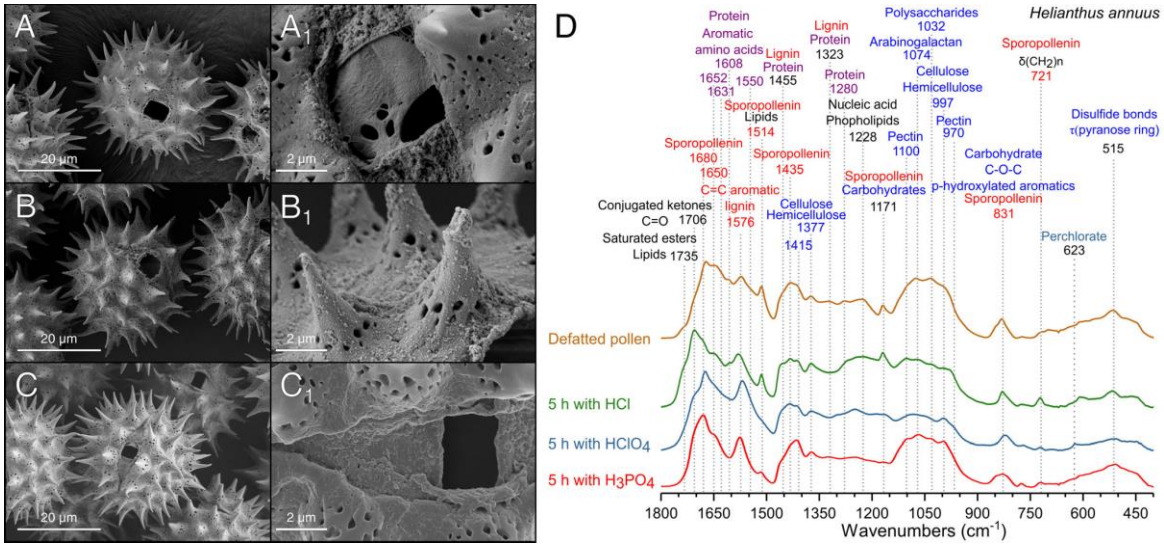

Figure 5. Scanning electron micrographs of defatted sunflower pollen treated with different acids. (**A**). HCl. (**B**). $HClO_4$. (**C**). H_3PO_4. (**D**). ATR-FTIR spectra of pollen samples after 5 h treatment.

H_3PO_4 yielded excellent results in the production of sunflower hollow pollen microcapsules (Figure 5C), as the relative intensity of the FTIR bands assignable to proteins (1631, 1608, 1550, 1455 cm^{-1}) and carbohydrates (1435, 1323, 1030 cm^{-1}) decreased sharply (Figure 5D) [41]. Treatment with H_3PO_4 did not reduce bands of hemicellulose and cellulose (Figure 5D), indicative of the preservation of intine, while the protein content after this treatment decreased to 4.4 ± 0.8 wt%. After H_3PO_4 treatment, the hollow sunflower microcapsules of different origin were indistinguishable in their FTIR spectra (Figure S1). Treatment with H_3PO_4 allowed the efficient production of hollow pollen, stable to dehydration or heating processes, without the requirement of additional neutralization steps. Optimization of this procedure is discussed in detail in Section 3.4.

In view of the results obtained with sunflower pollen, chamomile pollen was only treated with the best performing acids, i.e., HCl, $HClO_4$, and H_3PO_4 (**Figure 6**). The treatment with HCl for 5 h was not able to produce a homogeneous aperture of pollen (Figure 6A); however, protein bands reduced their relative intensity (Figure 6D), while bands related to polysaccharides and impurities remained unaltered.

HCl-treatment produced a shoulder at 1706 cm^{-1} in chamomile pollen, which, as observed in sunflower pollen (Figure 5D), is indicative of the formation of carboxylic acids [61]. The incubation with $HClO_4$ produced the aperture of the pollen (Figure 6B), but the signals of polysaccharides and mineral impurities did not decrease (Figure 6D). Perchlorate deposits were evident on the surface of the exine (Figure $6B_1$) and in the FTIR spectra (Figure 6D). The treatment with H_3PO_4 produced a uniform aperture of chamomile pollen grains (Figure 6C) and a drastic reduction of polysaccharides and protein bands (Figure 6D). The bands of mineral compounds present in chamomile pollen also disappeared from the FTIR spectra after H_3PO_4 treatment (Figure 6D). The efficacy of H_3PO_4 in the removal of minerals can be explained by its high reactivity forming soluble salts with metals such as calcium, aluminum, or iron [62], elements commonly found in minerals [53]. The treatment employed on sunflower showed similar results in chamomile, confirming that sunflower pollen was a good initial model that allowed the extension of the study to other members of the Asteraceae family.

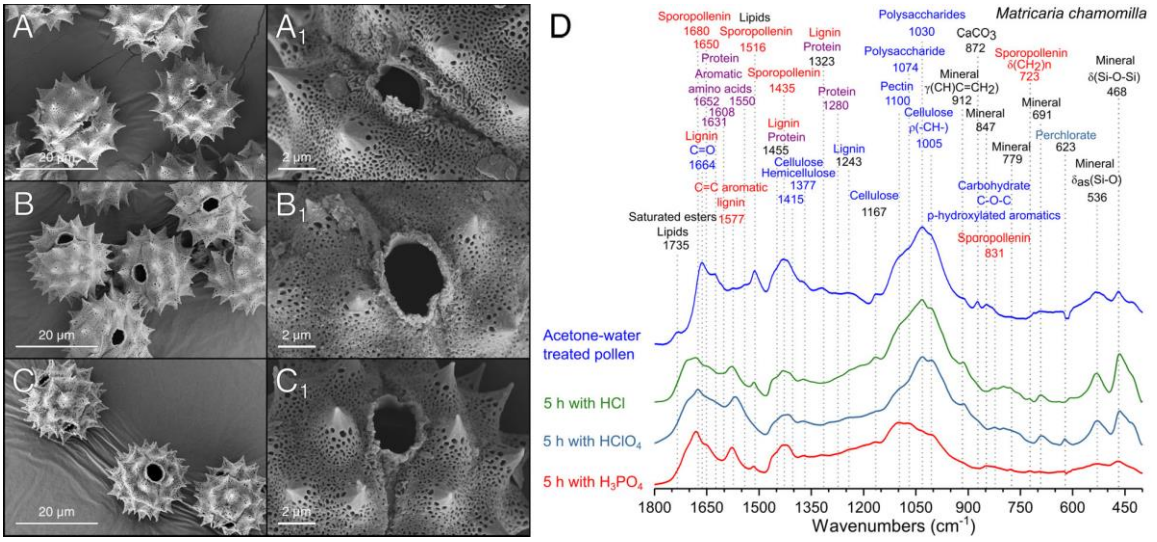

Figure 6. Scanning electron micrographs of acetone-water-treated chamomile pollen incubated with different acids. (**A**). HCl. (**B**). $HClO_4$. (**C**). H_3PO_4. (**D**). FTIR spectra of pollen samples after 5 h treatment.

3.4. Optimization of the Treatment with H_3PO_4

Since H_3PO_4 showed the best results in the production of hollow pollen microcapsules for both sunflower and chamomile (Figures 5C and 6C), we analyzed the time course of the purification process by confocal laser scanning microscopy (CLSM) and FTIR. CLSM has been employed as a reference technique in the characterization of sporopollenin microcapsules [17,18,27,45] due to the strong natural autofluorescence of pollen grains, derived from sporopollenin, flavonoids, and carotenoids [63]. Untreated sunflower pollen (**Figure 7A**) showed a strong overlapping fluorescence, hindering a clear distinction of the pollen layers. Defatted sunflower pollen presented a more defined autofluorescence pattern, with an internal cavity with a strong fluorescence (Figure 7B), due to the proteins and coenzymes present in the sporoplasm [63].

One hour of treatment with H_3PO_4 did not lead to large differences on defatted sunflower pollen (data not shown), but the permeabilization of the outer layer was observed after 2 h of treatment (Figure 7C), when sporoplasm components accumulated into the apertures. Definitive disappearance of the sporoplasm was not evident until 3 h (Figure 7D). At this point, fluorescent compounds remaining in exine and intine allowed a clear distinction between those layers. Pollen incubated with H_3PO_4 for 5 h (Figure 7E) had lower overall fluorescence but similar levels of autofluorescence of exine and intine. The lack of internal fluorescence confirmed the elimination of the sporoplasm [10]. For samples incubated for 14 h in H_3PO_4 (Figure 7F), the intine fluorescence signal decreased, and it appeared clearly detached from exine. This process led to unstable and fragile structures [64]. Despite the morphological changes, during the first 2 h of treatment there were no differences in the FTIR spectra as compared to defatted pollen. After 3 and 5 h of treatment with H_3PO_4, the bands of protein (1631, 1608, 1550, 1455 cm^{-1}) and carbohydrates (1435, 1323, 1030 cm^{-1}) virtually disappeared from FTIR spectra.

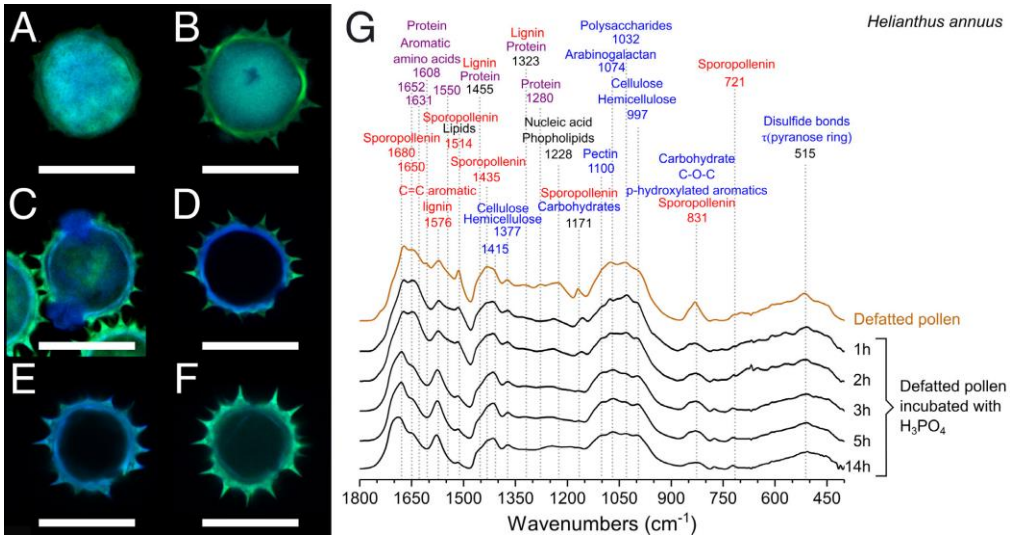

Figure 7. Confocal laser scanning micrographs of sunflower pollen samples. (**A**). Untreated pollen. (**B**). Defatted pollen. (**C**–**F**). Defatted pollen treated with H_3PO_4, 70 °C. (**C**). 2 h. (**D**). 3 h. (**E**). 5 h. (**F**). 14 h. Green channel: Exine. Blue channel: Intine and sporoplasm. (Scale bars represent 30 µm). (**G**). FTIR spectra of defatted pollen treated with H_3PO_4 at 70 °C fordifferent time points.

Our results confirmed that 5 h of treatment with H_3PO_4 were enough to produce hollow pollen microcapsules [17] resistant to dehydration or heating processes. After 5 h, the mass of the pollen was reduced by a total 30% compared to defatted samples and represented 12% of the raw pollen (Figure 3A). Because of the treatment (Table S1), sunflower hollow pollen (0.13 ± 0.01 g/cm^3, ~2.5 × 10^5 grains/mg,) had approximately three times less density than defatted (0.38 ± 0.06 g/cm^3, ~9.0 × 10^4 grains/mg). Protein content and morphology of hollow sunflower pollen obtained by this method were comparable to those reported for 5 h [17] and 10 h [10,17] treatments with H_3PO_4 after intensive washing procedures.

Chamomile pollen exine has a columnar structure and it forms a thicker wall (**Figure 8**) than sunflower exine (Figure 7). Its diffuse autofluorescence did not allow for differentiation of the intine. In addition, chamomile pollen was more sensitive to acid treatment than sunflower. After 1h of incubation, these pollen grains had already lost the sporoplasm fluorescence (Figure 8B), and the protein bands in FTIR (Figure 9G) reduced their relative intensity. The main difference observed as function of the incubation periods was polysaccharide content (1008, 1032 cm^{-1}) [41], which decreased with time. FTIR spectra and CLSM images of 5 h and 14 h treatments were almost identical (Figure 8G); however, a shoulder in the FTIR at 14 h at 1710 cm^{-1} indicated the oxidation of the sporopollenin [41,66]. The protein content and the remaining mass of chamomile pollen treated with H_3PO_4 were also similar among the incubation periods, stabilizing at 4.0 ± 1.3 wt% after 5 h. In contrast to sunflower pollen, the mass of hollow chamomile pollen represented 33% of the grain mass (Figure 3B). Similar to sunflower pollen (Table S1), 5 h H_3PO_4-treated chamomile pollen had significantly lower density (0.14 ± 0.01 g/cm^3, 1.0 × 10^6 grains/mg) than defatted pollen (0.44 ± 0.02 g/cm^3, 5.1 × 10^5 grains/mg).

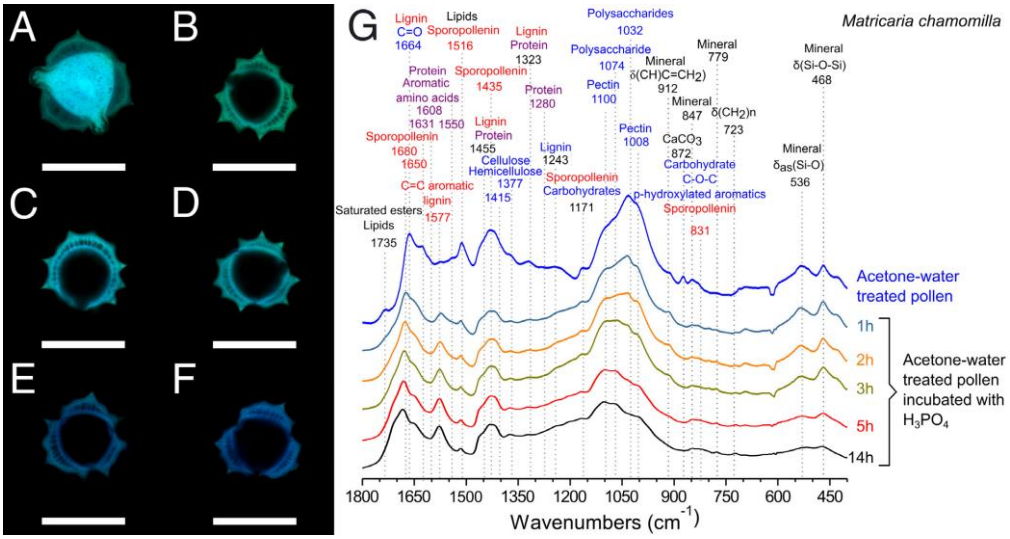

Figure 8. Confocal laser scanning micrographs of chamomile pollen samples. (**A**). Acetone-water-treated pollen. (**B**–**F**). Acetone-water-treated pollen incubated with H_3PO_4, 70 °C. (**B**). 1 h. (**C**). 2 h. (**D**). 3 h. (**E**). 5 h. (**F**). 14 h. Green channel: Exine. Blue channel: Intine and sporoplasm. (Scale bars represent 20 µm). (**G**). FTIR spectra of acetone-water-treated pol- len treated with H_3PO_4, 70 °C for different time points.

H_3PO_4 has been previously explored by other authors for the purification of hollow pollen grains. Nevertheless, those protocols involve extended incubation periods of defatting and acid treatment, with complex washing and neutralization processes, through multiple steps with organic solvents, acids, and bases [10,17,18,27]. The most common method for producing hollow pollen requires extensive treatments to eliminate acid residues, involving multiple washing steps, e.g.: water (5×), acetone (2×), 2M HCl, water (5×), acetone and ethanol (2×) [10,17,18]. The method proposed in this work (Figure 1) drastically reduces and shortens treatment and washing procedures (6 h of defatting at high temperature, > 10 steps after acidolysis vs. 10 min at room temperature and five steps of washing) and allowed the obtention of hollow pollen microcapsules with low protein content and preserved morphology, starting from pollen of different species and geographical origin.

3.5. Thermogravimetric Characterization of Hollow Pollen Platforms

Raw, defatted, hollow sunflower and chamomile pollen were analyzed by TGA (**Figure 9**, Table S2) to identify their thermal decomposition pattern. All samples showed a slight weight loss at low temperature (100 °C) due to the evaporation of absorbed water and humidity. Untreated sunflower pollen showed the highest variation of weight (ΔW) due to dehydration (Figure 9A), while defatted (Figure 9B) and hollow pollen followed a similar dehydration process (Figure 9C). Untreated sunflower pollen presented a thermal decomposition range (*T*onset) with five main stages (100–170 °C, volatile compounds; 170–250 °C, pectin and lipids; 250–300 °C, polysaccharides, proteins, lipids; 300–370 °C, cellulose, hemicellulose, sporopollenin; 370–480 °C, lignin, sporopollenin) [67–70], whereas defatted pollen and hollow pollen thermal decomposition was limited to three stages. Defatted pollen (Figure 9B, Table S2) presented the highest ΔW with a temperature of decomposition (*T*d) of ~320 °C (*T*onset: 225–400 °C, ΔW: 40%), in the case of hollow pollen (Figure 9C, Table S2) the main ΔW occurred at *T*d ~440 °C (*T*onset: 360–530 °C, ΔW: 38%). Similar *T*d has been reported for sporopollenin [70].

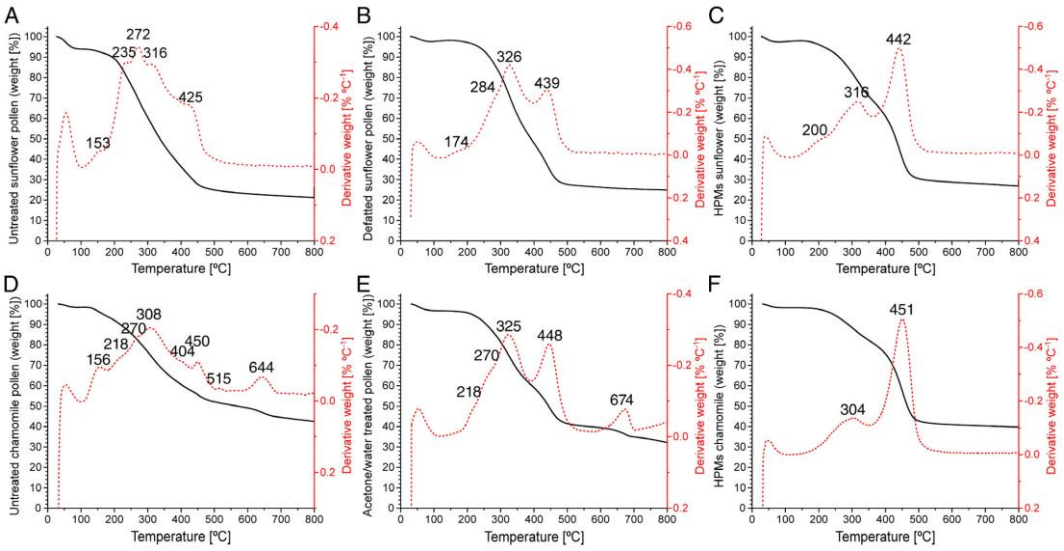

Figure 9. Thermogravimetric analysis of different pollen samples. (**A**). Untreated sunflower pollen. (**B**). Defatted sun- flower pollen. (**C**). Sunflower hollow pollen microcapsules. (**D**). Untreated chamomile pollen. (**E**). Defatted chamomile pollen. (**F**). Chamomile hollow pollen microcapsules. Black line: Weight percentage (%). Red dotted line: Derived thermo- gravimetry.

In the case of chamomile pollen, untreated pollen presented a complex decomposition pattern (Figure 9D, Table S2), indicating a higher percent of volatile compounds. Similarly, chamomile pollen had a lower percentage of lipids than sunflower pollen. In addition to that, the presence of Td at 515 °C and 644 °C indicated the presence of mineral components in the sample, aligning with the results obtained by FTIR (Figure 4D). After cleaning of the pollenkitt, the thermal degradation pattern of chamomile pollen was simplified. The ΔW attributable to sporopollenin increased up to 21%, but mineral debris was still present, as indicated by the *T*d at 674 (Figure 9E).

Despite sunflower and chamomile pollen (Figures 5 and 6) having differences in size (Table S1) and morphology (Figure 9A, D), the thermal degradation pattern of hollow chamomile pollen (Figure 9F, Table S2) was similar to sunflower (Figure 9C), indicating that, at this stage, both capsules have a very similar composition. In addition, after the purification with acid, the ΔW attributable to mineral compounds was absent, indicating that this treatment successfully cleaned these impurities. These results suggest that the main components of hollow pollen microcapsules were cellulose and sporopollenin, while defatted pollen had a higher content of polysaccharides and proteins, supporting the results obtained with other techniques.

3.6. Comparison between Hollow Sporopollenin Microcapsules from Sunflower and Chamomile

Sunflower and chamomile belong to the same family, Asteraceae [51], characterized by pollen grains with three apertures and an echinate surface [23,24]. However, they pre- sent considerable differences regarding their size (Table S1). In fact, the inner cavity of hollow sunflower pollen is approximately the same size of the entire hollow chamomile pollen (Table S1). Interestingly, the apertures of both pollens are similar, with 5.2 ± 0.6 µm × 3.4 ± 0.4 µm for sunflower and 4.0 ± 0.1 µm × 2.9 ± 0.6 µm ± 0.4 µm for chamomile, respectively. On the other hand, even though they do not present significant difference intheir densities (Table S1), the number of chamomile grains per unit of mass is one order of magnitude higher than sunflower (Table S1). This effect can be explained by their similar composition and different size (Figures 5D, 6D, and Table S1). The structure of the

exine is also different between species (Figures 7E and 8E). Chamomile has a thicker columnar structure connected with the exterior by nanopores. In the case of sunflower, those pores are mainly located on the base of the spines (Figure 5C1), while in chamomile their distribution is homogeneous along the surface (Figure 6C1). These differences may affect the capacity for loading and releasing substances. Both hollow pollens have similar composition (Figures 5D, 6D, and Table S1) and can be processed by the same procedure, but their different structural characteristics should play an important role in the loading and release of active ingredients. Moreover, hollow chamomile pollen could serve as an alternative to other small pollens with higher allergenicity, such as ragweed [38], for a variety of biomedical applications.

4. CONCLUSIONS

We have proposed an abridged protocol to produce pristine hollow sporopollenin microcapsules, as well as their complete physicochemical characterization throughout the purification process. The developed protocol can be applied to pollens from different species and/or origins, and it provides a faster and simplified procedure compared to those previously reported in the literature. By using this method, we also provide the first report on the production and characterization of purified pollen microcapsules from chamomile. Chamomile microcapsules present a nanoporous surface and a columnar inner structure of great interest for drug loading and release. In summary, the structure and characteristic of hollow sporopollenin microcapsules generated by the described purification methods make them promising candidates as devices for pharmaceutical applications.

PATENTS

M.G.-F. and N.C. are coinventors of the patents P201730151, P201730152 extended as PCT/ES2018/070092 “Purified pollen particles, their processing and application for the delivery of nanosystems”.

SUPPLEMENTARY MATERIALS

The following results are available online at www.mdpi.com/2073- 4360/13/13/2094/s1, Figure S1: ATR-FTIR spectra of pollen samples. A. Comparison spectra of sunflower pollen from Spain and Czech Republic. B. Spectra of chamomile pollen treated with extended extraction protocol, Figure S2: Time course study of the treatment of defatted sunflower pollen with $HClO_4$. A. SEM images at different magnifications. B. ATR-FTIR spectra of pollen samples indicating the band assignment, Table S1: Principal characteristics of sunflower and chamomile pollen samples, Table S2: TGA results for sunflower and chamomile pollen samples.

AUTHOR CONTRIBUTIONS

Conceptualization, J.M.A., M.G.-F., and N.C.; methodology, J.M.A.; validation, J.M.A.; investigation, J.M.A., S.R., and L.V.-F.; writing—original draft preparation, J.M.A. and S.R.; writing—review and editing, M.G.-F. and N.C.; supervision, M.G.-F. and N.C.; project administration and funding acquisition, N.C. All authors have read and agreed to the published version of the manuscript.

FUNDING

This work has received financial support from the Xunta de Galicia (Centro singular de investigación de Galicia, accreditation 2019-2022), the European Union (European Regional Development Fund—ERDF), and Ministerio de Ciencia e Innovación, Gobierno de España FEDER (PID2019-107500RB-I00 and ERC2018-092841).

DATA AVAILABILITY STATEMENT

Data presented in this study are available on request from the corresponding author.

ACKNOWLEDGMENTS

Authors would like to thank Raquel Antón Segurado for the acquisition of FESEM images, Ezequiel Vazquez Fernandez for FTIR analysis, both from the "Centro de Apoyo Científico y Tecnológico de la Universidad (CACTUS)" of the University of Santiago de Compostela.

CONFLICTS OF INTEREST

The authors declare no conflict of interest.

REFERENCES

1. Jiang, J.; Zhang, Z.; Cao, J. Pollen wall development: The associated enzymes and metabolic pathways. *Plant Biol.* **2013**, *15*, 249– 263, doi:10.1111/j.1438-8677.2012.00706.x.
2. Mackenzie, G.; Beckett, S.; Atkin, S.; Diego-Taboada, A. Pollen and spore shells—Nature's microcapsules. In *Microencapsulation in the Food Industry*; Academic Press: Cambridge, MA, USA, 2014; ISBN 9780124045682.
3. Punt, W.; Hoen, P.P.; Blackmore, S.; Nilsson, S.; Le Thomas, A. Glossary of pollen and spore terminology. *Rev. Palaeobot. Palynol.* **2007**, *143*, 1–81, doi:10.1016/j.revpalbo.2006.06.008.
4. Knox, R.B. The Pollen Grain. In *Embryology of Angiosperms*; Johri, B.M., Ed.; Springer: Berlin/Heidelberg, Germany, 1984; pp. 197–271; ISBN 9783642693045.
5. Qu, Z.; Meredith, J.C. The atypically high modulus of pollen exine. *J. R. Soc. Interface* **2018**, *15*, 20180533, doi:10.1098/rsif.2018.0533.
6. Mackenzie, G.; Boa, A.N.; Diego-Taboada, A.; Atkin, S.L.; Sathyapalan, T. Sporopollenin, The Least Known Yet Toughest Nat- ural Biopolymer. *Front. Mater.* **2015**, *2*, 66, doi:10.3389/fmats.2015.00066.
7. Li, F.; Phyo, P.; Jacobowitz, J.; Hong, M.; Weng, J. The molecular structure of plant sporopollenin. *Nat. Plants* **2019**, *5*, 41–46, doi:10.1038/s41477-018-0330-7.
8. Wang, Y.; Shang, L.; Chen, G.; Shao, C.; Liu, Y.; Lu, P.; Rong, F.; Zhao, Y. Pollen-inspired microparticles with strong adhesion for drug delivery. *Appl. Mater. Today* **2018**, *13*, 303–309, doi:10.1016/j.apmt.2018.09.016.
9. Traidl-Hoffmann, C.; Kasche, A.; Menzel, A.; Jakob, T.; Thiel, M.; Ring, J.; Behrendt, H. Impact of Pollen on Human Health: More Than Allergen Carriers? *Int. Arch. Allergy Immunol.* **2003**, *131*, 1–13, doi:10.1159/000070428.
10. Mundargi, R.C.; Potroz, M.G.; Park, J.H.; Seo, J.; Lee, J.H.; Cho, N.-J. Extraction of sporopollenin exine capsules from sunflower pollen grains. *RSC Adv.* **2016**, *6*, 16533–16539, doi:10.1039/C5RA27207F.
11. Fan, T.; Park, S.; Shi, Q.; Zhang, X.; Liu, Q.; Song, Y.; Chin, H.; Shahrudin, M.; Ibrahim,

B.; Mokrzecka, N.; et al. Transformation of hard pollen into soft matter. *Nat. Commun.* **2020**, *11*, 1449, doi:10.1038/s41467-020-15294-w.

12. Gonzalez-Cruz, P.; Uddin, M.J.; Atwe, S.U.; Abidi, N.; Gill, H.S. Chemical Treatment Method for Obtaining Clean and Intact Pollen Shells of Different Species. *ACS Biomater. Sci. Eng.* **2018**, *4*, 2319–2329, doi:10.1021/acsbiomaterials.8b00304.
13. Diego-Taboada, A.; Maillet, L.; Banoub, J.H.; Lorch, M.; Rigby, A.S.; Boa, A.N.; Atkin, S.L.; Mackenzie, G. Protein free micro- capsules obtained from plant spores as a model for drug delivery: Ibuprofen encapsulation, release and taste masking. *J. Mater. Chem. B* **2013**, *1*, 707–713, doi:10.1039/c2tb00228k.
14. Dyab, A.K.F.; Mohamed, M.A.; Meligi, N.M.; Mohamed, S.K. Encapsulation of erythromycin and bacitracin antibiotics into natural sporopollenin microcapsules: Antibacterial, cytotoxicity, in vitro and in vivo release studies for enhanced bioavailability. *RSC Adv.* **2018**, *8*, 33432–33444, doi:10.1039/C8RA05499A.
15. Wakil, A.; MacKenzie, G.; Diego-Taboada, A.; Bell, J.G.; Atkin, S.L. Enhanced bioavailability of eicosapentaenoic acid from fish oil after encapsulation within plant spore exines as microcapsules. *Lipids* **2010**, *45*, 645–649, doi:10.1007/s11745-010-3427-y.
16. Hamad, S.A.; Dyab, A.F.K.; Stoyanov, S.D.; Paunov, V.N. Encapsulation of living cells into sporopollenin microcapsules. *J. Mater. Chem.* **2011**, *21*, 18018–18023, doi:10.1039/c1jm13719k.
17. Potroz, M.G.; Mundargi, R.C.; Gillissen, J.J.; Tan, E.-L.; Meker, S.; Park, J.H.; Jung, H.; Park, S.; Cho, D.; Bang, S.-I.; et al. Plant-Based Hollow Microcapsules for Oral Delivery Applications: Toward Optimized Loading and Controlled Release. *Adv. Funct. Mater.* **2017**, *27*, 1700270, doi:10.1002/adfm.201700270.
18. Fan, T.; Park, J.H.; Pham, Q.A.; Tan, E.-L.; Mundargi, R.C.; Potroz, M.G.; Jung, H.; Cho, N.-J. Extraction of cage-like sporopol- lenin exine capsules from dandelion pollen grains. *Sci. Rep.* **2018**, *8*, 6565, doi:10.1038/s41598-018-24336-9.
19. Maric, T.; Nasir, M.Z.M.; Rosli, N.F.; Budanović, M.; Webster, R.D.; Cho, N.-J.; Pumera, M. Microrobots Derived from Variety Plant Pollen Grains for Efficient Environmental Clean Up and as an Anti-Cancer Drug Carrier. *Adv. Funct. Mater.* **2020**, *30*, 2000112, doi:10.1002/adfm.202000112.
20. Elmacı, G. Magnetic Hollow Biocomposites Prepared from *Lycopodium clavatum* Pollens as Efficient Recyclable Catalyst. *Chem- istrySelect* **2020**, *5*, 2225–2231, doi:10.1002/slct.201904152.
21. Singh, O.; Khanam, Z.; Misra, N.; Srivastava, M.K. Chamomile (*Matricaria chamomilla L.*): An overview. *Pharmacogn. Rev.* **2011**, *5*, 82–95, doi:10.4103/0973-7847.79103.
22. McKay, D.L.; Blumberg, J.B. A Review of the bioactivity and potential health benefits of chamomile tea (*Matricaria recutita* L.). *Phyther. Res.* **2006**, *20*, 519–530, doi:10.1002/ptr.1900.
23. Halbritter, H. *Matricaria chamomilla*. Available online: https://www.paldat.org/pub/Matricaria_chamomilla/301539;jsessionid=9C42510DC1E00F411213816DA650466B (accessed on 22 March 2021).
24. Halbritter, H.; Heig, H.; Svojtka, N. *Helianthus annuus*. Available online: https://www.paldat.org/pub/Helianthus_an- nuus/304619 (accessed on 2 April 2021).
25. Bashir, M.E.H.; Ward, J.M.; Cummings, M.; Karrar, E.E.; Root, M.; Mohamed, A.B.A.; Naclerio, R.M.; Preuss, D. Dual Function of Novel Pollen Coat (Surface) Proteins: IgE-

binding Capacity and Proteolytic Activity Disrupting the Airway Epithelial Barrier. *PLoS ONE* **2013**, *8*, e53337, doi:10.1371/journal.pone.0053337.

26. Sánchez Juárez, D.L.; Martínez Montes, G.; Rubio Rosas, E. Chemical Characterization of Yellow and Orange Pollen *(Helianthus annuus)* and its Effect in the Growth of Hydroxyapatite. *Mater. Sci. Forum* **2013**, *755*, 163–169, doi:10.4028/www.scientific.net/MSF.755.163.
27. Mundargi, R.C.; Potroz, M.G.; Park, J.H.; Seo, J.; Tan, E.-L.; Lee, J.H.; Cho, N.-J. Eco-friendly streamlined process for sporopol-lenin exine capsule extraction. *Sci. Rep.* **2016**, *6*, 1–14, doi:10.1038/srep19960.
28. Delaplane, K.S.; Dag, A.; Danka, R.G.; Freitas, B.M.; Garibaldi, L.A.; Goodwin, R.M.; Hormaza, J.I. Standard methods for polli- nation research with Apis mellifera. *J. Apic. Res.* **2013**, *52*, 1–28, doi:10.3896/IBRA.1.52.4.12.
29. Lin, H.; Gomez, I.; Meredith, J.C. Pollenkitt wetting mechanism enables species-specific tunable pollen adhesion. *Langmuir* **2013**, *29*, 3012–3023, doi:10.1021/la305144z.
30. Pappas, C.S.; Tarantilis, P.A.; Harizanis, P.C.; Polissiou, M.G. New Method for Pollen Identication by FT-IR Spectroscopy. *Appl. Spectrosc.* **2003**, *57*, 23–27.
31. Buta, E.; Cantor, M.; Tefan, R.; Pop, R.; Mitre, I.; Buta, M.; Sestra, R.E. FT-IR Characterization of Pollen Biochemistry, Viability, and Germination Capacity in Saintpaulia H. Wendl. Genotypes. *J. Spectrosc.* **2015**, *2015*, 1–7, doi:10.1155/2015/706370.
32. Anjos, O.; Santos, A.J.A.; Dias, T.; Estevinho, L.M. Application of FTIR-ATR spectroscopy on the bee pollen characterization. *J. Apic. Res.* **2017**, *8839*, 1–9, doi:10.1080/00218839.2017.1289657.
33. Grube, M.; Bekers, M.; Upite, D.; Kaminska, E. Infrared spectra of some fructans. *Spectroscopy* **2002**, *16*, 289–296, doi:10.1155/2002/637587.
34. Wiercigroch, E.; Szafraniec, E.; Czamara, K.; Pacia, M.Z.; Majzner, K.; Kochan, K.; Kaczor, A.; Baranska, M.; Malek, K. Raman and infrared spectroscopy of carbohydrates: A review. *Spectrochim. Acta Part A Mol. Biomol. Spectrosc.* **2017**, *185*, 317–335, doi:10.1016/j.saa.2017.05.045.
35. Schulte, F.; Lingott, J.; Panne, U.; Kneipp, J. Chemical Characterization and Classification of Pollen. *Anal. Chem.* **2008**, *80*, 9551– 9556, doi:10.1021/ac801791a.
36. Bağcıoğlu, M.; Zimmermann, B.; Kohler, A. A multiscale vibrational spectroscopic approach for identification and biochemical characterization of pollen. *PLoS ONE* **2015**, *10*, 1–19, doi:10.1371/journal.pone.0137899.
37. Farrán, A.; Cai, C.; Sandoval, M.; Xu, Y.; Liu, J.; Hernáiz, M.J.; Linhardt, R.J. Green Solvents in Carbohydrate Chemistry: From Raw Materials to Fine Chemicals. *Chem. Rev.* **2015**, *115*, 6811–6853, doi:10.1021/cr500719h.
38. Uddin, M.J.; Gill, H.S. Ragweed pollen as an oral vaccine delivery system: Mechanistic insights. *J. Control. Release* **2017**, *268*, 416– 426, doi:10.1016/j.jconrel.2017.10.019.
39. Ares, A.M.; Valverde, S.; Bernal, J.L.; Nozal, M.J.; Bernal, J. Extraction and determination of bioactive compounds from bee pollen. *J. Pharm. Biomed. Anal.* **2018**, *147*, 110–124, doi:10.1016/j.jpba.2017.08.009.
40. Schulz, S.; Arsene, C.; Tauber, M.; McNeil, J.N. Composition of lipids from sunflower pollen (*Helianthus annuus*). *Phytochemistry* **2000**, *54*, 325–336, doi:10.1016/S0031-9422(00)00089-3.
41. Schulz, H.; Baranska, M. Identification and quantification of valuable plant substances

by IR and Raman spectroscopy. *Vib. Spectrosc.* **2007**, *43*, 13–25, doi:10.1016/j.vibspec.2006.06.001.

42. Kinugasa, S.; Tanabe, K.; Tamura, T. SDBSWeb: National Institute of Advanced Industrial Science and Technology. Available online: https://sdbs.db.aist.go.jp (accessed on 22 June 2021).
43. Shearer, G.L. An Evaluation of Fourier Transform Infrared Spectroscopy for the Characterzation of Organic Compounds in Art and Archaeology. Ph.D. Thesis, University College London, London, UK, 1989.
44. Kędzierska-Matysek, M.; Matwijczuk, A.; Florek, M.; Barłowska, J.; Wolanciuk, A.; Matwijczuk, A.; Chruściel, E.; Walkowiak, R.; Karcz, D.; Gładyszewska, B. Application of FTIR spectroscopy for analysis of the quality of honey. *BIO Web Conf.* **2018**, *10*, 02008, doi:10.1051/bioconf/20181002008.
45. Fang, K.; Wang, Y.; Jinxing, L.; Yu, T.; Zhang, L.; Baluška, F.; Šamaj, J.; Lin, J. Isolation of de-exined pollen and cytological studies of the pollen intines of Pinus bungeana Zucc. Ex Endl. and Picea wilsonii Mast. *Flora Morphol. Distrib. Funct. Ecol. Plants* **2008**, *203*, 332–340, doi:10.1016/j.flora.2007.04.007.
46. Szymanska-Chargot, M.; Zdunek, A. Use of FT-IR Spectra and PCA to the Bulk Characterization of Cell Wall Residues of Fruits and Vegetables Along a Fraction Process. *Food Biophys.* **2013**, *8*, 29–42, doi:10.1007/s11483-012-9279-7.
47. Nicolson, S.W.; Human, H. Chemical composition of the "low quality" pollen of sunflower (*Helianthus annuus*, Asteraceae). *Apidologie* **2013**, *44*, 144–152, doi:10.1007/s13592-012-0166-5.
48. Domínguez, E.; Mercado, J.A.; Quesada, M.A.; Heredia, A. Pollen sporopollenin: Degradation and structural elucidation. *Sex. Plant Reprod.* **1999**, *12*, 171–178, doi:10.1007/s004970050189.
49. Ghosh, N.; Sircar, G.; Saha, B.; Pandey, N.; Bhattacharya, S.G. Search for allergens from the pollen proteome of sunflower (*He- lianthus annuus* L.): A major sensitizer for respiratory allergy patients. *PLoS ONE* **2015**, *10*, 1–20, doi:10.1371/journal.pone.0138992.
50. Hicks, D.M.; Ouvrard, P.; Baldock, K.C.R.; Baude, M.; Goddard, M.A.; Kunin, W.E.; Mitschunas, N.; Memmott, J.; Morse, H.; Nikolitsi, M.; et al. Food for Pollinators: Quantifying the Nectar and Pollen Resources of Urban Flower Meadows. *PLoS ONE* **2016**, *11*, e0158117, doi:10.1371/journal.pone.0158117.
51. Agatonovic-Kustrin, S.; Ristivojevic, P.; Gegechkori, V.; Litvinova, T.M.; Morton, D.W. Essential oil quality and purity evalua- tion via FT-IR spectroscopy and pattern recognition techniques. *Appl. Sci.* **2020**, *10*, 1–12, doi:10.3390/app10207294.
52. Dinant, S.; Wolff, N.; De Marco, F.; Vilaine, F.; Gissot, L.; Aubry, E.; Sandt, C.; Bellini, C.; Le Hir, R. Synchrotron FTIR and Raman spectroscopy provide unique spectral fingerprints for Arabidopsis floral stem vascular tissues. *J. Exp. Bot.* **2019**, *70*, 937– 948, doi:10.1093/jxb/ery396.
53. Chukanov, N.V. *Infrared Spectra of Mineral Species*; Springer: Dordrecht, The Netherlands, 2014; Volume 1; ISBN 9789400771277.
54. Süfer, Ö.; Bozok, F. Characterization of essential oil from *Matricaria sevanensis* by microwave-assisted distillation. *J. Therm. Anal. Calorim.* **2020**, *140*, 253–261, doi:10.1007/s10973-019-08829-x.
55. Taraj, K.; Malollari, I.; Andoni, A.; Ciko, L.; Lazo, P.; Ylli, F.; Osmeni, A.; Como, A. Eco-extraction of albanian chamomile essen- tial oils by liquid Co_2 at different temperatures

and characterisation by FTIR spectroscopy. *J. Environ. Prot. Ecol.* **2017**, *18*, 117– 124.
56. Kasai, T.; Furukawa, K.; Sakamura, S.J. Infrared and Mass Spectra of α-Amino Acid Amides. *J. Fac. Agric. Hokkaido Univ.* **1979**, *59*, 279–283.
57. Chen, X.; Li, H.; Sun, S.; Cao, X.; Sun, R. Effect of hydrothermal pretreatment on the structural changes of alkaline ethanol lignin from wheat straw. *Sci. Rep.* **2016**, *6*, 1–9, doi:10.1038/srep39354.
58. Aloisi, I.; Cai, G.; Serafini-Fracassini, D.; Del Duca, S. Polyamines in Pollen: From Microsporogenesis to Fertilization. *Front. Plant Sci.* **2016**, *7*, E305–E307, doi:10.3389/fpls.2016.00155.
59. Sasaki, Y.; Yasuda, H.; Ohba, Y.; Harada, H. Isolation and characterization of a novel nuclear protein from pollen mother cells of lily. *Plant. Physiol.* **1990**, *94*, 1467–1471, doi:10.1104/pp.94.3.1467.
60. Gouda, N.M.N.; Naika, S..; Gowda, N.M.N.; Naikar, S.B.; Reddy, G.K.N. Perchlorate Ion Complexes. *Adv. Inorg. Chem.* **1984**, *28*, 255–299, doi:10.1016/S0898-8838(08)60210-X.
61. Lutzke, A.; Morey, K.J.; Medford, J.I.; Kipper, M.J. Detailed characterization of *Pinus ponderosa* sporopollenin by infrared spec- troscopy. *Phytochemistry* **2020**, *170*, 112195, doi:10.1016/j.phytochem.2019.112195.
62. Boyd, C.E. Phosphorus. In *Water Quality: An Introduction*; Springer: Cham, Switzerland, 2015; pp. 243–261; ISBN 9783319174457.
63. Pöhlker, C.; Huffman, J.A.; Pöschl, U. Autofluorescence of atmospheric bioaerosols—Fluorescent biomolecules and potential interferences. *Atmos. Meas. Tech.* **2012**, *5*, 37–71, doi:10.5194/amt-5-37-2012.
64. Park, J.H.; Seo, J.; Jackman, J.A.; Cho, N.-J. Inflated Sporopollenin Exine Capsules Obtained from Thin-Walled Pollen. *Sci. Rep.* **2016**, *6*, 28017, doi:10.1038/srep28017.
65. She, D.; Xu, F.; Geng, Z.C.; Sun, R.C.; Jones, G.L.; Baird, M.S. Physicochemical characterization of extracted lignin from sweet sorghum stem. *Ind. Crop. Prod.* **2010**, *32*, 21–28, doi:10.1016/j.indcrop.2010.02.008.
66. Jardine, P.E.; Fraser, W.T.; Lomax, B.H.; Gosling, W.D. The impact of oxidation on spore and pollen chemistry. *J. Micropalaeon- tology* **2015**, *34*, 139–149, doi:10.1144/jmpaleo2014-022.
67. Soni, B.; Hassan, E.B.; Mahmoud, B. Chemical isolation and characterization of different cellulose nanofibers from cotton stalks. *Carbohydr. Polym.* **2015**, *134*, 581–589, doi:10.1016/j.carbpol.2015.08.031.
68. Ház, A.; Jablonský, M.; Orságová, A. Determination of Temperature Regions in Thermal Degradation of Lignin. In Proceedings of the 4 th International Conference on Renewable Energy Sources, Tatranské Matliare, Slovakia, 21–23 May 2013; pp. 1–6.
69. Gubbuk, I.H.; Gürfidan, L.; Erdemir, S.; Yilmaz, M. Surface modification of sporopollenin with calixarene derivative: Charac- terization and application for metal removal. *Water Air Soil Pollut.* **2012**, *223*, 2623–2632, doi:10.1007/s11270-011-1054-8.
70. Palazzo, I.; Mezzetta, A.; Guazzelli, L.; Sartini, S.; Pomelli, C.S.; Parker, W.O.; Chiappe, C. Chiral ionic liquids supported on natural sporopollenin microcapsules. *RSC Adv.* **2018**, *8*, 21174–21183, doi:10.1039/c8ra03455a.

CHAPTER II/CAPÍTULO II

Nanocarrier-loaded pollen microcapsules as multi-step delivery systems

In collaboration with:

Diabesity Group, Center for Research in Molecular Medicine and Chronic Diseases,
University of Santiago de Compostela
Department of Biochemistry and Molecular Biology, University of Santiago de Compostela

CHAPTER II/ CAPÍTULO II

Nanocarrier-loaded pollen microcapsules as multi-step delivery systems

Abstract

Transmucosal administration of nanocarriers is a promising strategy for solving complex drug delivery problems, but the premature removal of these nanocarriers from mucosal tissues still constitutes a great obstacle for their efficacy. Pollen grains are natural microstructures with a microneedle-like surface that enhances their mucosal–interaction. Over the past years, different methods have been developed to produce highly resistant hollow microcapsules from these pollen grains, of interest in drug encapsulation and delivery. In this work, we obtained hollow pollen microcapsules from *Helianthus annuus*, and we associated them with model nanoparticles of different sizes and surface properties. These nanoparticles allowed us to unravel their mechanisms of loading and their release kinetics in intestinal media. We also evaluated their interaction with immune cells, their mucosal interaction in an *ex vivo* intestine model, and their biodistribution after oral administration to rats. The results obtained with model nanoparticles were confirmed with biodegradable polymeric nanocapsules, specifically designed for oral drug delivery. This work systematically analyses the optimal size, surface charge, and loading method for the rational design of pollen microcapsules loaded with nanocarriers. The developed system combines the benefits of nanotechnology and the capacity of hollow pollen microcapsules to anchor in the mucosa for achieving a promising multistep delivery platform.

Graphical abstract

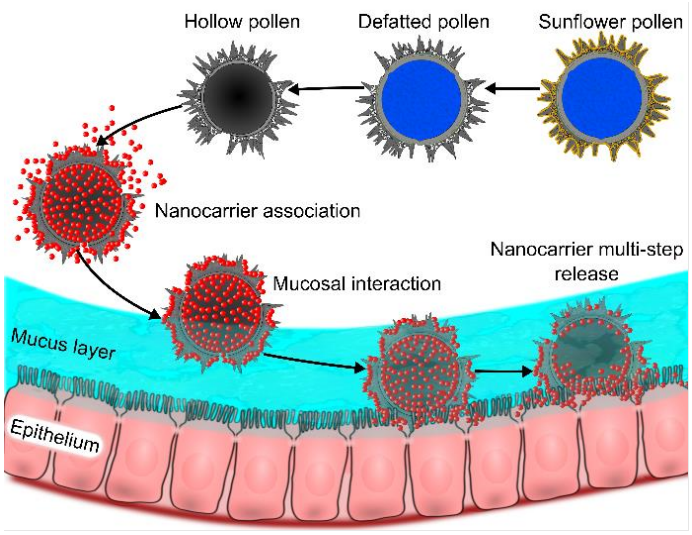

1. INTRODUCTION

Transmucosal administration of drugs offers an attractive possibility to overcome classical problems associated with injectable formulations, providing better access to the target site, and mimicking the natural release pathway of endogenous biomacromolecules [1]. Nanotechnology can enhance pharmacological efficacy by reducing side effects and improving the stability and bioavailability of drugs [2]. Polymeric nanocarriers have attracted great interest in drug delivery applications due to their safety, biocompatibility, and enhanced physical and biological stability [3]. Moreover, the high surface area of nanocarriers maximizes the functional surface for improving biological interactions [4]. However, despite the capacity of nanosystems to deliver high drug payloads and interact efficiently with mucosal tissue, the attempts to demonstrate consistently high and reproducible efficacy *in vivo* have failed so far [5, 6] due to their premature removal from the mucosa, resulting in limited bioavailability compared with other routes [7]. The integration of nanocarriers into functional platforms has already been studied by several authors as a so-called "multi-stage delivery strategy". These works mostly refer to parenterally administered nanomedicines and highlight particle size, shape, and morphology as key factors in the performance of each component of the multi-stage device [8]. Analogously, microencapsulated nanoparticles have also shown promising results in the mucosal administration of drugs [9, 10]. A major advantage for multi-stage delivery platforms has been their capacity to protect the nanocarriers in their inner core and transport them to the target region where they deliver their therapeutic cargo with higher efficiency. Within this context, plant pollen grains are naturally needle-like biological microstructures with attractive properties, such as high resistance and excellent bioadhesion. These structures consist of the external shell of pollen named exine and are mainly composed of the polymer sporopollenin [11]. As the pollen of some plant species is a source of allergens [12], several protocols have been developed for producing allergen-free pollen microcapsules with the preserved external structure of intact natural pollen grain [13, 14]. Among the reported pollen microcapsules, those obtained from sunflower (*Helianthus annuus*) pollen, echinate pollen with strong adhesive properties [15], have been explored for their high capacity for loading different compounds and for their enhanced mucoadhesion [16–18]. *H. annuus*'s distinct exine shell surface morphology provides an attachment site for insects during pollination, and could potentially promote adherence to the mucosa, leading to prolonged contact with biological surfaces, and improving drug absorption and bioavailability [19]. The main goal of this study is to design a three-dimensional bioadhesive platform, based on processed pollen grains resembling a microneedle-like surface morphology to improve nanocarrier-based transmucosal drug delivery. To this end, purified sunflower pollen grains were associated with model polystyrene nanoparticles of different sizes and surface charges, to unravel the mechanisms of loading and release from the pollen. Their *in vitro* interaction with immune cells as well as their *ex vivo* mucointeraction and their biodistribution were also evaluated upon oral administration. The results obtained with model nanosystems were also confirmed with biodegradable protamine nanocapsules, specifically designed for oral drug delivery. This technology combines the benefits of nanotechnology and the capacity of pollen grains to anchor in the mucosa for achieving a multi-step delivery platform.

2. MATERIALS AND METHODS

2.1. Materials

Sunflower pollen (*H. annuus*) was obtained from Pharmallerga (Czech Republic). Cyclohexane, acetone, ethanol, and 85 wt% orthophosphoric acid were purchased from Merck

KGaA (Germany). Low molecular weight protamine sulfate (5 kDa) was purchased from Yuki Gosei Kogyo, Ltd (Japan). Polyethylene glycol stearate 40 (PEGst 40) was provided by Croda Chemicals Europe Ltd. (United Kingdom) and sodium glycocholate (SGC) from Dextra Laboratories Ltd. (United Kingdom). Caprylic/capric/succinic triglyceride (Miglyol® 812) was purchased from IOI Oleo GmbH (Germany). 1,1'-Dioctadecyl-3,3,3',3'-tetramethylindodicarbocyanine, 4-chlorobenzene sulfonate salt (DiD) were provided by Thermo Fisher Scientific (USA), and pancreatin (8 % USP specification) was purchased from Biozym (Germany). Standard chemicals were purchased from Sigma Aldrich (Spain). Magenta fluorescent (Ex/Em: 588/612 nm) polystyrene latex nanoparticles (100, 200, and 500 nm) with different surface functionalization (unmodified, carboxylated, and aminated) were purchased from Magsphere Inc. (USA). Organic solvents were of HPLC grade, and all other products used were of reagent grade purity or higher. Ficoll-Paque™ PLUS was obtained from GE Healthcare Bio-Science AB, (Sweden), Medium Roswell Park Memorial Institute (RPMI-1640), and Dulbecco's Modified Eagle's Medium (DMEM) were obtained from GIBCO® (Thermo Fisher Scientific, Spain). Granulocyte-macrophage colony-stimulating factor (GM-CSF), interferon-gamma (IFNɣ), and interleukin 4 (IL-4) were obtained from Tonbo Biosciences (San Diego, CA). Fetal Bovine Serum (FBS), and PSG (Penicillin-Streptomycin-Glutamine) were provided from Sigma Aldrich. Lipopolysaccharide (LPS) from *Escherichia coli* was purchased from Invitrogen (Spain). For *in vitro* experiments sterile and autoclaved materials were used.

2.2. Obtention of *Helianthus annuus* hollow pollen microcapsules

Pollen of *H. annuus* was treated by sequential washing steps to remove the compounds coating the sporopollenin, as well as internal cellular and proteinaceous components, following a protocol developed by our group [20]. Briefly, 2 g of pollen were resuspended in 40 mL of ultra-pure water, homogenized, and filtered 5 times until obtaining a transparent eluent. This water-treated pollen was resuspended in 20 mL of acetone at 25 ºC and homogenized, filtered, and dried at 60 ºC for 24 h. The obtained acetone-treated pollen was resuspended in 20 mL of cyclohexane, vortexed and defatted. Pollen was recovered by filtration and was dried at 60 ºC for 24 h. For obtaining hollow pollen microcapsules, 10 mL of orthophosphoric acid (85%, 15.2 M H_3PO_4) was added per gram of defatted pollen and incubated at 70 ºC under gentle agitation for 5 h. Afterward, the solution was cooled, and the acid-treated pollen was recovered by filtration (5 washes of 50 mL of water), dried at 60 ºC for 24 h, and stored in a desiccant chamber until use.

2.3. Physicochemical characterization

Sections of frozen pollen were obtained using a cryotome (Leica CM 1850 UV; Leica Biosystems Nussloch GmbH, Germany) and visualized in a Field Emission Scanning Electron Microscopy (FESEM Ultra Plus, Zeiss, Germany). Samples were covered with Iridium on a carbon tape and micrographs were recorded with an acceleration voltage of 3.00 kV at different magnifications. The internal and external structure of pollen grains were studied by Confocal Laser Scanning Microscopy (CLSM, SP5 Leica AOBS-SP5, Leica Biosystems Nussloch GmbH). Natural fluorophores of pollen samples were excited at 405 nm, 492 nm, and 561 nm, and collected with photomultiplier tubes with emission filters of 414-479 nm, 505-554, and 571-635 nm [21]. The stability of the pollen samples was evaluated by the analysis of their integrity, shape, and surface morphology up to 2 h at 37 ºC after incubation in Simulated Intestinal Fluid (SIF, 15.4 mM sodium hydroxide, 50 mM monobasic potassium phosphate, pH 6.8) supplemented with pancreatin (1% w/w) according to USP specifications or Simulated Gastric Fluid (SGF, 0.03 M NaCl, pH 1.2) [22].

2.4. Loading with model polystyrene nanoparticles

The loading capacity of pollen samples was studied with commercial polystyrene NPs of different sizes (100, 200, and 500 nm), and surface functionalization (aminated, unmodified, and carboxylated) employing a fixed mass ratio of 1:1 and two loading techniques: lyophilization and vacuum. On one hand, a suspension of polystyrene NPs (1 wt%) was slowly dripped onto a fixed amount of dry pollen and incubated under rotatory agitation (400 rpm) at 37 ºC for 30 min and subsequently freeze-dried (50 h, -40 ºC, Labconco Corp., USA). On the other hand, for vacuum-assisted loading, the suspension of polystyrene NPs was added to the dry pollen drop by drop under rotatory motion until homogenization and then pollen and polystyrene NPs were subjected to vacuum (25 mbar) at 37 ºC for their association. For the determination of non-associated nanocarriers, loaded pollen samples were resuspended in water and centrifuged for 1 min at 5,000 *g* at 20 ºC, to avoid the precipitation of NP suspensions. The supernatant was collected and measured using a fluorimeter (Synergy H1 Hybrid Multi-Mode Microplate Reader, BioTek, Winooski, VT). Fluorescence quantification was performed using standard curves of known concentrations of NPs (λ_{ex}: 588 nm, λ_{em}: 612 nm). The internal and external structures of polystyrene NP-loaded pollen grains were studied by CLSM. For the observation of the nanoparticles, samples were excited at 588 nm and collected at 635-640 nm, following the supplier´s instructions. Images were assembled and analysed with the Leica Application Suite X (v3.7.2, Leica Biosystems Nussloch GmbH) software. Association efficiency (%), loading capacity (%), and loading content (w/w) of pollen samples were calculated using the following equations:

$$\text{Association efficiency (AE\%)} = \frac{\text{Nanocarriers associated}}{\text{Total of nanocarriers}} x\ 100$$

$$\text{Loading capacity (\%)} = \frac{\text{Mass of loaded nanocarriers}}{\text{Mass of pollen grains loaded with nanocarriers}} x\ 100$$

$$\text{Loading content (w/w)} = \frac{\text{Mass of loaded nanocarriers}}{\text{Mass of pollen grains}}$$

2.5. Release of polystyrene NPs and kinetic modelling

For *in vitro* release studies, pollen (10 mg) loaded with polystyrene NPs (ratio 1:1) was incubated at 37 ºC under horizontal agitation (700 rpm) in 1 mL of SIF. At specified time intervals (0, 0.25, 0.5, 1, 2, 3, 5, 8, 24, 48 up to 120 h) the supernatant was collected by centrifugation for 1 min at 5,000 *g* and the pellet was resuspended in fresh release medium. Polystyrene NPs release was quantified by the determination of fluorescence in the supernatant as previously described (section 2.4). Accumulative release (%) was determined considering the initial loading of each pollen sample. The mechanism of *in vitro* release of nanoparticles was studied by different kinetic models, where the employed formulas were adapted from the literature [23].

2.6. Interaction with immune cells

The interaction between pollen was studied by confocal microscopy in the macrophage cell line Raw 264.7 (ATCC, USA) and in a primary culture of human dendritic cells (DCs) [24]. Briefly, heparinized blood samples were obtained from healthy donors after informed consent. The *buffy coats* from anonymous donors were donated by the Organ and Blood Donation Agency (ADOS;

Santiago de Compostela). In all cases, the PBMCs from the blood samples were extracted within 24 h.

Peripheral blood mononuclear cells (PBMCs) were isolated using a Ficoll gradient centrifugation method. Briefly, blood was diluted with PBS (1:1) and layered onto Ficoll-Paque™ PLUS at a ratio of 2:1 (blood: Ficoll). Different components were isolated after centrifugation (Allegra X-12R, Beckman Coulter) at 400 *g* for 30 min at RT, and PBMCs were collected from the interface, washed twice with PBS, and centrifuged again at 300 *g* for 10 minutes at RT. Cells were resuspended in R_2 medium which consists of RPMI-1640 supplemented with 2% fetal bovine serum and 1% of Penicillin-Streptomycin-Glutamine (100 U/ml penicillin, 0.1 mg/ml streptomycin and 2mM L-glutamine). The density was adjusted to 1×10^6 cells/ml and 10 mL of cells were seeded into a 75 cm^2 cell culture flask for 2 h (37ºC, 5% CO_2). After the incubation period, nonadherent cells were washed with PBS and attached monocytes were cultured for another 6 days at 37ºC, 5% CO_2, renewing half of the medium after three days, in R_{10} medium (RPMI-1640 supplemented with 1% antibiotics and 10% FBS) in the presence of IL-4 and GM-CSF to allow the cells to differentiate into DCs. Immature DCs and macrophages were incubated with defatted and hollow pollen as well as with polystyrene NPs loaded hollow pollen grains. Samples were fixed on poly-L-lysine coated glass coverslips (Corning® BioCoat™, Thermo Fisher) with paraformaldehyde 4% and dried by sequential ethanol baths.

Raw 264.7 macrophages and pollen interaction were also analyzed under dynamic flow conditions in a µ-Slide I Luer channel slide (Ibidi GmbH, Germany) for 24 h by CLSM, as previously described in section 2.4.

2.7. Loading and release of biodegradable protamine nanocapsules

2.7.1. Protamine nanocapsules preparation and physicochemical characterization

Blank protamine nanocapsules (NCs) were prepared by the solvent displacement technique following the procedure previously described by our group [22]. The oily core was formed by 59 mg of Miglyol®812, 5 mg of sodium glycocholate, and 16 mg of PEGst-40, dissolved in 3 mL of ethanol. Thereafter, 1.95 mL of acetone was added to the ethanolic solution, and the organic phase was immediately poured over 10 mL of an aqueous phase containing 0.15% w/v protamine. The formulation was left under magnetic stirring for 10 min. The organic solvents were eliminated by evaporation under vacuum in a Rotary Evaporator (Rotavapor R-300, Buchi, Switzerland), to obtain NCs with a constant final volume of 5 mL. Subsequently, protamine NCs were isolated by ultracentrifugation (Optima™ L-90K, Ultracentrifuge, Beckman Coulter, USA) at 61,740 *g*, at 15 ºC for 1 h. The isolated formulation was resuspended in ultrapure water.

NCs were fluorescently labeled with DiD by adding 50 µg of a DiD solution in ethanol to the organic phase before NCs preparation. DiD encapsulation efficiency was determined by quantifying the amount of free dye after isolation of the NCs, by fluorescence spectroscopy in a multilabel plate reader EnVision® (λ_{ex}: 640 nm, λ_{em}: 675 nm, PerkinElmer; USA).

Protamine NCs were characterized in terms of mean particle size and polydispersity index (PDI) using photon correlation spectroscopy and the zeta potential was determined by laser doppler anemometry (Zetasizer Nano-ZSTM, Malvern Panalytical), after sample dilution in ultrapure water. Each analysis was performed in triplicate, at 25 ºC, and with a detection angle of 173°.

Fourier Transform InfraRed (FTIR) spectroscopy was performed to study the different functional groups present in NCs using a VARIAN FT-IR 670 (Varian Inc. Scientific Instr., USA) equipped with an attenuated total reflectance (ATR) accessory (GladiATR, PIKE technologies, USA) from 400 to 4,000 cm^{-1} at 4 cm^{-1} resolutions using 64 scans.

2.7.2. Loading of hollow pollen microcapsules with protamine NCs and release studies

The loading capacity of pollen samples was studied for DiD protamine NCs employing defatted and hollow pollen at ratios 1:1 and 1:2, by lyophilization and vacuum, as previously described for polystyrene NPs (section 2.4). For the determination of non-associated nanocapsules, loaded-pollen samples were resuspended in water and centrifuged for 1 min at 5,000 *g* at 20 ºC, and supernatants were excited at 640 nm and collected at 670-770 nm. The internal and external structure of DiD protamine NCs loaded pollen grains was studied by CLSM and association efficiency (%), loading capacity (%), and loading content (w/w) of pollen samples were calculated as described above. For *in vitro* release studies, pollen samples loaded with fluorescent protamine NCs were incubated in SIF and the accumulative release (%) was determined considering the initial loading of each pollen sample at different time intervals as described in section 2.5.

2.8. *Ex vivo* mucointeraction

Healthy, surplus stock Sprague-Dawley male rats (approx. 250 g) were employed for obtaining intestinal sacs. Rats were euthanized in a hypoxia chamber by inhalation in an atmosphere saturated with more than 90% CO_2, followed by cervical dislocation. Intestines were immediately extracted by an abdominal incision and washed with Krebs saline solution (7 g/L sodium chloride, 0.34 g/L potassium chloride, 1.8 g/L glucose, 0.25 g/L disodium hydrogen phosphate, 0.21 g/L sodium dihydrogen phosphate, and 46.8 mg/L magnesium chloride, pH 6.5) before the preparation of non-everted intestinal sacs [25]. After removing any remaining food residues from the standard laboratory diet, the ends of the intestinal sac were tied with a braided suture. Next, the different samples (hollow pollen microcapsules, DiD protamine NCs, and DiD protamine NCs loaded into hollow pollen microcapsules) were suspended in 1 mL of water and introduced into the sac using a syringe. The samples were then incubated horizontally at 37 ºC with continuous bubbling of carbogen (95% O2:5% CO2) for 3 h. The mucointeraction capacity of pollen samples and nanocarriers was visualized by CLSM and images were analyzed with ImageJ software version 1.52a (U.S. National Institutes of Health, Bethesda, MD, USA). Quantified red fluorescence intensity was expressed as raw integrated density divided by the analyzed area in square centimeters. An average area of 0.36±0.10 cm^2 of the intestinal sac was analyzed per sample.

2.9. *In vivo* biodistribution

Healthy Sprague-Dawley rats (approx. 250 g) were housed in ventilated polypropylene cages and received a standard laboratory diet of food and water *ad libitum*. Animals were fasted overnight and samples (hollow pollen microcapsules, DiD protamine NCs, and DiD protamine NCs loaded into hollow pollen microcapsules) were administered by oral gavage. As a control, non-treated rats were used. Biodistribution was assessed in triplicate on a semi-quantitative basis with an In Vivo Imaging System (IVIS, Living Image® System, Caliper Life Sciences, Hopkinton, MA) using body scanning with simultaneous, constant exposure times for all groups after 3 h. At predetermined time points after oral administration, rats were euthanized in a hypoxia chamber by inhalation in an atmosphere saturated with more than 90% CO_2, followed by cervical dislocation, and placed in the acquisition chamber for collecting a full body IVIS spectrum. After general image acquisition, the abdominal cavity was opened and visualized, and subsequently, the intestines were excised and washed carefully before their analysis. Images were captured using emission and excitation filters of 640/740 nm for DiD and 570/640

nm for hollow pollen microcapsules. The regions of interest (ROIs) to quantify the fluorescence intensity were acquired with Aura acquisition software, using identical illumination settings.

Statistical analysis

Statistical significance of the difference between the means was determined by analysis of variance (ANOVA) followed by pairwise multiple comparisons using Tukey's HSD method, employing the Statgraphics centurion XVII software (Statgraphics Technologies, Inc. The Plains, VA, USA). Differences were considered significant for $p < 0.05$.

3. RESULTS AND DISCUSSION

3.1. Obtention and physicochemical characterization of *Helianthus annuus* hollow pollen microcapsules

In order to obtain hollow pollen microcapsules derived from pollen grains for the subsequent encapsulation of nanoparticles, our group has developed a protocol to remove the compounds that cover the surface of the pollen, as well as the internal cellular and proteinaceous components from its internal cavity. All raw pollen grains are covered by an outermost matrix named pollenkitt, mainly composed of polysaccharides and lipids [26] followed by a multi-layered pollen wall (exine and intine) and an inner core of sporoplasm [27]. In turn, the exine, composed of the polymer sporopollenin, can be divided into two main layers, the ornamented external ectexine, and an internal laminated layer named endexine [28]. To remove pollen compounds, a sequential treatment was designed based on the differential solubility of the coating materials and taking advantage of the extraordinary toughness of sporopollenin, the principal component of the exine, and one of the most resistant biopolymers in nature [20]. The sequential water, acetone, and cyclohexane treatment resulted in defatted pollen. Upon treatment with H_3PO_4, purified (hollow) pollen microcapsules were obtained, and the sporoplasm was eliminated. As shown in **Figure 1**, surface-defatted and purified hollow pollen grains were similar to those previously reported for *H. annuus* [16, 17]. The defatted pollen had a defined (Fig. 1A) external layer, and an inner pollen core with the sporoplasm, both with specific autofluorescence patterns. In a closer look at the pollen surface (Fig. 1C and 1E), the nanopores surrounding the spines were visible in the defatted pollen, indicating the elimination of the pollenkitt compounds and environmental contaminants. The cavities of the ectexine appeared empty in the transversal section images (Fig. 1E), while the inner cavities appeared filled with compounds that probably remained from the pollen maturation process, such as tapetal debris [28]. Purified hollow pollen grains (Fig. 1B) showed a reduced overall fluorescence due to the complete elimination of the sporoplasm. Autofluorescence derived from exine was preserved. Overall, the treatment was effective for opening naturally existing pollen apertures (Fig. 1D), eliminating sporoplasm, and other components between the layers of the pollen wall (Fig. 1F). These changes results in a final multi-layered hollow structure, with the ectexine and endexine virtually intact (Fig. 1F), preserving the morphology and surface ornamentation of the pollen, and providing a support that prevents the collapse of the hollow pollen structure.

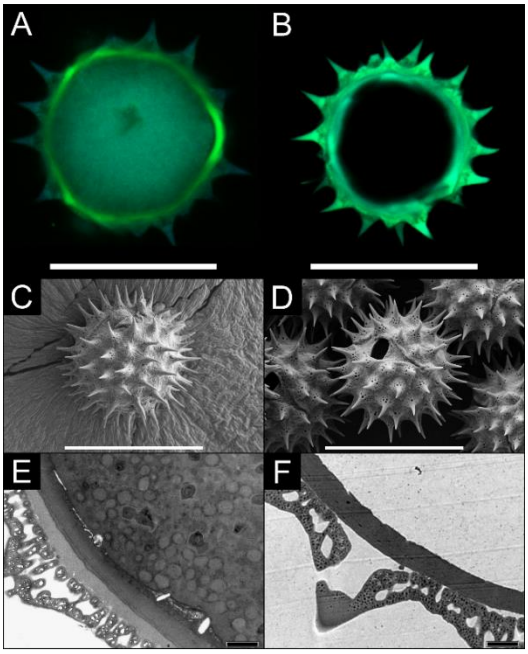

Figure 1. Microscopic images of defatted (A, C, and E) and hollow pollen microcapsules (B, D, and F) obtained from sunflower pollen grains. A and B: Confocal laser scanning microscopy (CLSM, scale bars represent 30 μm). C and D: Scanning electron microscopy (FESEM, scale bars represent 30 μm). E and F: Transmission electron microscopy (STEM, scale bars represent 1 μm).

3.2. Loading of sporopollenin microcapsules with model polystyrene NPs

As the first step of exploring the potential of nanocarrier-loaded hollow pollen grains for drug delivery purposes, non-biodegradable polystyrene NPs of different sizes (100, 200, and 500 nm) and surface chemical functionalizations (aminated, unmodified, and carboxylated) were associated by different methods (lyophilization and vacuum assisted loading) to hollow pollen microcapsules to determine the critical parameters of the loading process and release mechanisms in biorelevant media.

According to the SEM-analysis (**Figure 2**), after the vacuum-assisted loading process, 100 nm NPs coated completely the hollow pollen microcapsules up to spines, the internal areas of the endexine, and the ectexine pores. Similarly, 200 nm NPs formed a uniform coverage of external areas, thicker than 100 nm NPs. The inner part of the endexine appeared to be covered, however, the presence of NPs between the ectexine and endexine was lower than in the case of 100 nm NPs. Finally, 500 nm NPs were mainly attached to the surface of the pollen microcapsules, probably due to size exclusion effect, therefore, larger sizes would not be relevant. The effect of size on the loading efficiency was studied by fluorescence intensity analysis of non-modified NPs since the presence of different functional groups can alter the analysis of this specific interaction. As shown in **Table 1**, in the non-modified group, 100 nm and 500 nm NPs had similar AE% (between 67-80%), being 200 nm NPs notably higher, with values around 85%.

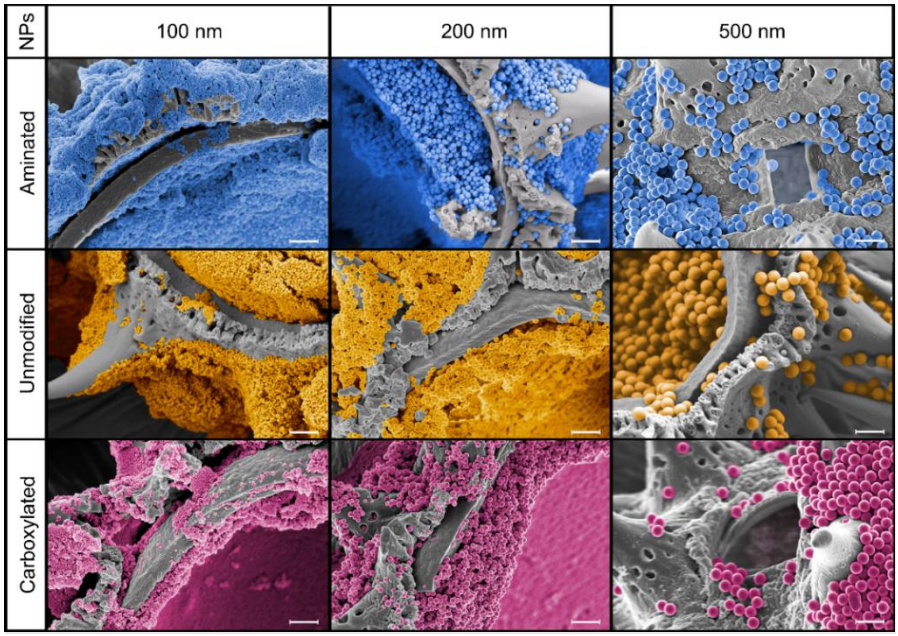

Figure 2. Images of scanning electron microscopy (SEM) of hollow pollen microcapsules loaded by vacuum with commercial nanoparticles (NPs; 100, 200, and 500 nm) with different functionalization. Bars represent 1 µm. NPs were artificially colored to increase the contrast with sporopollenin.

According to their loading method, loading of aminated NPs not importantly affect, with a similar AE% (76-77% vs. 69-81% for lyophilization and vacuum, respectively), while carboxylated NPs showed higher dependency on the loading method (59-69% vs. 78-89% AE% for lyophilization and vacuum, respectively). Lyophilization and vacuum-assisted loading produced similar AE% for aminated and unmodified nanoparticles, while vacuum loading yielded higher AE% for carboxylated NPs. The effect of the loading method seems to be also size-specific: when vacuum loading was employed, the AE% of 500 nm NPs increased more than 10% and 100 nm.

Table 1. Association efficiency (%) of polystyrene nanoparticles to hollow pollen microcapsules.

Loading method	**Modification**	**Size** (nm)		
		100	200	500
Lyophilization	Aminated	76.9±5.1	77.0±9.5	76.1±0.7
	Unmodified	68.9±6.8	85.0±3.6	67.5±1.8
	Carboxylated	69.4±0.5	59.1±5.8	60.4±2.4
Vacuum	Aminated	68.8±4.0	77.0±8.0	81.0±5.0
	Unmodified	73.4±6.5	85.2±8.7	80.7±8.1
	Carboxylated	87.7±7.3	89.6±1.2	78.7±9.6

Taken together, the AE% of the different NPs was higher compared with those reported for free drugs and biomolecules in pollen-derived platforms using different loading methods, such as pantoprazole-loaded in *Corylus avellana* (30%, passive loading) [29], imatinib mesylate loaded in *Betula* pendula (21%, passive loading) [30], bovine serum albumin loaded in ragweed (7%, vacuum loading) [31] or sunflower pollen microcapsules (37% and 65%, passive and vacuum loading, respectively) [16].

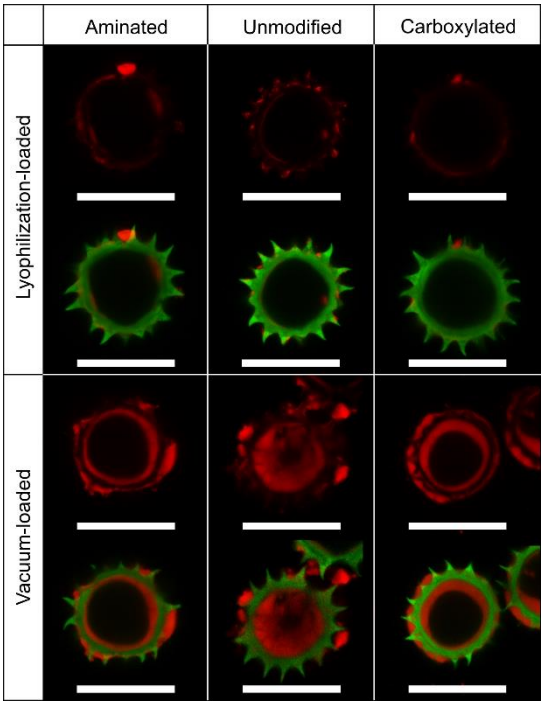

Figure 3. Images of confocal laser scanning (CLSM) microscopy of hollow pollen loaded with commercial polystyrene nanoparticles (200 nm) employing lyophilization and vacuum. Bars represent 30 µm. Green channel: pollen autofluorescence. Red channel: fluorescent polystyrene nanoparticles.

Since 200 nm NPs showed consistently high AE%, the influence of the different loading methods and surface functionalizations were further studied by CLSM for these nanoparticles (**Figure 3**). In general, vacuum loaded hollow pollen microcapsules had higher loading rates than those loaded by lyophilization, and unmodified and carboxylated NPs were prone to accumulate in the inner part of the pollen, while aminated NPs tended to remain in the external and internal surface of the pollen wall. The internal accumulation of unmodified and carboxylated nanoparticles can be explained by the different compositions of the endexine and ectexine, as the latter has negative groups on its surface(**Supplementary Table 1**) [32].

Nevertheless, the distribution of the cargo was not uniform among the pollen grains, as some pollen microcapsules presented a higher loading than others, but in general, vacuum method allowed the loading of higher mass ratios than lyophilization method. Similar behaviour has been described for bovine serum albumin (BSA) loaded in sunflower pollen-derived microcapsules [17], where the cargo entered through the apertures of the pollen and the loading varied in function of the mass ratio employed. It is to be noted, that the qualitative assessment of the apparent loading and distribution within the pollen by CLSM depends on the focal plane, and the orientation of the grain, and therefore, its utility for estimating the loading is limited and should be considered together with the above discussed quantitative determination.

3.3. Release polystyrene NPs from hollow pollen microcapsules and kinetic modeling

The release profile of polystyrene NPs (**Table 2**) from hollow pollen microcapsules showed a sustained release profile, with a fast release phase during the initial 8 h. In general, loading by lyophilization produced a higher burst release (**Figure 4**) than vacuum-loaded samples, achieving a steady phase after 24 h, while vacuum-loaded pollen produced a continuous release after 8 h and for up to 120 h. This can be explained by a preferential association of the NPs to

the external surface of the sporopollenin platforms when using lyophilization, which would produce their release more quickly, than after the use of vacuum conditions, where the NPs are located to a greater extent in the inner cavity due to the additional force applied in this case. Sporopollenin microcapsules loaded with drugs or nutrients typically show high initial burst release [16, 29, 33]; notwithstanding, in this study, associated nanoparticles showed a more controlled release, probably due to their larger size, high specific surface area and different association mechanisms

Table 2. Regression statistics and parameter estimates from the release models of polystyrene nanoparticles and hollow pollen microcapsules. Values in boldface represent the highest regression statistic of the studied release models.

Loading method	Size (nm)	Modification	Burst (%)	Release model			
				First-order	Higuchi	Korsmeyer-Peppas	
				R^2	R^2	R^2	n
Lyophilization	100	Aminated	9.9±2.1	0.934	0.972	**0.977**	**0.32**
		Unmodified	32.9±3.8	0.874	0.920	**0.951**	**0.33**
		Carboxylated	9.7±1.6	0.794	0.890	**0.951**	**0.09**
	200	Aminated	10.8±1.5	0.879	0.938	**0.963**	**0.40**
		Unmodified	30.4±3.4	0.879	0.938	**0.959**	**0.41**
		Carboxylated	11.8±2.5	0.962	**0.994**	**0.994**	**0.46**
	500	Aminated	10.0±1.8	0.770	0.868	**0.922**	**0.23**
		Unmodified	4.5±1.7	0.884	0.951	**0.967**	**0.43**
		Carboxylated	9.9±1.8	0.870	0.936	**0.955**	**0.46**
Vacuum	100	Aminated	3.8±1.6	0.880	0.944	**0.966**	**0.39**
		Unmodified	5.8±2.6	0.912	0.972	**0.984**	**0.54**
		Carboxylated	1.4±0.5	0.936	0.984	**0.993**	**0.37**
	200	Aminated	6.9±1.6	0.943	**0.987**	0.929	0.98
		Unmodified	10.3±2.6	0.986	**0.995**	0.992	0.65
		Carboxylated	6.6±3.8	0.950	**0.986**	0.978	0.90
	500	Aminated	5.2±1.4	0.930	**0.971**	0.963	0.72
		Unmodified	4.5±1.7	0.934	0.984	**0.990**	**0.54**
		Carboxylated	5.6±1.4	0.881	0.949	**0.961**	**0.81**

In addition to the lower burst, vacuum-loaded microcapsules showed a slower release profile compared with those loaded by lyophilization. This is possibly due to the internal localization of the NPs or and to a size-based exclusion mechanism by the exine pores. While the loading method mostly influenced the initial release; the size and surface functionalization of the NP further influenced the overall release profile with time. Unmodified NPs had the highest release profile, achieving 100 % in 100 nm and 200 nm NPs, while 500 nm NPs had a limited release, this could be due to their retention by aggregation, which can impede particle migration in porous materials like hollow pollen microcapsules [34]. On the other hand, aminated and carboxylated NPs showed a higher interaction with the pollen platform than unmodified NPs, since they produced a prolonged sustained release. However, regardless the surface functionalization, lyophilization resulted in an NPs release between 40-60%, while vacuum loading was lower, with values below 40% in all cases.

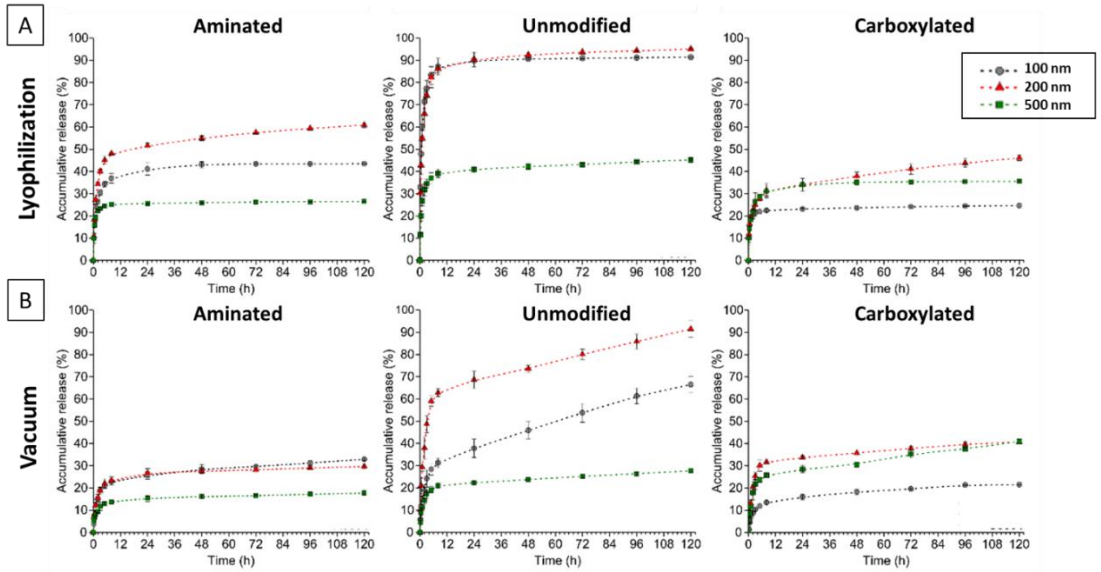

Figure 4. Time-course study of the accumulative release of nanoparticles (NPs) with different sizes, loaded into hollow pollen microcapsules by (A) lyophilization and (B) vacuum-assisted loading. ● 100 nm. ▲ 200 nm. ■ 500 nm. Error bars represent the standard deviation of the replicates (n=9).

To further understand the release mechanisms from the pollen microcapsules, the experimental release data were fitted to various kinetic models (**Table 2**). Sporopollenin is considered non-degradable in simulated biological fluids, consequently, the release of NPs is expected to follow a diffusion-driven mechanism [35]. However, it should also be considered that hollow pollen grains are flexible to some degree and have a complex micro and nanoporous structure. They can change their size and shape depending on the solvent, pH, or the degree of chemical modification of the exine [36, 37]. Moreover, NPs can be loaded onto the three-dimensional surface, the interior of the pollen grain (Fig. 3), or the internal channels of the exine, making it difficult to establish any initial assumption for a specific release model. Upon analysis (Table 2), it could be concluded that after the initial burst phase, the accumulative release data had a better approximation to models following a Fickian diffusion, since release data fitted with the Higuchi model or Korsmeyer-Peppas (with *n* in the 0.43 to 0.5 range) [38]. Fickian diffusion was also described in the release of pantoprazole encapsulated in *Corylus avellane* [29] and paracetamol-loaded *Platanus orientalis* hollow pollen microcapsules [39]. Vacuum-loaded NPs showed a slower release rate due to their higher entrapment inside the microcapsules and the decrease in the amount of the adsorbed nanocarriers. The receptor medium might take time to enter and release the entrapped NPs through the nanochannels on their surfaces, which also decreases the burst release effect. In general, the vacuum-loaded samples had a better approximation with the Fickian diffusion than lyophilization-loaded samples, where NPs followed a Fickian diffusion model (*n* value lower than 0.43) [38]. In the lyophilized NPs, they showed a faster release behavior, where a lower n value might be related to the porosity of the microcapsules; suggesting that the preferential passage of the solvent and NPs occurs across interconnected pores [23], present in the structure of exine. This mechanism has been previously described for erythromycin-loaded sporopollenin microcapsules [40]. Vacuum-loaded 200 and 500 nm NPs followed an anomalous transport release ($0.5<n<1$), which may be due to their lower specific surface area compared to 100 nm particles and their lower retention in the pores of the hollow microcapsules, which produces less adhesion to pollen and greater diffusion into the media. Pollen grains can absorb and release water to protect the male gametophyte against desiccation, being able to shift from dry to hydrated form and vice-versa. These two morphological conditions produce the folding of the pollen wall due to the elasticity

of the exine. This process, known as "harmomegathy", might produce a non-Fickian diffusion close to Case II, as diffusion is very rapid compared to relaxation [41]. A similar release pattern was also described for metformin delivery after its encapsulation in *L. clavatum* and *Phoenix dactylifera* sporopollenin microcapsules in simulated intestinal fluid (pH 7.4) [42].

3.4. *In vitro* immune cell interaction

Bee pollen is commonly used as a dietary supplement and has demonstrated antioxidant, anti-inflammatory, and antibacterial properties [43]. Even though oral administration of pollen is considered safe, proteins and lipids found in untreated pollen grains constitute the primary cause of pollen allergies. As detailed above, elimination of such components and possible environmental contaminants was confirmed by complementary analytical methods such as scanning electron microscopy, elemental analysis, or FTIR [20] to support safe use of the pollen -based vehicles for oral administration. Mucosal surfaces, such as those of the gastrointestinal tract, play a crucial role in immune regulation, where dendritic cells, macrophages, or intraepithelial lymphocytes act to provide intestinal homeostasis and immune tolerance [44]. Previous studies have shown that physical properties such as size, shape, and surface architecture influence pollen interaction and activation with human intestinal epithelial cells (in continuous crosstalk with immune cells by the release of multiple mediators [45]), macrophages and dendritic cells without causing an allergic response (IgE) [46]. The interaction of defatted and hollow pollen grains (empty or loaded with 200 nm polystyrene NPs) was evaluated with human dendritic cells (DCs) and Raw 264.7 macrophages to confirm the ability of sunflower spikes to provide cellular interaction and adhesion without undesired immune activation. As shown in Figure 5, the presence of pollen as well as nanocarriers triggered the recognition by immune system cells as macrophages (A-D) and dendritic cells (E-F), and they were attached to the pollen surface, surrounding the grains. These results suggest the importance of the specific topographic features of pollen surface affecting phagocytosis. Uddin *et al.* [46] previously stated that ragweed echinate pollen, with a morphology and size similar to sunflower pollen were able to reach the subepithelial region of the mucosa and be phagocytosed by macrophages, without the deterioration of cell integrity.

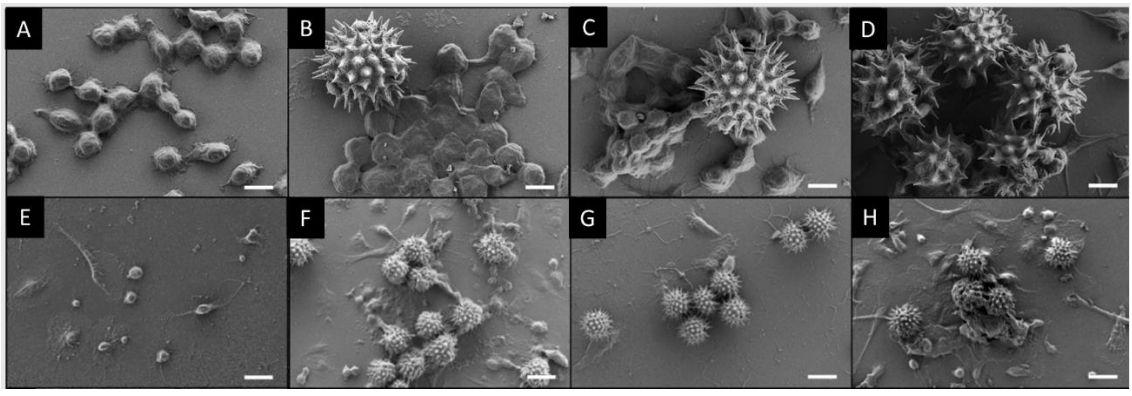

Figure 5. Images of scanning electron microscopy of Raw 264.7 cells (A-D) and dendritic cells (E-H) incubated with: defatted polle (B and F) hollow pollen microcapsules (C and G) and hollow pollen microcapsules loaded with 200 nm latex polystyrene nanoparticles (NPs, D and H). A-D white bars represent 30 µm and E-H bars represent 10 µm.

In a second step, Raw 264.7 macrophages were cultured with hollow pollen microcapsules, polystyrene NPs, and hollow pollen microcapsules loaded with NPs, in a microfluidics setup (Figure 6) that mimics the dynamics of the intestinal tract. Hollow pollen microcapsules were able to interact with cells, being retained in the cell layer (Figure 6A) despite the continuous

flow of the suspension medium (DMEM). By contrast, NPs were washed out by the perfusion media, as no visible fluorescence was observed (Figure 6B-C). Hollow pollen microcapsules loaded with NPs were retained by the cell layer (Figure 6D), and this prolonged interaction allowed subsequent internalization of the NPs, as shown by the red fluorescence observed inside the cells (Figure 6E-F). These results are coherent with the observations from static cultures, which indicate that loaded pollen acted as a multistep delivery device, first increasing the interaction with the cells, followed by a subsequent NPs release to the surrounding cells.

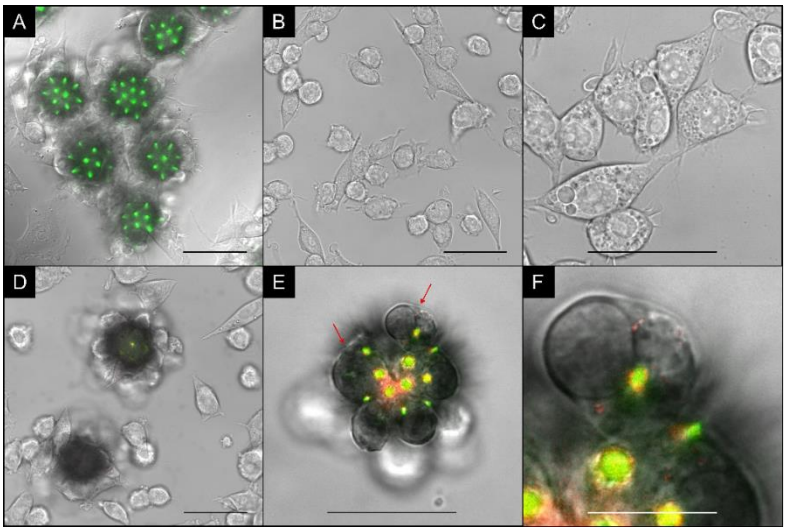

Figure 6. Confocal laser scanning micrographs of Raw 264.7 cells after the perfusion of **A**: hollow pollen microcapsules. **B** and **C**: fluorescent 200 nm polystyrene nanoparticles (NPs). **D** - **F**: Hollow pollen microcapsules loaded with fluorescent 200 nm polystyrene NPs. Red arrows indicate the presence of NPs in **E**. Green channel: Hollow pollen microcapsules autofluorescence. Red channel: NPs. (Scale bars represent 30 μm).

3.5. Loading and release of biodegradable protamine nanocapsules

Considering the results obtained with model polystyrene NPs, we explored the feasibility of associating biodegradable nanocarriers, using a core-shell protamine nanocapsule previously reported by our group [24]. As 200 nm NPs were more efficiently loaded than the other NPs regardless of the surface functionalization or the loading method employed, we developed protamine nanocapsules with a size close to 200 nm, low polydispersity index (<0.3), and neutral or slightly positive zeta potential. In addition, this polymeric nanocarrier, based on the combination of protamine (an arginine-rich polypeptide) [22–24], with oils and lipids was found to be a promising candidate for the oral delivery of peptides [47]. For monitoring the association of these nanocarriers to the pollen, a fluorescent dye (DiD) was efficiently encapsulated (96 ± 5%) within the oily core (**Table Supplementary S1**). Since in some studies, defatted [16] and hollow pollen grains [17] showed a similar capacity for loading drugs, we studied both, using different pollen: NCs ratios and loading procedures. As shown in **Table 3**, both lyophilization and vacuum-loading techniques yielded similar association efficiencies in the case of hollow pollen microcapsules. Defatted pollen showed lower NC association with the vacuum-assisted method. The obtained association efficiency was higher than that previously reported for other pollen samples and free drugs [17, 29–31, 39, 48], but lower than the data previously obtained with commercial NPs (see section 3.2.).

Table 3. Association efficiency, nanocapsules (NCs) loading capacity, and loading content of hollow pollen microcapsules (hollow) and defatted pollen (defatted) loaded by lyophilization and vacuum at different mass ratios.

Loading method	Ratio Pollen: NCs	Sample	Association efficiency (%)	Loading capacity (%)	Loading content (w/w)
Lyophilization	1:1	Hollow: NCs	60.4 ± 1.9	37.7 ± 0.8	0.60 ± 0.02
	1:2	Hollow: NCs	66.2 ± 7.6	56.8 ± 2.9	1.32 ± 0.15
	1:1	Defatted: NCs	63.3 ± 5.1	38.8 ± 1.9	0.63 ± 0.05
Vacuum	1:1	Hollow: NCs	65.8 ± 3.7	39.7 ± 1.4	0.66 ± 0.04
	1:2	Hollow: NCs	65.0 ± 6.7	56.4 ± 2.5	1.32 ± 0.13
	1:1	Defatted: NCs	52.1 ± 2.6	34.3 ± 1.0	0.52 ± 0.03

Thermogravimetric analysis (TGA) analysis of defatted pollen: NCs and hollow pollen: NCs at mass ratio 1:1 (**Supplementary Fig. S1**) also supported the fluorescence-based loading data. The mass variation at ~300 ºC of loaded samples was higher than unloaded (defatted or hollow) pollen, indicating the presence of NCs. CLSM analysis allowed us to localize the NCs within the pollen samples, and although defatted and hollow pollen loaded similar amounts of NCs (~60%), they presented different localization patterns within the pollen grains. Similar to polystyrene NPs, NCs were mostly located on the surface of defatted pollen (**Figure 7A**), while they were loaded both onto the surface, inside the wall, and in the core of the purified hollow pollen microcapsules (**Figure 7B-J**). At higher pollen: NCs ratios, the loading increased in this latter case, as more NCs were accumulated in the interior. Overall, hollow pollen microcapsules loaded with NCs by vacuum at a mass ratio of 1:2 showed the highest proportion of filled microcapsules.

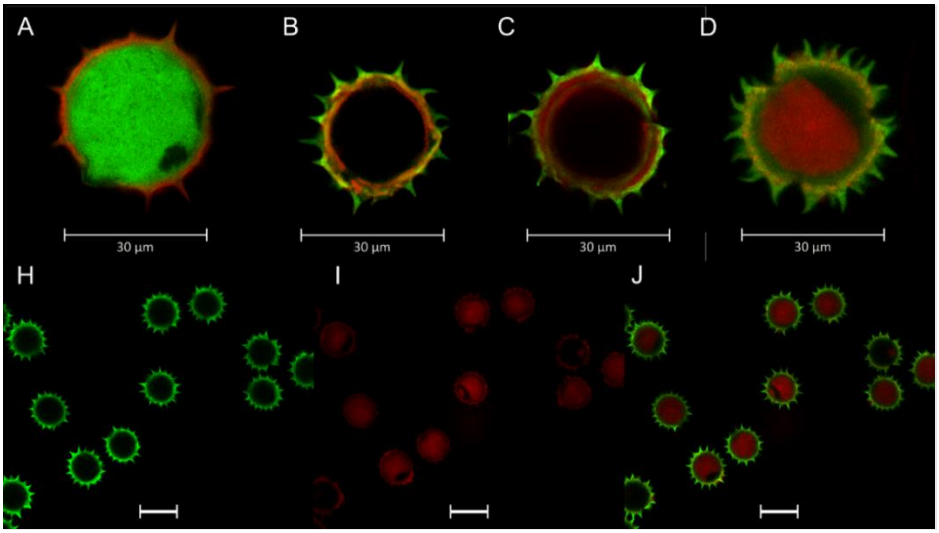

Figure 7. Confocal laser scanning micrographs of pollen samples (defatted and hollow) loaded with nanocapsules (NCs) at different mass ratios. **A**: Defatted pollen: NCs mass ratio of 1:1. **B**: Hollow pollen: NCs mass ratio of 1:1. **C**: Hollow pollen: NCs mass ratio of 1:2. **D-J:** Hollow pollen: NCs mass ratio of 1:2 loaded by vacuum. **H**: Green channel: pollen grain. **I**: Red channel: fluorescent NCs. **J**: Overlay. (Scale bars represent 30 µm).

The association of NCs to defatted and hollow pollen microcapsules was also studied by FTIR. The bands associated with the NCs (**Supplementary Figure 2**) were visible in addition to the FTIR spectra of the pollen. In general, NCs spectral intensity decreased with increased pollen: NCs mass ratio, indicating the successful NCs encapsulation in the internal cavity of the pollen microcapsules. In both defatted and hollow pollen microcapsules, the NCs' FTIR bands were higher when using a loading ratio of 1:1 (pollen: NCs) than the loading ratio of 1:2, suggesting the saturation of pollen, with a greater surface coverage. Interestingly, defatted pollen presented

higher NC band intensities than hollow pollen microcapsules, with the same loading. This can be explained by the penetration depth of FTIR (1 - 5 µm) at the wavelength used in this study [49]. This could indicate that the NCs are located on the surface of defatted pollen, whereas for hollow pollen microcapsules, more NCs would be present in the inner cavity. This explanation confirms the CLSM results (Figure 7).

Defatted and hollow pollen microcapsules loaded with NCs were incubated in simulated intestinal fluid (SIF) to investigate their *in vitro* release properties. Although both formulations were able to load similar amounts of NCs (**Table 2**), the cumulative release study (**Figure 8**) showed that defatted pollen had a limited maximum release of ~5% of loaded NCs over two days, while hollow pollen microcapsules reached ~40% of its payload over the same time interval. The release pattern of lyophilized and vacuum loaded NCs was similar, unlike the results obtained with NPs (**Figure 4**). This delayed NCs release in the case of defatted pollen could be related to a stronger interaction of NCs with the defatted pollen, due to the presence of proteins and carbohydrates on the surface and in the cytoplasm [20]. The materials providing this interaction would be absent after purification with phosphoric acid, that yields hollow structures composed by sporopollenin alone. Similar behavior was reported for BSA loaded into defatted and hollow pollen microcapsules. The low overall release of defatted samples indicates that the selected NCs have a strong affinity to the surface of the exine, being probably retained in its pores, while in hollow pollen grains, the additional release is produced by the NCs from the interior through the natural apertures [16].

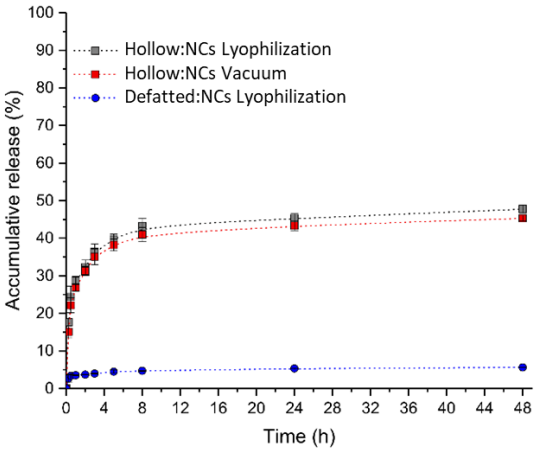

Figure 8. Accumulative release of protamine nanocapsules (NCs) loaded in defatted pollen and hollow pollen with a mass ratio 1:1 (w/w) employing lyophilization and vacuum-assisted loading methods. Error bars represent the standard deviation of the replicates (N=3).

After release, NCs size and polydispersity index (PDI) remained unchanged, and this was independent of the loading method (**Supplementary Table 1**). The release pattern was comparable to those observed with non-biodegradable aminated NPs (Fig. 4), indicating that the results obtained with the model NPs were predictive to a good extent to the behavior of the rationally designed, biodegradable nanocapsules. Defatted pollen: NCs (R^2=0.981) and hollow pollen microcapsules: NCs (R^2=0.991 for lyophilization and R^2=0.994) fitted to a Higuchi diffusion release kinetics, similar to that reported for 200 nm vacuum-loaded NPs. Therefore, the release kinetics were consistent with a diffusive mechanism.

3.6. *Ex vivo* mucointeraction

Pollen grains are characterized by natural bioadhesive properties, and thus we hypothesized that they could act as multi-stage delivery platforms and efficiently enhance the mucointeraction of associated nanocarriers. To confirm this idea, we tested the developed pollen microcapsules in an *ex vivo* model based on a non-everted rat intestinal sac. Our results showed that both defatted and hollow pollen microcapsules (**Supplementary Figure 3**) were able to attach to the intestinal mucosal surface and remained adhered to it over time. The surface of the sporopollenin microcapsules, with carboxyl and hydroxyl functional groups, could contribute to the formation of hydrogen bonds between mucin and sporopollenin and its morphology, mediated by the geometry of the spikes, could enhance its adhesion, and improve pollen microcapsules mucoadhesion on the intestinal wall. Similar behaviour has been previously described for other pollen grains from the same family, such as ragweed pollen, indicating that surface ornamentation of the pollen grain contributed to its adhesion to intestinal tissues and enhanced its interaction with the intestinal mucosa, resulting in a more efficient delivery of drugs [19][50]. Regarding the associated nanoparticles, supplementary Figure 3C shows a confocal microscopy image of the mucosal surface of the tissue after incubation with hollow pollen microcapsules loaded with polystyrene NPs. The attached pollen grains and the NPs are visible in the surrounding mucus.

When the same experiment was performed with biodegradable protamine NCs specifically designed for oral drug delivery and mucoadhesion, similar results were observed (**Figure 9**). Concretely, a high proportion of pollen microcapsules were found in contact with the mucosa. In general terms, the NCs administered alone presented a non-uniform distribution after 3 h of interaction, and the overall fluorescence intensity was found to be lower than for NCs associated with pollen-based microcapsules [25, 51]. In this case, the diffusion of the NCs to the mucosa could be also observed, surrounding the pollen grains. These results indicated that pollen microcapsules can modulate the NCs association and retention at the mucosa, improving their interaction and reducing the possibility of being prematurely eliminated from the absorption site.

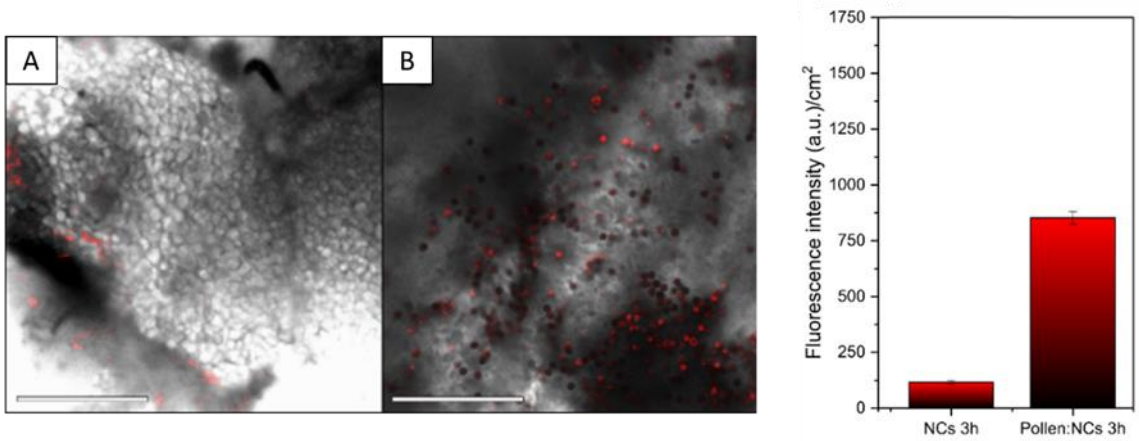

Figure 9. Confocal microscopy images of a top view of mucosal tissue of non-everted intestinal sacs incubated with. Protamine NCs after 3 h of incubation (A), hollow pollen microcapsules loaded with protamine NCs after 3h of incubation (B). Red channel: NCs. DIC: Differential Interference Contrast. Bars represent 500 µm. Quantification of red fluorescence in the tissue expressed as a form of raw integrated density per area of tissue (C). Error bars correspond to the standard error of the mean (n=3).

3.7. *In vivo* distribution upon oral administration

Finally, hollow pollen microcapsules, protamine NCs, and their combination were evaluated in terms of their distribution in the intestine after oral administration. The different preparations were given to healthy rats, and their fluorescence was analyzed by IVIS imaging [51, 52]. As the natural fluorophores of pollen samples emit across a broad spectrum of excitation wavelengths in the visible region [21], the mean fluorescence intensity of all images was adjusted [53] by extracting the signal produced by endogenous autofluorochromes such as hemoglobin. Those fluorochromes are present in living tissue [54] and cause background noise to the photon penetration process, interfering with imaging results [55, 56]. The biodistribution analysis at 3 h after oral administration suggests a lower accumulation of DiD-labelled protamine NCs in the small intestine of rats when they were administered alone as compared to the same NCs loaded into hollow pollen microcapsules (**Figure 10**). Similar retention times (2-4 h) were achieved after oral administration of free nanocarriers [51, 57], suggesting a rather quick removal from the intestinal mucosa. In the case of nanocarriers loaded into hollow pollen, a prolonged retention was observed, suggesting a progressive release, as corroborated by the *ex vivo* assay. The semi-quantitative analysis of the total fluorescence intensity of the region confirmed higher amounts of NCs when administered loaded on pollen platforms.

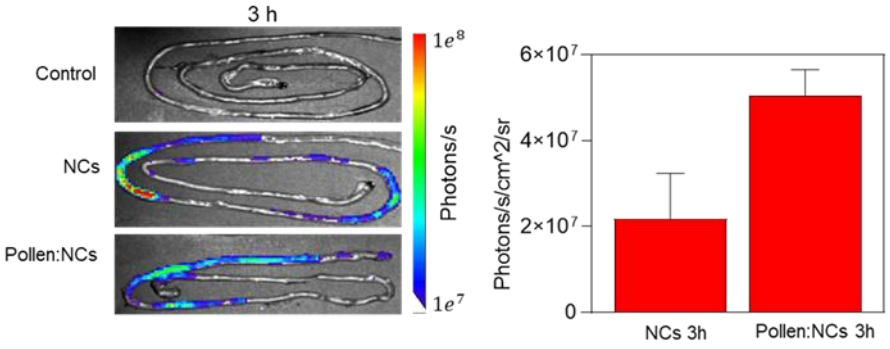

Figure 10. Fluorescence intensity signals and quantification (ROI) in the small intestine 3h after the oral administration of hollow pollen microcapsules (control), DiD-protamine nanocapsules (free NCs), and DiD-protamine NCs loaded into hollow pollen microcapsules (n=3; media± standard error of the mean).

It is important to highlight, that the developed pollen microcapsules did not require the use of external coatings, such as xanthan gum [58], alginate [16, 58], Eudragit L100 [17], or Eudragit RS 100 [33] to provide a sustained tuneable release, and/or protect from the low gastric pH during oral delivery. The NCs loaded into the pollen microcapsules were able to overcome the gastric environment and were effectively released to the intestinal mucosa, showing enhanced retention.

4. CONCLUSIONS

Microcapsules produced from spores and pollen have attracted great attention in the search for new drug delivery strategies. Pollen microcapsules derived from *H. annuus* are complex structures with a unique spike surface morphology that confers mucoadhesive properties. As one of the main problems in the administration of nanosystems is that they are quickly removed from biological surfaces, a combination of *H. annuus* pollen-based structures and nanocarriers should resolve those limitations. In this work, we have developed hollow pollen microcapsules and studied their capacity to load and release nanocarriers. To our knowledge, this is the first report on the association of pollen with nanocarriers of any kind, and the first to analyze the interactions between them and how those interactions depend on the nanocarriers'

physicochemical properties. Concretely, we have determined the optimal properties of the nanocarriers for effective loading in the hollow pollen microcapsules, and how nanocarrier size and surface modifications affect the release profile. Under specific conditions, hollow pollen microcapsules produce controlled release patterns. Besides this, hollow pollen microcapsules were also able to improve the interaction of the loaded nanocarriers with immune cells and the intestinal mucosa. In summary, this work provides information about the rational design of hollow pollen microcapsules loaded with nanocarriers, a multi-step delivery platform that combines the benefits of nanotechnology with the capacity of pollen grains to anchor to the mucosa. This combination of characteristics could be of interest for several applications.

SUPPLEMENTARY MATERIAL

Supplementary Table 1: Physicochemical characterization of employed nanocarriers (A) nanoparticles (NPs) and (B) protamine nanocapsules (NCs). DiD: 1,1'-Dioctadecyl-3,3,3',3'-tetramethylindodicarbocyanine, 4-chlorobenzenesulfonate salt.

(A) Sample	Size (nm)	PDI	ζ-potential (mV)
Aminated NPs 100 nm	141 ± 2	0.17	+47 ± 1
Unmodified NPs 100 nm	100 ± 2	0.02	-42 ± 0.3
Carboxylated NPs 100 nm	105 ± 2	0.02	-39 ± 1
Aminated NPs 200 nm	269 ± 6	0.06	+47 ± 1
Unmodified NPs 200 nm	194 ± 5	0.02	-50 ± 11
Carboxylated NPs 200 nm	234 ± 4	0.06	-39 ± 1
Aminated NPs 500 nm	451 ± 16	0.27	+43 ± 0.2
Unmodified NPs 500 nm	489 ± 28	0.39	-46 ± 1
Carboxylated NPs 500 nm	474 ± 19	0.15	-54 ± 1

(B) Sample	Size (nm)	PDI	ζ-potential (mV)
Protamine NCs	191 ± 3	0.10	+5 ± 1
Protamine- DiD NCs	246 ± 20	0.14	+3 ± 4
Protamine- DiD NCs released in SIF (lyophilization loading)	284 ± 10	0.30	-
Protamine- DiD NCs released in SIF (vacuum loading)	242 ± 2	0.20	-

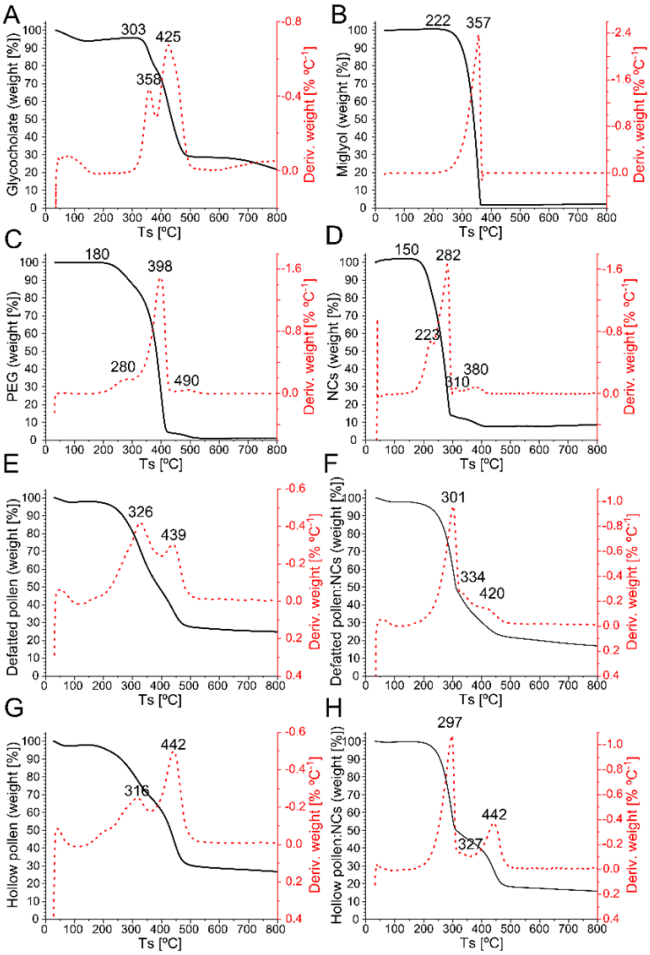

Supplementary Figure 1: Thermogravimetric analysis (TGA), and derivative thermogravimetry (DTG) curves of nanocapsules (NCs), their main components, defatted and hollow pollen, and NCs loaded pollen samples. **A**. Sodium glycocholate. **B**. Miglyol 812. **C**. PEG: Polyethylene glycol 40 stearate. **D**: NCs. **E**: Defatted pollen. **G**: Defatted pollen loaded with NCs at a mass ratio of 1:1. **G**: Hollow pollen microcapsules. **H**. Hollow pollen microcapsules loaded with NCs at a mass ratio of 1:1.

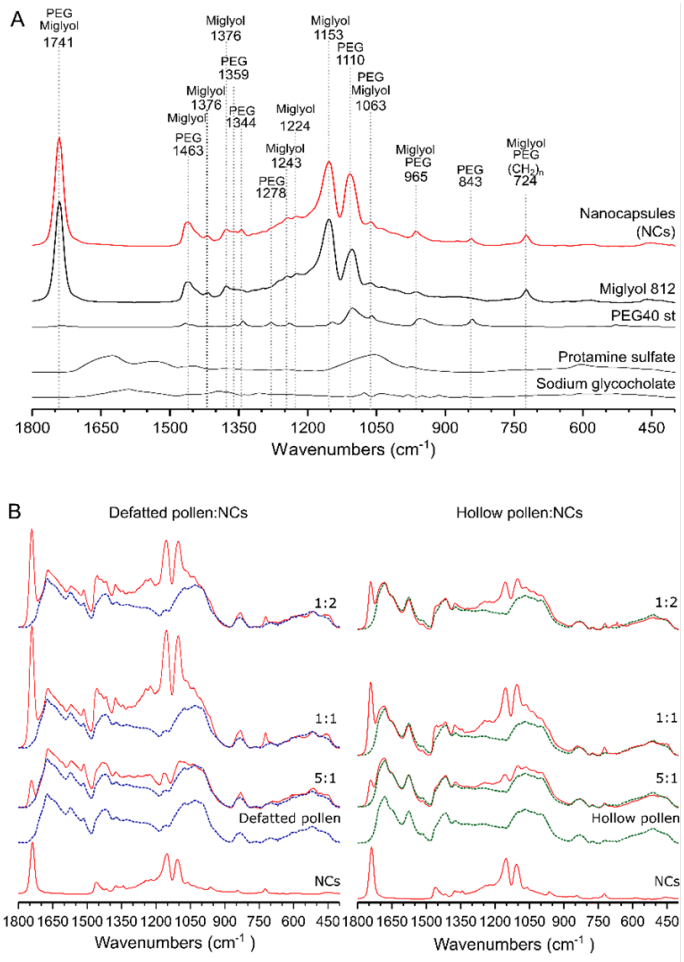

Supplementary Figure 2. FTIR spectra of nanocapsules (NCs), their components (A), defatted and hollow pollen, and NCs-loaded pollen samples (B) at different mass ratios. PEG40 st: Polyethylene glycol 40 stearate.

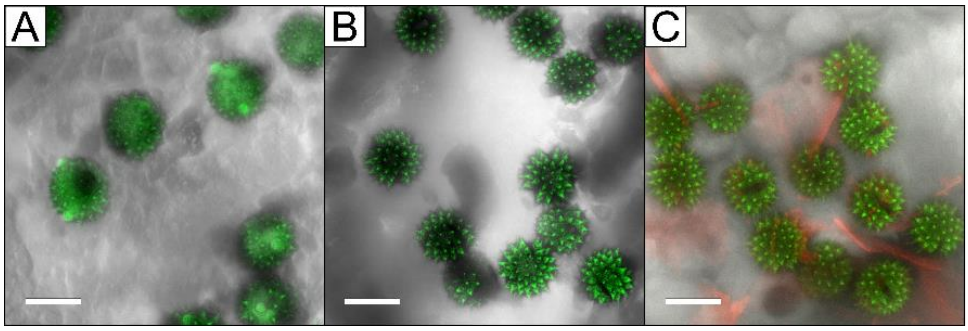

Supplementary Figure 3. Confocal microscopy images of a top view of mucosal tissue of a non-everted intestinal sac incubated with several samples. **A**. Defatted pollen. **B**. Hollow pollen. **C**. Hollow pollen loaded with 200 nm cationic polystyrene nanoparticles. Green channel: Pollen autofluorescence. Red channel: nanocapsules. DIC: differential interference contrast. White bars represent 30 µm.

REFERENCES

[1] Lakkireddy, H. R.; Urmann, M.; Besenius, M.; Werner, U.; Haack, T.; Brun, P.; Alié, J.; Illel, B.; Hortala, L.; Vogel, R.; et al. Oral Delivery of Diabetes Peptides - Comparing Standard Formulations Incorporating Functional Excipients and Nanotechnologies in the Translational Context. *Adv. Drug Deliv. Rev.*, **2016**, *106* (Pt B), 196–222. https://doi.org/10.1016/j.addr.2016.02.011.

[2] Ageitos, J. M.; Garcia-Fuentes, M. Advances in Drug Delivery Strategies for Microbial Healthcare Products. In *Pharmaceuticals from Microbes. The Bioengineering Perspective*; Arora, D., Sharma, C., Jaglan, S., Lichtfouse, E., Eds.; Springer International Publishing, 2019; pp 1–38. https://doi.org/10.1007/978-3-030-01881-8_1.

[3] Fosgerau, K.; Hoffmann, T. Peptide Therapeutics: Current Status and Future Directions. *Drug Discov. Today*, **2015**, *20* (1), 122–128. https://doi.org/10.1016/j.drudis.2014.10.003.

[4] Ageitos, J. M.; Chuah, J.-A.; Numata, K. Chapter 1. Design Considerations for Properties of Nanocarriers on Disposition and Efficiency of Drug and Gene Delivery. In *Nanomedicines: Design, Delivery and Detection*; Martin Braddock, Ed.; Royal Society of Chemistry, 2016; pp 1–22. https://doi.org/10.1039/9781782622536-00001.

[5] Thwala, L. N.; Préat, V.; Csaba, N. S. Emerging Delivery Platforms for Mucosal Administration of Biopharmaceuticals: A Critical Update on Nasal, Pulmonary and Oral Routes. *Expert Opin. Drug Deliv.*, **2017**, *14* (1), 23–36. https://doi.org/10.1080/17425247.2016.1206074.

[6] Ensign, L. M.; Cone, R.; Hanes, J. Oral Drug Delivery with Polymeric Nanoparticles: The Gastrointestinal Mucus Barriers. *Adv. Drug Deliv. Rev.*, **2012**, *64* (6), 557–570. https://doi.org/10.1016/j.addr.2011.12.009.

[7] Wu, L.; Shan, W.; Zhang, Z.; Huang, Y. Engineering Nanomaterials to Overcome the Mucosal Barrier by Modulating Surface Properties. *Adv. Drug Deliv. Rev.*, **2018**, *124*, 150–163. https://doi.org/10.1016/j.addr.2017.10.001.

[8] Serda, R. E.; Godin, B.; Blanco, E.; Chiappini, C.; Ferrari, M. Multi-Stage Delivery Nano-Particle Systems for Therapeutic Applications. *Biochim. Biophys. Acta - Gen. Subj.*, **2011**, *1810* (3), 317–329. https://doi.org/10.1016/j.bbagen.2010.05.004.

[9] Yu, F.; Li, Y.; Liu, C. S.; Chen, Q.; Wang, G. H.; Guo, W.; Wu, X. E.; Li, D. H.; Wu, W. D.; Chen, X. D. Enteric-Coated Capsules Filled with Mono-Disperse Micro-Particles Containing PLGA-Lipid-PEG Nanoparticles for Oral Delivery of Insulin. *Int. J. Pharm.*, **2015**, *484* (1–2), 181–191. https://doi.org/10.1016/j.ijpharm.2015.02.055.

[10] Gaspar, D. P.; Gaspar, M. M.; Eleutério, C. V.; Grenha, A.; Blanco, M.; Gonçalves, L. M. D.; Taboada, P.; Almeida, A. J.; Remuñán-López, C. Microencapsulated Solid Lipid Nanoparticles as a Hybrid Platform for Pulmonary Antibiotic Delivery. *Mol. Pharm.*, **2017**, *14* (9), 2977–2990. https://doi.org/10.1021/acs.molpharmaceut.7b00169.

[11] Wiermann, R.; Gubatz, S. Pollen Wall and Sporopollenin. *Int. Rev. Cytol.*, **1992**, *140*

(C), 35–72. https://doi.org/10.1016/S0074-7696(08)61093-1.

[12] Traidl-Hoffmann, C.; Kasche, A.; Menzel, A.; Jakob, T.; Thiel, M.; Ring, J.; Behrendt, H. Impact of Pollen on Human Health: More Than Allergen Carriers? *Int. Arch. Allergy Immunol.*, **2003**, *131* (1), 1–13. https://doi.org/10.1159/000070428.

[13] Barrier, S.; Diego-Taboada, A.; Thomasson, M. J.; Madden, L.; Pointon, J. C.; Wadhawan, J. D.; Beckett, S. T.; Atkin, S. L.; MacKenzie, G. Viability of Plant Spore Exine Capsules for Microencapsulation. *J. Mater. Chem.*, **2011**, *21* (4), 975–981. https://doi.org/10.1039/C0JM02246B.

[14] Alshehri, S. M.; Al-Lohedan, H. A.; Chaudhary, A. A.; Al-Farraj, E.; Alhokbany, N.; Issa, Z.; Alhousine, S.; Ahamad, T. Delivery of Ibuprofen by Natural Macroporous Sporopollenin Exine Capsules Extracted from *Phoenix Dactylifera* L. *Eur. J. Pharm. Sci.*, **2016**, *88*, 158–165. https://doi.org/10.1016/j.ejps.2016.02.004.

[15] Mundargi, R. C.; Potroz, M. G.; Park, J. H.; Seo, J.; Lee, J. H.; Cho, N.-J. Extraction of Sporopollenin Exine Capsules from Sunflower Pollen Grains. *RSC Adv.*, **2016**, *6* (20), 16533–16539. https://doi.org/10.1039/C5RA27207F.

[16] Mundargi, R. C.; Potroz, M. G.; Park, S.; Shirahama, H.; Lee, J. H.; Seo, J.; Cho, N.-J. Natural Sunflower Pollen as a Drug Delivery Vehicle. *Small*, **2016**, *12* (9), 1167–1173. https://doi.org/10.1002/smll.201500860.

[17] Potroz, M. G.; Mundargi, R. C.; Gillissen, J. J.; Tan, E.-L.; Meker, S.; Park, J. H.; Jung, H.; Park, S.; Cho, D.; Bang, S.-I.; et al. Plant-Based Hollow Microcapsules for Oral Delivery Applications: Toward Optimized Loading and Controlled Release. *Adv. Funct. Mater.*, **2017**, *27* (31), 1700270. https://doi.org/10.1002/adfm.201700270.

[18] Uddin, M. J.; Gill, H. S. Ragweed Pollen as an Oral Vaccine Delivery System: Mechanistic Insights. *J. Control. Release*, **2017**, *268* (October), 416–426. https://doi.org/10.1016/j.jconrel.2017.10.019.

[19] Diego-Taboada, A.; Beckett, S. T.; Atkin, S. L.; Mackenzie, G. Hollow Pollen Shells to Enhance Drug Delivery. *Pharmaceutics*, **2014**, *6* (1), 80–96. https://doi.org/10.3390/pharmaceutics6010080.

[20] Ageitos, J. M.; Robla, S.; Valverde-Fraga, L.; Garcia-Fuentes, M.; Csaba, N. Purification of Hollow Sporopollenin Microcapsules from Sunflower and Chamomile Pollen Grains. *Polymers (Basel).*, **2021**, *13* (13), 2094. https://doi.org/10.3390/polym13132094.

[21] Mundargi, R. C.; Potroz, M. G.; Park, J. H.; Seo, J.; Tan, E.-L.; Lee, J. H.; Cho, N.-J. Eco-Friendly Streamlined Process for Sporopollenin Exine Capsule Extraction. *Sci. Rep.*, **2016**, *6* (1), 1–14. https://doi.org/10.1038/srep19960.

[22] Thwala, L. N.; Beloqui, A.; Csaba, N. S.; González-Touceda, D.; Tovar, S.; Dieguez, C.; Alonso, M. J.; Préat, V. The Interaction of Protamine Nanocapsules with the Intestinal Epithelium: A Mechanistic Approach. *J. Control. Release*, **2016**, *243*, 109–120. https://doi.org/10.1016/j.jconrel.2016.10.002.

[23] Ageitos, J. M.; Pulgar, A.; Csaba, N.; Garcia-Fuentes, M. Study of Nanostructured Fibroin/Dextran Matrixes for Controlled Protein Release. *Eur. Polym. J.*, **2019**, *114* (February), 197–205. https://doi.org/10.1016/j.eurpolymj.2019.02.028.

[24] González-Aramundiz, J. V.; Presas, E.; Dalmau-Mena, I.; Martínez-Pulgarín, S.; Alonso, C.; Escribano, J. M.; Alonso, M. J.; Csaba, N. S. Rational Design of Protamine Nanocapsules as Antigen Delivery Carriers. *J. Control. Release*, **2017**, *245*, 62–69. https://doi.org/10.1016/j.jconrel.2016.11.012.

[25] Liu, W.; Pan, H.; Zhang, C.; Zhao, L.; Zhao, R.; Zhu, Y.; Pan, W. Developments in Methods for Measuring the Intestinal Absorption of Nanoparticle-Bound Drugs. *Int. J. Mol. Sci.*, **2016**, *17* (7). https://doi.org/10.3390/ijms17071171.

[26] Bashir, M. E. H.; Ward, J. M.; Cummings, M.; Karrar, E. E.; Root, M.; Mohamed, A. B. A.; Naclerio, R. M.; Preuss, D. Dual Function of Novel Pollen Coat (Surface) Proteins: IgE-Binding Capacity and Proteolytic Activity Disrupting the Airway Epithelial Barrier. *PLoS One*, **2013**, *8* (1), e53337. https://doi.org/10.1371/journal.pone.0053337.

[27] Knox, R. B. The Pollen Grain. In *Embryology of Angiosperms*; Johri, B. M., Ed.; Springer Berlin Heidelberg: Berlin, Heidelberg, 1984; pp 197–271. https://doi.org/10.1007/978-3-642-69302-1_5.

[28] Horner, H. T.; Pearson, C. B. Pollen Wall and Aperture Development in Helianthus Annuus (Compositae : Heliantheae). *Am. J. Bot.*, **1978**, *65* (3), 293–309. https://doi.org/10.2307/2442270.

[29] Akyuz, L.; Sargin, I.; Kaya, M.; Ceter, T.; Akata, I. A New Pollen-Derived Microcarrier for Pantoprazole Delivery. *Mater. Sci. Eng. C*, **2017**, *71*, 937–942. https://doi.org/10.1016/j.msec.2016.11.009.

[30] Sargin, I.; Akyuz, L.; Kaya, M.; Tan, G.; Ceter, T.; Yildirim, K.; Ertosun, S.; Aydin, G. H.; Topal, M. Controlled Release and Anti-Proliferative Effect of Imatinib Mesylate Loaded Sporopollenin Microcapsules Extracted from Pollens of *Betula Pendula*. *Int. J. Biol. Macromol.*, **2017**, *105*, 749–756. https://doi.org/10.1016/j.ijbiomac.2017.07.093.

[31] Lale, S. V.; Gill, H. S. Pollen Grains as a Novel Microcarrier for Oral Delivery of Proteins. *Int. J. Pharm.*, **2018**, *552* (1–2), 352–359. https://doi.org/10.1016/j.ijpharm.2018.10.016.

[32] Palazzo, I.; Mezzetta, A.; Guazzelli, L.; Sartini, S.; Pomelli, C. S.; Parker, W. O.; Chiappe, C. Chiral Ionic Liquids Supported on Natural Sporopollenin Microcapsules. *RSC Adv.*, **2018**, *8* (38), 21174–21183. https://doi.org/10.1039/c8ra03455a.

[33] Mundargi, R. C.; Potroz, M. G.; Park, S.; Park, J. H.; Shirahama, H.; Lee, J. H.; Seo, J.; Cho, N.-J. Lycopodium Spores: A Naturally Manufactured, Superrobust Biomaterial for Drug Delivery. *Adv. Funct. Mater.*, **2016**, *26* (4), 487–497. https://doi.org/10.1002/adfm.201502322.

[34] Babakhani, P. The Impact of Nanoparticle Aggregation on Their Size Exclusion during Transport in Porous Media: One- and Three-Dimensional Modelling Investigations. *Sci.*

Rep., **2019**, *9* (1), 1–12. https://doi.org/10.1038/s41598-019-50493-6.

[35] Fu, Y.; Kao, W. Drug Release Kinetics and Transport Mechanisms of Non-Degradable and Degradable Polymeric Delivery Systems. *Expert Opin. Drug Deliv.*, **2010**, *7* (4), 429–444. https://doi.org/10.1517/17425241003602259.Drug.

[36] Mackenzie, G.; Beckett, S.; Atkin, S.; Diego-Taboada, A. *Pollen and Spore Shells—Nature's Microcapsules*; Elsevier Inc., 2014. https://doi.org/10.1016/B978-0-12-404568-2.00024-8.

[37] Fan, T.; Park, S.; Shi, Q.; Zhang, X.; Liu, Q.; Song, Y.; Chin, H.; Shahrudin, M.; Ibrahim, B.; Mokrzecka, N.; et al. Transformation of Hard Pollen into Soft Matter. *Nat. Commun.*, **2020**, *11* (1), 1449. https://doi.org/10.1038/s41467-020-15294-w.

[38] Mathematical Models of Drug Release. In *Strategies to Modify the Drug Release from Pharmaceutical Systems*; Marcos Luciano Bruschi, Ed.; Elsevier, 2015; pp 63–86. https://doi.org/10.1016/B978-0-08-100092-2.00005-9.

[39] Mujtaba, M.; Sargin, I.; Akyuz, L.; Ceter, T.; Kaya, M. Newly Isolated Sporopollenin Microcages from *Platanus Orientalis* Pollens as a Vehicle for Controlled Drug Delivery. *Mater. Sci. Eng. C*, **2017**, *77*, 263–270. https://doi.org/10.1016/j.msec.2017.02.176.

[40] Dyab, A. K. F.; Mohamed, M. A.; Meligi, N. M.; Mohamed, S. K. Encapsulation of Erythromycin and Bacitracin Antibiotics into Natural Sporopollenin Microcapsules: Antibacterial, Cytotoxicity, in Vitro and in Vivo Release Studies for Enhanced Bioavailability. *RSC Adv.*, **2018**, *8* (58), 33432–33444. https://doi.org/10.1039/C8RA05499A.

[41] Korsmeyer, R. W.; Gurny, R.; Doelker, E.; Buri, P.; Peppas, N. A. Mechanisms of Solute Release from Porous Hydrophilic Polymers. *Int. J. Pharm.*, **1983**, *15* (1), 25–35. https://doi.org/10.1016/0378-5173(83)90064-9.

[42] Meligi, N. M.; Dyab, A. K. F.; Paunov, V. N. Sustained in Vitro and in Vivo Delivery of Metformin from Plant Pollen-Derived Composite Microcapsules. *Pharmaceutics*, **2021**, *13* (7), 9–12. https://doi.org/10.3390/pharmaceutics13071048.

[43] Pakolpakçıl, A.; Draczynski, Z. Green Approach to Develop Bee Pollen-Loaded Alginate Based Nanofibrous Mat. *Materials (Basel).*, **2021**, *14* (11). https://doi.org/10.3390/ma14112775.

[44] Turner, J. R. Intestinal Mucosal Barrier Function in Health and Disease. *Nat. Rev. Immunol.*, **2009**, *9* (11), 799–809. https://doi.org/10.1038/nri2653.

[45] Swamy, M.; Jamora, C.; Havran, W.; Hayday, A. Epithelial Decision Makers: In Search of the "Epimmunome." *Nat. Immunol.*, **2010**, *11* (8), 656–665. https://doi.org/10.1038/ni.1905.

[46] Uddin, M. J.; Gonzalez-Cruz, P.; Warzywoda, J.; Gill, H. S. Sporopollenin Spikes Augment Antigen-Specific Immune Response and Generate Long-Lived Humoral Immunity. *Adv. Ther.*, **2020**, *2000102*, 2000102.

https://doi.org/10.1002/adtp.202000102.

[47] Robla, S.; Alonso, M. J.; Csaba, N. Polyaminoacid-Based Nanocarriers: A Review of the Latest Candidates for Oral Drug Delivery. *Expert Opin. Drug Deliv.*, **2020**, *00* (00), 1–12. https://doi.org/10.1080/17425247.2020.1776698.

[48] Prabhakar, A. K.; Lai, H. Y.; Potroz, M. G.; Corliss, M. K.; Park, J. H.; Mundargi, R. C.; Cho, D.; Bang, S. I.; Cho, N.-J. Chemical Processing Strategies to Obtain Sporopollenin Exine Capsules from Multi-Compartmental Pine Pollen. *J. Ind. Eng. Chem.*, **2017**, *53*, 375–385. https://doi.org/10.1016/j.jiec.2017.05.009.

[49] Subramanian, A.; Rodriguez-Saona, L. Fourier Transform Infrared (FTIR) Spectroscopy. In *Infrared Spectroscopy for Food Quality Analysis and Control*; Da-Wen Sun, Ed.; Academic Press, 2009; pp 145–178. https://doi.org/10.1016/B978-0-12-374136-3.00007-9.

[50] Wang, Y.; Shang, L.; Chen, G.; Shao, C.; Liu, Y.; Lu, P.; Rong, F.; Zhao, Y. Pollen-Inspired Microparticles with Strong Adhesion for Drug Delivery. *Appl. Mater. Today*, **2018**, *13*, 303–309. https://doi.org/10.1016/j.apmt.2018.09.016.

[51] Thwala, L. N.; Delgado, D. P.; Leone, K.; Marigo, I.; Benetti, F.; Chenlo, M.; Alvarez, C. V.; Tovar, S.; Dieguez, C.; Csaba, N. S.; et al. Protamine Nanocapsules as Carriers for Oral Peptide Delivery. *J. Control. Release*, **2018**, *291* (June), 157–168. https://doi.org/10.1016/j.jconrel.2018.10.022.

[52] Komesli, Y.; Burak Ozkaya, A.; Ugur Ergur, B.; Kirilmaz, L.; Karasulu, E. Design and Development of a Self-Microemulsifying Drug Delivery System of Olmesartan Medoxomil for Enhanced Bioavailability. *Drug Dev. Ind. Pharm.*, **2019**, *45* (8), 1292–1305. https://doi.org/10.1080/03639045.2019.1607868.

[53] Barone, F. C.; Marcinkiewicz, C.; Li, J.; Feng, Y.; Sternberg, M.; Lelkes, P. I.; Rosenbaum-Halevi, D.; Gerstenhaber, J. A.; Feuerstein, G. Z. Long-Term Biocompatibility of Fluorescent Diamonds-(NV)-Z~800 Nm in Rats: Survival, Morbidity, Histopathology, Particle Distribution and Excretion Studies (Part IV). *Int. J. Nanomedicine*, **2019**, *14*, 1163–1175. https://doi.org/10.2147/IJN.S189048.

[54] Hansch, A.; Sauner, D.; Hilger, I.; Böttcher, J.; Malich, A.; Frey, O.; Bräuer, R.; Kaiser, W. A. Autofluorescence Spectroscopy in Whole Organs with a Mobile Detector System. *Acad. Radiol.*, **2004**, *11* (11), 1229–1236. https://doi.org/10.1016/j.acra.2004.07.027.

[55] Cao, J.; Zhu, B.; Zheng, K.; He, S.; Meng, L.; Song, J.; Yang, H. Recent Progress in NIR-II Contrast Agent for Biological Imaging. *Front. Bioeng. Biotechnol.*, **2020**, *7* (January), 1–21. https://doi.org/10.3389/fbioe.2019.00487.

[56] Weissleder, R. A Clearer Vision for in Vivo Imaging: Progress Continues in the Development of Smaller, More Penetrable Probes for Biological Imaging. *Nat. Biotechnol.*, **2001**, *19* (4), 316–317. https://doi.org/10.1038/86684.

[57] Niu, Z.; Samaridou, E.; Jaumain, E.; Coëne, J.; Ullio, G.; Shrestha, N.; Garcia, J.; Durán-Lobato, M.; Tovar, S.; Santander-Ortega, M. J.; et al. PEG-PGA Enveloped

Octaarginine-Peptide Nanocomplexes: An Oral Peptide Delivery Strategy. *J. Control. Release*, **2018**, *276* (October 2017), 125–139. https://doi.org/10.1016/j.jconrel.2018.03.004.

[58] Prabhakar, A. K.; Potroz, M. G.; Tan, E. L.; Jung, H.; Park, J. H.; Cho, N.-J. Macromolecular Microencapsulation Using Pine Pollen: Loading Optimization and Controlled Release with Natural Materials. *ACS Appl. Mater. Interfaces*, **2018**, *10* (34), 28428–28439. https://doi.org/10.1021/acsami.8b09952.

CHAPTER III/CAPÍTULO III

A ready-to-use dry powder formulation based on protamine nanocarriers for pulmonary drug delivery

Sandra Robla[1], Rubén Varela Calviño[2], Rita Ambrus[3] & Noemi Csaba[1]

1. Center for Research in Molecular Medicine and Chronic Diseases (CiMUS) and Department of Pharmacology, Pharmacy and Pharmaceutical Technology, University of Santiago de Compostela, A Coruña, Spain
2. Department of Biochemistry and Molecular Biology, University of Santiago de Compostela, A Coruña, Spain
3. Faculty of Pharmacy, Institute of Pharmaceutical Technology and Regulatory Affairs, University of Szeged, Szeged, Hungary

Sandra Robla, Rubén Varela Calviño, Rita Ambrus & Noemi Csaba (2023) A ready-to-use dry powder formulation based on protamine nanocarriers for pulmonary drug delivery. European Journal of Pharmaceutical Sciences; 185:106442.

DOI:*https://10.1016/j.ejps.2023.106442*

Author contributions: Formal analysis, Investigation, Methodology, Software, Visualization & Writing.

CHAPTER III/ CAPÍTULO III

A ready-to-use dry powder formulation based on protamine nanocarriers for pulmonary drug delivery

Abstract

The use of oral antibiotic therapy for the treatment of respiratory diseases such as tuberculosis has promoted the appearance of side effects as well as resistance to these treatments. The low solubility, high metabolism, and degradation of drugs such as rifabutin, have led to the use of combined and prolonged therapies, which difficult patient compliance. In this work, we develop inhalable formulations from biomaterials such as protamine to improve the therapeutic effect. Rifabutin-loaded protamine nanocapsules (NCs) were prepared by solvent displacement method and were physico-chemically characterized and evaluated for their dissolution, permeability, stability, cytotoxicity, hemocompatibility, internalization, and aerodynamic characteristics after a spray-drying procedure. Protamine NCs presented a size of around 200 nm, positive surface charge, and drug association up to 54%. They were stable as suspension under storage, as well as in biological media and as a dry powder after lyophilization in the presence of mannitol. Nanocapsules showed a good safety profile and cellular uptake with no tolerogenic effect on macrophages and showed good compatibility with red blood cells. Moreover, the aerodynamic evaluation showed a fine particle fraction deposition up to 30% and a mass median aerodynamic diameter of about 5 µm, suitable for the pulmonary delivery of therapeutics.

Keywords

protamine nanocapsules, rifabutin, mannitol, pulmonary drug delivery, anti-tuberculotic treatment.

Graphical abstract

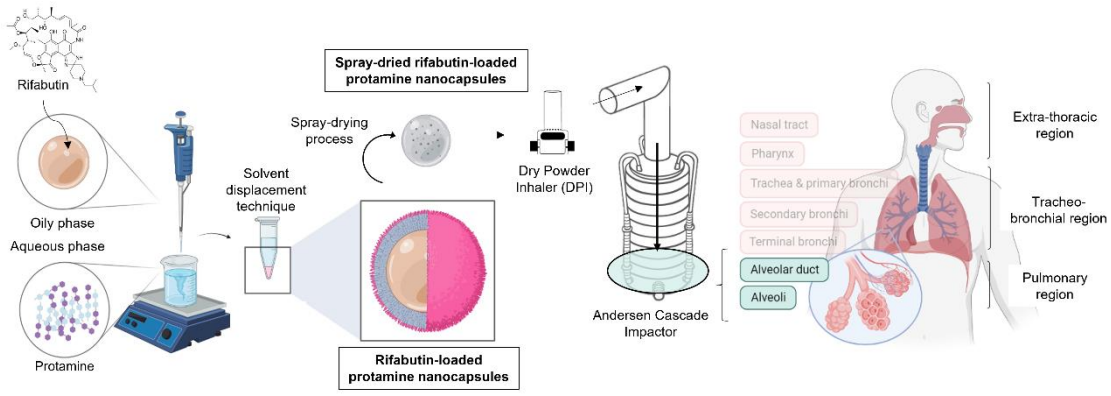

1. INTRODUCTION

Tuberculosis (TB) is an infectious disease caused by the Gram+ bacteria *Mycobacterium tuberculosis* (Mtb). TB's global mortality of 1.4 million people (WHO, 2019) constitutes a significant public health challenge (Chae et al., 2021). Pulmonary TB is the most characteristic form of disease, where Mtb, once inhaled, is phagocytosed by alveolar macrophages, multiplying and giving rise to an inflammatory reaction and characteristic tissue damage in the upper lobes of the lungs (Lado, 2002). TB treatment consists of 6 months of oral administration of the first-line drugs isoniazid, rifampicin, ethambutol, and pyrazinamide. A second-line TB treatment extends up to 9 or 20 months in case of isoniazid or rifampicin resistance, respectively, and includes the use of oral or parenteral drugs such as kanamycin, moxifloxacin or levofloxacin (Suárez et al., 2019). The oral route is the most suitable and least expensive for TB treatment, however, extended administration of high doses is required, and only sub-therapeutic levels of anti-TB drugs reach the site of action due to elevated first-pass metabolism and degradation (Sosnik et al., 2010). Compared to the oral route, the pulmonary route allows rapid action and higher bioavailability due to the large surface area and high vascularization of alveoli (70-140 m^2) for the achievement of high concentrations at the site of Mtb action, the alveolar macrophages (Chae et al., 2021), thereby reducing unwanted systemic effects. However, this route is constituted by a set of physical and biological barriers with complex geometry and high humidity, mucociliary clearance, or the presence of macrophages and alveolar enzymes which pose a great challenge for the administration of drugs (El-Sherbiny et al., 2015). Although studies of inhalation therapy for TB began in the late 1940s, after oral treatment began to show resistance (Traini and Young, 2017), they are still in preclinical development with no anti-tubercular inhalable formulation available in the market (Braunstein et al., 2019).

Rifabutin is a derivative of rifamycin, which has shown tolerability and safety in the treatment of disseminated intracellular infection by *Mycobacterium avium*, with significant advantages over rifampicin in the treatment of *M. tuberculosis* (Aristoff et al., 2010). It has shown a minimum inhibitory concentration *in vitro* and lower protein binding than rifampicin, with greater accumulation in cells and lipid solubility, which provides a larger volume of distribution (Davies et al., 2007). Therapeutic strategies based on nanotechnology offer the possibility of overcoming biological barriers and protecting biomacromolecules against degradation. The few reports available on rifabutin-based nanotechnology-based drug delivery systems comprised liposomes and solid lipid nanoformulations for intravenous, oral or pulmonary (Gaspar et al., 2016, 2008; Nimje et al., 2009; Nirbhavane et al., 2017) TB treatment, as well as Chron's disease (Rouco et al., 2020) or *M. avium* infection (Gaspar et al., 2000). However, upon pulmonary administration their nanometric size results have low inertia, which carries the risk of exhalation (up to 80%) without being deposited in the airways (Yang et al., 2008). Recent advances in particle engineering and materials science have opened a door for improving the efficacy of inhalation by the production of porous microparticulate powders with the optimal size for drug deposition at the targeted site (El-Sherbiny et al., 2015). Microparticle administration in the form of dry powder inhalers (DPIs) constitutes a promising strategy, with highly effective drug lung deposition and patient adherence (Nainwal et al., 2022). The controlled agglomeration of nanoparticles into micron-sized particles has been used as an effective delivery method using DPIs. These platforms act as an intermediate delivery system until reaching the alveoli, where the redispersion of the agglomerates of nanoparticles occurs, causing their release (Malamatari et al., 2020). The present study aimed to design and develop a drug delivery system to overcome the limitations related to anti-tuberculosis therapy.

Rifabutin was encapsulated into protamine nanocapsules, and formulations were characterized and spray-dried with mannitol for the obtention of a DPI. The present work demonstrates the potential of the developed nanocarriers evaluating their distribution in the lung and showing their suitability for pulmonary administration.

2. EXPERIMENTAL SECTION

2.1. Materials

Rifabutin was acquired from Chemos GmbH (Germany). Low molecular weight protamine sulphate (5 kDa) was purchased from Yuki Gosei Kogyo, Ltd (Japan). Polyethylene glycol stearate 40 (PEGst 40) was provided by Croda Chemicals Europe Ltd. (United Kingdom) and sodium glycocholate (SGC) was purchased from Dextra laboratories Ltd. (United Kingdom). Caprylic/capric/succinic triglyceride (Miglyol® 812) was obtained from IOI Oleo GmbH (Germany). D-Mannitol was obtained from Molar Chemical KFT. 3-(4,5-dimethyl-2-thiazolyl)-2,5-diphenyl-2H-tetrazolium bromide (MTT) and 4,6-diamidino-2-phenylindole (DAPI) dye were purchased from Sigma-Aldrich (St. Louis, MO, USA). 1,1'-Dioctadecyl-3,3,3',3'-tetramethylindodicarbocyanine, 4-chlorobenzenesulfonate salt (DiD) was provided by Thermo Fisher Scientific (USA). Ficoll-Paque™ PLUS was obtained from GE Healthcare Bio-Science AB, (Sweden), Medium Roswell Park Memorial Institute (RPMI-1640), and Dulbecco's Modified Eagle's Medium (DMEM) were obtained from GIBCO® (Thermo Fisher Scientific, Spain). Granulocyte-macrophage colony-stimulating factor (GM-CSF) was obtained from Tonbo Biosciences (San Diego, CA, USA). Fetal Bovine Serum (FBS), and PSG (Penicillin-Streptomycin-Glutamine) were provided by Sigma Aldrich. A549 human alveolar lung carcinoma cell line and Raw 264.7 cell line were obtained from ATCC (Manassas, VA, USA). Sodium chloride (NaCl), sodium hydrogen carbonate ($NaHCO_3$), glycine ($C_2H_5NO_2$), calcium chloride dihydrate ($CaCl_2$), sulfuric acid (H_2SO_4) and sodium phosphate hydrated ($NaH_2PO_4\ H_2O$) were purchased from Sigma Aldrich (St. Louis, MO, USA), Trifluoroacetic acid was obtained from Merck Schuchardt OHG (Germany). All other reagents were of analytical grade and were used without further purification.

2.2. Preparation and characterization of protamine nanocapsules

Protamine nanocapsules were prepared by solvent displacement technique following the procedure described by our group, with modifications (Thwala et al., 2016). An oily core of 29.5 mg of Miglyol®812, 2.5 mg of SGC, 8 mg of PEGst-40 an acetone up to a final volume of 2.5 mL was poured over 5 mL of an aqueous phase of 0.15% protamine, and the formulation was left under magnetic stirring at 1,000 rpm for 10 min. The organic solvents were evaporated under vacuum in a Rotary Evaporator (Rotavapor R-215, Büchi, Switzerland) and finally, nanocapsules were isolated by centrifugation (Hermle Labnet universal centrifuge Z323K, Labnet international) at 15,000 g at 15ºC for 1 h. The isolated formulation was resuspended in ultrapure water. For the preparation of rifabutin-loaded protamine nanocapsules, rifabutin was dissolved in acetone (1, 2.5, and 5% of theoretical drug over total nanocapsules weight) and incorporated into the liquid lipid phase prior to nanocapsule formation.

Blank and rifabutin-loaded protamine nanocapsules were optionally freeze-dried for 48 h using Scanvac, Coolsafe 100-9 apparatus (LaboGeneApS, Lynge, Denmark) including mannitol in a ratio of 80/20 (w/w) as a cryoprotectant. Subsequently the nanoparticles process yield was calculated by gravimetry:

$$\text{Process yield (Y\%)} = \frac{\text{Weight of nanocapsules}}{\text{Theoretical weight of nanocapsules}} \text{x } 100$$

Nanocapsules were characterized in terms of mean particle size (nm), polydispersity index (PDI), and Z potential (mV) using photon correlation spectroscopy (Zetasizer Nano-ZSTM, Malvern Panalytical), after dilution in ultrapure water (dilution 1:250 at 25°C and with a detection angle of 173°) and Nanoparticle Tracking Analysis (NTA, NanoSight 142 NS3000, Malvern analytical Ltd., Malvern, UK). For NTA analysis, NCs were diluted 1:1,000 in order to keep the concentration within the instrument measuring range.

The morphology of the nanocapsules (dilution 1:1,000) was analyzed by field emission scanning electron microscopy (FESEM; Gemini-SEM, Zeiss, Germany) after coating the samples with iridium in an argon atmosphere.
Lyophilized protamine NCs were characterized by Fourier Transform infrared spectroscope (FTIR) (Thermo Nicolet AVATAR 330, Waltham, MA, USA) at 4 cm^{-1} resolution at the wavenumber range of 400–4000 cm^{-1}. The crystallinity of the NCs was evaluated by X-Ray Powder Diffraction (XRPD) using a Bruker D8 Advance X-ray diffractometer (Bruker AXS GmbH, Karlsruhe, Germany). The XRPD and FTIR spectra were analyzed using OriginPro 2017 (OriginLab Corporation, USA) and Spectragryph v1.2.16.1 software, respectively.

2.3. Encapsulation efficiency and drug loading

Associated rifabutin was quantified using an Acquity UPLC H-Class Plus system equipped with a C_{18} column (Waters® symmetry 1.7 µm, 2.1x 50 mm) adapting a protocol developed by Rouco et al (Rouco et al., 2020). Briefly, 10 µL of each sample were injected and eluted with a mobile phase composed of (A) a mixture of sodium acetate 0.05 M/potassium dihydrogen phosphate 0.05 M (pH adjusted to 4.0 with acetic acid) and (B) acetonitrile in a ratio A:B 53:47 (v/v). Drug quantification was performed at a wavelength of 278 nm, with a 0.2 mL/min flow rate. The Limit of Detection (LOD) was 0.016 ng/mL and the Limit of Quantification (LOQ) was 0.048 ng/mL, with a retention time of 1.7 min. Rifabutin was analyzed in the range of 5–35 µg/mL, showing a correlation coefficient of R= 0.9997. NCs were dissolved with a mixture of acetonitrile/sodium acetate/potassium dihydrogen in the same ratio as the mobile phase and centrifuged (Eppendorf 5430R®) at 12,000 g and 4ºC for 30 min for drug isolation. This procedure was repeated, and samples were filtered before UPLC measurement by 0.22-micron syringe filters. The rifabutin encapsulation efficiency (EE%) and drug loading (DL%) in protamine nanocapsules were calculated according to the following equations:

$$\text{Encapsulation efficiency (EE\%)} = \frac{\text{Weight of initial drug} - \text{Weight of free drug}}{\text{Weight initial drug}} \text{x } 100$$

$$\text{Drug loading (DL\%)} = \frac{\text{Weight of loaded drug}}{\text{Weight lipid core}} \text{x } 100$$

2.4. Colloidal stability of the nanocapsules

The colloidal stability of rifabutin-loaded protamine NCs were evaluated in aqueous suspension under storage at 4°C and in freeze-dried form at room temperature (RT) for 30 days. Stability was also evaluated in cell culture media and simulated lung media (SLM, pH 7.4) composed of 116 mM NaCl, 27 mM $NaHCO_3$, 5 mM $C_2H_5NO_2$, 1.1 mM NaH_2PO_4 (H_2O), 0.18 mM $CaCl_2$ and 0.5 mM 0.1 M H_2SO_4 in distilled water at pH 7.4 (Parlati, 2008). The mean particle diameter (nm), PDI, derived count rate (kcps) and zeta potential (mV) were analyzed using Zetasizer Nano-ZS™ as described in section 2.2.

2.5. *In vitro* dissolution studies

In vitro dissolution studies were performed in simulated lung medium (SLM) to evaluate the release kinetics of rifabutin from the nanocapsules. The nanopowder quantity equivalent to 0.75 mg of rifabutin was dispersed in 10 mL of SLM. The stirring was adjusted at 200 rpm and the sampling was performed up to 1 h at 37ºC. 1 mL of the dissolution medium was collected into microcentrifuge tubes (Eppendorf) at time intervals of 5, 10, 15, 20, 30, 40, 50, and 60 min and replaced every time with fresh medium upon sample withdrawal. Release samples were centrifuged at 7,500 g and the collected supernatant was analyzed spectroscopically by using a UV–visible spectrophotometer (V-730 UV-visible Spectrophotometer, Jasco Deutschland) at a wavelength of 237 nm. All experiments were conducted in triplicate. The kinetics of the *in vitro* drug release were evaluated to Zero order, First-order, Higuchi, and Korsmeyer–Peppas to understand the drug release mechanism.

2.6. *In vitro* permeability studies

The permeability study of rifabutin was performed on a modified horizontal diffusion side-by-side cell-type apparatus (Grown Glass, New York) (Gieszinger et al., 2021). Briefly, 9 mL of phosphate buffer (pH 7.4) was used in the acceptor chamber while the same volume of simulated lung media was used as donor media. Subsequently, 0.75 mg of raw rifabutin and rifabutin-loaded nanocapsules equivalent to 0.75 mg of rifabutin were dispersed into the donor chamber. Chambers were separated by an artificial membrane (Isopore™ membrane filter, 0.45 µm) impregnated in isopropyl myristate, with a diffusion area of 0.69 cm^2. The temperature was kept at 37°C and stirred at 100 rpm. The amount of rifabutin diffused from protamine nanocapsules in the acceptor phase was measured for 1 h spectrophotometrically at 238 nm using a FDP-7UV200 probe and a Avaspec-ULS2048-USB2 spectrophotometer (Avantes, Apeldoorn, The Netherlands). The flux (J) (µg/cm^2/h) of rifabutin was calculated from the amount of drug (µg) permeated through the side-by-side membrane (m), divided by the surface of the membrane (A) and the time (t) following the equation:

$$J = \frac{m}{A * t}$$

The permeability coefficient (Kp) (cm/h) was determined from the flux and the initial rifabutin concentration in the donor phase (Cd) (g/cm^3), according to the equation:

$$Kp = \frac{J}{Cd}$$

2.7. *In vitro* toxicity studies

The cytotoxicity of rifabutin-loaded protamine nanocapsules was evaluated using MTT reduction, a water-soluble tetrazolium dye that is converted by viable cells to a water-insoluble and purple compound, formazan. Cell viability was assessed in A549 and Raw 264.7 cells after 24h of incubation of different concentrations of nanocapsules. The day before the experiment, cells were seeded in a 96-well plate in DMEM culture medium supplemented with 10% FBS, and 1% Penicillin/Streptomycin at a cell density of $1x10^4$ cells/well at 37ºC and 5% CO_2. On the next day, the medium was replaced by medium containing the formulations, and cells were incubated for 24h. Fresh medium was used as the negative control and Triton x100 (1% v/v) was used as the positive control. After 24h, the medium was replaced by 0.5 mg/mL of MTT

dissolved in PBS, and cells were incubated for 4h at 37ºC and darkness. MTT solution was discarded, and the formazan crystals were dissolved by the addition of 0.04 N HCl in isopropanol. Absorbance was measured at 570 nm using a microplate reader (Synergy H1 Hybrid Multi-Mode, BioTek, Winooski, VT, USA). Cells treated with equivalent rifabutin concentrations were used as control. The cell viability (%) compared to control cells was calculated following the equation:

$$\text{Cell toxicity (\%)} = \frac{\text{Absorbance sample} - \text{Absorbance positive control}}{\text{Absorbance negative control} - \text{Absorbance positive control}} \text{ x } 100$$

2.8. Quantitative nanocapsules uptake

Rifabutin-loaded protamine nanocarriers were labeled by incorporating 20 µL DiD (2.5 mg/mL) in ethanol into the organic phase prior to nanocapsule formation. Physicochemical characterization and drug loading were evaluated to confirm that the dye did not interfere with the physico-chemical properties of the formulation before in vitro assays.
A549 and Raw 264.7 cells were grown in 8-µwell slides ibidiTreat (Ibidi GmbG, Gräfelfing, Germany) (0.8 cm^2/well) at 2.5x10^4 cells/well and DiD-labeled rifabutin-loaded protamine NCs were added and incubated for 24h. Then, formulations were removed with PBS pH 7.4 (x3) and cells were fixed with 4% paraformaldehyde (PFA) for 15 min at RT and 150 rpm. Then, PFA was removed with PBS (x3) and the nucleus was stained with DAPI for 5 min. Finally, cells were washed with PBS (x3) and mounted in glycerol. Nanocapsules internalization was studied by Confocal Laser Scanning Microscopy (CLSM, SP5 Leica AOBS-SP5, Leica Biosystems Nussloch GmbH). Fluorescence measurements were performed at DAPI-dye excitation λmax= 359 nm and emission λmax= 457 nm and DiD-dye excitation λmax=640 nm and emission λmax= 675 nm.
To quantify the A549 cells and Raw 364.7 internalized with rifabutin-loaded protamine NCs, a study based on flow cytometry was carried out. 6x10^4 cells were seeded in a 24-well plate at 37 °C for 24h and 5% CO_2. The medium was replaced with formulations and cells were incubated for 24h, washed with PBS and detached with trypsin (5 min, 37 °C). Cells were centrifuged at 1,000 g (Eppendorf 5430R®) for 10 min, and the pellet was resuspended in 500 µL PBS. Non-treated cells were used as negative control. Events were counted employing a cytometer (BD FACSCalibur™, Becton Dickinson) and were analyzed by flowing software 2.5.1 (Cell Imaging Core, Turku Centre for Biotechnology). The study was carried out in triplicate.

2.9. IDO assay

Tolerogenic phenotype of the developed rifabutin-loaded protamine NCs was evaluated on human-derived macrophages in terms of T cell suppression and tolerance promotion by quantification of 2,3-Indoleamine dioxygenase (IDO) expression. Buffy coats were donated by the Organ and Blood Donation Agency (ADOS; Santiago de Compostela, Spain) after informed consent. Briefly, the blood was diluted with PBS (1:1) and peripheral blood mononuclear cells (PBMCs) were isolated using the Ficoll density gradient separation method (blood/Ficoll ratio of 2:1) by centrifugation (Allegra X-12R, Beckman Coulter) at 400 g for 30 min at RT on deceleration mode. Red Blood Cells (RBCs) were kept for blood compatibility assays (section 2.10.) and the PBMC layer was washed with PBS by centrifugation at 300 g for 10 min. 10 mL of the obtained cells (1.2 × 10^6 cells/mL) were then resuspended in an R_2 media (RPMI-1640 supplemented with 2% FBS and 1% of Penicillin-Streptomycin-Glutamine, PSG) for 2h (37ºC, 5% CO_2). After this time, the non-adherent cells, peripheral blood lymphocytes, were washed

with PBS. The attached monocytes were cultured for 6 days in R_{10} media (RPMI-1640 supplemented with 10% FBS and 1% of PSG), replacing the media on the third day and adding 0.1 µg GM-CSF for the differentiation of monocytes to macrophages.

Macrophages were seeded onto a 48-well plate, followed by their incubation with different formulations in a final volume of 0.5 mL and by adding 1.25 µL of L-tryptophan (100 µM) 4h before the end of the culture period. After 24h, cells were centrifuged (1,000 g, 5 min at RT) and supernatants were mixed with 30% trifluoroacetic acid (2:1 v/v). Cells were centrifuged again and Ehrlich Reagent (1:1 v/v) was added to the supernatant. Absorbance was read using a microplate reader (Synergy H1 Hybrid Multi-Mode, BioTek, Winooski, VT, USA) at 490 nm. A total of 3 different donors were used and were plotted along with the standard error.

2.10. Blood compatibility test

As described in section 2.9., after the Ficoll density gradient separation method, freshly collected RBCs were collected, washed with PBS (x3, pH 7.4), and centrifuged at 1,000 g for 5 min at RT. The RBC pellet was resuspended in PBS and placed in a 96-well plate and was treated with rifabutin-loaded protamine NCs (0.1 mg/mL) at 37ºC for 4 h and 24 h. Triton x100 (1% v/v) was used as the positive control while PBS was used as the negative control. A total of 3 different donors were used and results were plotted along with the standard error. At signaled time points the absorbance of released hemoglobin was measured at 570 nm (Synergy H1 Hybrid Multi-Mode, BioTek, Winooski, VT, USA), and percentage hemolysis was calculated using the following equation:

$$\%\ \text{Haemolysis} = \frac{\text{Absorbance sample} - \text{Absorbance negative control}}{\text{Absorbance positive control} - \text{Absorbance negative control}} \text{x } 100$$

2.11. Thermal analysis

The influence of temperature on the physicochemical properties of rifabutin-loaded protamine NCs was evaluated by DLS. Samples (dilution 1:250) were placed in a quartz cell and particle size, PDI, and count rate measurement was performed by heating the sample from 25ºC up to 90ºC at a heating rate of 1ºC/min. Measurements were performed in triplicate.

2.12. Preparation of dry powders containing rifabutin protamine nanocapsules

Mannitol was used as an excipient for dry powder preparation and samples were spray-dried using the Nano Spray Dryer B-90 HP Nano SD (Büchi Labortechnik AG, Falwil, Switzerland) with an inlet air temperature of 100ºC, an outlet Tª of 31ºC a pump flow rate of 20%, and aspirator capacity of 100%. Protamine nanocapsules were suspended in an aqueous solution of mannitol to achieve a theoretical mannitol/nanocapsules ratio of 80/20 (w/w) (Grenha et al., 2007) and a final solid content of 1.25% (w/v), as it is expected to lead to the production of microparticles with adequate morphologic and aerodynamic characteristics for pulmonary administration. The spray-dried powders were stored in a desiccator at RT until use. Samples were analyzed by Differential Scanning Calorimetry (DSC) was performed using a Mettler-Toledo 821e DSC (Mettler-Toledo GmbH, Gießen, Germany) at the temperature interval of 30 to 450ºC under constant purging of argon. DSC spectra were analyzed using the STARe thermal analysis program V9.1 (Mettler Inc., Schwerzenbach, Switzerland). The crystallinity was also evaluated by XRPD using a Bruker D8 Advance X-ray diffractometer as described in section 2.2. The spray-dried particles were dissolved in water to achieve in-water dispersed rifabutin-

loaded protamine NCs and were subsequently evaluated by dynamic light scattering as previously described in section 2.2. The morphology of the spray-dried nanocapsules was analyzed by scanning electron microscopy (SEM) (Hitachi S4700, Hitachi Scientific Ltd., Tokyo, Japan) after coating the samples with gold-palladium (SEM) in an argon atmosphere.

2.13. *In vitro* aerodynamic evaluation

The *in vitro* distribution profile of the spray-dried protamine NCs was evaluated using the Andersen cascade impactor (ACI, Copley Scientific Ltd., Nottingham, UK). The used methodology respected the United States Pharmacopeia and Ph. Eur. 2.9.18 requirements. ACI separates particles according to their aerodynamic diameter by cut-offs of the stages from −1 to 6 (8.60, 6.50, 4.40, 3.20, 1.90, 1.20, 0.55, and 0.26 µm). A glass fiber filter (Pall corporation, Mexico, 1.0 µm pore size and aerosol retention of 99.98%) was placed right below stage six. Collection plates were coated with Span 80 + cyclohexane solution (1 + 99 w/w %) to prevent particle bounce. An amount of 8 mg of spray-dried protamine NCs was loaded into 4 hard gelatin capsules (transparent, size 3, Capsugel, Germany) and aerosolized using a DPI Breezhaler® single dose device (Novartis International AG, Basel, Switzerland). The content of the four capsules was discharged for each experiment, and the experiments were performed in triplicate. The flow rate was adjusted at 60 L/min using a DFM 2000 Flow Meter (Copley Scientific, Nottingham, UK), and the test duration time was adjusted at 4 s. The DPI device, the mouthpiece, the induction port, the eight stages of the impactor, and the end filter were weighed before and after the experiment, and parameters (MMAD, FPD, ED, and FPF) were quantified by gravimetry. The *in vitro* aerodynamic properties were evaluated with Inhalytix™ (Copley Scientific LTD., Nottingham, United Kingdom) data analysis software.

Mass median aerodynamic diameter (MMAD) was determined by plotting the cumulative percentage of mass for each stage on a probability scale versus the aerodynamic diameter of the stage on a logarithmic scale. The fine particle dose (FPD) corresponded to the mass of particles with a size <5 µm, while fine particle fraction (FPF) was established as the percentage of particles <5 µm, while emitted dose (ED) was the percentage of particles leaving the device and reaching the impactor. Time-of-flight (TOF) particle size analyzer Aerosizer® (TSI Instruments Ltd. UK) connected with Aero-Disperser® was also used to confirm the aerodynamic size distribution by timing the flight of the individual spray-dried nanocarriers. A small amount of powder (around 5 mg) was placed in the sample cup of the aerodisperser and measurements were performed using laser current 41 mA, a nozzle type 200 µm, a size range from 0.1 to 200 µm and a run length of 30 sec.

Statistical analysis

The statistical significance of the difference between the means was determined by GraphPad Prism 8 and OriginPro 9.0. All data are shown as mean±SD or mean± SEM (IDO and hemolysis assay) and one-way and two-way analyses of variance (ANOVA) were performed to compare multiple independent groups. Differences were considered statistically significant at $P<0.05$.

3. RESULTS AND DISCUSSION

3.1. Preparation and characterization of rifabutin protamine nanocapsules

In this work, we use protamine, a natural arginine-rich polypeptide with remarkable stability in simulated biological fluid, widely used in the design of polymeric nanocarriers for drug and vaccine delivery (Jakubiak et al., 2017). The attachment of protamine to the oily core was

possible after the incorporation of an anionic surfactant, and the developed protamine nanocapsules were stabilized by incorporating PEG-stearate. The different rifabutin formulations were prepared at theoretical loadings of 1%, 2.5%, and 5% (w/w) (**Supplementary Figure 1**). To evaluate the incorporation of rifabutin in the oily phase of the nanocapsules, nanoemulsions were first analyzed by DLS and UPLC (**Supplementary Table 1**), and then, protamine nanocapsules were prepared by solvent displacement technique. The mean hydrodynamic diameter of unloaded and rifabutin-loaded protamine nanocapsules is presented in **Table 1** and was found to be around 200 nm for all formulations. No statistical differences were observed between loaded and unloaded nanocapsules, suggesting that rifabutin incorporation does not influence the particle diameter and surface charge, which was found to be positive (from +11 to +17 mV). It has been shown that a hydrodynamic diameter > 100 nm and a positive surface charge significantly improve the particle-macrophage interaction and internalization, since phagocytic activity depends on particle size and macrophages present sialic acid on their surface, which gives them a negative surface charge (Lee et al., 2015). In all cases, high rifabutin incorporations were obtained, as shown in **Table 1**. The satisfactory encapsulation as well as the high yields achieved (up to 90%) confirm the suitability of the developed nanocarriers for rifabutin incorporation.

Table 1. Physicochemical characterization, association efficiency (AE), and Drug Load (DL) of non-loaded and rifabutin-loaded (1, 2.5, and 5%) protamine nanocapsules (NCs). Particle hydrodynamic diameter and polydispersity index (PDI) were obtained by Dynamic Light Scattering. Data represents mean ± SD, N>3.

Formulation	Size (nm)	PDI	Charge (mV)	AE (%)	DL (%)	Yield (%)
Blank NCs	199 ± 17	<0.2	11 ± 10	-	-	91 ± 2
1% Rifabutin NCs	185 ± 13	<0.2	9 ± 10	54 ± 18	0.87	79 ± 19
2.5% Rifabutin NCs	199 ± 15	<0.2	9 ± 8	46 ± 6	1.88	91 ± 4
5% Rifabutin NCs	198 ± 19	<0.2	11 ± 10	42 ± 7	3.55	86 ± 3

Their structural characterization is represented in **Figure 1** after their lyophilization process in the presence of mannitol. As shown in the FTIR spectrum (Figure 1A), the developed nanocapsules presented the typical signal of protamine sulfate at around 1,100-1150 cm^{-1} attributed to arginine (that constitutes 67% of the total amino acid content of protamine) (Awotwe-Otoo et al., 2012), as well as D-Mannitol δ-phase bands at 931, 967, 1023, 1086 and 1193 cm^{-1} (Barreneche et al., 2013). Moreover, characteristic bands of glycocholate acid were observed at 1582 and 1394 cm^{-1} (COO- stretching), 1308 (C−H bending) and 1037 cm^{-1} (ammonium stretching vibration) (Benbow et al., 2021). C-H scissor and bending at the region between 1450-1292 cm^{-1}, can be attributed to PEG-stearate 40 (Khairuddin et al., 2016). XRPD diffractogram (Figure 1B) of rifabutin showed a distinctive drug sharp peak, indicative of the crystalline nature of rifabutin, whereas it faded away in the diffractogram of rifabutin-loaded protamine NCs. This reduction in relative integrated intensity of peak, with no distinct peak of rifabutin, suggests that drug was entirely incorporated into the oily core of the nanocapsules. In addition, it is indicative of amorphous material, which had shown to increase solubility compared to crystalline material (Nighute and Bhise, 2009).

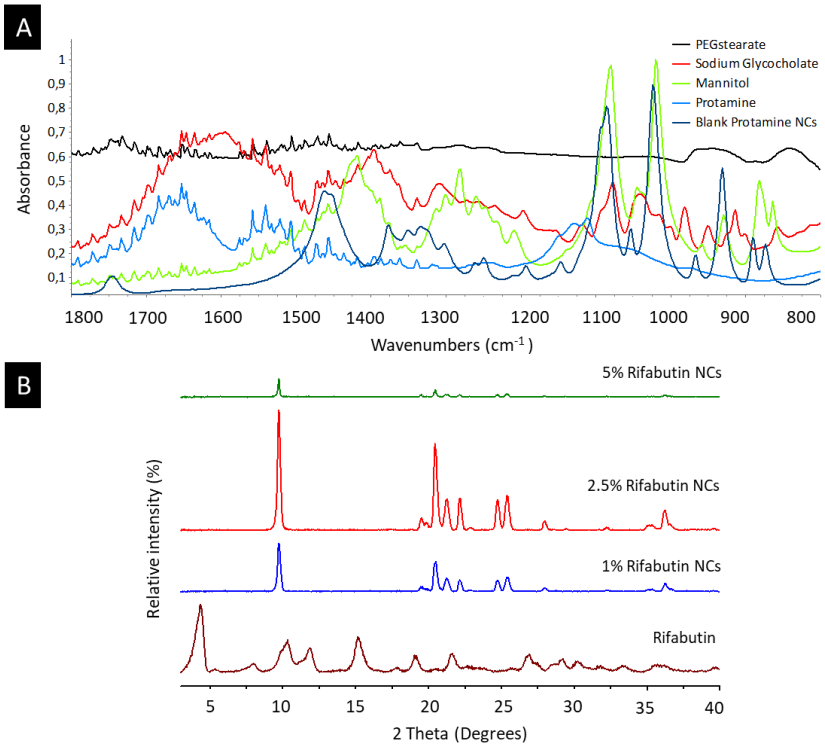

Figure 1. (A) FTIR spectra of lyophilized protamine nanocapsules (NCs) and their components and (B) XRPD spectra of rifabutin and 1, 2.5, and 5% rifabutin-loaded protamine NCs.

A uniform shape, smooth surface and spherical morphology were observed by FESEM microscopy (**Figure 2** without aggregation of the nanocapsules. The NTA analysis further supported the above disclosed DLS and FESEM data and similar hydrodynamic particle sizes were reported (between 132-148 nm), slightly lower than those obtained by DLS measurement.

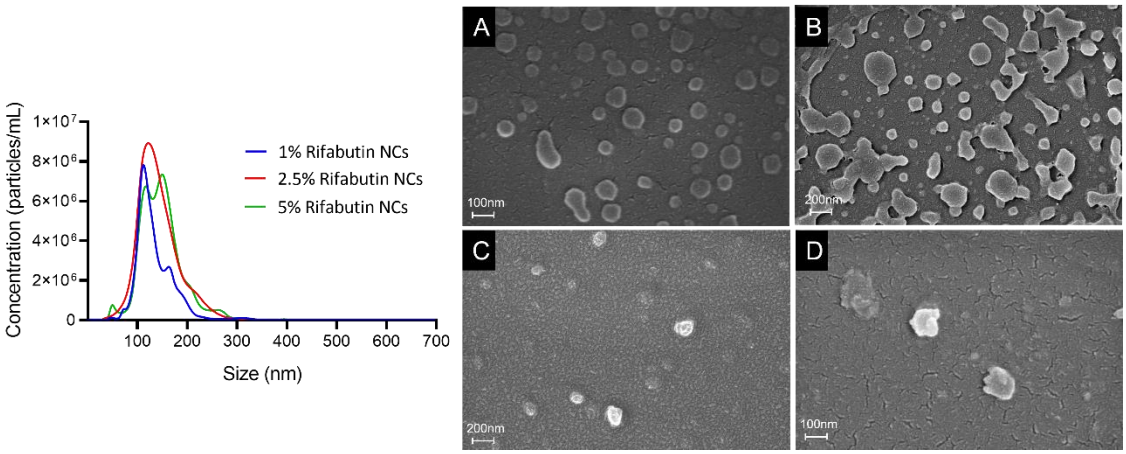

Figure 2. (Left) Representative image of the particle size distribution by Nanoparticle Tracking Analysis of nanocapsules in solution and (Right) scanning electron microscopy images of blank (A) and rifabutin-loaded 1 (B), 2.5 (C) and 5% (D) protamine nanocapsules. Scale bars represent 100 nm.

3.2. Stability studies

The size of the nanocarriers remained unchanged upon storage in suspension, and no signs of aggregation were observed for 30 days nor after the freeze-drying process. Mannitol was

included as an inert carrier and stabilizer in the process, and it was completely dissolved after incubation of the lyophilized nanocapsules in an aqueous medium, inducing no significant changes in their physicochemical characteristics. The slight increase in zeta potential as compared with non-lyophilized nanocapsules, indicative of the stability of the colloidal system, was also reported previously for chitosan nanoparticles recovery from mannitol dry powders (Grenha et al., 2005) (**Table 2**).

Table 2. Physicochemical characterization of blank and rifabutin-loaded (1, 2.5, and 5%) protamine nanocapsules (NCs) after one month of storage as suspension (at 4ºC) or as a freeze-dried powder (RT). Particle size and polydispersity index were obtained by Dynamic Light Scattering. Data represent mean ± SD, N=3.

Conditions	Freeze-dried (RT)			Suspension (4ºC)		
Formulation	Size (nm)	PDI	Charge (mV)	Size (nm)	PDI	Charge (mV)
Blank NCs	222 ± 32	<0.3	12 ± 9	229 ± 52	<0.2	11 ± 9
1% Rifabutin NCs	202 ± 36	<0.3	17 ± 8	229 ± 64	<0.2	9 ± 10
2.5% Rifabutin NCs	199 ± 23	<0.3	13 ± 7	208 ± 30	<0.2	13 ± 11
5% Rifabutin NCs	204 ± 19	<0.3	13 ± 9	213 ± 35	<0.2	13 ± 8

SLM was prepared based on a modification of Gamble's original solution (Parlati, 2008) and was suitable for flow through dynamic systems. Following a protocol developed by Kanapilly et al., glycine was included to prevent clogging of filter pores in a dynamic flow system (Kastury et al., 2017). When incubated in SLM and cell culture media **(Figure 3),** rifabutin-loaded protamine NCs exhibited satisfactory stability over time. In addition, the derived count rate (kilo counts per second, kcps) provided information about the concentration of nanoparticles remaining *in situ* in suspension after incubation and its degradation (Woods et al., 2020). Results showed no reduction in intact particle number following exposure to the cell culture media or SLM up to 24h, strongly suggesting efficient physical and biological stabilization mechanisms of the developed formulations.

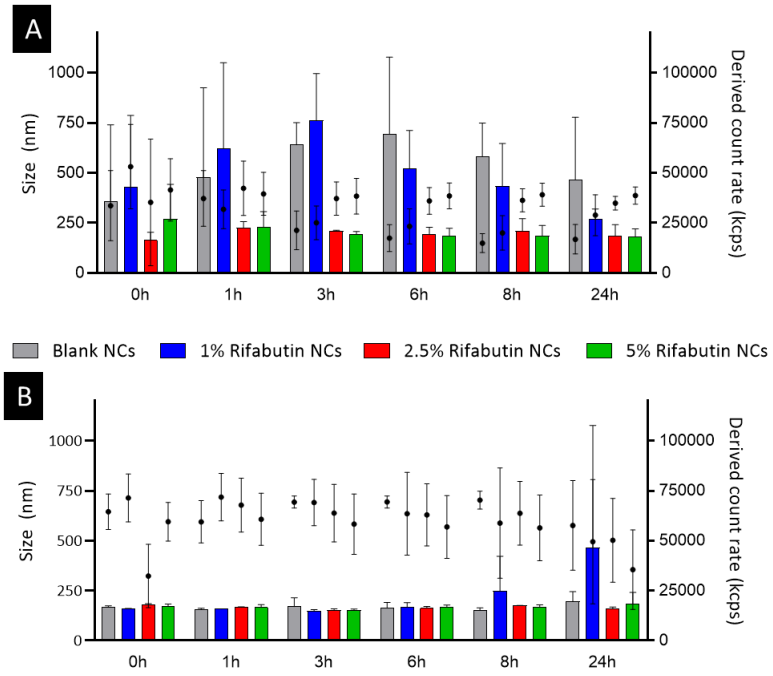

Figure 3. Stability of rifabutin-loaded protamine nanocapsules (NCs) after incubation in (A) cell culture media DMEM and (B) Simulated Lung Media at 37ºC by Dynamic Light Scattering. Size=Bars, Derived count rate= Dots. Data represent mean ± SD, N=5 independent measurements.

3.3. *In vitro* dissolution studies

To predict the *in vivo* efficacy of the formulations, an *in vitro* release of rifabutin from protamine NCs was performed in simulated lung media and results were analyzed using drug release kinetics models. *In vitro* rifabutin release from 1% loaded protamine NCs presented a drug release profile where all encapsulated rifabutin was released (96 ± 13%), while in the case of 2.5 and 5% rifabutin-loaded protamine NCs was of 71 ± 12 and 66 ± 27%, respectively, over 1 hour (**Figure 4**). Rifabutin dissolution was statistically significant (one way ANOVA $P<0.05$) for 1% rifabutin protamine NCs when compared with raw drug dissolution. Formulations showed a linear drug-release pattern with a higher drug release compared with the poorly water-soluble raw API (38 ± 3%). Similar rifabutin dissolution profiles were reported from glyceryl dibehenate and glyceryl tristearate solid-lipid nanoparticles (65 and 80 % after 1 h, respectively) (Gaspar et al., 2016).

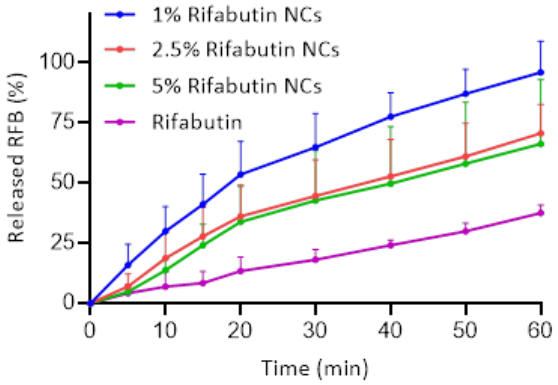

Figure 4. *In vitro* dissolution results of the drug from the developed 1%, 2.5 %, and 5% rifabutin-loaded protamine nanocapsules (NCs). Data represent mean ± SD, N=3 independent measurements.

Various kinetic models were used to evaluate the drug release pattern of protamine NCs using DDSolver software (Zhang et al., 2010), and the best-fitted models were selected based on the adjusted coefficient of determination R^2, adj R^2, and Akaike Information Criterion (ACI) (**Supplementary Table 2**). Protamine NCs were found to be a better fit for both the First Order and Korsmeyer-Peppas > Higuchi model, which explains a concentration-dependent drug release (first-order kinetics) but also a diffusion of the drug from the polymeric matrix (Korsmeyer-Peppas). The n value indicated that 1 and 5% rifabutin formulations followed a non-Fickian diffusion of the drug (n= 0.82 and 0.94, respectively) while 2.5% followed Fickian drug diffusion (n=0.28), thus observing a change in the sorption process once the equilibrium by the surface concentration of drugs was achieved. (ACI) values confirmed that first-order kinetics gave the best fit out of the set of models. Rifabutin release profile from nanocapsules was similar to that obtained with other previously reported rifabutin-based formulations, supporting that the matrix is responsible of the release pattern: rifabutin release was faster in the case of formulations that used hydrophilic polymers devoid of crosslinking agents, such as low molecular weight chitosan or fucoidan, while it slowed down when viscous solutions such as locust bean gum or chitosan with a higher degree of crosslinking were used (Rodrigues et al., 2020).

3.4. *In vitro* permeability studies

The amount of Active Pharmaceutical Ingredient (API) dispersed from the simulated lung media through the epithelium was evaluated by diffusion in a modified side-by-side® model, and the measurements took place in real time. The maximum permeability of rifabutin was

about 70 µg/cm^2 after 35 minutes, not observing a greater increase in permeability and reaching a plateau at this point. However, the diffusion of rifabutin-loaded nanocapsules was slower and more progressive, as shown in **Figure 5**, with a linear trend. In the case of 1% and 5% rifabutin-loaded protamine NCs diffusion was apparently faster (90 ± 14 and 78 ± 32 µg/cm^2 after 1h), while in the case of 2.5% was 57 ± 5 µg/cm^2.

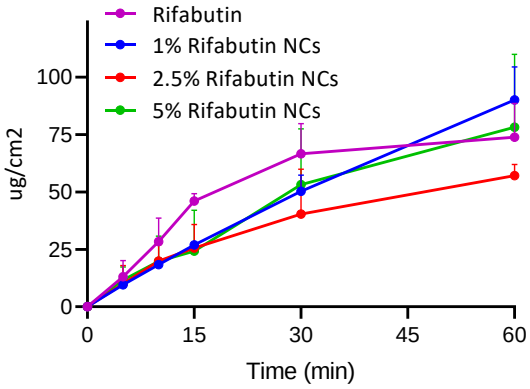

Figure 5. *In vitro* results of the API (rifabutin) permeability from the developed 1%, 2.5%, and 5% rifabutin-loaded protamine nanocapsules (NCs) compared with the raw drug. Data represent mean ± SD, N=3 independent measurements.

Despite rifabutin is characterized by its high permeability and low solubility (Nighute and Bhise, 2009), stagnation takes place without observing further increase in the permeability after 35 min. The flux (J) and the permeability coefficient (Kp) (**Table 3**) of the nanocapsules were higher than that of the raw rifabutin for all the formulations except 2.5% rifabutin-loaded protamine NCs. However, a progressive and constant permeability of the drug through the membrane with a linear tendency was observed and the growing trend is expected to exceed the maximum obtained from the raw drug at more extended times.

Table 3. *In vitro* permeability results of the samples. Data represent mean ± SD, N=3 independent measurements.

Formulation	J (µg/cm^2/h)	Kp (cm/h)
Raw Rifabutin	73.82	0.0984
1% Rifabutin NCs	90.08	0.1201
2.5% Rifabutin NCs	57.07	0.0761
5% Rifabutin NCs	78.15	0.1042

3.5. *In vitro* toxicity assays

An MTT assay was performed to investigate the cytotoxicity of the developed nanocapsules in lung derived A549 cells and Raw 264.7 macrophages. The cell viability was observed to be concentration-dependent (from 0.1 to 1 mg/mL NCs concentrations) after 24 h, as reported in **Figure 6**. The rifabutin-loaded NCs showed more than 50% cell viability at 0.25 mg/mL and more than 75% viability at concentrations of 0.1 mg/mL. The toxicity values obtained at high concentrations of nanocapsules may be due to the affinity of cationic nanocarriers towards macrophages, which leads to a greater electrostatic attraction with their negatively charged cell surface (Robla et al., 2021), thus increasing the metabolic activity of macrophages. For all formulations, the toxicity of the encapsulated drug was similar to the reported for free rifabutin (>50% toxicity at 12.5 µg/mL for Raw 264.7 cells and 20 µg/mL for A549 cells, data not shown). 1mg/mL formulations were equivalent to 10, 25, and 50 µg/mL of encapsulated drug of 1, 2.5, and 5% rifabutin protamine NCs, respectively.

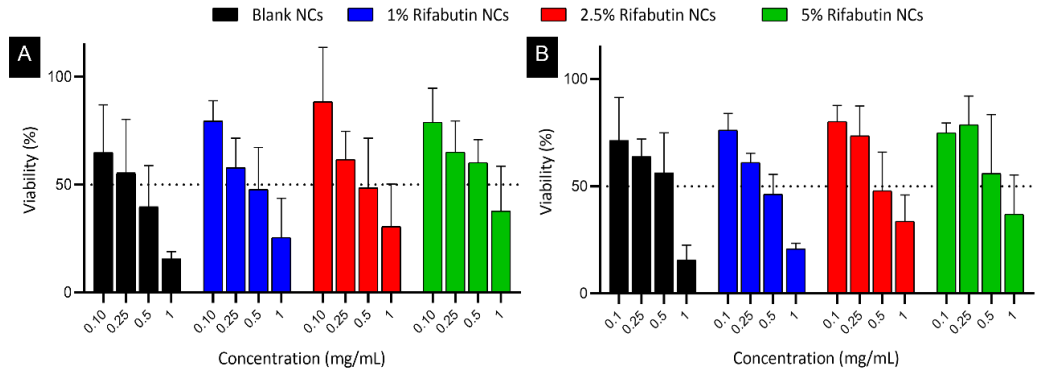

Figure 6. *In vitro* evaluation of the effect of the developed 1%, 2.5%, and 5% rifabutin-loaded protamine nanocapsules (NCs) on the viability of A549 cells (A) and Raw 264.7 macrophages (B). Data represent mean ± SD, N=3 independent measurements.

3.6. Quantitative nanocapsule uptake

Confocal laser scanning microscopy (CLSM) was performed for the qualitative assessment of the fluorescent-DiD labeled rifabutin-loaded protamine NCs in human alveolar epithelial cells A549 and macrophages Raw 264.7. For this purpose, protamine nanocapsules were initially formulated with the drug as described above, carrying out the incorporation of DiD dye in the oily phase. Its physicochemical properties were characterized by DLS and drug association by UPLC (**Supplementary Table 3**) showing sizes similar to those previously reported and with a slightly lower association of rifabutin, which could be related to drug-rifabutin competition in the oily nucleus. NCs internalization with a cytoplasmatic distribution was observed in both cell lines (**Figure 7**) when compared with control (untreated cells). Bright-field analysis (**Supplementary Figure 2**) allows us to delimit the different cells, confirming that an internalization or adsorption of the NCs takes place in the plasma membrane surrounding cell nuclei.

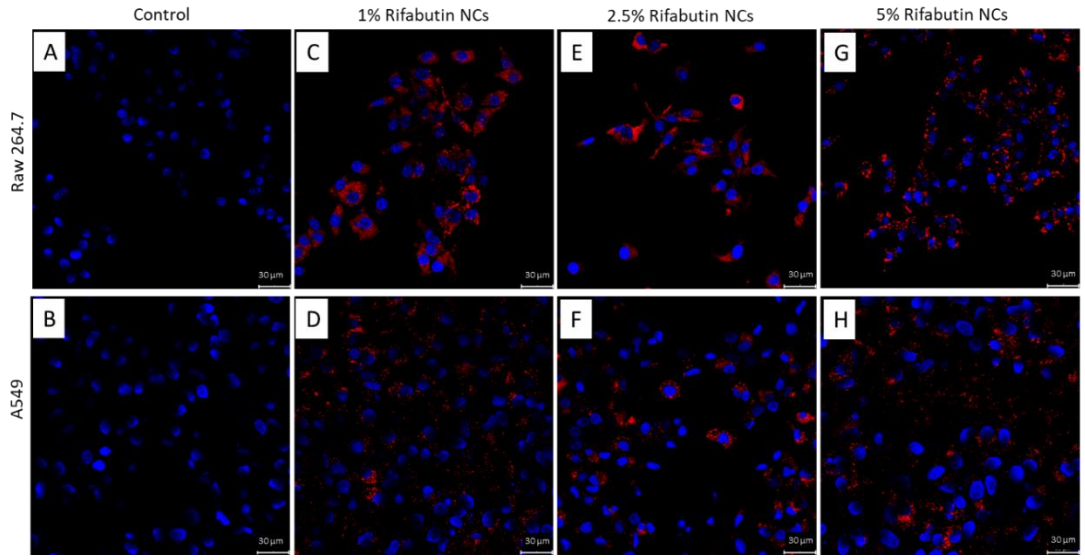

Figure 7. Cellular internalization study via confocal imaging of Raw 264.7 (A, C, E, and G) and A549 (B, D, F, and G) cell lines. DAPI-dye (blue channel; Excitation λmax = 359 nm, Emission λmax = 457 nm); DiD-dye (red channel; Excitation λmax=640 nm, Emission λmax= 675 nm). The scale bar represents 30 µm.

Quantification of the percentage of DiD-labeled rifabutin-loaded NCs uptake was also performed by flow cytometry (**Figure 8**). Histograms of the control cells were compared with those of A549 and Raw264.7 cells treated with 1, 2.5, and 5% rifabutin-loaded protamine NCs. Internalization was found to be of >90% in all cases (93, 95, 98, and 96% of the A549 cells, and 96, 97, 99, and 98% of the Raw 264.7 cells were internalized by blank, 1, 2.5, and 5% rifabutin-loaded protamine NCs, respectively). The internalization of the rifabutin-loaded protamine NCs in the A549 cells after evaluation of the Mean Fluorescence Intensity (MFI) was found to be 8-12 times higher compared with control. Raw 264.7 macrophages showed an MFI 2-3 times higher than untreated cells, for blank, 1%, 2.5 and 5% rifabutin-loaded protamine NCs, respectively. It has been reported that the physicochemical characteristics of nanoparticles influence their mechanism of entry into cells, (Lee et al., 2015) thus, the size of the developed nanocapsules could also lead to their internalization through phagocytic and non-phagocytic mechanisms, such as micropinocytosis.

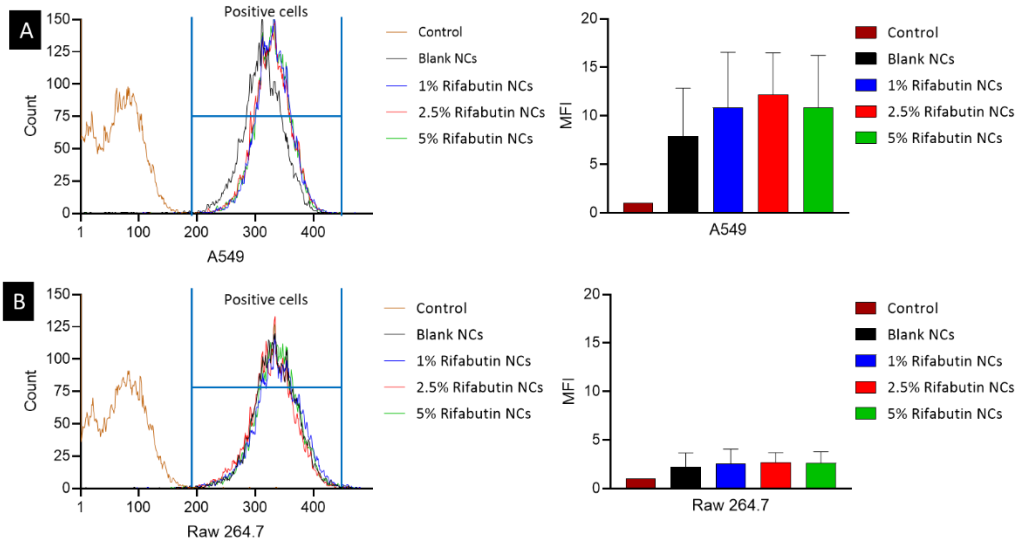

Figure 8. Flow cytometry histograms and Mean Fluorescent Intensity (MFI) of (A) A549 cells and (B) Raw 264.7 cells after incubation with rifabutin-loaded protamine nanocapsules (NCs). MFI=1 was established for control (non-treated cells).

3.7. IDO assay

IDO is an immune-suppressive enzyme in macrophages and dendritic cells involved in tryptophan catabolism into kynurenine, which induces Th_1 cell apoptosis *in vitro*. Th_1 are the main effector CD4+ T lymphocytes during TB, contributing to protection against TB by secreting IFN-γ (Lyadova and Panteleev, 2015). As IDO expression can impact peripheral tolerance and immune regulation, we evaluated the tolerogenic response of the rifabutin-loaded protamine NCs by quantifying the IDO enzymatic activity in human monocyte-derived macrophages. We observed that the response was similar for all the formulations compared to non-treated macrophages used as control (**Figure 9**), indicating no tolerogenic effect (pro-inflammatory response) of the formulations. Given that macrophages are capable of internalizing rifabutin-loaded protamine NCs, and that Mtb suppresses the antimicrobial response of macrophages (Bekale et al., 2019), the developed systems could be interesting in terms of macrophage immune modulation, being able to activate these immune cells and creating a hostile environment for Mtb.

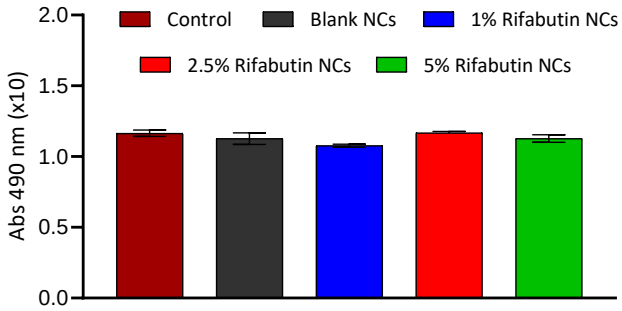

Figure 9. Indoleamine 2,3-dioxygenase (IDO) activity in human-derived macrophage cultures after incubation with rifabutin-loaded protamine nanocapsules (NCs). Data represents mean ± SEM (Standard Error Mean); N=3 different donors.

3.8. Blood compatibility test

Although inhaled particles do not come in contact with blood immediately, the high permeability of air-blood barrier of the alveoli (with a thickness of 0.1–0.2 μm) allows fast uptake of particles (Fröhlich, 2017). A hemolysis assay was performed to demonstrate nanocarrier biocompatibility with the bloodstream to get insight into the behavior of formulations for *in vivo* applications. As shown in **Figure 10**, the rifabutin-loaded nanocapsules posed no toxicity on the RBCs in the concentration range used in this study, indicating their hemocompatibility and the preservation of integrity and functionality of erythrocytes. Although positively charged nanoparticles interact electrostatically with the erythrocyte membrane, which can cause its rupture (Singh et al., 2020), the developed nanocapsules did not influence hemotoxicity. Similar results were also reported for cationic chitosan nanoparticles for the pulmonary delivery of isoniazid (Mukhtar et al., 2022).

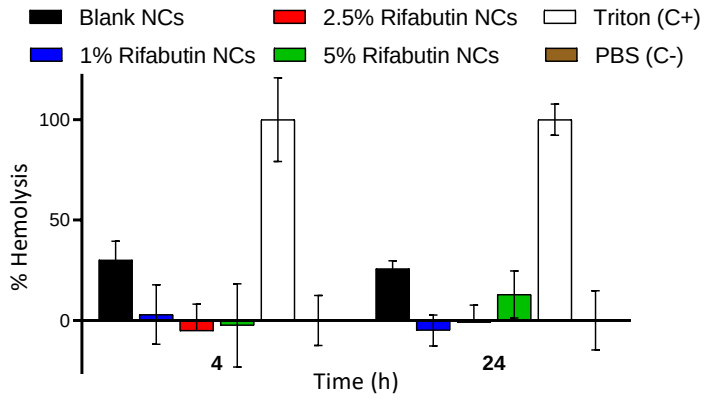

Figure 10. *In vitro* hemolysis assay after 4 and 24h was performed on fresh human blood obtained from donors after consent. NCs: Nanocapsules, C+: Positive control, C-: Negative control. Results are expressed as mean ± SEM (Standard Error Mean), N=3 different donors.

3.9. Thermal analysis using DLS

To perform a spray drying process where an increase in the temperature of the formulations is required, it is necessary to previously evaluate its effect on particle size. The low hygroscopic nature of mannitol allows for a low drying temperature for the preparation of dry powder (Munir et al., 2022). Likewise, the use of the Nano Spray Dryer allows outlet temperatures between

28ºC and 59ºC for aqueous solutions. Furthermore, even if a high inlet temperature were used, it has been shown that has minimal impact on particle size during the spray drying process (Arpagaus, 2011). As shown in **Figure 11**, the heating process did not induce particle size changes in the developed protamine nanocapsules up to 90ºC, as their size remained unchanged during the whole thermal analysis. Therefore, we can conclude that the developed systems meet the compatibility requirements for their spray-drying and are not expected to suffer degradation under the processing conditions.

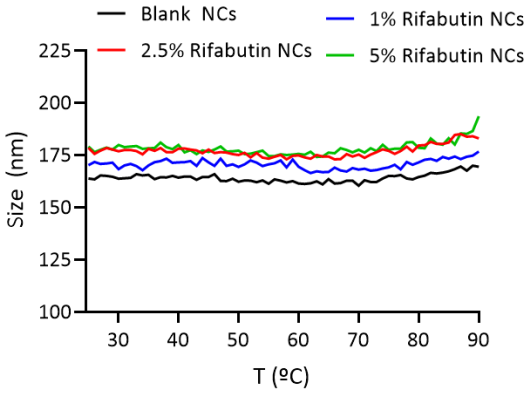

Figure 11. DLS thermograms blank, 1, 2.5, and 5% rifabutin-loaded protamine nanocapsules (NCs) from 25ºC to 90ºC. Results are expressed as mean, N=3. SD values were <10%.

3.10. Preparation of pulmonary dry powders containing rifabutin protamine nanocapsules

D-mannitol is a non-toxic and degradable carbohydrate widely used as excipients for dry powder inhalers, approved by the Food and Drug Administration (FDA) (Sham et al., 2004). D-mannitol is a non-reducing and non-hygroscopic compound widely used in aerosolization. During this process, it can give rise to different pure polymorphs (mainly α, β, or δ), with greater kinetic stability than its hydrated and amorphous form (Altay Benetti et al., 2021). Mannitol is approved as a dry powder formulation for the treatment of bacterial infections in cystic fibrosis (Bronchitol®) (Burness and Keating, 2012). Although its effect in TB treatment has not been reported, its high aqueous solubility and osmolarity properties make it an interesting candidate to overcome the mucus absorption barrier, reaching alveoli tuberculosis-infected macrophages. The 80/20 (mannitol/nanocapsules) ratio used and the solid content was established according to previous studies with mannitol that showed that 20% (w/w) of nanoparticles allowed the obtaining of dry non-aggregated powders with desirable droplet size (Al-Qadi et al., 2012; Grenha et al., 2005). It was also considered because as Miglyol® is a lipid with a low melting point, higher excipient amounts were required to protect it from high temperatures during the spray-drying process, as also reported for lipids such as glyceryl dibehenate and glyceryl tristearate (Gaspar et al., 2017). The rifabutin-loaded protamine NCs were co-spray dried with D-mannitol (section 2.12) and then characterized using DSC, Andersen Cascade Impactor, and Aerosizer® LD.

As reported in DSC thermograms (**Figure 12A**), the spray-dried nanoparticles exhibited a sharp peak at 165ºC (endothermic peak) due to the presence of D-mannitol in the spray-drying process. The presence of a melting peak at 155ºC followed by an exothermic recrystallization peak at about 157ºC and a final melting around 165ºC is attributable to a change from a mixture

of α-β D-mannitol forms to a δ polymorph (Altay Benetti et al., 2021). The disappearance of the peak for the pure drug, which shows a melting endotherm at approximately 149ºC (Gaspar et al., 2016), could be attributed to its encapsulation inside the developed spray-dried NCs (Chokshi et al., 2018). XRPD pattern (**Figure 12B**) confirmed the crystalline structure of the spray-dried formulation and showed an intense peak at 9.7° 2-theta which is typical of δ-form mannitol (Kwok et al., 2015). δ-mannitol polymorph has been described as having better compaction behavior, tabletability, and friability compared to α- and β-mannitol (De Pauw et al., 2022; Vanhoorne et al., 2016). Rifabutin peaks at 10.75, 12.63, 15.50, 17.9, 18.9, and 22.8 2-theta are indicative of its crystalline state (Shanmuga Priya et al., 2013). The XRPD pattern of the spray-dried rifabutin-loaded NCs also manifests the effective inclusion of the drug in the system as groups responsible for the crystalline of rifabutin is included in the spray-dried formulations.

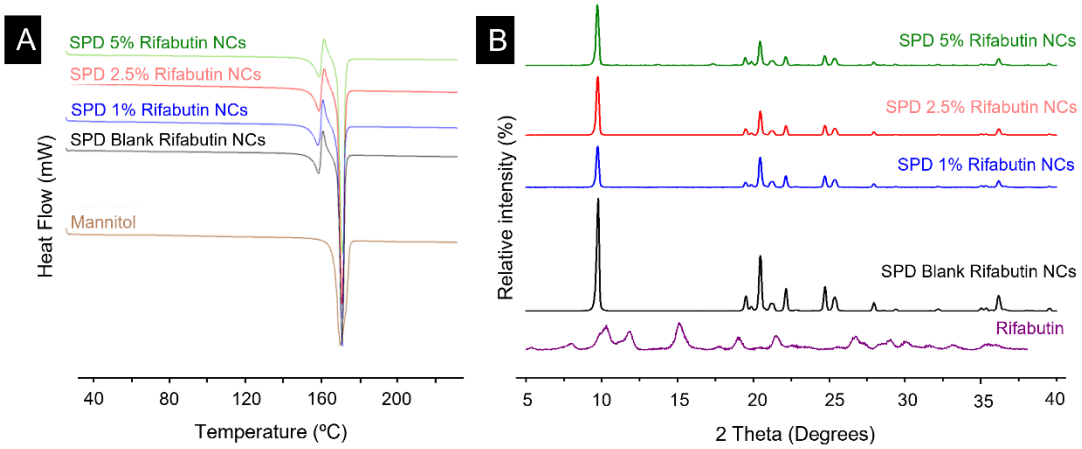

Figure 12. (A) DSC thermograms and (B) XRPD diffractograms of the raw materials and the spray-dried (SPD) blank and 1, 2.5, and 5% rifabutin-loaded nanocapsules (NCs).

3.11. *In vitro* drug deposition evaluation

Andersen cascade impactor evaluation was performed for the aerodynamic evaluation of the spray-dried powders and the distribution of the SPD nanocapsules was determined during the aerodynamic assessment. The *in vitro* aerodynamic results calculated by the Inhalytix™ software are presented in **Table 4**, and the ED, FPF, and MMAD obtained indicated the DPI performance. The ED percentages were remarkably high for all the formulations as were obtained in the range of 69-80%. The co-spray-dried powders exhibited appropriate aerosolization properties with an FPF of 19 to 32%, indicative of the proportion of the dose delivered to the smaller airways (<5µm). Similar FPF values for the low-resistance inhaler have been reported for the Breezhaler® device, which was selected because of its suitability for use in patients with a range of disease severities (Chapman et al., 2011). The breathing parameters affect DPI airway deposition for this device, as shown for commercialized Onbreez Breezhaler®, which presented sensitive changes of FPF, with values no higher than 36% for 90 L/min (r^2=0.81) (Horváth et al., 2020). MMADs ranged from 4.2 to 5.8 µm and were optimal for depositing in the bronchi and alveoli (Carvalho et al., 2011). Spray-dried NCs redispersion and size analysis confirmed the stability of colloidal systems during the drying process, as all formulations were kept on the nano-range size fulfilling our aim. However, an increase of 2.8 and 2.3-fold was observed in the reconstituted 2.5 and 5% rifabutin-loaded NCs compared to the nanocapsules before the spray-dried process. These changes in size were also reported in

the development of mannitol spray-dried rifabutin-loaded solid-lipid nanoparticles (Gaspar et al., 2017).

Table 4. *In vitro* aerodynamic properties of the mannitol spray-dried (SPD) powders at a ratio of 80/20. FPD: Fine Particle Dose; FPF: Fine Particle Fraction (<5µm); ED: Emitted Dose; MMAD: Mean Medium Aerodynamic Diameter. Data represent mean ± SD, N=3 independent measurements.

Spray-dried powder	Andersen Cascade Impactor				Dynamic Light Scattering		
	FPF (%)	FPD (mg)	ED (%)	MMAD (µm)	Size (nm)	PDI	Charge (mV)
SPD Blank NCs	32 ± 10	1.8 ± 1	77 ± 8	4.2 ± 0.8	290 ± 34	<0.4	19 ± 6
SPD 1% Rifabutin NCs	26 ± 6	1.1 ± 0.4	75 ± 11	5.8 ± 1.4	259 ± 32	<0.3	18 ± 7
SPD 2.5% Rifabutin NCs	19 ± 8	0.8 ± 0.6	69 ± 25	5.8 ± 1.3	564 ± 104	<0.6	19 ± 2
SPD 5% Rifabutin NCs	26 ± 8	1.2 ± 0.6	80 ± 9	5.5 ± 1.8	487 ± 96	<0.7	14 ± 3

Figure 13 illustrates the stage-by-stage deposition profiles of spray-dried rifabutin NCs in the ACI after aerosolization. The use of mannitol improved the aerosolization of the nanocapsules as they were successfully released from the capsule in large amounts. Spray-dried rifabutin NCs were distributed mainly through the extra-thoracic region (63-79% of the total amount), especially on the trachea (25-30%). However, the spray-dried powders reached the fourth stage (15-18%), which corresponds to the bronchial area, as well as the alveolar region (1-9% of the total amount).

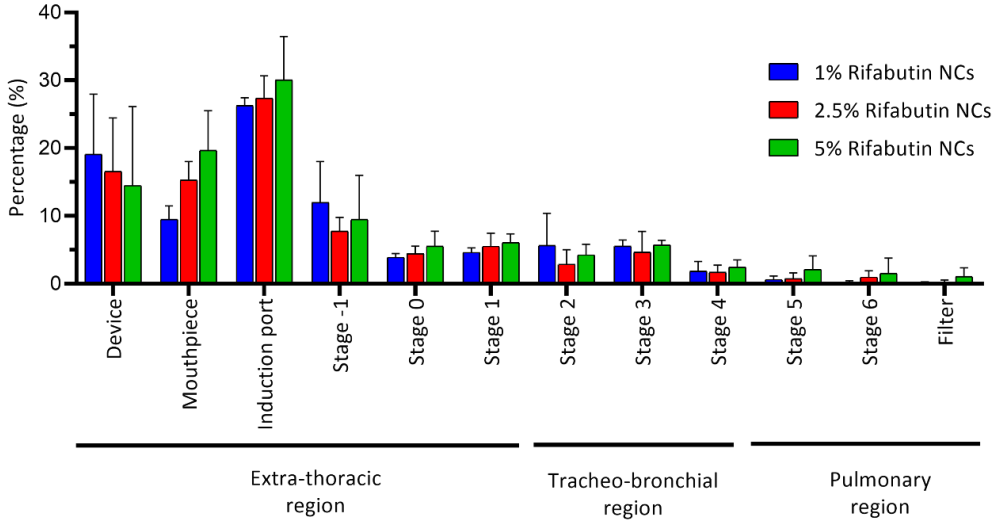

Figure 13. *In vitro* aerodynamic deposition of spray-dried, rifabutin-loaded protamine nanocapsules (NCs) in the Andersen cascade impactor. Values represent mean±SD, N=3 independent measurements.

Particle size distributions were confirmed by the time-of-flight measurements using an Aerosizer LD (**Supplementary Figure 3**). For all the samples, similar aerodynamic size distributions were obtained for the whole set of experimental conditions with an average diameter of 2.9 ±1.9, 2.5 ±2, 2.3±1.9 and 2.4±1.8 µm with specific surface areas of 0.62, 0.48, 0.67 and 0.84 m^2/g for blank, 1, 2.5 and 5% rifabutin protamine NCs, respectively. The slight decrease in size when using this technique compared to the ACI analysis may be due to the use of maximum shear pressure (Adi et al., 2006) which can cause a slight particle breakage (Bennett et al., 2011). However, this shear is recommended for the analysis of size powders

(<20 µm), being of 3 PSI with normal deagglomeration and a medium feed rate of 5,000 cts/sec. Microscopy evaluation was performed to support the quantitative evaluation, and the size distribution was corroborated by SEM photomicrographs (**Figure 14**), where the rifabutin spray-dried NCs presented mainly a spherical shape with a homogeneous distribution, and we could observe the nanosized active ingredient particles. The diameter of the spray-dried NCs was measured with the Image-J program. The size range obtained was between 4.1 and 5.1 µm and was correlated with the results of the aerodynamic characterization.

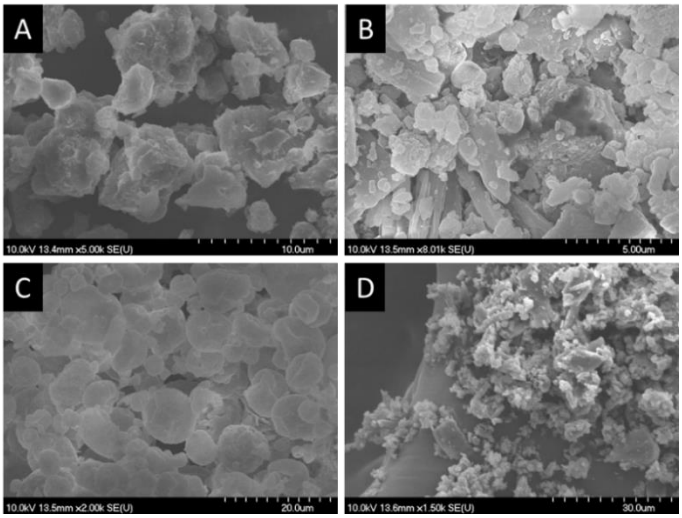

Figure 14. Electron microscopy scanning images of blank (A), 1% (B), 2.5% (C), and 5% (D) rifabutin-loaded protamine nanocapsules (NCs) after mannitol spray-drying process.

The inspiratory flow generated by the patient and the specific resistance of the device are the two driving forces affecting DPIs. In the case of Breezhaler®, a low air-resistance device, its low specific intrinsic resistance (R_D) of 0.060 (cm H_2O)$^{0.5}$ [L/min]$^{-1}$ requires a lower inhalation effort (30 L/min or below), allowing for a greater flow rate. Breezhaler® PIF (peak inspiratory flow rate) is achieved at 108 L/min and requires an inspiratory effort (ΔP) in the of about 4 kPa, lower than Diskus®, Turbuhaler® or Handihaler® (Altman et al., 2018; Dal Negro, 2015; Molimard et al., 2021). Tuberculosis results in impaired lung function, in the form of obstructive lung disease or through reduced lung function, factors that may influence the reduction in PIF (Chushkin and Ots, 2017). Therefore, a flow of 60 L/min was established according to previous works in the field (Gaspar et al., 2017; Grenha et al., 2020; Mukhtar et al., 2021) Considering a flow rate of 60 L/min, 4 s was established as time to achieve the normal forced inhalation volume of an average sized male (4 L) (Momin et al., 2019). Following the equation $\Delta P^{1/2} = R_D Q$ (Tee et al., 2000), the inspiratory effort (drop pressure) generated at 60 L/min was found to be of 1.44 kPa, which could underestimate the real performance of the Breezhaler®, comparing with drop pressure at PIF, which assures an optimal drug delivery to distal airways. This could explain the emitted dose achieved, as small amounts of the DPI were left in the capsule after the first inhalation. This could be improved with repeated inhalations to ensure full dose delivery.

Finally, to provide a higher concentration in the extrapulmonary region, doses between 10–100 mg of drug are estimated as necessary in the treatment of tuberculosis, which is less than the conventional oral/parenteral dose of the drug (Momin et al., 2018). Spray-drying technique produces voluminous powders, limiting the amount in a single dose capsule. In this case, the use of 4 capsules (type 3 hard gelatin) would allow to fill of around 1.82 grams of powder (1.52

g/mL Aerosizer®, data not shown), equivalent to 30 mg of drug for 5% rifabutin protamine nanocapsules. However, it is to be highlighted that drug activity in alveolar macrophages would be required to establish the necessary dose of rifabutin, which we estimate to be far below the theoretically calculated value.

4. CONCLUSIONS

In this study, the developed rifabutin-loaded protamine nanocapsules presented a high encapsulation rate of the drug and have shown promising results on the improvement of dissolution and permeability of the drug. The developed formulation is well tolerated by alveolar macrophages and has a strong capacity to be internalized and activate them. Furthermore, rifabutin-loaded protamine nanoparticles could be successfully incorporated in microparticles by co-spray drying with mannitol for the obtention of a dry powder with adequate aerodynamic properties. The developed ready-to-use pulmonary dry powder system holds great promise for inhalable therapy of pulmonary tuberculosis. Future studies will be required to evaluate the antibacterial efficacy of the systems developed after *in vivo* pulmonary administration.

ACKNOWLEDGMENTS

This research was funded by Ministerio de Ciencia e Innovacion RETOS - PID2019-107500RB-I00, Ministry of Human Capacities, Hungary grant TKP2021-EGA-32 and the Erasmus+ program of the European Union.

CRediT AUTHORSHIP CONTRIBUTION STATEMENT

Sandra Robla: Formal analysis, Investigation, Methodology, Software, Visualization, Roles/Writing - original draft, Writing - review & editing. **Rubén Varela-Calviño**: Supervision, Writing - review & editing. **Rita Ambrus**: Conceptualization, Funding acquisition, Resources, Supervision, Validation, Visualization, Writing - review & editing. **Noemi Csaba**: Conceptualization, Funding acquisition, Resources, Project administration, Supervision, Validation, Visualization Writing - review & editing.

ETHICS APPROVAL

Informed consent was obtained from all subjects involved in the study. All the procedures were carried out under the ethical standard of the institute and national committee on human experiments and the Declaration of Helsinki. Permission was acquired from the Institutional Ethics Committee (Comité Ético de Investigación Clínica de Galicia, CEIC), approval number 2014/543.

CONFLICTS OF INTEREST

The authors declare no conflict of interest.

SUPPLEMENTARY MATERIAL

Supplementary material associated with this article can be found in the online version, at doi:10.1016/j.ejps.2023.106442.

REFERENCES

Adi, H., Larson, I., Chiou, H., Young, P., Traini, D., Stewart, P., 2006. Agglomerate Strength and Dispersion of Salmeterol Xinafoate from Powder Mixtures for Inhalation. Pharm. Res. 23, 2556–2565. https://doi.org/10.1007/s11095-006-9082-6

Al-Qadi, S., Grenha, A., Carrión-Recio, D., Seijo, B., Remuñán-López, C., 2012. Microencapsulated chitosan nanoparticles for pulmonary protein delivery: In vivo evaluation of insulin-loaded formulations. J. Control. Release 157, 383–390. https://doi.org/10.1016/j.jconrel.2011.08.008

Altay Benetti, A., Bianchera, A., Buttini, F., Bertocchi, L., Bettini, R., 2021. Mannitol Polymorphs as Carrier in DPIs Formulations: Isolation Characterization and Performance. Pharmaceutics 13, 1113. https://doi.org/10.3390/pharmaceutics13081113

Altman, P., Wehbe, L., Dederichs, J., Guerin, T., Ament, B., Moronta, M.C., Pino, A.V., Goyal, P., 2018. Comparison of peak inspiratory flow rate via the Breezhaler®, Ellipta® and HandiHaler® dry powder inhalers in patients with moderate to very severe COPD: A randomized cross-over trial. BMC Pulm. Med. 18, 1–8. https://doi.org/10.1186/s12890-018-0662-0

Aristoff, P.A., Garcia, G.A., Kirchhoff, P.D., Hollis Showalter, H.D., 2010. Rifamycins – Obstacles and opportunities. Tuberculosis 90, 94–118. https://doi.org/10.1016/j.tube.2010.02.001

Arpagaus, C., 2011. Nano Spray Dryer B-90: Literature review and applications. Büchi Inf. Bull. 8.

Awotwe-Otoo, D., Agarabi, C., Keire, D., Lee, S., Raw, A., Yu, L., Habib, M.J., Khan, M.A., Shah, R.B., 2012. Physicochemical Characterization of Complex Drug Substances: Evaluation of Structural Similarities and Differences of Protamine Sulfate from Various Sources. AAPS J. 14, 619–626. https://doi.org/10.1208/s12248-012-9375-0

Barreneche, C., Gil, A., Sheth, F., Inés Fernández, A., Cabeza, L.F., 2013. Effect of d-mannitol polymorphism in its thermal energy storage capacity when it is used as PCM. Sol. Energy 94, 344–351. https://doi.org/10.1016/j.solener.2013.05.023

Bekale, R.B., Du Plessis, S.M., Hsu, N.J., Sharma, J.R., Sampson, S.L., Jacobs, M., Meyer, M., Morse, G.D., Dube, A., 2019. Mycobacterium Tuberculosis and Interactions with the Host Immune System: Opportunities for Nanoparticle Based Immunotherapeutics and Vaccines. Pharm. Res. 36. https://doi.org/10.1007/s11095-018-2528-9

Benbow, N.L., Rozenberga, L., McQuillan, A.J., Krasowska, M., Beattie, D.A., 2021. ATR FTIR Study of the Interaction of TiO2Nanoparticle Films with β-Lactoglobulin and Bile Salts. Langmuir 37, 13278–13290. https://doi.org/10.1021/acs.langmuir.1c01830

Bennett, M., Christie, S.M., Graham, A., Thomas, B.S., Vishnyakov, V., Morris, K., Peters, D.M., Jones, R., Ansell, C., 2011. Composition of Smoke Generated by Landing Aircraft. Environ. Sci. Technol. 45, 3533–3538. https://doi.org/10.1021/es1027585

Braunstein, M., Hickey, A.J., Ekins, S., 2019. Why Wait? The Case for Treating Tuberculosis with Inhaled Drugs. Pharm. Res. 36, 166. https://doi.org/10.1007/s11095-019-2704-6

Burness, C.B., Keating, G.M., 2012. Mannitol dry powder for inhalation: in patients with cystic fibrosis. Drugs 72, 1411–21. https://doi.org/10.2165/11208950-000000000-00000

Carvalho, T.C., Peters, J.I., Williams III, R.O., 2011. Influence of particle size on regional lung

deposition – What evidence is there? Int. J. Pharm. 406, 1–10. https://doi.org/10.1016/j.ijpharm.2010.12.040

Chae, J., Choi, Y., Tanaka, M., Choi, J., 2021. Inhalable nanoparticles delivery targeting alveolar macrophages for the treatment of pulmonary tuberculosis. J. Biosci. Bioeng. 132, 543–551. https://doi.org/10.1016/j.jbiosc.2021.08.009

Chapman, K.R., Fogarty, C.M., Peckitt, C., Lassen, C., Jadayel, D., Dederichs, J., Dalvi, M., Kramer, B., 2011. Delivery characteristics and patients' handling of two single-dose dry-powder inhalers used in COPD. Int. J. Chron. Obstruct. Pulmon. Dis. 6, 353–63. https://doi.org/10.2147/COPD.S18529

Chokshi, N. V., Khatri, H.N., Patel, M.M., 2018. Formulation, optimization, and characterization of rifampicin-loaded solid lipid nanoparticles for the treatment of tuberculosis. Drug Dev. Ind. Pharm. 44, 1975–1989. https://doi.org/10.1080/03639045.2018.1506472

Chushkin, M.I., Ots, O.N., 2017. Impaired pulmonary function after treatment for tuberculosis: the end of the disease? J. Bras. Pneumol. 43, 38–43. https://doi.org/10.1590/s1806-37562016000000053

Dal Negro, R.W., 2015. Dry powder inhalers and the right things to remember: A concept review. Multidiscip. Respir. Med. 10, 2–5. https://doi.org/10.1186/s40248-015-0012-5

Davies, G.R., Cerri, S., Richeldi, L., 2007. Rifabutin for treating pulmonary tuberculosis. Cochrane Database Syst. Rev. https://doi.org/10.1002/14651858.CD005159.pub2

De Pauw, E., Vervaet, C., Vanhoorne, V., 2022. Formation of delta-mannitol by co-spray drying: enhancing the tabletability of paracetamol/mannitol formulations. J. Drug Deliv. Sci. Technol. 77, 103907. https://doi.org/10.1016/j.jddst.2022.103907

El-Sherbiny, I.M., El-Baz, N.M., Yacoub, M.H., 2015. Inhaled nano- and microparticles for drug delivery. Glob. Cardiol. Sci. Pract. 2015, 2. https://doi.org/10.5339/gcsp.2015.2

Fröhlich, E., 2017. Hemocompatibility of inhaled environmental nanoparticles: Potential use of in vitro testing. J. Hazard. Mater. 336, 158–167. https://doi.org/10.1016/j.jhazmat.2017.04.041

Gaspar, D.P., Faria, V., Gonçalves, L.M.D., Taboada, P., Remuñán-López, C., Almeida, A.J., 2016. Rifabutin-loaded solid lipid nanoparticles for inhaled antitubercular therapy: Physicochemical and in vitro studies. Int. J. Pharm. 497, 199–209. https://doi.org/10.1016/j.ijpharm.2015.11.050

Gaspar, D.P., Gaspar, M.M., Eleutério, C. V., Grenha, A., Blanco, M., Gonçalves, L.M.D., Taboada, P., Almeida, A.J., Remuñán-López, C., 2017. Microencapsulated Solid Lipid Nanoparticles as a Hybrid Platform for Pulmonary Antibiotic Delivery. Mol. Pharm. 14, 2977–2990. https://doi.org/10.1021/acs.molpharmaceut.7b00169

Gaspar, M.M., Cruz, A., Penha, A.F., Reymão, J., Sousa, A.C., Eleutério, C.V., Domingues, S.A., Fraga, A.G., Filho, A.L., Cruz, M.E.M., Pedrosa, J., 2008. Rifabutin encapsulated in liposomes exhibits increased therapeutic activity in a model of disseminated tuberculosis. Int. J. Antimicrob. Agents 31, 37–45. https://doi.org/10.1016/j.ijantimicag.2007.08.008

Gaspar, M.M., Neves, S., Portaels, F., Pedrosa, J., Silva, M.T., Cruz, M.E.M., 2000. Therapeutic Efficacy of Liposomal Rifabutin in a Mycobacterium avium Model of Infection. Antimicrob. Agents Chemother. 44, 2424–2430. https://doi.org/10.1128/AAC.44.9.2424-2430.2000

Gieszinger, P., Kiss, T., Szabó-Révész, P., Ambrus, R., 2021. The Development of an In Vitro Horizontal Diffusion Cell to Monitor Nasal Powder Penetration Inline. Pharmaceutics 13, 809. https://doi.org/10.3390/pharmaceutics13060809

Grenha, A., Alves, A.D., Guerreiro, F., Pinho, J., Simões, S., Almeida, A.J., Gaspar, M.M.,

2020. Inhalable locust bean gum microparticles co-associating isoniazid and rifabutin: Therapeutic assessment in a murine model of tuberculosis infection. Eur. J. Pharm. Biopharm. 147, 38–44. https://doi.org/10.1016/j.ejpb.2019.11.009

Grenha, A., Seijo, B., Remuñán-López, C., 2005. Microencapsulated chitosan nanoparticles for lung protein delivery. Eur. J. Pharm. Sci. 25, 427–437. https://doi.org/10.1016/j.ejps.2005.04.009

Grenha, A., Seijo, B., Serra, C., Remuñán-López, C., 2007. Chitosan nanoparticle-loaded mannitol microspheres: Structure and surface characterization. Biomacromolecules 8, 2072–2079. https://doi.org/10.1021/bm061131g

Horváth, A., Farkas, Á., Szipőcs, A., Tomisa, G., Szalai, Z., Gálffy, G., 2020. Numerical simulation of the effect of inhalation parameters, gender, age and disease severity on the lung deposition of dry powder aerosol drugs emitted by Turbuhaler®, Breezhaler® and Genuair® in COPD patients. Eur. J. Pharm. Sci. 154. https://doi.org/10.1016/j.ejps.2020.105508

Jakubiak, P., Thwala, L.N., Cadete, A., Préat, V., Alonso, M.J., Beloqui, A., Csaba, N., 2017. Solvent-free protamine nanocapsules as carriers for mucosal delivery of therapeutics. Eur. Polym. J. 93, 695–705. https://doi.org/10.1016/j.eurpolymj.2017.03.049

Kastury, F., Smith, E., Juhasz, A.L., 2017. A critical review of approaches and limitations of inhalation bioavailability and bioaccessibility of metal(loid)s from ambient particulate matter or dust. Sci. Total Environ. 574, 1054–1074. https://doi.org/10.1016/j.scitotenv.2016.09.056

Khairuddin, Pramono, E., Utomo, S.B., Wulandari, V., Zahrotul W, A., Clegg, F., 2016. FTIR studies on the effect of concentration of polyethylene glycol on polimerization of Shellac. J. Phys. Conf. Ser. 776, 012053. https://doi.org/10.1088/1742-6596/776/1/012053

Kwok, P.C.L., Grabarek, A., Chow, M.Y.T., Lan, Y., Li, J.C.W., Casettari, L., Mason, A.J., Lam, J.K.W., 2015. Inhalable spray-dried formulation of D-LAK antimicrobial peptides targeting tuberculosis. Int. J. Pharm. 491, 367–374. https://doi.org/10.1016/j.ijpharm.2015.07.001

Lado, F.L.L., 2002. Clínica de la tuberculosis 39, 181–192.

Lee, W.H., Loo, C.Y., Traini, D., Young, P.M., 2015. Nano- and micro-based inhaled drug delivery systems for targeting alveolar macrophages. Expert Opin. Drug Deliv. 12, 1009–1026. https://doi.org/10.1517/17425247.2015.1039509

Lyadova, I. V., Panteleev, A. V., 2015. Th1 and Th17 Cells in Tuberculosis: Protection, Pathology, and Biomarkers. Mediators Inflamm. 2015, 1–13. https://doi.org/10.1155/2015/854507

Malamatari, M., Charisi, A., Malamataris, S., Kachrimanis, K., Nikolakakis, I., 2020. Spray drying for the preparation of nanoparticle-based drug formulations as dry powders for inhalation. Processes 8. https://doi.org/10.3390/pr8070788

Molimard, M., Kottakis, I., Jauernig, J., Lederhilger, S., Nikolaev, I., 2021. Performance Characteristics of Breezhaler® and Aerolizer® in the Real-World Setting. Clin. Drug Investig. 41, 415–424. https://doi.org/10.1007/s40261-021-01021-w

Momin, M.A.M., Rangnekar, B., Sinha, S., Cheung, C.Y., Cook, G.M., Das, S.C., 2019. Inhalable dry powder of bedaquiline for pulmonary tuberculosis: In vitro physicochemical characterization, antimicrobial activity and safety studies. Pharmaceutics 11. https://doi.org/10.3390/pharmaceutics11100502

Momin, M.A.M., Tucker, I.G., Das, S.C., 2018. High dose dry powder inhalers to overcome the challenges of tuberculosis treatment. Int. J. Pharm. 550, 398–417. https://doi.org/10.1016/j.ijpharm.2018.08.061

Mukhtar, M., Csaba, N., Robla, S., Varela-Calviño, R., Nagy, A., Burian, K., Kókai, D., Ambrus, R., 2022. Dry Powder Comprised of Isoniazid-Loaded Nanoparticles of Hyaluronic Acid in Conjugation with Mannose-Anchored Chitosan for Macrophage-Targeted Pulmonary Administration in Tuberculosis. Pharmaceutics 14, 1543. https://doi.org/10.3390/pharmaceutics14081543

Mukhtar, M., Szakonyi, Z., Farkas, Á., Burian, K., Kókai, D., Ambrus, R., 2021. Freeze-dried vs spray-dried nanoplex DPIs based on chitosan and its derivatives conjugated with hyaluronic acid for tuberculosis: In vitro aerodynamic and in silico deposition profiles. Eur. Polym. J. 160. https://doi.org/10.1016/j.eurpolymj.2021.110775

Munir, M., Kett, V.L., Dunne, N.J., McCarthy, H.O., 2022. Development of a Spray-Dried Formulation of Peptide-DNA Nanoparticles into a Dry Powder for Pulmonary Delivery Using Factorial Design. Pharm. Res. 39, 1215–1232. https://doi.org/10.1007/s11095-022-03256-4

Nainwal, N., Sharma, Y., Jakhmola, V., 2022. Dry powder inhalers of antitubercular drugs. Tuberculosis 135, 102228. https://doi.org/10.1016/j.tube.2022.102228

Nighute, A.B., Bhise, S.B., 2009. Enhancement of dissolution rate of rifabutin by preparation of microcrystals using solvent change method. Int. J. PharmTech Res. 1, 142–148.

Nimje, N., Agarwal, A., Saraogi, G.K., Lariya, N., Rai, G., Agrawal, H., Agrawal, G.P., 2009. Mannosylated nanoparticulate carriers of rifabutin for alveolar targeting. J. Drug Target. 17, 777–787. https://doi.org/10.3109/10611860903115308

Nirbhavane, P., Vemuri, N., Kumar, N., Khuller, G.K., 2017. Lipid Nanocarrier-Mediated Drug Delivery System to Enhance the Oral Bioavailability of Rifabutin. AAPS PharmSciTech 18, 829–837. https://doi.org/10.1208/s12249-016-0559-2

Parlati, C., 2008. Respirable microparticles of aminoglycoside antibiotics for pulmonary administration. Dipatamento Farm. PhD, 161.

Robla, S., Prasanna, M., Varela-Calviño, R., Grandjean, C., Csaba, N., 2021. A chitosan-based nanosystem as pneumococcal vaccine delivery platform. Drug Deliv. Transl. Res. 11, 581–597. https://doi.org/10.1007/s13346-021-00928-3

Rodrigues, S., da Costa, A.M.R., Flórez-Fernández, N., Torres, M.D., Faleiro, M.L., Buttini, F., Grenha, A., 2020. Inhalable spray-dried chondroitin sulphate microparticles: Effect of different solvents on particle properties and drug activity. Polymers (Basel). 12, 1–13. https://doi.org/10.3390/polym12020425

Rouco, H., Diaz-Rodriguez, P., Gaspar, D.P., Gonçalves, L.M.D., Cuerva, M., Remuñán-López, C., Almeida, A.J., Landin, M., 2020. Rifabutin-loaded nanostructured lipid carriers as a tool in oral anti-mycobacterial treatment of crohn's disease. Nanomaterials 10, 1–18. https://doi.org/10.3390/nano10112138

Sham, J.O.H., Zhang, Y., Finlay, W.H., Roa, W.H., Löbenberg, R., 2004. Formulation and characterization of spray-dried powders containing nanoparticles for aerosol delivery to the lung. Int. J. Pharm. 269, 457–467. https://doi.org/10.1016/j.ijpharm.2003.09.041

Shanmuga Priya, A., Sivakamavalli, J., Vaseeharan, B., Stalin, T., 2013. Improvement on dissolution rate of inclusion complex of Rifabutin drug with β-cyclodextrin. Int. J. Biol. Macromol. 62, 472–480. https://doi.org/10.1016/j.ijbiomac.2013.09.006

Singh, N., Sahoo, S.K., Kumar, R., 2020. Hemolysis tendency of anticancer nanoparticles changes with type of blood group antigen: An insight into blood nanoparticle interactions. Mater. Sci. Eng. C 109, 110645. https://doi.org/10.1016/j.msec.2020.110645

Sosnik, A., Carcaboso, Á.M., Glisoni, R.J., Moretton, M.A., Chiappetta, D.A., 2010. New old challenges in tuberculosis: Potentially effective nanotechnologies in drug delivery. Adv. Drug Deliv. Rev. 62, 547–559. https://doi.org/10.1016/j.addr.2009.11.023

Suárez, I., Fünger, S.M., Kröger, S., Rademacher, J., Fätkenheuer, G., Rybniker, J., 2019. The Diagnosis and Treatment of Tuberculosis. Dtsch. Arztebl. Int. 116, 729–735. https://doi.org/10.3238/arztebl.2019.0729

Tee, S.K., Marriott, C., Zeng, X.M., Martin, G.P., 2000. The use of different sugars as fine and coarse carriers for aerosolised salbutamol sulphate. Int. J. Pharm. 208, 111–123. https://doi.org/10.1016/S0378-5173(00)00553-6

Thwala, L.N., Beloqui, A., Csaba, N.S., González-Touceda, D., Tovar, S., Dieguez, C., Alonso, M.J., Préat, V., 2016. The interaction of protamine nanocapsules with the intestinal epithelium: A mechanistic approach. J. Control. Release 243, 109–120. https://doi.org/10.1016/j.jconrel.2016.10.002

Traini, D., Young, P.M., 2017. Drug delivery for tuberculosis: is inhaled therapy the key to success? Ther. Deliv. 8, 819–821. https://doi.org/10.4155/tde-2017-0050

Vanhoorne, V., Van Bockstal, P.-J., Van Snick, B., Peeters, E., Monteyne, T., Gomes, P., De Beer, T., Remon, J.P., Vervaet, C., 2016. Continuous manufacturing of delta mannitol by cospray drying with PVP. Int. J. Pharm. 501, 139–147. https://doi.org/10.1016/j.ijpharm.2016.02.001

Woods, A., Andrian, T., Sharp, G., Bicer, E.M., Vandera, K.-K.A., Patel, A., Mudway, I., Dailey, L.A., Forbes, B., 2020. Development of new in vitro models of lung protease activity for investigating stability of inhaled biological therapies and drug delivery systems. Eur. J. Pharm. Biopharm. 146, 64–72. https://doi.org/10.1016/j.ejpb.2019.11.005

Yang, W., Peters, J.I., Williams, R.O., 2008. Inhaled nanoparticles—A current review. Int. J. Pharm. 356, 239–247. https://doi.org/10.1016/j.ijpharm.2008.02.011

Zhang, Y., Huo, M., Zhou, J., Zou, A., Li, W., Yao, C., Xie, S., 2010. DDSolver: An Add-In Program for Modeling and Comparison of Drug Dissolution Profiles. AAPS J. 12, 263–271. https://doi.org/10.1208/s12248-010-9185-1

CHAPTER V/ CAPÍTULO V

A bioinspired delivery platform for ocular nanotherapeutics

In collaboration with:

Department of Biochemistry and Molecular Biology, University of Santiago de Compostela, Instituto Universitario Fernández-Vega, Fundación de Investigación Oftalmológica, University of Oviedo and Instituto de Investigación Sanitaria del Principado de Asturias (ISPA)

CHAPTER V/ CAPÍTULO V

A bioinspired delivery platform for ocular nanotherapeutics

Abstract

Topical administration constitutes a challenge in the ocular delivery of biopharmaceutics. Despite its easy accessibility, the eye is protected by extraordinary anatomical and physiological barriers, causing the premature removal of nanocarriers, their enzymatic degradation, and their elimination by immune cells. In this work, we developed an ocular microneedle-like drug delivery platform based on natural pollen grains to enhance the mucointeraction and the residence time of an antihistamine drug, for the topical treatment of allergic rhinoconjunctivitis. First, purification of *Helianthus annuus* pollen grains was performed, and then the obtained pollen microcapsules were associated with previously characterized bilastine-loaded protamine nanocapsules. Toxicity, cell internalization, and macrophage activation were evaluated *in vitro*. The analysis of the interaction of the developed carriers with the ocular epithelium was carried out in an artificial 3D cornea model of the human corneal epithelium and biocompatibility and physical irritation effects were evaluated upon ocular instillation in rats. The developed pollen microcapsules preserved the original external 3D structure of the intact pollen grain but were free of its internal compounds and did not induce immune cell activation *in vitro* or *in vivo*. Furthermore, preservation of epithelial integrity and high tolerability were also observed both *in vitro* and after *in vivo* topical administration. Their biocompatibility, allergen-free composition, and mucoadhesive properties make these pollen microcapsules an interesting strategy to overcome the biological and mechanical barriers of ocular drug delivery.

Graphical abstract

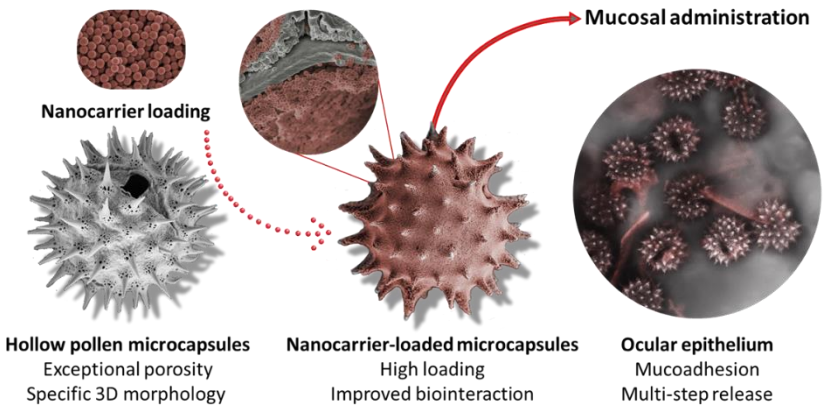

1. INTRODUCTION

The eye is the most common site of allergic inflammatory disorders. Allergic conjunctivitis is the most frequent ocular allergy presentation, affecting 10-25% of the population's quality of life. Seasonal or intermittent allergic conjunctivitis starts in childhood (>80% of individuals before the age of 30 years) and it is usually accompanied by allergic rhinitis, causing redness, itching, tearing, and swelling, as well as blurred vision, sensitivity to light, or even eye pain [1–3]. As the ocular surface is highly exposed to pathogens and other foreign particles, there is a basal immunological unresponsiveness state. This mucosal immune tolerance to ocular antigens and pathogens is initiated by dendritic cells (DCs) in the anterior chamber, which activate Treg cells inhibiting mucosal inflammation [4]. The anterior chamber of the eye is an immune-privileged site, with an anti-inflammatory and immunosuppressive microenvironment [5]. However, during allergic inflammation, there is a breakdown of mucosal tolerance [4], and DCs are recruited to the conjunctiva to initiate an adaptive immune response [6]. Allergic rhinoconjunctivitis is an immediate IgE-mediated hypersensitivity (type I) reaction [7], where allergens are taken by antigen-presenting cells (APCs) and supplied to T cells, with consequent activation of Th_2 response and production of IgE antibodies [7]. The interaction of these antibodies to IgE receptors on mast cells and basophils leads to their degranulation and histamine release, with subsequent allergic symptoms [8]. Effects of histamine are mediated through the H_1 histamine receptor, leading to calcium mobilization and inflammatory response [9].

Bilastine is a histamine inverse agonist with a high affinity for H_1 receptors [10] initially developed by Faes Farma (Bilaxten®) and currently available as Ibis® (Menarini), Obalix® (GSK) and as a generic drug and approved in more than 120 countries for the treatment of allergic rhinoconjunctivitis through oral administration of 20 mg per day. It is characterized by a fast onset of action and a prolonged effect compared with first-generation antihistamines and no sedative properties, with an oral bioavailability of 60%, reduced to 30% when taken together with food [11]. In this context, the use of topical eye drops containing antihistamines, mast cell stabilizers, or corticosteroids is being developed to relieve eye symptoms, and ophthalmic formulation of 0.6% bilastine are currently under investigation (clinical trials NCT03231969 and NCT03479307) [12]. Topical drug delivery for the treatment of conditions of the anterior segment of the eye is a simple, non-invasive, and convenient route for local treatment, however, the eye's anatomy constitutes a challenge in the ophthalmic delivery of pharmaceutics [13]. Factors such as nasolacrimal drainage and tear fluid turnover limit the residence time of ophthalmic formulations, which constitutes the major drawback for topical application. Different ophthalmic delivery strategies as the use of nanocarriers using mucoadhesive polymers such as PLGA [14], protamine [15], or chitosan [16] have emerged to interact closely with ocular surface structures, resulting in increased concentration and longer retention of the drug [17]. Other strategies, such the use of mucus penetrating particles (MPP) were reported with a specific covalent or non-covalent coating that allows diffusion into mucus pores, by minimizing adhesive interactions with mucin fibers. INVELTYS® is an ophthalmic suspension approved by FDA using MPP technology (Kala Pharmaceuticals, Inc.) specifically indicated for treating inflammation and pain following ocular surgery [18]. Besides, the development of drug delivery systems that act as drug reservoirs prolonging their residence time and controlling their release is becoming a key strategy for ocular drug delivery [19]. The use of microneedles constitutes a minimally-invasive alternative in ocular administration, offering a long-term localized drug delivery in the treatment of eye diseases [20]. Previously it has been proposed that microneedle-like surface of pollen grains such as sunflower (*Helianthus annuus)* can largely facilitate mucosal adhesion [21]. Pollen grains have been identified as a promising

candidate for drug encapsulation and delivery [22] due to their chemically stable and biocompatible biopolymer outer wall, the sporopollenin, which can be processed to create an allergen-free hollow platform with a large inner cavity, which can serve as a drug delivery vehicle that protects by encapsulating drugs [23]. Based in this previous information, in this work, we explored the feasibility of encapsulating bilastine-containing polymeric nanocapsules into hollow pollen platforms of *H. annuus* for ocular administration with improved mucointeraction to allow efficient local delivery for the treatment of allergy.

2. MATERIALS AND METHODS

2.1. Materials

Low molecular weight protamine sulphate (LMWP 5 kDa, Yuki Gosei Kogyo, Ltd., Japan), polyethylene glycol stearate 40 (PEGst 40, Croda Chemicals Europe Ltd., UK), sodium glycocholate (SGC, Dextra Laboratories Ltd., UK), Miglyol® 812 (IOI Oleo GmbH, Germany), Bilastine Normon 20mg tablets EFG (Normon, Spain), *Helianthus annuus* pollen (Control Bio, Spain). 1,1'-Dioctadecyl-3,3,3',3'-tetramethylindodicarbocyanine, 4-chlorobenzenesulfonate salt (DiD) and medium Roswell Park Memorial Institute RPMI-1640 GIBCO® (Thermo Fisher Scientific, Spain), 3-(4,5-dimethyl-2-thiazolyl)-2,5-diphenyl-2H-tetrazolium bromide (MTT), fetal Bovine Serum (FBS), Penicillin-Streptomycin-Glutamine (PSG) and standard chemicals (Sigma Aldrich, USA), normal goat serum (Vector Laboratories, Burlingame, USA), 6-diamidino-2-phenylindole (DAPI) (Molecular Probes, USA), allophycocyanin (APC)-conjugated anti-human CD83 (CD83-APC), phycoerythrin (PE)-conjugated anti-human CD80 (CD80-PE), (Miltenyi Biotec, Germany), anti-mouse CD4-FITC (Tonbo Bioscience, USA), rabbit mab-TNFα and rabbit man anti-b catenin (Abcam, UK) mouse mab-CamKII (Cell Signaling Technology, USA), Alexa Fluor 488 goat anti-mouse and Alexa Fluor 594 goat anti-rabbit (Molecular Probes, USA), rabbit polyclonal anti-S100 (Dako, Denmark) and fluorescent mounting medium (Dako®, Denmark), ketamine 100 mg/mL (Imalgene®, Merial, France), xylazine 20 mg/mL (Rompun®, Bayer, Germany) and sodium pentobarbital 200 mg/mL (Dolethal®, Vetoquinol, France).

2.2. Bilastine purification and characterization

Pure bilastine was extracted from commercial 20 mg bilastine tablets, after homogenization by physical mixing and dissolution in a 1:1 (v/v) water: chloroform solution. The organic fraction was collected and evaporated under vacuum at 150 rpm (Rotavapor R-300, Buchi, Switzerland) and the solid powder was dried in a vacuum oven at 35-40°C to constant weight. Bilastine was characterized by H_1-NMR spectrometry (Bruker BRX-500), Fourier Transform infrared spectroscope (FTIR) (Thermo Nicolet AVATAR 330, Waltham, MA, USA) at 4 cm^{-1} resolution at a range of 400–4000 cm^{-1} and X-Ray Powder Diffraction (XRPD) (Bruker AXS GmbH, Karlsruhe, Germany). The H_1-NMR spectra was analyzed by NMR processing software ACD/1D NMR Processor and XRPD and FTIR spectra were evaluated using OriginPro 2017 Spectragryph v1.2.16.1 software, respectively.

2.3. Preparation and physicochemical characterization of bilastine-loaded protamine NCs

Bilastine-containing nanoemulsions (NEs) were prepared by the solvent displacement technique following the procedure previously described and optimized by our group [24], by adding 29.5 mg of Miglyol®812, 2.5 mg of SGC and 8 mg of PEGst-40 dissolved in 1.5 mL of ethanol. Thereafter, 2.5 mg of bilastine (5% w/w) were dissolved in 0.975 mL of acetone and were added over the ethanolic solution. The organic phase was immediately poured over 5 mL

of water under magnetic stirring for 10 min. Then, the organic solvents were eliminated by evaporation under vacuum in a Rotary Evaporator (Rotavapor R-300, Buchi, Switzerland), to obtain NEs with a constant final volume of 5 mL and NEs were isolated by ultracentrifugation (Optima™ L-90K, Ultracentrifuge, Beckman Coulter, USA) at 61,740 *g*, at 15 ºC for 1 h and resuspended in 1 mL of ultrapure water. Blank and bilastine-loaded protamine nanocapsules (NCs) were prepared by changing the aqueous phase to a solution containing 0.15% w/v protamine.
The hydrodynamic diameter, polydispersity index (PDI), derived count rate, and zeta potential values were measured by using a Zetasizer Nano-S (Malvern Instruments; Malvern, UK). Bilastine-loaded NEs and protamine NCs were diluted 1:50 in ultrapure water (MilliQ®, Merck, USA) before the measurement. Nanoparticle Tracking Analysis (NTA) was conducted using the NanoSight 142 NS3000 system from Malvern Analytical Ltd. in Malvern, UK, and the NCs were diluted (1:1,000) to ensure that their concentration fell within the measuring range of the instrument (~10^7- 10^9 particles/mL).

After coating the samples with iridium in an argon atmosphere, the morphology of the nanocapsules (dilution 1:1,000) was examined using field emission scanning electron microscopy (FESEM; Gemini-SEM, Zeiss, Germany).

2.4. Encapsulation efficiency and drug loading

The efficiency of encapsulation of bilastine was quantified using an Acquity UPLC H-Class Plus system equipped with a C_{18} column (Waters symmetry 1.7 µm, 2.1 x 50 mm). Throughout UPLC analysis, 10 µL of each sample was injected and eluted with a mobile phase composed of (A) methanol (B) acetonitrile, and (C) phosphoric acid buffer pH 2.1 in a ratio A:B: C (21:33:46 v/v) based on a procedure previously described by Ashish S. Jain *et al* [25]. The phosphoric acid buffer solution was prepared by adding 24.59 mM of sodium phosphate monobasic hydrated ($NaH_2PO_4H_2O$) and 75.40 mM of sodium phosphate dibasic heptahydrate (Na_2HPO_4 $7H_2O$) in distilled water in a final volume of 800 mL and adjusting the pH to 2.1. A standard stock solution was prepared by dissolving pure bilastine in a range of 0 and 25 µg/mL in mobile phase, showing a correlation coefficient of R= 0.9976. Isolated bilastine-loaded NCs were digested in acetonitrile to extract the encapsulated bilastine in the NCs and they were centrifuged twice at (Eppendorf 5430R®) at 12,000 g and 4ºC for 30 min. Samples were filtered by 0.22-micron syringe filters before UPLC measurement. The limit of detection (LOD) was found to be 0.0544 ng/mL. and the Limit of quantification (LOQ) was found to be 0.1649 ng/mL. Suitability, linearity, precision, and specificity of the analytical method were also evaluated. The retention time was 1.87 min. Bilastine quantification was performed at 278 nm, with a 0.1 mL/min flow rate.

$$\text{Encapsulation efficiency (EE\%)} = \frac{\text{Weight of initial drug} - \text{Weight of free drug}}{\text{Weight of initial drug}} \text{ x } 100$$

$$\text{Drug loading (DL\%)} = \frac{\text{Weight of loaded drug}}{\text{Weight of lipid core}} \text{ x } 100$$

2.5. Stability studies

The colloidal stability of the nanocapsules before and after the freeze-drying procedure was evaluated *in vitro* in water and Simulated Lacrimal Fluid (SLF) at 37ºC, composed of 0.18%

KCl, 0.63% NaCl, 0.006% $CaCl_2$ and 0.01% $MgCl_2$ (pH adjusted to 7.4) at 37°C [26] to mimic the ocular environment after drop instillation.
For the freeze-drying process, blank and bilastine-loaded protamine nanocapsules were lyophilized (Labconco Corp, USA) in the presence of 5% (w/v) trehalose as a cryoprotectant, using different ratios and trehalose: nanocapsules (1:1, 2:1, 3:1, 4:1 and 5:1 v/v). Samples were frozen in a freeze-drying glass vial at -80°C in a high vacuum atmosphere and they were subjected to a drying step for 24 h. The freeze-dried formulations were resuspended with ultrapure water to their initial concentration by vortexing. At different time points under moderate shaking (0, 1, 3, 6, 8, and 24 h) and the evolution of mean particle diameter (nm), PDI, and derived count rate were analyzed using Zetasizer Nano-ZS^{TM} as previously described (section 2.3). Stability under storage for 30 days at 4°C was also monitored. All experiments were performed in triplicates. The nanoparticles process yield was calculated by gravimetry following the equation:

$$\text{Process yield (Y\%)} = \frac{\text{Weight of nanocapsules}}{\text{Theoretical weight of nanocapsules}} \text{x } 100$$

2.6. Obtention of *H. annuus* pollen platforms

Pollen of *Helianthus annuus* was treated in several washing steps to remove the external and internal cellular components following a protocol developed by our group [23]. Briefly, pollen was initially washed with water to remove the hydrophilic compounds. After that, the water-washed pollen was washed with acetone to remove organic components. Once acetone-treated pollen was obtained, it was resuspended with cyclohexane for the obtention of defatted *H. annuus* sporopollenin microcapsules. Finally, for the obtention of hollow platforms, defatted pollen was incubated with H_3PO_4 at a 1:10 ratio (w/v) at 70ºC for 5 h. Acid-treated (hollow) pollen was collected through filtration and washed with water until neutral pH and was subsequently dried and stored in a desiccant chamber until needed.

2.7. Loading of bilastine protamine nanocapsules in hollow pollen microcapsules

Bilastine nanocapsules were loaded into *H. annuus* hollow pollen microcapsules under vacuum (25 mbar) using a mass ratio of 1:1 (w/w) in a Rotary Evaporator (Rotavapor R-300, Buchi, Switzerland) at 150 rpm, 37 ºC for 30 minutes. For the determination of non-associated nanocapsules, pollen vehicles were resuspended in water and centrifuged for 1 min at 15,000 *g* at room temperature. Non-loaded nanocapsules were removed from the supernatant by using a syringe and samples were filtered (0.22 µm-micron filters) and freeze-dried for 24 h using (Labconco Corp, USA). All experiments were conducted in triplicate. Encapsulation efficiency (EE%), loading capacity (LC%), and loading content (w/w) of pollen samples were calculated by gravimetry using the following equations:

$$\text{Encapsulation efficiency (EE\%)} = \frac{\text{Nanocarriers associated}}{\text{Total of nanocarriers}} \text{x } 100$$

$$\text{Loading Capacity (LC\%)} = \frac{\text{Mass of loaded nanocarriers}}{\text{Mass of pollen platforms loaded with nanocarriers}} \text{x } 100$$

$$\text{Loading Content (w/w)} = \frac{\text{Mass of loaded nanocarriers}}{\text{Mass of pollen platforms}} \text{x } 100$$

Nanocapsules internalization into *H. annuus* sporopollenin microcapsules was analyzed by Confocal Laser Scanning Microscopy (CLSM, SP5 Leica AOBS-SP5, Leica Biosystems Nussloch GmbH). Bilastine-loaded protamine NCs were labeled by incorporating 0.02 mL of a DiD solution in ethanol (0.25% w/v) to the organic phase before NCs preparation, and its physicochemical characterization was evaluated by DLS as described in Section 2.3., to confirm that the dye did not alter the formulations and is suitable for the *in vitro* assays. CLSM visualization was performed at DAPI-dye excitation λ_{max}= 359 nm and emission λ_{max}= 457 nm and DiD-dye excitation λ_{max}=640 nm and emission λ_{max}= 675 nm. Natural fluorophores of pollen were excited at λ_{max}=405 nm, 492 nm, and 561 nm, and collected with emission filters of λ_{max}= 414-479, 505-554, and 571-635 nm [27].

2.8. *In vitro* release studies

In vitro dissolution studies were performed in SLF to evaluate the release kinetics of bilastine from the nanocapsules and the *H. annuus* pollen microcapsules. A suspension of nanocapsules containing 4 mg of loaded pollen microcapsules (equivalent to 250 µg of bilastine) was dispersed in 10 mL of SLF at 200 rpm up to 24h at 37ºC. 1 mL of the dissolution medium was collected into microcentrifuge tubes (Eppendorfs®) at time intervals of 30 min, 1, 2, 3, 4, 6, and 24 h, and centrifuged at 7,500 *g* during 1 min at RT, filtered (0.22 µm-micron filters) and the supernatant was analyzed spectroscopically by using a UV–visible spectrophotometer (FLUOstar Omega, BMGLabtech, Germany) at a wavelength of 278 nm. An equal volume of fresh SLF was added to replace the withdrawn volume. A calibration curve was constructed from standard solutions of bilastine diluted in SLF over the concentration range of 0–50 µg/mL. y= 0.0075x – 0.0112 (R= 0.9825). All experiments were conducted in triplicate. The kinetics of the *in vitro* drug release were evaluated by fitting to Zero order, First-order, Higuchi, and Korsmeyer–Peppas models to understand the drug release mechanism.

2.9. *In vitro* cytotoxicity studies

The cytotoxicity of the developed bilastine-loaded protamine NCs in suspension or loaded into *H. annuus* hollow pollen platforms was evaluated using MTT reduction, a soluble tetrazolium dye converted by viable cells into insoluble formazan. 200 µl of non-adherent human monocyte-like THP-1 cells were seeded in a 24-well plate at $2.3x10^5$ cells/mL in RPMI culture medium, supplemented with 10% inactivated fetal serum bovine, 100 units/ml of penicillin G (sodium salt) and 100 µg/mL of streptomycin sulfate. Cells viability was assessed after 24 h of cell incubation with 200 µL of different concentrations of blank and bilastine-loaded nanocapsules (1, 0.5, 0.25, and 0.1 mg/mL), hollow pollen microcapsules and bilastine NCs loaded into hollow microcapsules (1, 0.5, 0.25 and 0.1 mg/mL of NCs), considering a loading ratio of pollen: NCs of 1:1 (w/w). Non-treated cells were used as control. Then, cells were centrifuged (5 min 1,000 g at room temperature), the medium was replaced by 0.05% MTT in PBS, and cells were incubated for 4 h at 37ºC in darkness in a 24-well plate. After that time, MTT solution was discarded by centrifugation (5 min 1,000 *g* at RT), and cells were transferred to a 96-well plate. Formazan crystals were dissolved by the addition of 0.04 N HCl in isopropanol. Absorbance was measured at 570 nm using a microplate reader (Synergy H1 Hybrid Multi-Mode, BioTek, Winooski, VT, USA). All MTT assays were performed in triplicates.

2.10. Quantitative nanocapsule uptake

Coverslips previously treated with Poly-L-Lysine for cell adhesion were placed in a 6-well plate and $1x10^6$ cells were added to each well. The different formulations (DiD bilastine-loaded NCs, hollow sporopollenin microcapsules, and DiD bilastine-loaded NCs-loaded into pollen microcapsules) were incubated with the THP-1 cells at a final concentration of 0.1 mg/mL during 24 h at 37ºC and 5% CO_2. After this time, formulations were removed, and cells were fixed with 4% paraformaldehyde (PFA) for 20 minutes at room temperature. Subsequently, cells were washed 3x with PBS pH 7.4 and samples were mounted in glycerol. Bilastine-loaded nanocapsules internalization in THP-1 cells was evaluated by Confocal Laser Scanning Microscopy (CLSM, SP5 Leica AOBS-SP5, Leica Biosystems Nussloch GmbH). Non-treated cells were used as control. Fluorescence measurements were analyzed by LAS X Life Science Software as previously described in section 2.7. The percentage and fluorescence intensity of internalized bilastine-loaded NCs was quantified by flow cytometry analysis (BD FACSCalibur™, Becton Dickinson) after THP-1 cells incubation with the bilastine-loaded formulations for 24 h. Cells were washed (1,000 *g*, 5 min at room temperature) and filtered through 20 µm cell strainer filters (PluriStrainer mini®) to remove excess of NCs and NCs loaded pollen microcapsules and resuspended in PBS pH 7.4 before flow cytometry analysis and were analyzed by Flowing Software 2.5.1 (Cell Imaging Core, Turku Bioscience).

2.11. Immune cell activation

Non-adherent THP-1 cells were seeded in a 24-well plate at 37 °C and 5% CO_2 and incubated with the different formulations (blank and bilastine-loaded nanocapsules, hollow pollen microcapsules, bilastine NCs loaded into pollen microcapsules and bilastine). After 24h, cells were washed (1,000 *g*, 5 min at room temperature) to remove excess of NCs and resuspended in PBS pH 7.4 (100 µL/well). Staining with the different antibodies (CD80-PE and CD83-APC) was carried out for 25 min at room temperature in darkness. Then, 1 mL of PBS pH 7.4 was added and cells were centrifuged to remove unbound markers (1,000 *g*, 5 min at room temperature), and resuspended in a final volume of 0.5 mL of PBS before flow cytometry analysis. The studies were carried out in triplicate. CD80/CD83 antibody expression was analyzed by Flowing Software 2.5.1. Non-treated cells were used as a negative control and cells treated with lipopolysaccharide (LPS) at 1 µg/mL were used as a positive control.

2.12. *In Vitro* 3D corneal epithelium integrity assay

An artificial 3D cornea ephitelium model (QobuR-Reconstructed human Corneal Epithelium [28, 29]) was performed from the human sclerocorneal limbus stem cells. Cells were seeded in 1.12 cm^2 poluester cell culture inserts with serum-free medium at standard culture conditions and were maintained with medium contacting both the apical and basolateral sides. At confluence, the medium was removed from the apical side and the cells were exposed to an air–liquid interface to stimulate tissue maturation for a week. Formulations of hollow pollen microcapsules, DiD-labeled bilastine NCs loaded pollen microcapsules, and DiD-labeled bilastine NCs were incubated with the QobuR models at 1 mg/mL for 4 h at 37ºC and 5% CO_2. To analyze the morphology and integrity of the epithelial barrier in the QobuR-RhCE models, samples were fixed in 4% (*w/v*) buffered paraformaldehyde for 1 h at RT and cryoprotected in 30% (*w/v*) sucrose. Membranes were isolated from the insert, embedded in Optimum Cutting Temperature compound (OCT) (Tissue-Teck® Sakure, Japan) compound and snap frozen in liquid Nitrogen. Transversal sections of 10 µm were obtained using a by cryostat microtome (Microm HM550 cryostat, Microm International GmbH) and collected on microscope slides.

3D sections were washed with distilled water for 20 minutes to remove the OCT compound. Then, excess water was removed, samples were washed with PBS-Triton 0.03% (3x10 min) then, they were incubated with primary antiserum Rb mab β-Catenin E247 (1:200) in 10% normal goat serum for blocking non-specific binding and PBS-Triton x100 0.03%) for 24 h in a humid chamber at RT. Next, all sections were washed in PBS (3x10 min) and incubated with the polyclonal secondary antibodies Alexa Fluor 488 goat anti-rabbit (1:500) for 2 h ar TR and protected from light. After 3 additional PBS washes, cell nuclei were counterstained with DAPI (2 µg/mL) for 10. 3D epithelium models morphology was was evaluated under a Leica DM 6000 fluorescence microscope and DiD-labeled NCs internalization was analyzed by using a Thunder microscope (Leica Microsystems, GmB) and the LAS X Life Science Software (Leica Microsystems), at DiD-dye excitation at λmax=640 nm and emission at λmax= 675 nm and Alexa Fluor 488, with excitation at λmax=490 nm and emission at λmax= 520 nm.

2.13. *In vivo* ocular distribution and immunohistological analysis

Wistar rats (weighing 250-300 g) were used to evaluate the ocular tolerance and distribution of protamine NCs and NCs loaded pollen microcapsules. 20 µL samples (1 mg/mL) were topically instilled onto the ocular surface and they were examined for signs of ocular irritation. Untreated rats were used as control. The presence of animal discomfort, symptoms, and signs was evaluated according to the guidelines for ocular irritation testing (OECD TG 405 [30]). Formulations were maintained in the ocular surface for 30 minutes and then rats were anesthetized intraperitoneally with Ketamine (Imalgene®, 100 mg/mL) and Xilacine (Rompun®, 20 mg/mL), ratio 80:20 and intracardiac euthanized with sodium pentobarbital (200 mg/mL). The eye tissues (ocular globe and eyelids) were eviscerated and fixed with 4% formaldehyde overnight, washed in 0.1 M PBS pH 7.4, and cryoprotected with 30% (*w/v*) sucrose solution. Eyes were embedded in the OCT compound and frozen in isopentane. For immunohistological analysis, transversal sections of 10 µm were obtained using a cryostat microtome and collected in microscope slides**.** Slides were washed with distilled water for 20 min to remove the OCT compound. Then, excess water was removed, and samples were washed with PBS-Triton 0.03% (3x10 min). They were divided into two groups, and they were incubated with primary antiserum. The first group was stained with primary antibodies anti-mouse CD4-FITC, and rabbit polyclonal anti-S100 (1:400), and the second group with rabbit mab TNFα (1:200) and mouse mab CamKII (1:200), both in 10% normal goat serum for blocking non-specific binding and triton X100 0.03%) during 24 h in a humid chamber at RT. Subsequently, all sections were washed in PBS pH 7.4 (3x10 min) and incubated with the polyclonal secondary antibodies Alexa Fluor 488 goat anti-mouse (1:500) for primary CAMKII and Alexa Fluor 594 goat anti-rabbit (1:500) for primary S100 and TNFα for 2 h protected from light at RT and washed again with PBS (3x10 min). Finally, cell nucleus staining was performed, using DAPI (2 µg/mL) solution for 10 min. The expression of activation markers was compared with the expression induced by defatted pollen (positive control). Samples were mounted with Dako Fluorescent Mounting Media and stored at -20ºC until use. Sections were visualized under a Leica DM 6000B fluorescence microscope (Leica Microsystems, Wetziar, Germany) using LAS X software (Leica Microsystems) at Alexa Fluor 488 (λex=490 nm and λem= 520 nm), Alexa Fluor 594 (λex=590 nm and λem= 617 nm) and FITC (λex=490 nm and λem= 525 nm).

Statistical analysis

The statistical significance of the difference between the means was determined by GraphPad Prism 8. All data are shown as mean±SD and one-way and two-way analyses of variance (ANOVA) were performed to compare multiple independent groups. Differences were considered statistically significant at $P<0.05$.

3. RESULTS AND DISCUSSION

3.1. Bilastine purification and characterization

Bilastine ($C_{28}H_{37}N_3O_3$, molecular weight 463.6 g/mol) is a second-generation antihistamine, a histamine receptor antagonist, developed by Faes Farma in 2011 and approved by the EU for oral administration of 20 mg for the treatment of allergic rhinoconjunctivitis and urticaria [31]. In this work, we developed a method for preparing a bilastine crystalline form, using chloroform as the isolation solvent. To characterize the obtained product, H_1-NMR analysis (**Figure 1**) was recorded from 0 to 10 ppm using a proton NMR spectrometer and the bilastine spectra was confirmed as previously reported for the development of an alternative synthesis of bilastine [32]. The typical bilastine signals were detected at δ ~7.11 and 7.32, corresponding to H_{11} and H_{13} protons of the benzene rings, which is fused to an imidazole ring, the signals at δ ~2.23, 3.36, and 3.38 which correspond to H_3, H_5, and H_6 of piperidine, respectively, and the signal at δ ~1.40 of the H_2 from the metilpropanoic acid.

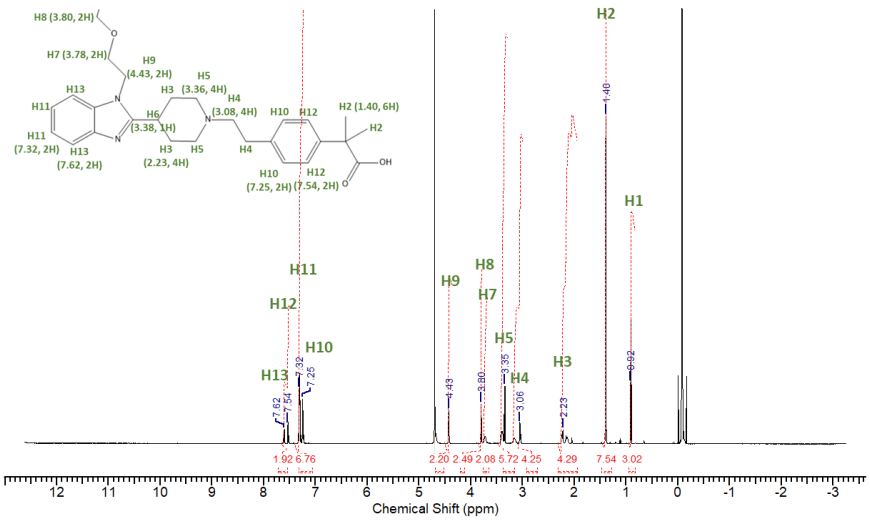

Figure 1. H_1-NMR (400 MHz, D_2O) spectra and integration peaks of purified bilastine and its respective chemical structures. All chemical shifts are expressed as δ in parts per million (ppm).

Previous studies describe three bilastine polymorphs, I, II, and III, where the active substance with pharmacological activity corresponds to polymorph I. FTIR spectra (**Figure 2A**) of the purified bilastine showed strong characteristic intensity bands at 2970, 1509, 1459, 1121, and 742 cm^{-1} in the infrared spectrum [33] as well as medium and strong intensity bands in the functional group region at 2929, 2883, 2857 (N-H, C-H) and 1667 cm^{-1} (C=O) as well as in the fingerprint region at 1481, 1431, 1346, 1326 cm^{-1} (C-N, C-C) typical from polymorph I of bilastine, and not observed in polymorphs II and III (EP1505066).

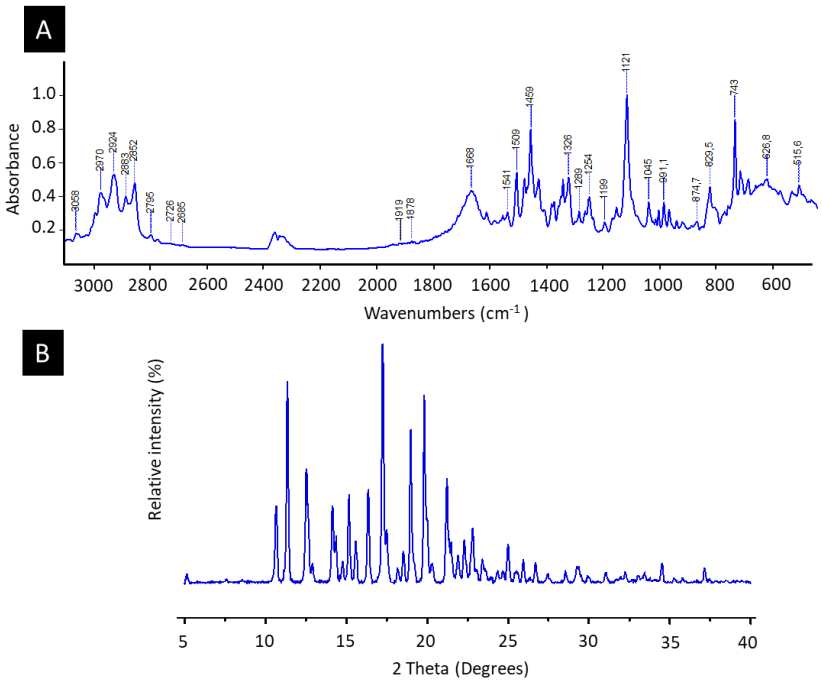

Figure 2. (A) FTIR spectra and (B) XRPD spectra of bilastine.

The XRPD spectra (**Figure 2B**) confirmed the presence of polymorph I as described in WO2014/026657, the stable form and with pharmacological activity, with the characteristic absorption peaks at 2 Theta relative intensity at 10.66 (31.65%), 11.36 (80,86%), 12.57 (34.83%), 14.20 (24.41%, 15.16 (35.23%), 16.36 (38.93%), 17.25 (100%), 17.49 (20.33%), 18.98 (59,76%), 19.81 (56.74%), 19.92 (28,86%), 21.24 (34.52%) and 22.79 (19.29%).

3.2. Preparation and physicochemical characterization of bilastine-loaded NCs

Despite eyedrops representing 90% of the marketed formulations for anterior or intraocular eye pathologies [34], at present, bilastine is only available orally because of its poor water solubility (<0.5 mg/mL in the pH range of 5-8), which hinders the creation of acceptable pharmaceutical methods for administering these compounds in liquid form (EP3170817A1). The development of nanocapsules allows to increase the ocular permeation of lipophilic drugs through the corneal epithelium and improves bioavailability, which is limited by the precorneal clearance, a challenge in the ocular delivery of therapeutics [35]. As bilastine is soluble in organic solvents, nanoemulsions (NEs) containing bilastine were initially formed using the polar solvent acetone as the internal phase to evaluate the drug association and to subsequently develop protamine nanocapsules. The use of liquid lipids such as Miglyol® has been used in topical ophthalmic formulations due to their good ocular tolerance [36]. Further, a partition coefficient of greater than 1 is considered adequate to permeate the corneal epithelium, and Miglyol® showed a partition coefficient of n-octanol/water > 8 (pH 6.2) [20]. In addition, the use of non-ionic surfactants such as polyethylene-glycol (present in PEGst-40) with low toxicity and irritancy, disperse the oil in the aqueous phase and enhance formulations stability, while sodium glycocholate confers penetration enhancing properties to the delivery system [37]**.** As shown in **Table 1**, bilastine NEs showed a hydrodynamic diameter of around 200 nm with a pH of 6.6 ± 0.3 and a greater polydispersity index.

Table 1. Physicochemical characterization, association efficiency (AE), and Drug Load (DL) of non-loaded and 5% bilastine loaded nanoemulsions (NEs) and protamine nanocapsules (NCs). Particle size and polydispersity index were obtained by dynamic light scattering. Data represent mean ± SD, N=3.

Formulation	Size (nm)	PDI	ZP (mV)	AE (%)	DL (%)
Bilastine-loaded NEs	200 ± 52	0.2	-11 ± 6	12 ± 4	0.7
Blank protamine NCs	209 ± 9	0.1	11 ± 9	-	-
Bilastine-loaded protamine NCs	196 ± 10	0.1	-1 ± 1	12 ± 2	0.6

The use of a cationic polymer shell can enhance mucoadhesiveness and interaction of delivery carriers with the ocular surface, improving its corneal penetration [38, 39], so cationic polypeptide protamine was selected due to its wide use in oral, nasal, or transdermic delivery, high biocompatibility and permeation enhancer properties [40]. The developed bilastine-loaded protamine NCs showed a homogeneous mean size in the range of 200 nm and a narrow size distribution (PDI<0.2). The entrapment of the antihistaminic drug bilastine into the oily core did not influence the size of protamine nanocapsules, with encapsulation efficiency values up to 12%, and a neutral surface charge when the drug was included in the oily core of the nanocapsules. The zwitterionic character of bilastine, ionized at physiological pH with a zero net charge, can influence the final surface charge of the NCs, since it is reduced in comparison to the non-loaded NCs. Bilastine-loaded protamine NCs showed an appropriate pH (6.9 ± 0.4) for ocular delivery which is considered acceptable in a range between 6.8-8.2, as high or low pH are not tolerated well by the eye [17, 34]. FESEM and STEM micrographs of bilastine-loaded NCs confirmed their spherical shape (**Figure 3**), and NTA analysis further corroborated DLS and FESEM data, and found similar sizes between 145 and 161 nm, slightly smaller than those measured by DLS, and a homogeneous population with a particle concentration between 1-2 x10^7 particles/mL.

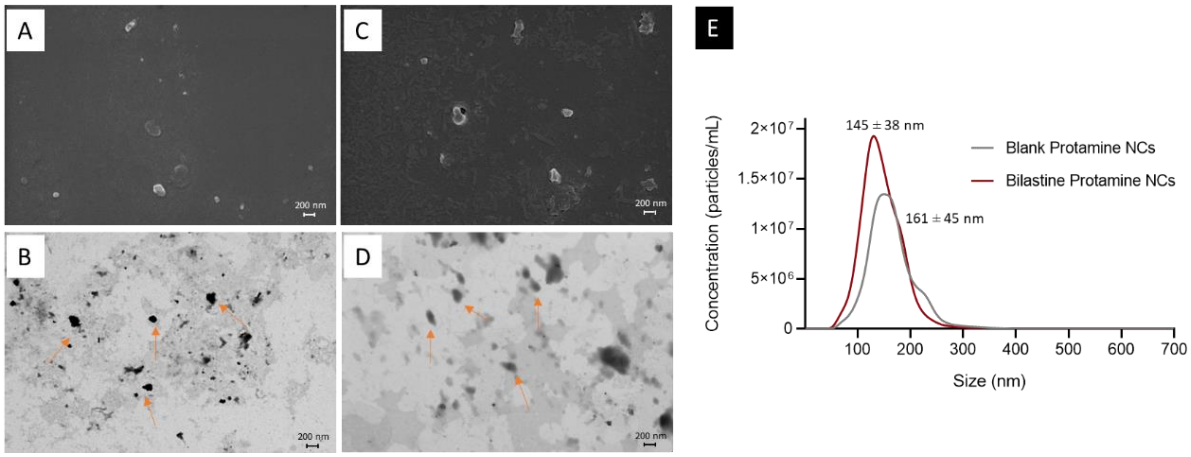

Figure 3. Scanning electron microscopy (A and C) and transmission (B and D) images of blank (A and B) and bilastine loaded protamine nanocapsules (NCs) (C and D). Scale bars are indicated in each image (50 Kx). (E) particle size distribution by nanoparticle tracking analysis of blank and bilastine loaded nanocapsules. Orange arrows point out the protamine NCs.

3.3. Stability studies

The robustness of the freshly prepared bilastine-loaded protamine NCs was confirmed after stability evaluation, which was maintained for at least 30 days at 4ºC in dispersion with a minor increase in size and polydispersity index, of great interest in the development of eye drop formulations (**Figure 4A**). Additionally, the stability of the NCs after lyophilization was evaluated using trehalose as the preferable cryoprotectant due to its less hygroscopicity, low

chemical reactivity, and capacity to interact with nanoparticles and form hydrogen bonds [41]. Reconstituted protamine nanocapsules showed good stability in the presence of trehalose 5% [42] as they maintained their nanometric size when the ratio trehalose: nanocarrier 4:1 and 5:1 was used (**Figure 4B**). The particle size and degree of dispersion gradually decreased as the amount of trehalose increased, stabilizing from the 4:1 ratio onwards. The ocular administration of drugs strict conditions of sterility, pH, and isotonicity, as well as, in most cases, the addition of preservatives to maintain their properties. This latter has been associated, with the appearance of hypersensitivity and other undesired side effects [8, 34]. Therefore, the conservation and storage of NCs in lyophilized form, in addition to simplifying logistics, would avoid the use of preservatives, allowing for extemporaneous reconstitution of the product as a sterile suspension for topical instillation to the eye.

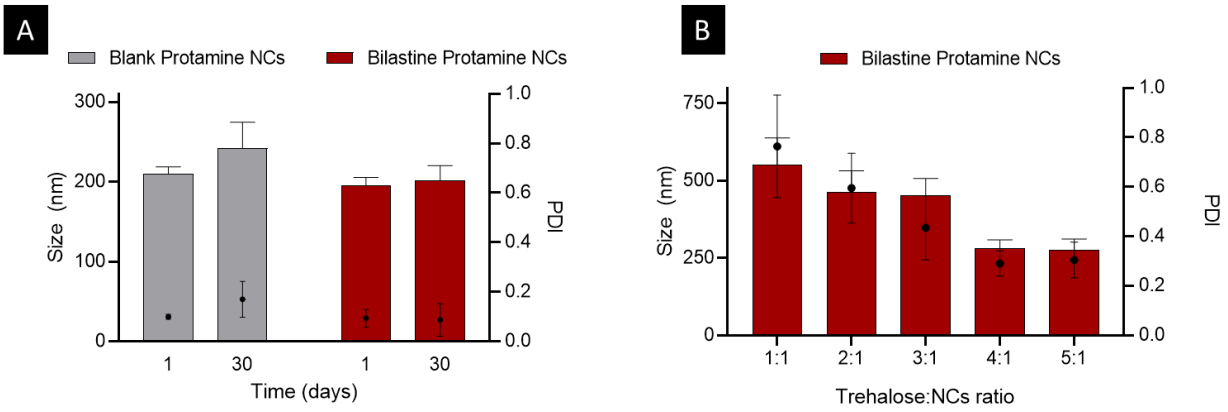

Figure 4. (A) Stability of blank and bilastine loaded protamine nanocapsules (NCs) one month under storage at 4ºC in suspension by dynamic light scattering and (B) stability of reconstituted 5% bilastine loaded protamine NCs after different trehalose ratio addition. Size=Bars, PDI=Dots. Data represent mean ± SD, N=3 independent measurements.

We also evaluated the stability of bilastine nanocapsules upon contact with simulated lachrymal fluid by monitoring blank and bilastine-loaded protamine NCs size and PDI for 24 h (**Figure 5**). The size remained constant upon contact with lachrymal fluid for up to 8 h, both for freshly prepared and freeze-dried and reconstituted formulations. While the size and polydispersity of blank protamine nanocapsules remained stable, the size of the freeze-dried reconstituted bilastine-loaded nanocapsules increased gradually over time, however, nanometric size was maintained in all cases for time periods far exceeding tear film turnover and expected residence times. Overall, the remarkable stability observed both under different storage conditions and in biorelevant media, as well as the satisfactory yields achieved (56 ± 8 %) confirm the suitability of the developed nanocarriers for ocular applications.

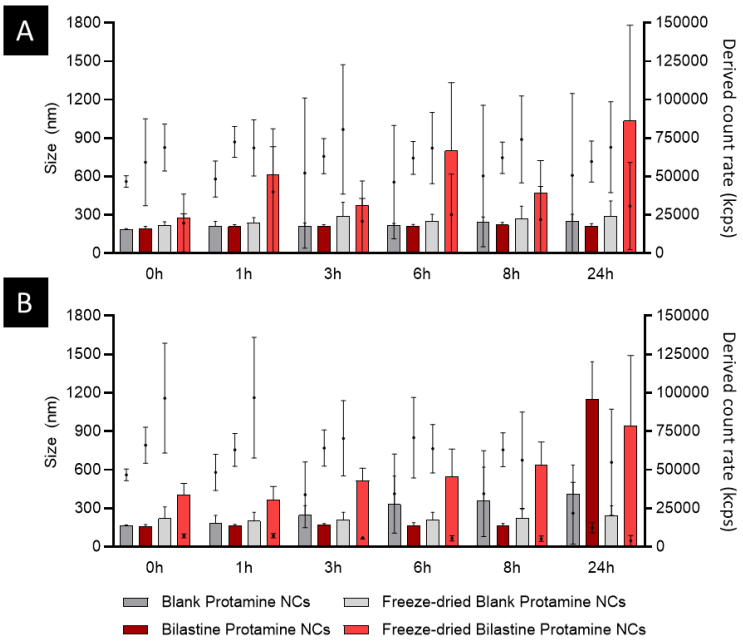

Figure 5. Stability of blank and bilastine loaded protamine NCs in suspension, freshly prepared and after lyophilization in (A) water and (B) simulated lacrimal fluid. Bars represent size (nm), and dots represent derived count rate (kcps). Data represent mean ± SD, N=3 independent measurements.

3.4. Purification of *H. annuus* pollen microcapsules

Pollen microcapsules were obtained from *H. annuus* (sunflower), from the Asteraceae family, with a diameter of approximately 35 µm and an echinate and tricolporate structure. Initially, pollen was processed to obtain completely purified pollen microcapsules with a nanoporous surface and an empty inner cavity [16], with the preservation of the structural integrity of the sporopollenin wall. Pollen allergies vary depending on the species and its dispersion capacity, and studies on *Corylus avellana* and *Betula pendula* pollen have shown to damage tear film components and attack ocular surface cells [43], while *Ambrosia artemisiifolia* has shown allergic potential causing rhinoconjunctivitis [8]. Even though allergies are not common for Asteraceae family [44] and in the case of sunflower pollen, there is no substantial biochemical evidence on their allergenic potential [45]. The developed protocol pollen has been chemically purified to remove allergenics compounds as proteins, the native biomolecules that cause allergies [46], creating clean and intact hollow microcapsules. After the performed purification protocol, the protein content of the *H. annuus* pollen was determined by elemental analysis and decreased from ~33 wt% to 4.4 wt%, which successfully confirmed their removal and non-allergenicity [16], ensuring its safe use for drug delivery applications.

3.5. Loading of bilastine protamine nanocapsules in hollow pollen microcapsules

The vacuum-assisted loading method [47, 48] and a 1:1 (w/w) ratio of drug-to-pollen loading [49, 50] have previously demonstrated higher encapsulation efficiency compared to other strategies for encapsulating substances in hollow pollen microcapsules. **Table 2** shows a high encapsulation efficiency of bilastine protamine NCs into hollow pollen microcapsules (71%), and similarly high loading capacity (74%). BSA encapsulation into *H. annuus* encapsulating by using a vacuum-based loading process also reported similar encapsulation efficiency (65.7% ±

1.8%), which was attributed to the external force provided by vacuum, in addition to the passive uptake during the natural pollen rehydration process [51].

Table 2. Encapsulation efficiency (EE%), loading capacity (LC%), and loading content of *H. annuus* hollow pollen microcapsules with 5% bilastine nanocapsules (NCs) by vacuum at mass ratio 1:1. Data represent mean ± SD, N=3 independent measurements.

Formulation	Encapsulation Efficiency (%)	Loading Capacity (%)	Loading Content (w/w)	Yield (%)
5% Bilastine NCs-loaded pollen platform	71.8 ± 11	74.1 ± 11.9	0.72 ± 0.11	48.6 ± 3

Scanning electron analysis (**Figure 6**) of the pollen microcapsules after their loading with bilastine protamine NCs confirmed the presence of the nanocarriers on the external surface of the pollen vehicle. Bilastine-loaded nanocapsules showed a rough monolayer arranged on the sporopollenin surface, which partially covered the nanopores of the pollen wall, and completely visible in the hollow pollen after its purification process. However, the loaded pollen microcapsules still exhibited well-defined spikes with uniform size, thus preserving the initial structural and morphological features of the pollen grain [52], responsible for their adhesion to mucosal surfaces. . The use of phosphoric acid in the production of sporopollenin microcapsules from natural pollen grains introduced ionizable groups such as carboxylic acid and carboxylate salt onto their surface, leading to a negative surface charge [53]. Sporopollenin interfacial properties could promote the interaction with the developed nanocapsules via electrostatic interaction, and their surface adsorption due to the positive character of the arginine-rich polymeric shell of the protamine nanocapsules.

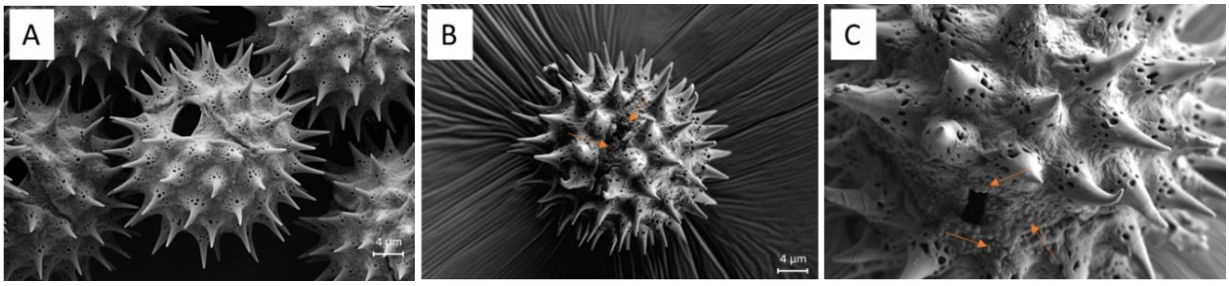

Figure 6. Scanning electron microscopy images of (A) hollow *Helianthus annuus* sporopollenin microcapsules and (B and C) *H. annuus* sporopollenin microcapsules loaded with bilastine protamine NCs. The orange arrows point to the NCs on the zoom-in image (C).

The successful association of the bilastine-loaded nanocapsules to *H. annuus* sporopollenin microcapsules was further confirmed by confocal microscopy (**Figure 7**). The vacuum reduced the pressure in the pollen cavity, causing the NCs suspension to be drawn inside the pollen vehicle. Fluorescent DiD-labeled NCs were observed inside the sporopollenin (Figure 7C and D) microcapsules, in contrast with the absence of red fluorescence in empty pollen microcapsules (Figure 7A and B).

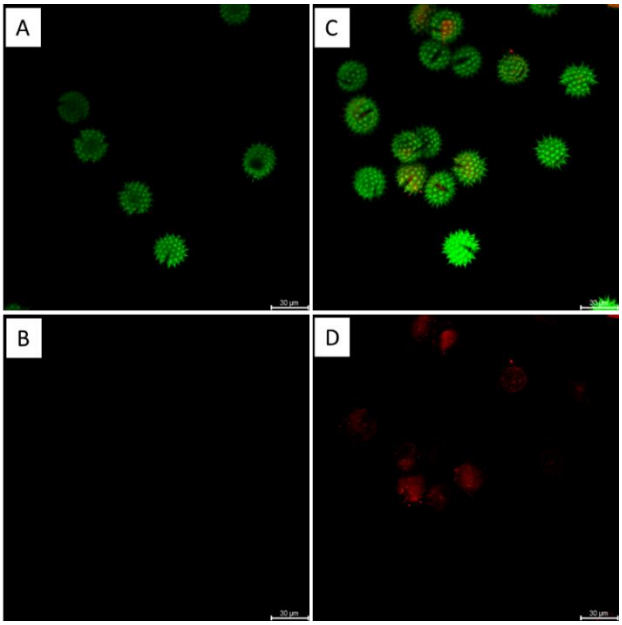

Figure 7. Non-loaded sporopollenin microcapsules (A and B) and DiD-labeled bilastine loaded protamine (NCs) encapsulation into hollow *H. annuus* pollen microcapsules (C and D) by Confocal Laser Scanning Microscopy compared. DiD dye (red channel, B and D) Excitation λ_{max}=640 nm, Emission λ_{max}= 675 nm; Pollen (green channel, A and C) Excitation λ_{max}= 405, 492, 561 nm, Emission λ_{max}= 414-479, 505-554 and 571-635 nm. The scale bar represents 30 µm.

3.6. *In vitro* release studies

To assess the suitability of pollen microcapsules for bilastine delivery, we conducted *in vitro* release studies in simulated lacrimal fluid, comparing the behavior of bilastine-loaded NCs and bilastine NCs-loaded pollen microcapsules over a 24 h period. As shown in **Figure 8**, the developed protamine nanocapsules exhibited a biphasic pattern, with a fast initial release of the drug, with values around 80% after 6 h followed by a sustained release and reaching a total bilastine release after 24 h, as also reported for insulin from protamine NCs in simulated intestinal fluid at pH 6.5 [37]. However, in the bilastine NCs loaded pollen microcapsules, during the first 6 h the drug was initially released at a faster rate and gradually slowed down over 24 h, with a cumulative percentage of free drug of 64 ± 2 % during the evaluated period. The drug release from the NCs encapsulated in the pollen microcapsules was slower compared with the non-encapsulated NCs due to their accumulation and retention inside the pollen microcapsules and slower diffusion from the nano-channels of the pollen wall to the lacrimal fluid. This could be related to the selected vacuum-assisted loading method, which resulted in the internal encapsulation of the NCs as well as their external association with the surface of the pollen platforms, as previously described in section 3.5. Bilastine- loaded protamine NCs adsorbed on the surface of *H. annuus* pollen microcapsules were rapidly released into the simulated lacrimal medium, while drug-loaded protamine NCs trapped inside the pollen platforms exhibited more controlled release behavior. Although there are no studies analyzing drug or nanocarrier release pattern from pollen platforms in simulated lacrimal fluid, studies have reported greater release profiles at neutral pHs, such as simulated intestinal fluid, compared to acidic pHs like simulated gastric fluid, where the release was found to be more delayed [54, 55]. The obtained cumulative bilastine release was slightly higher than that reported for other drugs as paracetamol from *Platanus orientalis* pollen microcapsules, of 56% within 24 h when the release was performed in the same pH conditions (PBS pH= 7.4) [56].

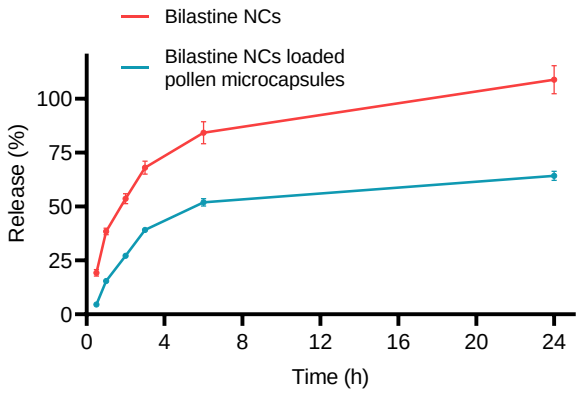

Figure 8. *In vitro* bilastine release in simulated lacrimal fluid from the developed protamine NCs and NCs loaded into hollow *H. annuus* hollow sporopollenin microcapsules.

Different kinetic models were used to evaluate the drug release pattern of NCs-load pollen platforms in this study. DDSolver software was used to analyze the data and determine the coefficient of determination (R^2), adjusted R^2, and Akaike Information Criterion (ACI) for each model. The best-fitted model was selected based on these parameters. Based on the results presented in Table 2, the Korsmeyer-Peppas model was found to be the best-fitted model for bilastine release from NCs, which explains drug diffusion from a polymeric matrix. On the other hand, it can be concluded that the accumulative release of bilastine from the NCs, loaded pollen microcapsules, followed Fickian diffusion (n< 0.5) after the initial burst phase and the Higuchi model was found to be the best approximation for the release data, also reported for paracetamol release in the same pH conditions [56].

Table 2. Kinetics of bilastine-loaded NCs and bilastine NCs loaded into *H. annuus* sporopollenin microcapsules.

	Parameters	Zero-order	1st order	Higuchi	Korsmeyer-Peppas
Bilastine-loaded protamine NCs	R^2	0.7419	0.9437	0.6693	**0.9692**
	adj R^2	0.7419	0.9437	0.6693	0.9539
	AIC	56.6137	35.9690	46.6215	18.0425
	K	5.5532	0.3360	26.9962	33.4354 n= 0.6866
Bilastine NCs loaded sporopollenin microcapsules	R^2	0.0643	0.5187	**0.7822**	0.7401
	adj R^2	0.0643	0.5187	0.7822	0.6751
	AIC	49.3693	44.5969	39.8485	19.6174
	K	3.2638	0.0753	15.5335	12.7506 n= 0.3221

3.7. *In vitro* cytotoxicity evaluation

The interaction between protamine NCs, pollen microcapsules, and the biological environment was analyzed *in vitro* by the MTT assay to ensure both efficacy and safety of the developed formulations. THP-1 leukemic promonocytic cell line is used as a model for human monocytes, which transform into cytokine-producing inflammatory cells in response to pathogens or inflammation [57]. We evaluated the biocompatibility of the protamine nanocapsules and pollen platforms with THP-1 cells by analyzing their recognition and activation. As shown in **Figure 9**, THP-1 cellular viability remained high for 0.1 mg/mL for both blank NCs (79 ± 8%) and bilastine-loaded NCs (88 ± 8%). Conversely, the administration of bilastine NCs-loaded pollen microcapsules showed lower cell viability values, regardless of the NCs concentration,

as similar values were obtained by increasing the NCs concentration up to 0.5 mg/mL. The EC_{50} value was determined to be 229 µg/mL for hollow pollen microcapsules and 856 µg/mL for bilastine NCs loaded pollen microcapsules after 24 h of treatment.

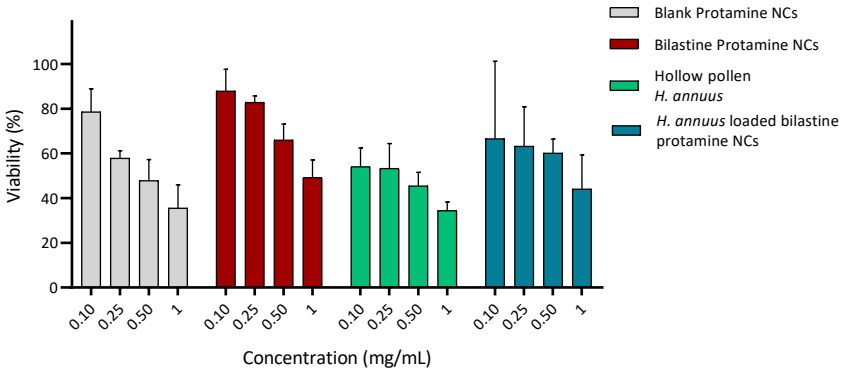

Figure 9. *In vitro* evaluation of the effect of the developed blank, bilastine-loaded protamine nanocapsules (NCs) and pollen-loaded prototypes on the viability of THP-1 cells. Data represent mean ± SD, N=3 independent measurements.

On the one hand, bilastine encapsulation into protamine NCs does not affect its toxicity, as no changes were observed in the viability of the monocytes. On the other hand, due to their dimensions, pollen microcapsules are rapidly deposited over the cell monolayer in these static *in vitro* conditions. This direct contact could cause greater cellular stress than NCs, that remained suspended in the medium for a long period of time (see Section 3.3).
Similar cell viability values (60-80%) were reported for other pollen-based microcapsules as in the case of *B. pendula* (with microechinate, regulate surface) pollen microcapsules at 0.1 mg/mL, [58], while cell viability values over 90% were reported for *L .clavatum* (reticular microstructure and ornamentation) [59] and *P. dactylifera* [60] (with a "psilate"/smooth surface) pollen microcapsules. This indicates that pollen morphology and surface ornamentation could influence pollen-cell interaction and thus, the final cellular viability.
Finally, it is important to mention that the apparently increased viability observed in the loaded pollen microcapsules compared with the hollow microcapsules could be attributed to the different density between both platforms. Although the concentration of established pollen was the same in both cases, the loaded platforms showed a higher density as the inner core was partially filled with bilastine protamine NCs, resulting in a decrease in the final number of the administered pollen vehicles (2 x 10^5 grains/mg) compared with hollow vehicles (2.45 x 10^5 grains/mg) and ultimately impacting cell viability.

Taken together these findings, we established a NCs concentration of 0.1 mg/mL as well-tolerated for the subsequent evaluation of NCs internalization and immune cell activation.

3.8. Nanocapsules uptake by immune cells

We evaluated the recognition of bilastine NCs and bilastine NCs loaded pollen platforms by antigen-presenting cells using fluorescent DiD-loaded protamine NCs. The results indicated that the size of these fluorescent particles was consistent with previous reports. DiD-labeled bilastine NCs presented a nanometric size (162 ± 3 nm), low disperstiy (PDI <0.1), and positive surface charge of 6 ± 3 mV. The DiD-labeled bilastine NCs were subjected to a qualitative evaluation by CLSM upon incubation with THP-1 cells for 24h. **Figure 9** confirmed the NC's internalization (Figures 9C and D) compared with untreated cells (control). This internalization

could be explained due to the mucoadhesive character of arginine-rich biomaterials as protamine (<70% of arginine in its structure) presenting a great potential to interact with cells and biological membranes [61] producing in this case, efficient NCs uptake by THP-1 cells.

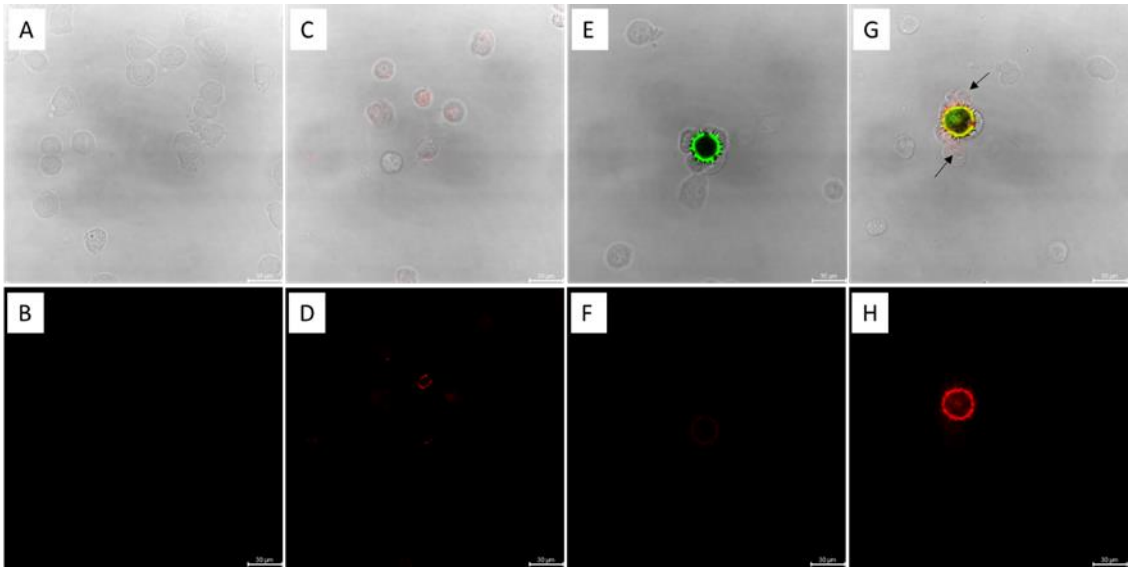

Figure 10. Cellular internalization of DiD-labeled bilastine nanocapsules (NCs) In THP-1 cells. Merged bright-field (upper row) and fluorescent confocal images (bottom row) acquired for A and B: THP-1 cells, C and D: nanocapsules, E and F: hollow pollen microcapsules, G and H: DiD bilastine NCs loaded into hollow pollen microcapsules. DiD dye (red channel) Excitation λ_{max}=640 nm, Emission λ_{max}= 675 nm; Pollen (green channel) Excitation λ_{max}= 405, 492, 561 nm, Emission λ_{max}= 414-479, 505-554 and 571-635 nm. The scale bar represents 30 µm.

On the other hand, as shown in Figure 9E-H, both hollow and bilastine NCs-loaded pollen microcapsules exhibited adhesion to THP-1 cells, resulting in the efficient internalization of bilastine NCs into the cells and their distribution within the cytoplasm. Previous studies have demonstrated that physical characteristics of particulate structures such as native ragweed pollen (*Ambrosia artemisifoliia*), with a size of around 17 micrometers and surface architecture similar to that of *H. annuus* pollen, play a crucial role in their phagocytosis by mouse macrophages and dendritic cells without triggering an allergic response (IgE secretion) [62].

Flow cytometry (**Figure 11**) was used to quantify the percentage of DiD-labeled bilastine-loaded NCs uptake. Control histograms of untreated cells were compared with those of THP-1 cells treated with free or bilastine NCs-loaded pollen vehicles after 24 h. The results indicated that NCs internalization occurred in over 96% of the cells for bilastine-loaded protamine NCs, while in the case of bilastine NCs loaded pollen platforms, the percentage of NCs internalized cells was 6.6%. However, after evaluating the Mean Fluorescence Intensity (MFI), the internalization of bilastine-loaded protamine NCs was found to be 4.8±0.2 times higher than the control, while bilastine NCs previously loaded pollen microcapsules showed an MFI 3.6±0.5 times higher than untreated cells.

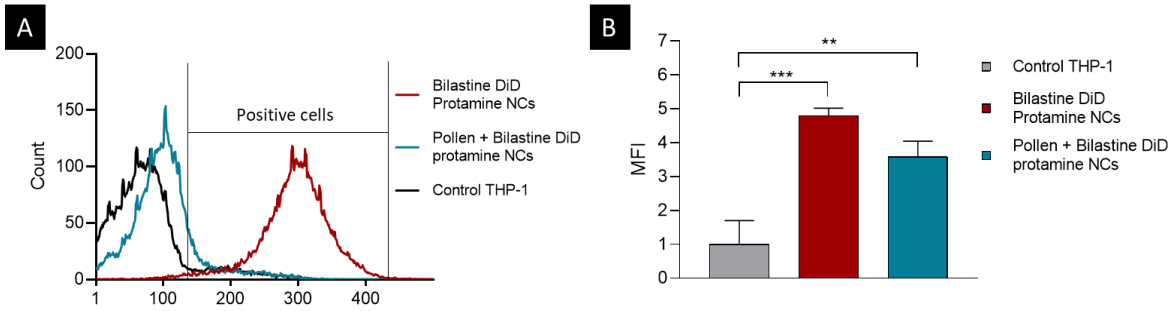

Figure 11. (A) Flow cytometry histograms and (B) Mean Fluorescent Intensity (MFI) of THP-1 cells after incubation with bilastine-loaded protamine nanocapsules (NCs) and bilastine NCs loaded into hollow sporopollenin microcapsules. MFI=1 was established for the control (non-treated cells). Data represent mean ± SD, N=3 independent measurements.

Therefore, the bilastine NCs internalize uniformly in all cells, however, in the case of bilastine NCs loaded pollen, this internalization is localized to those cells in direct contact with the pollen, which could be of interest for targeted and sustained delivery.

3.9. Immune cell activation

Immune cells derived from the bone marrow of the central cornea (avascular and without lymphatics), can phenotypically mature into cells expressing costimulatory molecules during an inflammation process, leading to the recruitment of innate immune cells in the peripheral cornea and conjunctiva [63]. As uptake by these cells was previously observed for the formulations, we also evaluated their recognition by THP-1 monocytes in order to elucidate the generation of a possible immune response *in vivo*. The H_4 monocyte receptor plays a key role in mediating histamine's effects, both inflammatory and pruritic responses. It has been linked to the chemotaxis of mast cells, eosinophils, and DCs, as well as the production of cytokines from T cells and dendritic cells (DCs) [9][64]. Changes in the expression of co-stimulatory molecules CD80 and CD83 were evaluated after THP-1 monocytes incubation with polarizing stimulus as blank and bilastine-loaded NCs and hollow pollen microcapsules and bilastine NCs loaded into pollen microcapsules. In a basal condition, THP-1 monocytes do not show CD80 surface expression [65], while the CD83 expression is a lineage-specific marker during monocyte differentiation into mature DCs [66], upregulated by stimulation factors like LPS, playing a role in the development of CD4+ T cells [67].

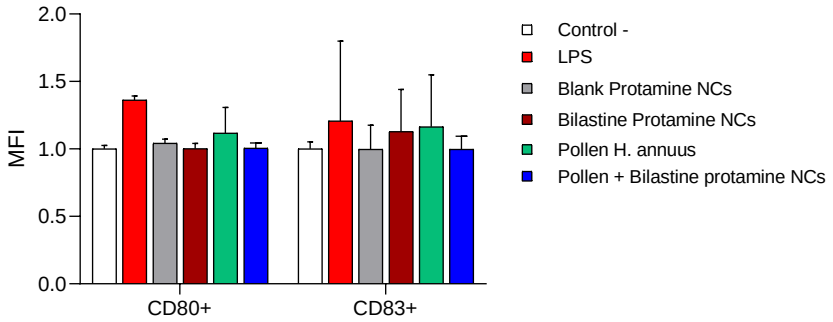

Figure 12. Mean Fluorescent Intensity of THP-1 maturation markers CD80 and CD83 after incubation with the different blank and bilastine-loaded nanocapsules (NCs) and H. annuus sporopollenin microcapsule prototypes. MFI=1 was established for the control (non-treated cells). Data represent mean ± SD, N=3 independent measurements.

As shown in **Figure 12**, the expression levels of CD83, characteristic of activated DCs, confirmed that the developed platforms did not induce the differentiation of monocytes into DCs. THP-1 cells have been shown to acquire DCs properties upon stimulation, and LPS induced the expression of CD83 on the cell surface, resulting in their differentiation into DCs after 24 h of contact (**Supplementary Figure 1**). Studies have shown that microcapsules from ragweed pollen or pollen-mimetic metal-organic framework (MOFs) based on Spanish-needle (*Bidens pilosa*) displayed markedly higher levels of CD80 surface markers compared to untreated cells. They are suggested to have an increased ability to interact with resident immune cells, leading to an upregulation of activation and CD80 maturation molecules that lead to increased attachment and internalization. However, this activation, as observed in THP-1 cells, is apparently lower [68, 69] and would enable the use of the developed delivery strategy for the ocular administration of antiallergic substances.

3.10. *In vitro* 3D Corneal permeability

In the design of ocular delivery carriers, the combination of the biomaterials influence the interaction and internalization with the ocular surface [70]. The use of cationic polymers have shown promising properties, due to their enhanced interaction with negatively charged mucus and/or their penetration capacity into the corneal tissue [71]. We evaluated the nanocapsules internalization by using an *in vitro* 3D corneal tissue model (**Figure 13**), resembling the morphologic features of the human corneal epithelium [72, 73].

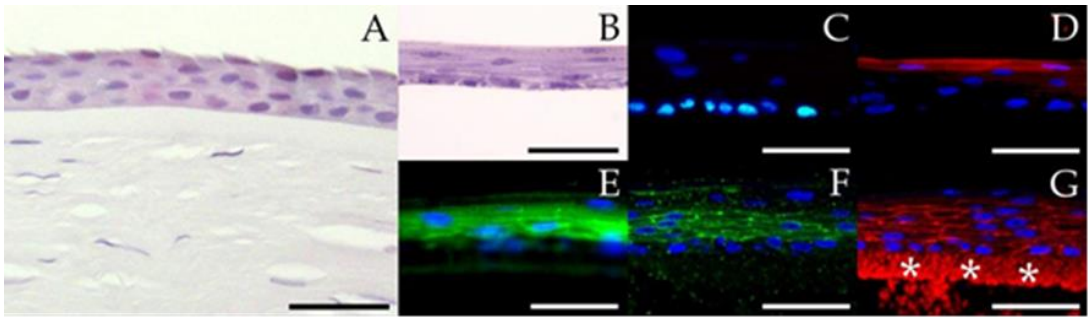

Figure 13. Histological analysis. (A): Human cornea; (B): QobuR; (C): p63 (green); (D): Cytokeratin 3 (red); (E): Zonula occludens-1 (green); (F): Connexin-43 (green); (G): β-catenin (red). Scale bar 50 µm. Nuclei stained in blue (DAPI). (*): Unspecific background stain of the polyester Transwell membrane (adapted with permission from [28]).

QobuR human corneal epithelial models, developed from primary cultures of human limbal epithelial cells, express β-catenin adherent junction protein, which regulates actin organization, providing strong mechanical binding. The evaluation of the immunofluorescence for β-catenin to assess barrier damage caused by cell junctions and the morphology of the cell membrane (**Figure 14**) was performed, and the intense expression of β-catenin confirmed the integrity of the epithelial barrier as well as the distribution of the DiD-labeled NCs through the Qobur external layer (**Supplementary Figure 2**). These results confirmed the reversible permeabilization capability of both formulations through 3D corneal models. The mechanism of this interaction is probably mediated by endocytosis, increasing the corneal penetration of nanocarriers without inducing permanent cell damage [74]. These results are also consistent with previous *in vivo* studies, where topical instillation of polypeptide and polyaminoacid NC-based formulations preserved the epithelial ocular barrier integrity without producing irritation or abnormal secretions in healthy mice [15].

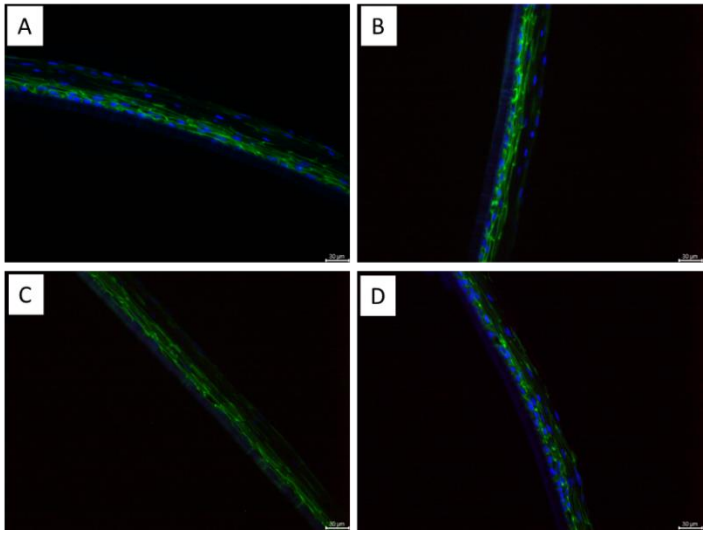

Figure 14. Microscopy images of Immunofluorescent staining of the 3D cornea: ß catenin (green) proteins after incubation with (A) hollow pollen microcapsules, (B) protamine NCs, (C) protamine NCs loaded pollen microcapsules exposure compared with (D) control. Nucleus are stained with DAPI (blue). Scale bars represent 30 µm.

3.11. *In vivo* ocular distribution and histological analysis

We evaluated the ocular distribution of the free and pollen-associated protamine NCs and the secretion of proinflammatory cytokines after *in vivo* topical administration in rat eyes. As shown in **Figure 15**, after 30 minutes of instillation, NCs-loaded pollen microcapsules could be detected in the cornea, resisting the rapid renewal rate of the tear fluid and the blinking reflex, which normally limits ocular drug residence to a maximum of 5-6 min [70]. This could be due to the surface morphology and size of the sporopollenin-based platforms, larger than the tear film thickness (<12 µm) [19], which leads to a decrease in precorneal loss and results in an increase of the contact time between the nanocapsules and the corneal tissue.

Regarding the cytokine and protein expression, protamine NCs nor pollen loaded with protamine NCs (Figures 15A and C) showed expression of TNFα, a cytokine secreted by conjunctival mast cells and detected in the tear fluid and conjunctival epithelium of patients with allergic disorders [75, 76]. No calcium/calmodulin Kinase II (CamKII) expression was observed either. CamKII is protein produced by macrophages during the inflammation process, which is altered in allergic conjunctivitis and stimulate mucin secretion in goblet cells [77]. Furthermore, (Figures 15B and D), expression of S100A proteins on corneal epithelium was also not detectable, which would be early markers of pathological inflammatory and immunoregulatory processes of the ocular surface [78, 79]. These proteins play a role in DCs differentiation and maturation status [80] and effector CD4+ T helper cells on corneal DCs or LCs, responsible of cytokines secretion and destruction of pathogens and inflammatory cells activation [81].

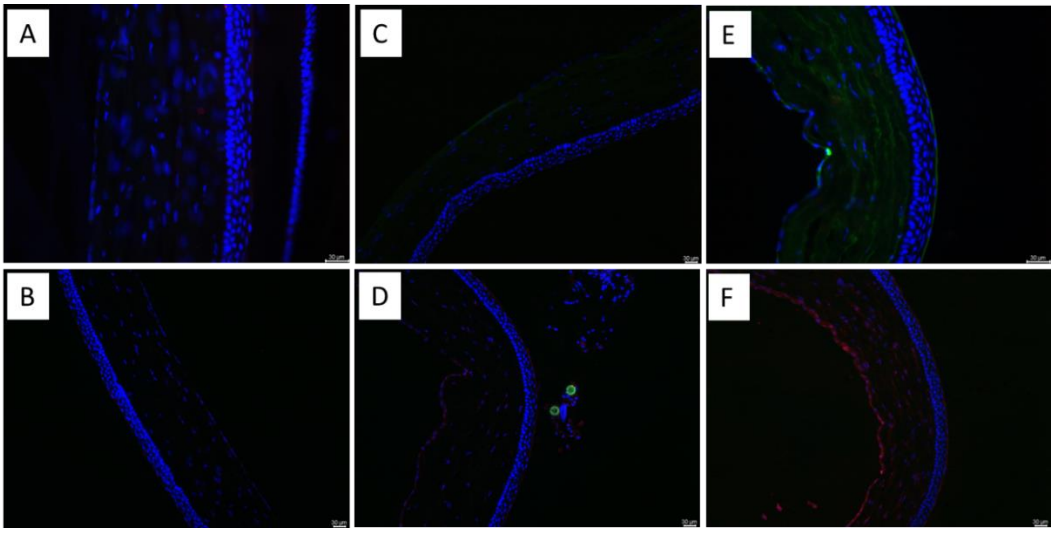

Figure 15. Immunofluorescent staining of TNF α (green) and CamKII (red) proteins (A, C, E), CD4 lymphocytes (green), and S100 (red) (B, D, F) proteins in rat corneal epithelia after topical protamine NCs (A, B) and NCs-loaded *H. annuus* pollen microcapsules (C, D) administration compared with control (E, F). The nucleus was counter-stained blue with DAPI.

Although these studies were conducted on drug-free formulations, their tolerability and compatibility, as well as the increased residence time, support their suitability as drug delivery system, considering their preferential distribution accross the conjunctiva and cornea [82]. Bilastine NCT03231969 phase II and NCT04810390, NCT03479307 phase III studies also assessed the safety and tolerability of this drug after topical ophthalmic solution for the treatment of allergic conjunctivitis. Therefore, for the ongoing experiments evaluating drug-loaded pollen platforms we envisage results similar to those observed herein for blank NCs and pollen microcapsules.

4. CONCLUSIONS

In this work, we report for the first time the encapsulation of bilastine in polymeric nanocapsules, as well as the use of pollen-based microcapsule platforms for the ocular delivery of drugs. The developed nanocarriers proved efficient delivery of lipophilic bilastine and enhanced retention and penetration through the corneal epithelium and internalization into immune cells, with remarkable stability in simulated biological fluids. The successful loading of the drug containing nanocarriers into hollow *H. annuus* sporopollenin platforms was confirmed and the developed delivery system showed no signs of immune activation *in vitro* nor *in vivo* after ocular topical instillation. Enhanced residence time was also observed after the administration of the sporopollenin-based platforms with the preservation of integrity of the corneal epithelial barrier. This bifunctional strategy combines the increase of drug penetration by the nanocarriers and the decrease of the precorneal drug loss by the sporopollenin platforms and constitutes a promising strategy for the treatment of ocular allergies.

Ethics

Sprague-Dawley rats were housed in ventilated polypropylene cages and received a standard laboratory diet of food and water *ad libitum*. Animals were handled and housed following the standards of best animal care practices, according to the ARVO Statement for the Use of Animals in Ophthalmic and Vision Research, as well as guidelines of the EU (2003/65/EC) and the Spanish Government (RD 53/2013) and the Ethics Committee of the University of Oviedo.

SUPPLEMENTARY MATERIAL

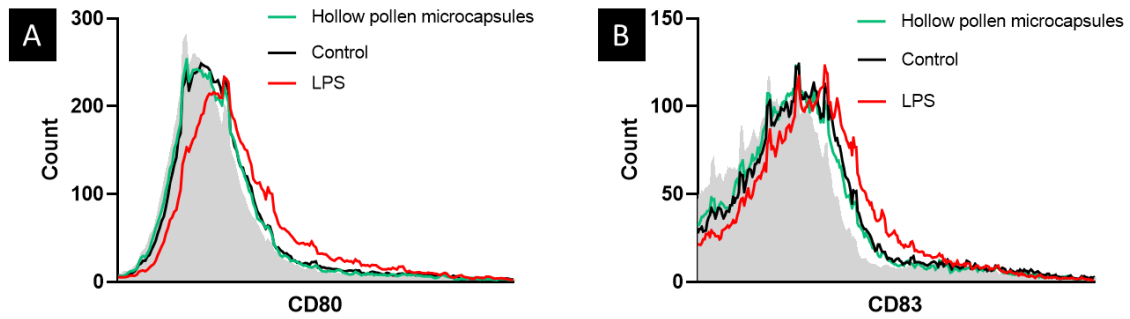

Supplementary Figure 1. Cell surface expression of activation and maturation markers CD80 (A) and CD83 (B) after treatment with 100 µg/mL of hollow pollen microcapsules in THP-1 cells. The filled histogram represents unstained cells.

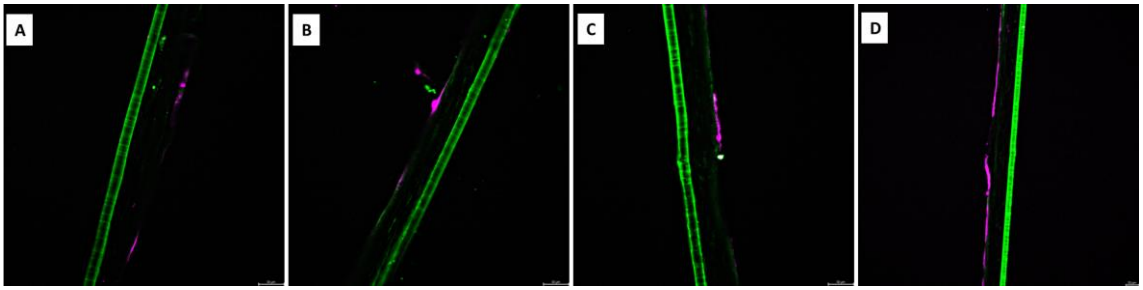

Supplementary Figure 2. Fluorescent microscopy images of the 3D cornea after administration of DiD-labeled protamine NCs (A and B) and DiD-labeled protamine NCs loaded *H. annuus* pollen microcapsules (C and D). Scale bars represent 30 µm.

REFERENCES

[1] Bielory, L. Ocular Allergy. *Mt. Sinai J. Med. A J. Transl. Pers. Med.*, **2011**, *78* (5), 740–758. https://doi.org/10.1002/msj.20291.

[2] Bartra, J.; Mullol, J.; Montoro, J.; Jáuregui, I.; del Cuvillos, A.; Dávila, I.; Ferrer, M.; Sastre, J.; Valero, A. Effect of Bilastine upon the Ocular Symptoms of Allergic Rhinoconjunctivitis. *J. Investig. Allergol. Clin. Immunol.*, **2011**, *21 Suppl 3*, 24–33.

[3] Church, M. K.; Tiongco-Recto, M.; Ridolo, E.; Novák, Z. Bilastine: A Lifetime Companion for the Treatment of Allergies. *Curr. Med. Res. Opin.*, **2020**, *36* (3), 445–454. https://doi.org/10.1080/03007995.2019.1681134.

[4] Galletti, J. G.; Guzmán, M.; Giordano, M. N. Mucosal Immune Tolerance at the Ocular Surface in Health and Disease. *Immunology*, **2017**, *150* (4), 397–407. https://doi.org/10.1111/imm.12716.

[5] Streilein, J. W. Ocular Immune Privilege: The Eye Takes a Dim but Practical View of Immunity and Inflammation. *J. Leukoc. Biol.*, **2003**, *74* (2), 179–185. https://doi.org/10.1189/jlb.1102574.

[6] Ohbayashi, M.; Manzouri, B.; Flynn, T.; Toda, M.; Ikeda, Y.; Nakamura, T.; Ono, S. J. Dynamic Changes in Conjunctival Dendritic Cell Numbers, Anatomical Position and Phenotype during Experimental Allergic Conjunctivitis. *Exp. Mol. Pathol.*, **2007**, *83* (2), 216–223. https://doi.org/10.1016/j.yexmp.2007.04.007.

[7] Averbeck, M.; Gebhardt, C.; Emmrich, F.; Treudler, R.; Simon, J. C. Immunologic Principles of Allergic Disease. *JDDG - J. Ger. Soc. Dermatology*, **2007**, *5* (11), 1015–1027. https://doi.org/10.1111/j.1610-0387.2007.06538.x.

[8] Bielory, L. Allergic Diseases of the Eye. *Med. Clin. North Am.*, **2006**, *90* (1), 129–148. https://doi.org/10.1016/j.mcna.2005.08.013.

[9] Thurmond, R. L.; Gelfand, E. W.; Dunford, P. J. The Role of Histamine H1 and H4 Receptors in Allergic Inflammation: The Search for New Antihistamines. *Nat. Rev. Drug Discov.*, **2008**, *7* (1), 41–53. https://doi.org/10.1038/nrd2465.

[10] Wang, X. Y.; Lim-Jurado, M.; Prepageran, N.; Tantilipikorn, P.; Wang, D. Y. Treatment of Allergic Rhinitis and Urticaria: A Review of the Newest Antihistamine Drug Bilastine. *Ther. Clin. Risk Manag.*, **2016**, *12*, 585–597. https://doi.org/10.2147/TCRM.S105189.

[11] Sádaba, B.; Gómez-Guiu, A.; Azanza, J. R.; Ortega, I.; Valiente, R. Oral Availability of Bilastine. *Clin. Drug Investig.*, **2013**, *33* (5), 375–381. https://doi.org/10.1007/s40261-013-0076-y.

[12] Torrens, I.; Ganza, Á.; Hernández, G.; Gonzalo, A.; Zazpe, A. Ocular Biodistribution of Once-Daily 0.6% Bilastine Eye Drops Reveals Highest Levels in Conjunctiva Up to 24 h Postadministration. *J. Ocul. Pharmacol. Ther.*, **2022**, *38* (9), 617–625. https://doi.org/10.1089/jop.2022.0024.

[13] Morrison, P. W. J.; Khutoryanskiy, V. V. Advances in Ophthalmic Drug Delivery. *Ther. Deliv.*, **2014**, *5* (12), 1297–1315. https://doi.org/10.4155/tde.14.75.

[14] Gupta, H.; Aqil, M.; Khar, R. K.; Ali, A.; Bhatnagar, A.; Mittal, G. Biodegradable Levofloxacin Nanoparticles for Sustained Ocular Drug Delivery. *J. Drug Target.*, **2011**, *19* (6), 409–417. https://doi.org/10.3109/1061186X.2010.504268.

[15] Reimondez-Troitiño, S.; Alcalde, I.; Csaba, N.; Íñigo-Portugués, A.; de la Fuente, M.; Bech, F.; Riestra, A. C.; Merayo-Lloves, J.; Alonso, M. J. Polymeric Nanocapsules: A Potential New Therapy for Corneal Wound Healing. *Drug Deliv. Transl. Res.*, **2016**, *6* (6), 708–721. https://doi.org/10.1007/s13346-016-0312-0.

[16] De Campos, A. M.; Sánchez, A.; Alonso, M. J. Chitosan Nanoparticles: A New Vehicle for the Improvement of the Delivery of Drugs to the Ocular Surface. Application to Cyclosporin A. *Int. J. Pharm.*, **2001**, *224* (1–2), 159–168.

[17] Wilson*, C. G.; Tan, L. E. Chapter 4.1. Nanostructures Overcoming the Ocular Barrier: Physiological Considerations and Mechanistic Issues; **2012**; pp 173–189. https://doi.org/10.1039/9781849735292-00173.

[18] Popov, A. Mucus-Penetrating Particles and the Role of Ocular Mucus as a Barrier to Micro- And Nanosuspensions. *J. Ocul. Pharmacol. Ther.*, **2020**, *36* (6), 366–375. https://doi.org/10.1089/jop.2020.0022.

[19] Achouri, D.; Alhanout, K.; Piccerelle, P.; Andrieu, V. Recent Advances in Ocular Drug Delivery. *Drug Dev. Ind. Pharm.*, **2013**, *39* (11), 1599–1617. https://doi.org/10.3109/03639045.2012.736515.

[20] Thakur Singh, R. R.; Tekko, I.; McAvoy, K.; McMillan, H.; Jones, D.; Donnelly, R. F.

Minimally Invasive Microneedles for Ocular Drug Delivery. *Expert Opin. Drug Deliv.*, **2017**, *14* (4), 525–537. https://doi.org/10.1080/17425247.2016.1218460.

[21] Lin, H.; Gomez, I.; Meredith, J. C. Pollenkitt Wetting Mechanism Enables Species-Specific Tunable Pollen Adhesion. *Langmuir*, **2013**, *29* (9), 3012–3023. https://doi.org/10.1021/la305144z.

[22] Potroz, M. G.; Mundargi, R. C.; Gillissen, J. J.; Tan, E.-L.; Meker, S.; Park, J. H.; Jung, H.; Park, S.; Cho, D.; Bang, S.-I.; et al. Plant-Based Hollow Microcapsules for Oral Delivery Applications: Toward Optimized Loading and Controlled Release. *Adv. Funct. Mater.*, **2017**, *27* (31), 1700270. https://doi.org/10.1002/adfm.201700270.

[23] Ageitos, J. M.; Robla, S.; Valverde-Fraga, L.; Garcia-Fuentes, M.; Csaba, N. Purification of Hollow Sporopollenin Microcapsules from Sunflower and Chamomile Pollen Grains. *Polymers (Basel).*, **2021**, *13* (13), 2094. https://doi.org/10.3390/polym13132094.

[24] González-Aramundiz, J. V.; Presas, E.; Dalmau-Mena, I.; Martínez-Pulgarín, S.; Alonso, C.; Escribano, J. M.; Alonso, M. J.; Csaba, N. S. Rational Design of Protamine Nanocapsules as Antigen Delivery Carriers. *J. Control. Release*, **2017**, *245*, 62–69. https://doi.org/10.1016/j.jconrel.2016.11.012.

[25] Padte, C. K.; Batwal, P. R.; Patil, M. S.; Jain, A. S. Development and Validation of Analytical Method for Estimation of Bilastine in Bulk and Pharmaceutical (Tablet) Dosage Form. *J. Indian Chem. Soc.*, **2021**, *98* (11), 100172. https://doi.org/10.1016/j.jics.2021.100172.

[26] Diebold, Y.; Jarrín, M.; Sáez, V.; Carvalho, E. L. S.; Orea, M.; Calonge, M.; Seijo, B.; Alonso, M. J. Ocular Drug Delivery by Liposome-Chitosan Nanoparticle Complexes (LCS-NP). *Biomaterials*, **2007**, *28* (8), 1553–1564. https://doi.org/10.1016/j.biomaterials.2006.11.028.

[27] Mundargi, R. C.; Potroz, M. G.; Park, J. H.; Seo, J.; Tan, E.-L.; Lee, J. H.; Cho, N.-J. Eco-Friendly Streamlined Process for Sporopollenin Exine Capsule Extraction. *Sci. Rep.*, **2016**, *6* (1), 1–14. https://doi.org/10.1038/srep19960.

[28] Chacón, M.; Vázquez, N.; Berisa, S.; Persinal, M.; Sánchez, M.; Baamonde, B.; Alfonso, J. F.; Fernández-Vega Cueto, L.; Merayo-Lloves, J.; Meana, Á. QobuR – A New in Vitro Human Corneal Epithelial Model for Preclinical Drug Screening. *Eur. J. Pharm. Biopharm.*, **2019**, *136* (January), 164–173. https://doi.org/10.1016/j.ejpb.2019.01.023.

[29] Chacón, M.; Vázquez, N.; Persinal-Medina, M.; Alonso-Alonso, S.; Alcalde, I.; Merayo-Lloves, J.; Meana, Á. In-House Performance Assessment of 3D QobuR-Reconstructed Human Cornea-Like Epithelium (RhCE) for the Evaluation of Eye Hazard. *Toxicol. Vitr.*, **2022**, *82* (January). https://doi.org/10.1016/j.tiv.2022.105390.

[30] OECD. *Test No. 492: Reconstructed Human Cornea-like Epithelium (RhCE) Test Method for Identifying Chemicals Not Requiring Classification and Labelling for Eye Irritation or Serious Eye Damage*; OECD Guidelines for the Testing of Chemicals, Section 4; OECD, 2019. https://doi.org/10.1787/9789264242548-en.

[31] Wang, X. Y.; Lim-Jurado, M.; Prepageran, N.; Tantilipikorn, P.; Wang, D. Y. Treatment of Allergic Rhinitis and Urticaria: A Review of the Newest Antihistamine Drug Bilastine. *Ther. Clin. Risk Manag.*, **2016**, *12* (April), 585–597.

https://doi.org/10.2147/TCRM.S105189.

[32] Collier, S. J.; Wu, X.; Poh, Z.; Rajkumar, G. A.; Yet, L. Alternative Synthesis of Bilastine. *Synth. Commun.*, **2011**, *41* (9), 1394–1402. https://doi.org/10.1080/00397911.2010.486506.

[33] Anuradha P. Prajapati, S. B. N. S. D. A. A. N. T. Formulation Development and Evaluation of Sublingual Drug Delivery System of Bilastine for Allergic Rhinoconjunctivitis. *Indo Am. J. Pharm. Sci.*, **2021**, *08* (04), 166–181. https://doi.org/10.5281/4710587.

[34] Alvarez-Trabado, J.; Diebold, Y.; Sanchez, A. *Designing Lipid Nanoparticles for Topical Ocular Drug Delivery*; Elsevier B.V., **2017**; Vol. 532. https://doi.org/10.1016/j.ijpharm.2017.09.017.

[35] Calvo, P.; Alonso, M. J.; Vila-Jato, J. L.; Robinson, J. R. Improved Ocular Bioavailability of Indomethacin by Novel Ocular Drug Carriers. *J. Pharm. Pharmacol.*, **1996**, *48* (11), 1147–1152. https://doi.org/10.1111/j.2042-7158.1996.tb03911.x.

[36] Battaglia, L.; Serpe, L.; Foglietta, F.; Muntoni, E.; Gallarate, M.; Del Pozo Rodriguez, A.; Solinis, M. A. Application of Lipid Nanoparticles to Ocular Drug Delivery. *Expert Opin. Drug Deliv.*, **2016**, *13* (12), 1743–1757. https://doi.org/10.1080/17425247.2016.1201059.

[37] Thwala, L. N.; Delgado, D. P.; Leone, K.; Marigo, I.; Benetti, F.; Chenlo, M.; Alvarez, C. V.; Tovar, S.; Dieguez, C.; Csaba, N. S.; et al. Protamine Nanocapsules as Carriers for Oral Peptide Delivery. *J. Control. Release*, **2018**, *291* (October), 157–168. https://doi.org/10.1016/j.jconrel.2018.10.022.

[38] Calvo, P.; Vila-Jato, J. L.; Alonso, M. J. Evaluation of Cationic Polymer-Coated Nanocapsules as Ocular Drug Carriers. *Int. J. Pharm.*, **1997**, *153* (1), 41–50. https://doi.org/10.1016/S0378-5173(97)00083-5.

[39] Calvo, P.; Alonso, M. J.; Sur, C. Development of Positively Charged Colloidal Drug Carriers : Chitosan-Coated Polyester Nanocapsules and Submicron-Emulsions. **1996**.

[40] Robla, S.; Alonso, M. J.; Csaba, N. Polyaminoacid-Based Nanocarriers: A Review of the Latest Candidates for Oral Drug Delivery. *Expert Opin. Drug Deliv.*, **2020**, *00* (00), 1–12. https://doi.org/10.1080/17425247.2020.1776698.

[41] Abdelwahed, W.; Degobert, G.; Stainmesse, S.; Fessi, H. Freeze-Drying of Nanoparticles: Formulation, Process and Storage Considerations. *Adv. Drug Deliv. Rev.*, **2006**, *58* (15), 1688–1713. https://doi.org/10.1016/j.addr.2006.09.017.

[42] González-Aramundiz, J. V.; Peleteiro, M.; González-Fernández, Á.; Alonso, M. J.; Csaba, N. S. Protamine Nanocapsules for the Development of Thermostable Adjuvanted Nanovaccines. *Mol. Pharm.*, **2018**, *15* (12), 5653–5664. https://doi.org/10.1021/acs.molpharmaceut.8b00852.

[43] Rabensteiner, D. F.; Rabensteiner, J.; Horwath-Winter, J.; Lang-Loidolt, D.; Wedrich, A.; Heidinger, A.; Schwantzer, G.; Schmut, O. Extracts of Different Pollen Species and Their Effect on Human Tear Fluid and an Epithelial Cell Line. *Cutan. Ocul. Toxicol.*, **2019**, *38* (1), 93–103. https://doi.org/10.1080/15569527.2018.1530259.

[44] Smith, M.; Jäger, S.; Berger, U.; Šikoparija, B.; Hallsdottir, M.; Sauliene, I.; Bergmann, K. C.; Pashley, C. H.; De Weger, L.; Majkowska-Wojciechowska, B.; et al. Geographic and Temporal Variations in Pollen Exposure across Europe. *Allergy Eur. J. Allergy Clin. Immunol.*, **2014**, *69* (7), 913–923. https://doi.org/10.1111/all.12419.

[45] Ghosh, N.; Sircar, G.; Saha, B.; Pandey, N.; Bhattacharya, S. G. Search for Allergens from the Pollen Proteome of Sunflower (Helianthus Annuus L): A Major Sensitizer for Respiratory Allergy Patients. *PLoS One*, **2015**, *10* (9), 1–20. https://doi.org/10.1371/journal.pone.0138992.

[46] Guryanova, S. V.; Finkina, E. I.; Melnikova, D. N.; Bogdanov, I. V.; Bohle, B.; Ovchinnikova, T. V. How Do Pollen Allergens Sensitize? *Front. Mol. Biosci.*, **2022**, *9* (June), 1–17. https://doi.org/10.3389/fmolb.2022.900533.

[47] Mundargi, R. C.; Tan, E. L.; Seo, J.; Cho, N.-J. Encapsulation and Controlled Release Formulations of 5-Fluorouracil from Natural *Lycopodium Clavatum* Spores. *J. Ind. Eng. Chem.*, **2016**, *36*, 102–108. https://doi.org/10.1016/j.jiec.2016.01.022.

[48] Diego-taboada, A.; Sathyapalan, T.; Courts, F.; Lorch, M.; Walther, T.; Almutairi, F.; Burke, B. P.; Harris, K.; Kruusm, M.; Booth, J.; et al. Spore Exines Increase Vitamin D Clinical Bioavailability by Mucoadhesion and Bile Triggered Release ☆. **2022**, *350* (January), 244–255. https://doi.org/10.1016/j.jconrel.2022.08.017.

[49] Meligi, N. M.; Dyab, A. K. F.; Paunov, V. N. Sustained in Vitro and in Vivo Delivery of Metformin from Plant Pollen-Derived Composite Microcapsules. *Pharmaceutics*, **2021**, *13* (7), 9–12. https://doi.org/10.3390/pharmaceutics13071048.

[50] Diego-Taboada, A.; Maillet, L.; Banoub, J. H.; Lorch, M.; Rigby, A. S.; Boa, A. N.; Atkin, S. L.; Mackenzie, G. Protein Free Microcapsules Obtained from Plant Spores as a Model for Drug Delivery: Ibuprofen Encapsulation, Release and Taste Masking. *J. Mater. Chem. B*, **2013**, *1* (5), 707–713. https://doi.org/10.1039/c2tb00228k.

[51] Mundargi, R. C.; Potroz, M. G.; Park, S.; Shirahama, H.; Lee, J. H.; Seo, J.; Cho, N.-J. Natural Sunflower Pollen as a Drug Delivery Vehicle. *Small*, **2016**, *12* (9), 1167–1173. https://doi.org/10.1002/smll.201500860.

[52] Goodwin, W. B.; Gomez, I. J.; Fang, Y.; Meredith, J. C.; Sandhage, K. H. Conversion of Pollen Particles into Three-Dimensional Ceramic Replicas Tailored for Multimodal Adhesion. *Chem. Mater.*, **2013**, *25* (22), 4529–4536. https://doi.org/10.1021/cm402226w.

[53] Uddin, M. J.; Liyanage, S.; Warzywoda, J.; Abidi, N.; Gill, H. S. Role of Sporopollenin Shell Interfacial Properties in Protein Adsorption. *Langmuir*, **2022**, *38* (9), 2763–2776. https://doi.org/10.1021/acs.langmuir.1c02682.

[54] Alshehri, S. M.; Al-Lohedan, H. A.; Chaudhary, A. A.; Al-Farraj, E.; Alhokbany, N.; Issa, Z.; Alhousine, S.; Ahamad, T. Delivery of Ibuprofen by Natural Macroporous Sporopollenin Exine Capsules Extracted from *Phoenix Dactylifera* L. *Eur. J. Pharm. Sci.*, **2016**, *88*, 158–165. https://doi.org/10.1016/j.ejps.2016.02.004.

[55] Raish, M.; Kalam, M. A.; Ahmad, A.; Shahid, M.; Ansari, M. A.; Ahad, A.; Ali, R.; Jardan, Y. A. B.; Alshamsan, A.; Alkholief, M.; et al. Eudragit-Coated Sporopollenin Exine Microcapsules (Semc) of Phoenix Dactylifera l. of 5-Fluorouracil for Colon-

Specific Drug Delivery. *Pharmaceutics*, **2021**, *13* (11). https://doi.org/10.3390/pharmaceutics13111921.

[56] Thwala, L. N.; Delgado, D. P.; Leone, K.; Marigo, I.; Benetti, F.; Chenlo, M.; Alvarez, C. V.; Tovar, S.; Dieguez, C.; Csaba, N. S.; et al. Protamine Nanocapsules as Carriers for Oral Peptide Delivery. *J. Control. Release*, **2018**, *291* (June), 157–168. https://doi.org/10.1016/j.jconrel.2018.10.022.

[57] Cutone, A.; Frioni, A.; Berlutti, F.; Valenti, P.; Musci, G.; Bonaccorsi di Patti, M. C. Lactoferrin Prevents LPS-Induced Decrease of the Iron Exporter Ferroportin in Human Monocytes/Macrophages. *BioMetals*, **2014**, *27* (5), 807–813. https://doi.org/10.1007/s10534-014-9742-7.

[58] Sargin, I.; Akyuz, L.; Kaya, M.; Tan, G.; Ceter, T.; Yildirim, K.; Ertosun, S.; Aydin, G. H.; Topal, M. Controlled Release and Anti-Proliferative Effect of Imatinib Mesylate Loaded Sporopollenin Microcapsules Extracted from Pollens of *Betula Pendula*. *Int. J. Biol. Macromol.*, **2017**, *105*, 749–756. https://doi.org/10.1016/j.ijbiomac.2017.07.093.

[59] Dyab, A. K. F.; Mohamed, M. A.; Meligi, N. M.; Mohamed, S. K. Encapsulation of Erythromycin and Bacitracin Antibiotics into Natural Sporopollenin Microcapsules: Antibacterial, Cytotoxicity, in Vitro and in Vivo Release Studies for Enhanced Bioavailability. *RSC Adv.*, **2018**, *8* (58), 33432–33444. https://doi.org/10.1039/C8RA05499A.

[60] Alshehri, S. M.; Al-Lohedan, H. A.; Al-Farraj, E.; Alhokbany, N.; Chaudhary, A. A.; Ahamad, T. Macroporous Natural Capsules Extracted from Phoenix Dactylifera L. Spore and Their Application in Oral Drugs Delivery. *Int. J. Pharm.*, **2016**, *504* (1–2), 39–47. https://doi.org/10.1016/j.ijpharm.2016.02.049.

[61] Reynolds, F.; Weissleder, R.; Josephson, L. Protamine as an Efficient Membrane-Translocating Peptide. *Bioconjug. Chem.*, **2005**, *16* (5), 1240–1245. https://doi.org/10.1021/bc0501451.

[62] Uddin, M. J.; Gonzalez-Cruz, P.; Warzywoda, J.; Gill, H. S. Sporopollenin Spikes Augment Antigen-Specific Immune Response and Generate Long-Lived Humoral Immunity. *Adv. Ther.*, **2020**, *2000102*, 2000102. https://doi.org/10.1002/adtp.202000102.

[63] Dana, M. R. Corneal Antigen-Presenting Cells: Diversity, Plasticity, and Disguise. The Cogan Lecture. *Investig. Ophthalmol. Vis. Sci.*, **2004**, *45* (3), 722–727. https://doi.org/10.1167/iovs.03-0803.

[64] Shahid, M.; Tripathi, T.; Sobia, F.; Moin, S.; Siddiqui, M.; Khan, R. A. Histamine, Histamine Receptors, and Their Role in Immunomodulation: An Updated Systematic Review. *Open Immunol. J.*, **2009**, *2* (1), 9–41. https://doi.org/10.2174/1874226200902010009.

[65] Forrester, M. A.; Wassall, H. J.; Hall, L. S.; Cao, H.; Wilson, H. M.; Barker, R. N.; Vickers, M. A. Similarities and Differences in Surface Receptor Expression by THP-1 Monocytes and Differentiated Macrophages Polarized Using Seven Different Conditioning Regimens. *Cell. Immunol.*, **2018**, *332*, 58–76. https://doi.org/10.1016/j.cellimm.2018.07.008.

[66] An, S.; Kim, S.; Huh, Y.; Lee, T. R.; Kim, H. K.; Park, K. L.; Eun, H. C. Expression of Surface Markers on the Human Monocytic Leukaemia Cell Line, THP-1, as Indicators for the Sensitizing Potential of Chemicals. *Contact Dermatitis*, **2009**, *60* (4), 185–192. https://doi.org/10.1111/j.1600-0536.2009.01528.x.

[67] Park, M. C.; Kim, D.; Lee, Y.; Kwon, H. J. CD83 Expression Induced by CpG-DNA Stimulation in a Macrophage Cell Line RAW 264.7. *BMB Rep.*, **2013**, *46* (9), 448–453. https://doi.org/10.5483/BMBRep.2013.46.9.023.

[68] Uddin, M. J.; Gill, H. S. Ragweed Pollen as an Oral Vaccine Delivery System: Mechanistic Insights. *J. Control. Release*, **2017**, *268* (October), 416–426. https://doi.org/10.1016/j.jconrel.2017.10.019.

[69] Chen, P. M.; Pan, W. Y.; Luo, P. K.; Phung, H. N.; Liu, Y. M.; Chiang, M. C.; Chang, W. A.; Tien, T. L.; Huang, C. Y.; Wu, W. W.; et al. Pollen-Mimetic Metal-Organic Frameworks with Tunable Spike-Like Nanostructures That Promote Cell Interactions to Improve Antigen-Specific Humoral Immunity. *ACS Nano*, **2021**, *15* (4), 7596–7607. https://doi.org/10.1021/acsnano.1c01129.

[70] Reimondez-Troitiño, S.; Csaba, N.; Alonso, M. J.; de la Fuente, M. Nanotherapies for the Treatment of Ocular Diseases. *Eur. J. Pharm. Biopharm.*, **2015**, *95* (Pt B), 279–293. https://doi.org/10.1016/j.ejpb.2015.02.019.

[71] de Campos, A. M.; Diebold, Y.; Carvalho, E. L. S.; Sánchez, A.; Alonso, M. J. Chitosan Nanoparticles as New Ocular Drug Delivery Systems: In Vitro Stability, in Vivo Fate, and Cellular Toxicity. *Pharm. Res.*, **2004**, *21* (5), 803–810.

[72] Zorn-Kruppa, M.; Tykhonova, S.; Beige, G.; Bednarz, J.; Diehl, H. A.; Engelke, M. A Human Corneal Equivalent Constructed from SV40-Immortalised Corneal Cell Lines. *ATLA Altern. to Lab. Anim.*, **2005**, *33* (1), 37–45. https://doi.org/10.1177/026119290503300107.

[73] Kaluzhny, Y.; Kinuthia, M. W.; Truong, T.; Lapointe, A. M.; Hayden, P.; Klausner, M. New Human Organotypic Corneal Tissue Model for Ophthalmic Drug Delivery Studies. *Investig. Ophthalmol. Vis. Sci.*, **2018**, *59* (7), 2880–2898. https://doi.org/10.1167/iovs.18-23944.

[74] CALVO, P.; THOMAS, C.; ALONSO, M.; VILAJATO, J.; ROBINSON, J. Study of the Mechanism of Interaction of Poly(ϵ-Caprolactone) Nanocapsules with the Cornea by Confocal Laser Scanning Microscopy. *Int. J. Pharm.*, **1994**, *103* (3), 283–291. https://doi.org/10.1016/0378-5173(94)90179-1.

[75] Ji, Y. W.; Byun, Y. J.; Choi, W.; Jeong, E.; Kim, J. S.; Noh, H.; Kim, E. S.; Song, Y. J.; Park, S. K.; Lee, H. K. Neutralization of Ocular Surface TNF-α Reduces Ocular Surface and Lacrimal Gland Inflammation Induced by in Vivo Dry Eye. *Investig. Ophthalmol. Vis. Sci.*, **2013**, *54* (12), 7557–7566. https://doi.org/10.1167/iovs.12-11515.

[76] Leonardi, A. The Central Role of Conjunctival Mast Cells in the Pathogenesis of Ocular Allergy. *Curr. Allergy Asthma Rep.*, **2002**, *2* (4), 325–331. https://doi.org/10.1007/s11882-002-0061-7.

[77] Olsen, M. V.; Lyngstadaas, A. V.; Bair, J. A.; Hodges, R. R.; Utheim, T. P.; Serhan, C. N.; Dartt, D. A. Maresin 1, a Specialized Proresolving Mediator, Stimulates Intracellular

[Ca2+] and Secretion in Conjunctival Goblet Cells. *J. Cell. Physiol.*, **2021**, *236* (1), 340–353. https://doi.org/10.1002/jcp.29846.

[78] Nubile, M.; Lanzini, M.; Calienno, R.; Mastropasqua, R.; Curcio, C.; Mastropasqua, A.; Agnifili, L.; Mastropasqua, L. S100 A and B Expression in Normal and Inflamed Human Limbus. *Mol. Vis.*, **2013**, *19* (January), 146–152.

[79] Tong, L.; Lan, W.; Lim, R. R.; Chaurasia, S. S. S100A Proteins as Molecular Targets in the Ocular Surface Inflammatory Diseases. *Ocul. Surf.*, **2014**, *12* (1), 23–31. https://doi.org/10.1016/j.jtos.2013.10.001.

[80] Wilkinson, A.; Kawaguchi, N.; Geczy, C.; Di Girolamo, N. S100A8 and S100A9 Proteins Are Expressed by Human Corneal Stromal Dendritic Cells. *Br. J. Ophthalmol.*, **2016**, *100* (9), 1304–1308. https://doi.org/10.1136/bjophthalmol-2016-308827.

[81] Akpek, E. K.; Gottsch, J. D. Immune of Defense at the Ocular Surface. *Eye*, **2003**, *17* (8), 949–956. https://doi.org/10.1038/sj.eye.6700617.

[82] Ochoa, D.; Román, M.; Belmonte, C.; Martín-Vilchez, S.; Mejía-Abril, G.; Abad-Santos, F.; Hernández, G.; Arranz, P.; Elgezabal, L.; Fernández, N. Pharmacokinetics and Safety of a Bilastine Once-Daily, Preservative-Free, Ophthalmic Formulation. *Adv. Ther.*, **2021**, *38* (7), 4070–4081. https://doi.org/10.1007/s12325-021-01801-y.

OVERALL DISCUSSION

OVERALL DISCUSSION

Pollen grains possess a unique morphology characterized by a uniform size and a resistant outer wall composed of sporopollenin, a chemically stable and biocompatible biopolymer that enables the pollen to protect its genetic material [1]. Different plants produce numerous variations of pollen with differing sizes, morphologies, and physicochemical structures in nature. These morphological characteristics have been extensively studied in taxonomic and phylogenetic research. Furthermore, the surface of pollen can exhibit different decorations and/or apertures, which vary in number and location among species [2]. In this context, plant pollen from the Asteraecae family such as sunflower (*Helianthus annuus*) or chamomile pollen (*Matricaria chamomilla*), exhibit a unique spiny surface morphology that enables the attachment to insects during pollination, and could potentially promote adhesion to mucosal surfaces, leading to extended contact with biological surfaces compared with other pollen species [3] (**Figure 1**).

Over the past few years, various types of pollen have been identified as potential candidates for drug encapsulation and delivery. Methods such as alkaline lysis [4], acidolysis [5], or enzymatic treatments [6] have been developed to produce hollow platforms that can serve as a drug delivery systems by offering protection and allowing the encapsulation of both polar and non-polar drugs. These methods are executed under specific reflux conditions and temperatures to ensure minimal harm to the exine surface, thereby maintaining its structural integrity. However, these methods must be optimized based on the nature and composition of each pollen to obtain intact sporopollenin microcapsules. In the case of *H. annuus*, it was found to be destroyed by an alkaline lysis treatment (KOH 60°C, 12 h) or an acidolysis treatment (HCl 70°C, 24 h) [7], while the use of phosphoric acid (H_3PO_4) was more effective in the production of sporopollenin microcapsules [8–10]. H_3PO_4 and diethyl ether [11, 12] or a combination of acetone, diethyl ether, and alkaline lysis (KOH at 80ºC 12 h), were also reported to produce flexible and softer sunflower sporopollenin structures, losing some of their natural toughness and structure [13].

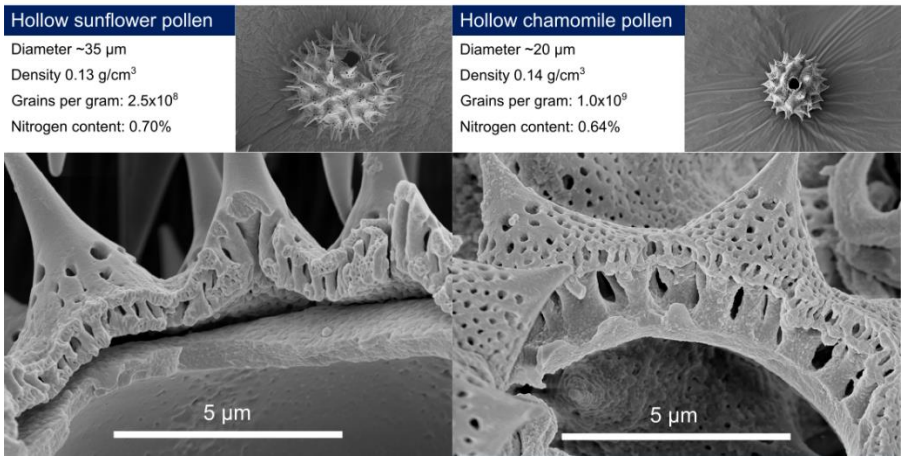

Figure 1. Scanning Electron Microscopy of a section of *Helianthus annuus* and *Matricaria chamomilla* hollow pollen microcapsules after their purification procedure.

Our group has developed a new, simplified method for producing hollow *H. annuus* microcapsules by performing a pre-treatment with water and acetone, followed by a cyclohexane washing step. Different acids (HCl, $HClO_4$, H_3PO_4, CF_3COOH, H_2SO_4, or HNO_3)

were tested for acidolysis, with various ratios (1:10 w/v), incubation times (1 to 14 h), and temperatures (25 and 70°C) to optimize solubilization and removal of internal components (**Figure 2**). Treatment with H_3PO_4 for 5 h at 70ºC was found to be the most effective method to produce hollow pollen microcapsules. We also applied a similar protocol for the direct extraction of dried *M. chamomilla*, for which, until now, no treatment or use had been reported, and we obtained hollow sporopollenin microcapsules with a final protein content of < 4%, similar to that obtained for sunflower [14]. On the one hand, the use of a preliminary water-washing step is infrequent in the literature, where it is more common to treat pollen directly with organic solvents. However, the low solubility of polysaccharides and proteins in organic solvents leads to suboptimal purification of the samples [15]. On the other hand, the use of shorter extraction processes with acetone at lower temperatures (25ºC) have shown to produce similar results to prolonged incubation times and hot acetone, a widely used method for producing defatted pollen [16], and could be advantageous to avoid any thermal alteration of the product. Finally, the additional washing step using cyclohexane allowed the removal of saturated lipids and proteins that could not be eliminated with a standard acetone treatment.

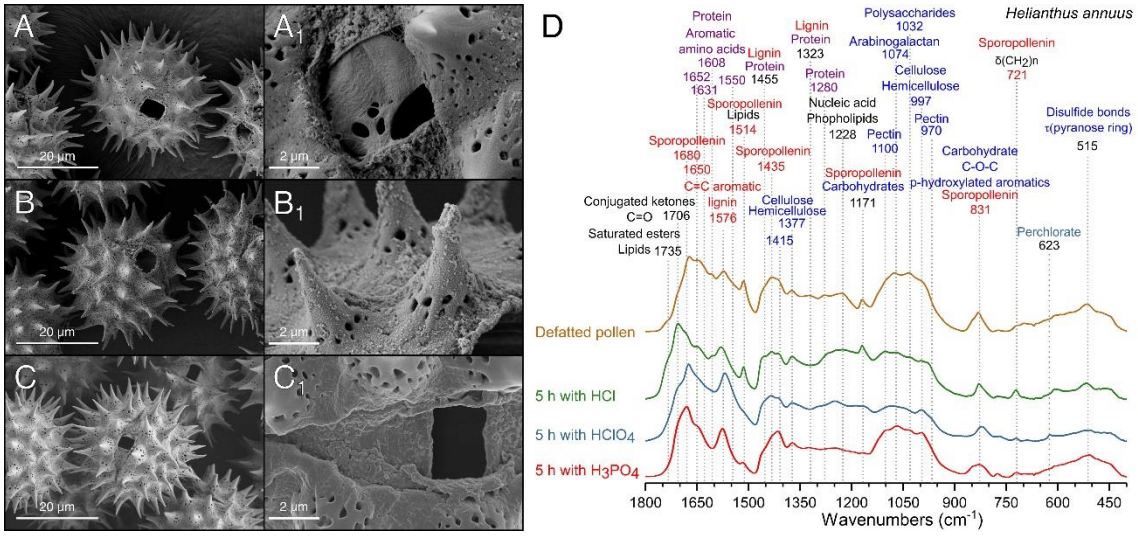

Figure 2. Scanning Electron Micrographs of defatted sunflower pollen treated with different acids. (A) HCl, (B) $HClO_4$, (C) H_3PO_4, (**D**) ATR-FTIR spectra of pollen samples after 5 h treatment.

Up to date, the sunflower sporopollenin microcapsules have been tested for loading with BSA [6, 8, 17, 18], β-Galactosidase [9, 10], or doxorubicin [12], while *M. chamomilla* sporopollenin microcapsules have not yet been investigated for biomedical purposes. In this context of drug delivery, nanotechnology-based therapeutic approaches provide an opportunity to overcome biological barriers and protect biomacromolecules from degradation, enhancing their stability and availability [19]. However, *in vivo* studies have yet to consistently demonstrate high and reproducible efficacy due to their premature removal from the mucosa, leading to limited bioavailability compared to other delivery routes [20]. Our group has reported, for the first time, the combination of pollen grains with nanoparticles (NPs) of varying size (100, 200 and 500nm) and surface functionalization (aminated, carboxylated or unmodified), with a focus on understanding the physical and chemical interactions to achieve adequate loading and sustained release patterns.

The association efficiency (AE%) of the different NPs (**Table 1**) to hollow pollen microcapsules, with values between 60-90%, was higher compared to the reported association of free drugs and biomolecules in *H. annuus* pollen platforms, with a BSA encapsulation of 54% [6], 42% [8], and 66% after vacuum-loading and an AE% of 37-38% after passive or compression-loading [17]. This AE% was also higher compared to drug loading into other pollen-derived platforms, using either the same or different loading methods, for example, pantoprazole (30%) [21], or imatinib mesylate [22] into *Corylus avellana* and *Betula pendula* pollen, respectively.

Table 1. Association efficiency (%) of polystyrene nanoparticles and hollow pollen microcapsules.

Loading method	Modification	Size (nm)		
		100	200	500
Lyophilization	Aminated	76.9±5.1	77.0±9.5	76.1±0.7
	Unmodified	68.9±6.8	85.0±3.6	67.5±1.8
	Carboxylated	69.4±0.5	59.1±5.8	60.4±2.4
Vacuum	Aminated	68.8±4.0	77.0±8.0	81.0±5.0
	Unmodified	73.4±6.5	85.2±8.7	80.7±8.1
	Carboxylated	87.7±7.3	89.6±1.2	78.7±9.6

Regarding the release kinetics, lyophilization produced a higher burst release within the first 15 minutes compared to vacuum-assisted loading, which resulted in a continuous release lasting from 8 to 120 h. While it was commonly observed that drug-loaded sporopollenin microcapsules tend to have a significant initial burst release [17, 21, 23], in our case, the NPs displayed a more controlled release pattern. The degree of total release reached in some of the prototypes with values of up to 100% without any need for surface modification, preserving the morphology and spines of the platforms, which allow for the retention of their mucointeraction properties.

200 nm NPs showed a higher loading and overall release, indicating that the specific surface area could influence the size-exclusion effect. Based on the findings obtained with commercial polystyrene NPs, the possibility of incorporating biodegradable nanocarriers was evaluated by utilizing a core-shell protamine nanocapsule prototype that had been previously reported by our group for the transmucosal delivery of insulin [24, 25]. Biodegradable protamine nanocapsules [26–28] were successfully developed and loaded into hollow pollen microcapsules. Although their AE% was lower than the data previously obtained with commercial NPs (85% *vs* 60% for lyophilization and 85% *vs* 65% for the vacuum-assisted loading method using a 1:1 ratio), the release pattern in simulated intestinal fluid exhibited similarities with aminated NPs, suggesting that the findings obtained with the model NPs were able to anticipate the expected behavior of protamine NCs. Protamine NCs adhered strongly to the intestinal mucosal surface *ex vivo* and also maintained a more prolonged adhesion to the small intestine after 3 h oral administration when they were loaded into hollow pollen microcapsules, as compared with free administered NCs (**Figure 3**). These results indicated that pollen grains can modulate nanocarrier retention and absorption by the mucosa, improving their interaction and reducing the possibility of being prematurely eliminated from the absorption site. Besides, these results suggested a controlled and sustained intestinal release of the developed NCs from the pollen microcapsules without the use of any external coatings, such as xanthan gum, alginate [17, 29], Eudragit L100 [8], or Eudragit RS 100 [23] reported as possible strategies to delay the release of encapsulated molecules or protect them from gastric conditions.

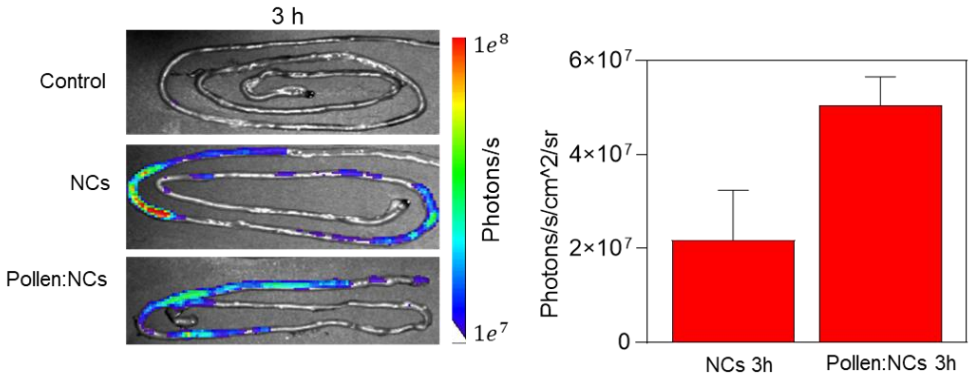

Figure 3. Fluorescence intensity signals and quantification (ROI) in the small intestine 3h after the oral administration of hollow pollen microcapsules (control), DiD-protamine nanocapsules (free NCs), and DiD-protamine NCs loaded into hollow pollen microcapsules (n=3; media± SEM).

In addition to the use of protamine-based nanocapsules for oral delivery, we evaluated their utility in the pulmonary administration of rifabutin for the treatment of tuberculosis (TB). As compared to systemic administration, the large pulmonary surface area and high vascularization of alveoli offer a rapid action and higher bioavailability of anti-TB drugs in alveolar macrophages, however, its complex geometry, high humidity, or mucociliary clearance limits their availability [30]. For that reason, inhalable anti-TB formulations are still in preclinical development, and no product is currently available in the market [31]. Besides, when nanocarriers are administered via the pulmonary route, their nanoscale size results in low inertia, increasing the risk of exhalation (up to 80%) without deposition in the airways [32]. Dry powder inhalers (DPIs) are a promising strategy for the administration of microparticles, as they allow for highly effective drug deposition in the lungs and improved patient adherence [33]. Our group has developed a large carrier(lactose)-free DPI based on spray-dried microparticles from rifabutin NCs.

For the development of spray-dried microparticles from rifabutin, we initially designed rifabutin-load protamine NCs. Previous reports on rifabutin-based drug delivery systems using nanotechnology have described liposomes and solid lipid nanoparticles (SLN) for tuberculosis treatment via intravenous, oral, or pulmonary administration [34–37]. However, in some cases, they showed the greater size and polydisperse values (345 nm and PDI >0.3 [34]; 389 nm and PDI> 0.4 [36]) and a negative surface charge (between -3 and -33 mV for liposomes [35], and -10-20 mV for mannosylated-SLNs [36] and SLNs [37]) which could decrease their interaction with the negatively charged alveolar macrophages compared with our rifabutin protamine NCs, with a size of 200 nm and a slightly positive surface charge (**Figure 4**) [38]. The developed protamine NCs showed uptake of >90%, remarkably higher than those reported for SLNs (between 27-43%) [37] in lung cell lines and macrophages after 24 h.

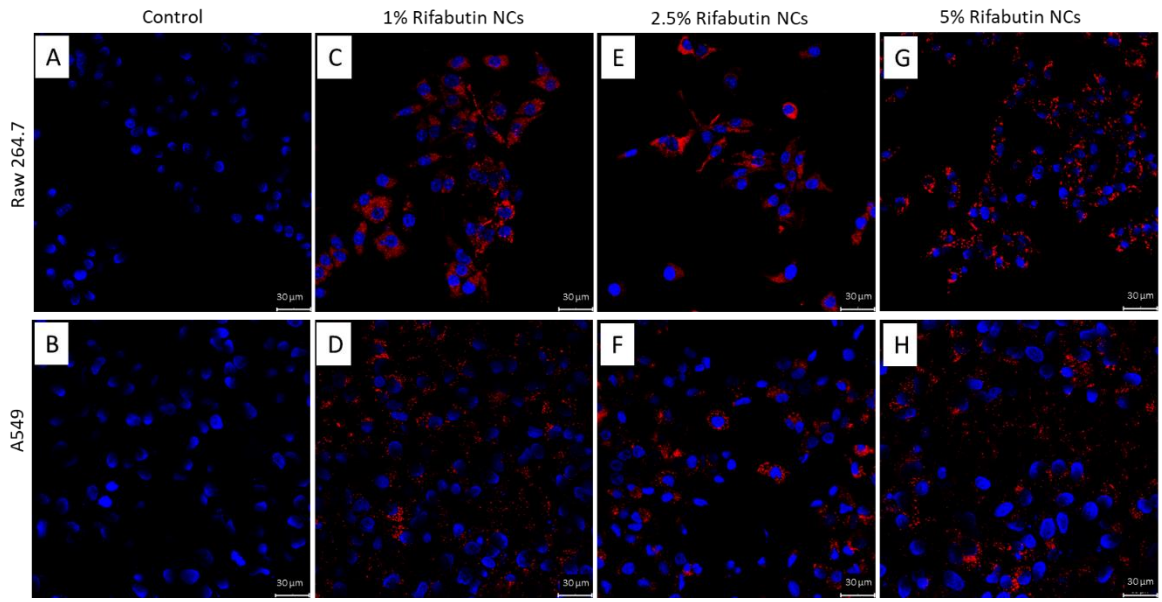

Figure 4. Cellular internalization study via confocal imaging of Raw 264.7 (A, C, E, and G) and A549 (B, D, F, and G) cell lines. DAPI-dye (blue channel; Excitation λ_{max} = 359 nm, Emission λ_{max} = 457 nm); DiD-dye (red channel; Excitation λ_{max}=640 nm, Emission λ_{max}= 675 nm). The scale bar represents 30 µm.

The drug-release pattern of the formulations in simulated lung media was linear and resulted in a higher drug release between 66-96% depending on the concentration of encapsulated drug, compared to the poorly water-soluble rifabutin (38 ± 3%). Similar rifabutin dissolution profiles were reported from glyceryl dibehenate and glyceryl tristearate SLNs (65 and 80% after 1 h, respectively) [37], supporting that the polymeric matrix is responsible for the release pattern. The developed spray-dried microcapsules showed an aerodynamic diameter of 5.8 µm, comparable to those reported for spray-dried locust bean gum microparticles combining isoniazid and rifabutin [39], and were able to reach the respiratory region of the lung. The spray-dried NCs redispersion and size analysis confirmed the stability of colloidal systems during the drying process, as all formulations remained in the nano-range size.

-Párrafos afectados por la protección de derechos-

Finally, the use of protamine-based nanocapsules for ocular delivery of bilastine was also explored in this thesis, and its loading into hollow pollen microcapsules was performed to prolong their residence time and control their release. Bilastine (Bilaxten®, Ibis®, Obalix®) is a histamine inverse agonist with a high affinity for H_1, approved in more than 120 countries for the treatment of allergic rhinoconjunctivitis through oral administration. However, bilastine´s poor water solubility, as well as factors such as nasolacrimal drainage and tear fluid turnover, limit the residence time of topical formulations in the anterior eye segment. Therefore, ophthalmic formulations of bilastine are currently not available on the market, even though several studies are currently under investigation (clinical trials NCT03231969 and NCT03479307) [40]. Stable and active polymorph I of bilastine was successfully obtained from commercial tablets using chloroform as isolation solvent. The obtained bilastine was encapsulated into 200 nm protamine NCs, which showed an appropriate final pH (6.9 ± 0.4) for ocular delivery. Bilastine-loaded protamine NCs achieved an encapsulation efficiency of 71%

and a loading capacity of up to 74% into *H. annuus* hollow microcapsules, similar to those reported BSA encapsulation using vacuum- loading (66%) [17].

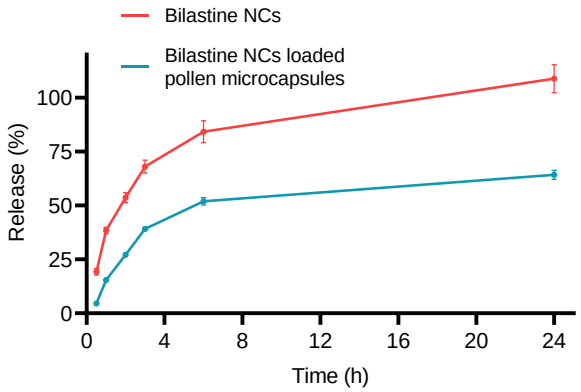

Figure 6. *In vitro* bilastine dissolution in simulated lacrimal fluid from the developed protamine NCs in suspension and loaded into hollow *H. annuus*sporopollenin microcapsules.

The release profile of bilastine from pollen microcapsules was biphasic (**Figure 6**), with a rapid initial release in simulated lacrimal fluid over the first 6 h, followed by a slower release over the next 18 h, resulting in a total cumulative release of 64 ± 2%. The study showed that bilastine NCs adsorbed on the surface of *H. annuus* pollen microcapsules had a faster release, than those trapped inside the pollen platforms, with a more controlled pattern. Although there are no studies analyzing drug release from pollen platforms in simulated lacrimal fluid, studies have shown a pH influence, with greater release observed at neutral pH as simulated intestinal fluids compared to acidic pHs like simulated gastric fluid, where the release was found to be more delayed [41, 42]. As previously reported for ragweed pollen, with a surface architecture similar to *H. annuus*, its physical characteristics were crucial for their phagocytosis by mouse macrophages and dendritic cells [43]. As shown in **Figure 7**, *H. annuus* surface morphology produced a localized adhesion of the developed bilastine NCs-loaded pollen platforms to THP-1 cells (6.6% of the cells).

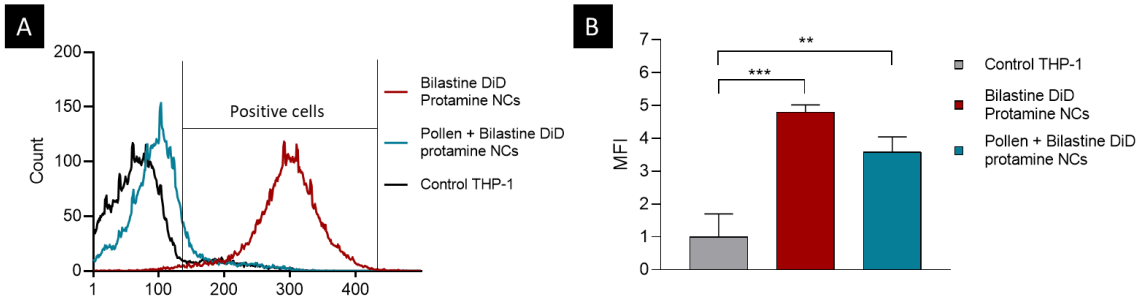

Figure 7. (A) Flow cytometry histograms and (B) Mean Fluorescent Intensity (MFI) of THP-1 cells after incubation with bilastine-loaded protamine nanocapsules (NCs) and bilastine NCs loaded into hollow sporopollenin microcapsules. MFI=1 was established for the control (non-treated cells).

In addition, internalization of NCs into the adhered cells was similar to the free bilastine NCs, which is particularly useful for targeted and sustained drug delivery. Furthermore, in contrast to ragweed microcapsules, their adhesion did not induce the expression of immune cells maturation markers as CD80 [44] greater than the lipopolysaccharide. Adhesion of pollen did not cause cellular damage *in vitro* in a 3D QobuR human corneal epithelial model, nor upon *in*

vivo topical instillation in rat eye, where no irritation, abnormal secretions, or release of proinflammatory cytokines were observed.

Overall, the results obtained during this Ph.D. thesis provide a deeper insight on the potential of using pollen grains as drug delivery vehicles. Considering the administration route, the design of our nanocarrier-loaded purified pollen vehicles must meet different technological requirements to achieve effective release of the encapsulated APIs.
Firstly, the presence of spines is crucial for achieving optimal mucoadhesion, making pollen from the Asteraceae family particularly attractive due to their echinate surface morphology. In addition, as indicated by the results obtained for the **oral route**, the species-dependent surface ornamentation, as well as the diameter and dimensions of the inner cavity can also play an important role in the loading capacity, mucointeraction and overall efficacy of these vehicles.

-Párrafo afectado por la protección de derechos-

Finally, an additional consideration has been considered for the use of pollen-based microcapsules delivery through **ocular route**, as it is essential to avoid any allergic or hypersensitization effect derived from the size and composition of the platforms, to improve patient tolerance and preserve unaltered epithelial barrier function.

Considering the above, the developed pollen microcapsules offer an adjustable and adaptable multi-stage delivery strategy, of high interest for biomedical applications. These platforms, based on innovative biomaterials such as sporopollenin, constitute a suitable, promising, biocompatible, cost-effective, and simple approach to enhance effectiveness in drug delivery to mucosal tissues.

REFERENCES

[1] Barrier, S.; Diego-Taboada, A.; Thomasson, M. J.; Madden, L.; Pointon, J. C.; Wadhawan, J. D.; Beckett, S. T.; Atkin, S. L.; MacKenzie, G. Viability of Plant Spore Exine Capsules for Microencapsulation. *J. Mater. Chem.*, **2011**, *21* (4), 975–981. https://doi.org/10.1039/C0JM02246B.

[2] Halbritter, H.; Ulrich, S.; Grímsson, F.; Weber, M.; Zetter, R.; Hesse, M.; Buchner, R.; Svojtka, M.; Frosch-Radivo, A. *Illustrated Pollen Terminology*; 2018. https://doi.org/10.1007/978-3-319-71365-6.

[3] Diego-Taboada, A.; Beckett, S. T.; Atkin, S. L.; Mackenzie, G. Hollow Pollen Shells to Enhance Drug Delivery. *Pharmaceutics*, **2014**, *6* (1), 80–96. https://doi.org/10.3390/pharmaceutics6010080.

[4] Zetzsche, F.; Huggler, K. Untersuchungen Über Die Membran Der Sporen Und Pollen. I. 1. *Lycopodium Clavatum* L. *Justus Liebig's Ann. der Chemie*, **1928**, *461* (1), 89–109. https://doi.org/10.1002/jlac.19284610105.

[5] Cain, S. A. Pollen Analysis as a Paleo-Ecological Research Method. *Bot. Rev.*, **1939**, *5* (12), 627–654. https://doi.org/10.1007/BF02871650.

[6] Fan, T.; Park, J. H.; Pham, Q. A.; Tan, E.-L.; Mundargi, R. C.; Potroz, M. G.; Jung, H.; Cho, N.-J. Extraction of Cage-like Sporopollenin Exine Capsules from Dandelion Pollen Grains. *Sci. Rep.*, **2018**, *8* (1), 6565. https://doi.org/10.1038/s41598-018-24336-9.

[7] Mundargi, R. C.; Potroz, M. G.; Park, J. H.; Seo, J.; Lee, J. H.; Cho, N.-J. Extraction of

Sporopollenin Exine Capsules from Sunflower Pollen Grains. *RSC Adv.*, **2016**, *6* (20), 16533–16539. https://doi.org/10.1039/C5RA27207F.

[8] Potroz, M. G.; Mundargi, R. C.; Gillissen, J. J.; Tan, E.-L.; Meker, S.; Park, J. H.; Jung, H.; Park, S.; Cho, D.; Bang, S.-I.; et al. Plant-Based Hollow Microcapsules for Oral Delivery Applications: Toward Optimized Loading and Controlled Release. *Adv. Funct. Mater.*, **2017**, *27* (31), 1700270. https://doi.org/10.1002/adfm.201700270.

[9] Deng, Z.; Wang, S.; Zhou, B.; Li, J.; Zhou, P.; Li, B.; Liang, H. Carboxymethylpachymaran-Zein Coated Plant Microcapsules-Based β-Galactosidase Encapsulation System for Long-Term Effective Delivery. *Food Res. Int.*, **2020**, *128*, 108867. https://doi.org/10.1016/j.foodres.2019.108867.

[10] Deng, Z.; Pei, Y.; Wang, S.; Zhou, B.; Hou, X.; Li, J.; Li, B.; Liang, H. Designable Carboxymethylpachymaran/Metal Ion Architecture on Sunflower Sporopollenin Exine Capsules as Delivery Vehicles for Bioactive Macromolecules. *J. Agric. Food Chem.*, **2020**, *68* (47), 13990–14000. https://doi.org/10.1021/acs.jafc.0c05169.

[11] Wang, H.; Potroz, M. G.; Jackman, J. A.; Khezri, B.; Marić, T.; Cho, N.-J.; Pumera, M. Bioinspired Spiky Micromotors Based on Sporopollenin Exine Capsules. *Adv. Funct. Mater.*, **2017**, *27* (32), 1–9. https://doi.org/10.1002/adfm.201702338.

[12] Maric, T.; Nasir, M. Z. M.; Rosli, N. F.; Budanović, M.; Webster, R. D.; Cho, N.-J.; Pumera, M. Microrobots Derived from Variety Plant Pollen Grains for Efficient Environmental Clean Up and as an Anti-Cancer Drug Carrier. *Adv. Funct. Mater.*, **2020**, *2000112*, 1–13. https://doi.org/10.1002/adfm.202000112.

[13] Fan, T.; Park, S.; Shi, Q.; Zhang, X.; Liu, Q.; Song, Y.; Chin, H.; Shahrudin, M.; Ibrahim, B.; Mokrzecka, N.; et al. Transformation of Hard Pollen into Soft Matter. *Nat. Commun.*, **2020**, *11* (1), 1449. https://doi.org/10.1038/s41467-020-15294-w.

[14] Ageitos, J. M.; Robla, S.; Valverde-Fraga, L.; Garcia-Fuentes, M.; Csaba, N. Purification of Hollow Sporopollenin Microcapsules from Sunflower and Chamomile Pollen Grains. *Polymers (Basel).*, **2021**, *13* (13), 2094. https://doi.org/10.3390/polym13132094.

[15] Farrán, A.; Cai, C.; Sandoval, M.; Xu, Y.; Liu, J.; Hernáiz, M. J.; Linhardt, R. J. Green Solvents in Carbohydrate Chemistry: From Raw Materials to Fine Chemicals. *Chem. Rev.*, **2015**, *115* (14), 6811–6853. https://doi.org/10.1021/cr500719h.

[16] Mundargi, R. C.; Potroz, M. G.; Park, J. H.; Seo, J.; Tan, E.-L.; Lee, J. H.; Cho, N.-J. Eco-Friendly Streamlined Process for Sporopollenin Exine Capsule Extraction. *Sci. Rep.*, **2016**, *6* (1), 1–14. https://doi.org/10.1038/srep19960.

[17] Mundargi, R. C.; Potroz, M. G.; Park, S.; Shirahama, H.; Lee, J. H.; Seo, J.; Cho, N.-J. Natural Sunflower Pollen as a Drug Delivery Vehicle. *Small*, **2016**, *12* (9), 1167–1173. https://doi.org/10.1002/smll.201500860.

[18] Wang, L.; Jackman, J. A.; Ng, W. B.; Cho, N.-J. Flexible, Graphene-Coated Biocomposite for Highly Sensitive, Real-Time Molecular Detection. *Adv. Funct. Mater.*, **2016**, *26* (47), 8623–8630. https://doi.org/10.1002/adfm.201603550.

[19] Ageitos, J. M.; Garcia-Fuentes, M. Advances in Drug Delivery Strategies for Microbial Healthcare Products. In *Pharmaceuticals from Microbes. The Bioengineering*

Perspective; Arora, D., Sharma, C., Jaglan, S., Lichtfouse, E., Eds.; Springer International Publishing, 2019; pp 1–38. https://doi.org/10.1007/978-3-030-01881-8_1.

[20] Wu, L.; Shan, W.; Zhang, Z.; Huang, Y. Engineering Nanomaterials to Overcome the Mucosal Barrier by Modulating Surface Properties. *Adv. Drug Deliv. Rev.*, **2018**, *124*, 150–163. https://doi.org/10.1016/j.addr.2017.10.001.

[21] Akyuz, L.; Sargin, I.; Kaya, M.; Ceter, T.; Akata, I. A New Pollen-Derived Microcarrier for Pantoprazole Delivery. *Mater. Sci. Eng. C*, **2017**, *71*, 937–942. https://doi.org/10.1016/j.msec.2016.11.009.

[22] Sargin, I.; Akyuz, L.; Kaya, M.; Tan, G.; Ceter, T.; Yildirim, K.; Ertosun, S.; Aydin, G. H.; Topal, M. Controlled Release and Anti-Proliferative Effect of Imatinib Mesylate Loaded Sporopollenin Microcapsules Extracted from Pollens of *Betula Pendula*. *Int. J. Biol. Macromol.*, **2017**, *105*, 749–756. https://doi.org/10.1016/j.ijbiomac.2017.07.093.

[23] Mundargi, R. C.; Potroz, M. G.; Park, S.; Park, J. H.; Shirahama, H.; Lee, J. H.; Seo, J.; Cho, N.-J. Lycopodium Spores: A Naturally Manufactured, Superrobust Biomaterial for Drug Delivery. *Adv. Funct. Mater.*, **2016**, *26* (4), 487–497. https://doi.org/10.1002/adfm.201502322.

[24] Thwala, L. N.; Delgado, D. P.; Leone, K.; Marigo, I.; Benetti, F.; Chenlo, M.; Alvarez, C. V.; Tovar, S.; Dieguez, C.; Csaba, N. S.; et al. Protamine Nanocapsules as Carriers for Oral Peptide Delivery. *J. Control. Release*, **2018**, *291* (October), 157–168. https://doi.org/10.1016/j.jconrel.2018.10.022.

[25] Thwala, L. N.; Beloqui, A.; Csaba, N. S.; González-Touceda, D.; Tovar, S.; Dieguez, C.; Alonso, M. J.; Préat, V. The Interaction of Protamine Nanocapsules with the Intestinal Epithelium: A Mechanistic Approach. *J. Control. Release*, **2016**, *243*, 109–120. https://doi.org/10.1016/j.jconrel.2016.10.002.

[26] Thwala, L. N.; Beloqui, A.; Csaba, N. S.; González-Touceda, D.; Tovar, S.; Dieguez, C.; Alonso, M. J.; Préat, V. The Interaction of Protamine Nanocapsules with the Intestinal Epithelium: A Mechanistic Approach. *J. Control. Release*, **2016**, *243*, 109–120. https://doi.org/10.1016/j.jconrel.2016.10.002.

[27] Ageitos, J. M.; Pulgar, A.; Csaba, N.; Garcia-Fuentes, M. Study of Nanostructured Fibroin/Dextran Matrixes for Controlled Protein Release. *Eur. Polym. J.*, **2019**, *114* (February), 197–205. https://doi.org/10.1016/j.eurpolymj.2019.02.028.

[28] González-Aramundiz, J. V.; Presas, E.; Dalmau-Mena, I.; Martínez-Pulgarín, S.; Alonso, C.; Escribano, J. M.; Alonso, M. J.; Csaba, N. S. Rational Design of Protamine Nanocapsules as Antigen Delivery Carriers. *J. Control. Release*, **2017**, *245*, 62–69. https://doi.org/10.1016/j.jconrel.2016.11.012.

[29] Prabhakar, A. K.; Potroz, M. G.; Tan, E. L.; Jung, H.; Park, J. H.; Cho, N.-J. Macromolecular Microencapsulation Using Pine Pollen: Loading Optimization and Controlled Release with Natural Materials. *ACS Appl. Mater. Interfaces*, **2018**, *10* (34), 28428–28439. https://doi.org/10.1021/acsami.8b09952.

[30] Chae, J.; Choi, Y.; Tanaka, M.; Choi, J. Inhalable Nanoparticles Delivery Targeting Alveolar Macrophages for the Treatment of Pulmonary Tuberculosis. *J. Biosci. Bioeng.*, **2021**, *132* (6), 543–551. https://doi.org/10.1016/j.jbiosc.2021.08.009.

[31] Braunstein, M.; Hickey, A. J.; Ekins, S. Why Wait? The Case for Treating Tuberculosis with Inhaled Drugs. *Pharm. Res.*, **2019**, *36* (12), 166. https://doi.org/10.1007/s11095-019-2704-6.

[32] Yang, W.; Peters, J. I.; Williams, R. O. Inhaled Nanoparticles—A Current Review. *Int. J. Pharm.*, **2008**, *356* (1–2), 239–247. https://doi.org/10.1016/j.ijpharm.2008.02.011.

[33] Nainwal, N.; Sharma, Y.; Jakhmola, V. Dry Powder Inhalers of Antitubercular Drugs. *Tuberculosis*, **2022**, *135* (February), 102228. https://doi.org/10.1016/j.tube.2022.102228.

[34] Nirbhavane, P.; Vemuri, N.; Kumar, N.; Khuller, G. K. Lipid Nanocarrier-Mediated Drug Delivery System to Enhance the Oral Bioavailability of Rifabutin. *AAPS PharmSciTech*, **2017**, *18* (3), 829–837. https://doi.org/10.1208/s12249-016-0559-2.

[35] Gaspar, M. M.; Cruz, A.; Penha, A. F.; Reymão, J.; Sousa, A. C.; Eleutério, C. V.; Domingues, S. A.; Fraga, A. G.; Filho, A. L.; Cruz, M. E. M.; et al. Rifabutin Encapsulated in Liposomes Exhibits Increased Therapeutic Activity in a Model of Disseminated Tuberculosis. *Int. J. Antimicrob. Agents*, **2008**, *31* (1), 37–45. https://doi.org/10.1016/j.ijantimicag.2007.08.008.

[36] Nimje, N.; Agarwal, A.; Saraogi, G. K.; Lariya, N.; Rai, G.; Agrawal, H.; Agrawal, G. P. Mannosylated Nanoparticulate Carriers of Rifabutin for Alveolar Targeting. *J. Drug Target.*, **2009**, *17* (10), 777–787. https://doi.org/10.3109/10611860903115308.

[37] Gaspar, D. P.; Faria, V.; Gonçalves, L. M. D.; Taboada, P.; Remuñán-López, C.; Almeida, A. J. Rifabutin-Loaded Solid Lipid Nanoparticles for Inhaled Antitubercular Therapy: Physicochemical and in Vitro Studies. *Int. J. Pharm.*, **2016**, *497* (1–2), 199–209. https://doi.org/10.1016/j.ijpharm.2015.11.050.

[38] Lee, W. H.; Loo, C. Y.; Traini, D.; Young, P. M. Nano- and Micro-Based Inhaled Drug Delivery Systems for Targeting Alveolar Macrophages. *Expert Opin. Drug Deliv.*, **2015**, *12* (6), 1009–1026. https://doi.org/10.1517/17425247.2015.1039509.

[39] Grenha, A.; Alves, A. D.; Guerreiro, F.; Pinho, J.; Simões, S.; Almeida, A. J.; Gaspar, M. M. Inhalable Locust Bean Gum Microparticles Co-Associating Isoniazid and Rifabutin: Therapeutic Assessment in a Murine Model of Tuberculosis Infection. *Eur. J. Pharm. Biopharm.*, **2020**, *147*, 38–44. https://doi.org/10.1016/j.ejpb.2019.11.009.

[40] Torrens, I.; Ganza, Á.; Hernández, G.; Gonzalo, A.; Zazpe, A. Ocular Biodistribution of Once-Daily 0.6% Bilastine Eye Drops Reveals Highest Levels in Conjunctiva Up to 24 h Postadministration. *J. Ocul. Pharmacol. Ther.*, **2022**, *38* (9), 617–625. https://doi.org/10.1089/jop.2022.0024.

[41] Alshehri, S. M.; Al-Lohedan, H. A.; Chaudhary, A. A.; Al-Farraj, E.; Alhokbany, N.; Issa, Z.; Alhousine, S.; Ahamad, T. Delivery of Ibuprofen by Natural Macroporous Sporopollenin Exine Capsules Extracted from *Phoenix Dactylifera* L. *Eur. J. Pharm. Sci.*, **2016**, *88*, 158–165. https://doi.org/10.1016/j.ejps.2016.02.004.

[42] Raish, M.; Kalam, M. A.; Ahmad, A.; Shahid, M.; Ansari, M. A.; Ahad, A.; Ali, R.; Jardan, Y. A. B.; Alshamsan, A.; Alkholief, M.; et al. Eudragit-Coated Sporopollenin Exine Microcapsules (Semc) of Phoenix Dactylifera l. of 5-Fluorouracil for Colon-Specific Drug Delivery. *Pharmaceutics*, **2021**, *13* (11).

https://doi.org/10.3390/pharmaceutics13111921.

[43] Uddin, M. J.; Gonzalez-Cruz, P.; Warzywoda, J.; Gill, H. S. Sporopollenin Spikes Augment Antigen-Specific Immune Response and Generate Long-Lived Humoral Immunity. *Adv. Ther.*, **2020**, *2000102*, 2000102. https://doi.org/10.1002/adtp.202000102.

[44] Uddin, M. J.; Gill, H. S. Ragweed Pollen as an Oral Vaccine Delivery System: Mechanistic Insights. *J. Control. Release*, **2017**, *268* (October), 416–426. https://doi.org/10.1016/j.jconrel.2017.10.019.

CONCLUSIONS

CONCLUSIONS

The experimental work described in this thesis has been focused on the design of hollow pollen-based microcapsules, the study of their association with model nanoparticles and rationally designed, drug-loaded polymeric nanocapsules and the evaluation of their potential for mucosal administration. The main conclusions from the results obtained in this thesis are the following:

1. A simplified protocol based on sequential washing steps using water, acetone, cyclohexane, and phosphoric acid could remove external and internal compounds from pollen grains, allowing the production of hollow pollen microcapsules from sunflower (*Helianthus annuus*) pollen grains, preserving their surface morphology and structural integrity. This method could be also applied for other pollen species (e.g., *Matricaria chamomilla*), with a low final protein content which supports its safe use for pharmaceutical purposes.

2. Nanoparticle size, surface functionalization the loading methodology constitute critical parameters which influence their association and spatial distribution in the pollen microcapsules, as well as their release kinetics in biorelevant media.

3. Based on the results obtained in the systematic studies performed with non-biodegradable nanocarriers, a biodegradable polymeric nanocapsule prototype was successfully designed and loaded into pollen microcapsules. *Ex vivo* and *in vivo* mechanistic studies carried out with this prototype provided proof of concept for our hypothesis, showing improved adherence to the intestinal mucosal tissue.

4. The encapsulation of rifabutin in nanosystems improved its dissolution and permeability, enhancing its internalization by alveolar macrophages. The use of pharmaceutical excipients such as mannitol allowed the atomization of the nanocapsules for obtaining a dry powder with adequate aerodynamic properties for inhalable tuberculosis therapy.

   -Párrafo afectado por la protección de derechos-

5. Purified pollen grains lack the capacity to induce potential allergic or hypersensitivity reactions. Their preserved surface morphology enhances residence time at the ocular surface, while preserving corneal barrier integrity in the ocular delivery of pharmaceutics.

Overall, the developed sporopollenin microcapsules provide a flexible and versatile multi-stage delivery system, suitable for improving mucointeraction and drug delivery to mucosal tissues.

AGRADECIMIENTOS

Mindenekelőtt a témavezetőimnek szeretnék köszönetet mondani. Csaba Noéminek a segítségéért és azért, hogy lehetővé tette, hogy együtt dolgozhassunk és számos projektjében is részt vehessek. Ambrus Ritának is köszönettel tartozom, aki mindig mindenben segített és ezáltal otthon érezhettem magam Szegeden.

Gracias a Rubén Varela Calviño, Ignacio Alcalde, Sulay Tovar, Marcos García-Fuentes y Carmen Remuñán, por vuestra cercanía, vuestro tiempo, y por haberme permitido trabajar con vosotros y llevar a cabo este trabajo tan multidisciplinar.

Thanks to my lab colleagues and friends, both those who accompanied me from the beginning, integrating me as part of the group, and those to whom I pass the baton. I have been very happy with all of you. To Maruthi, the best master's supervisor, for been there from the beginning to the end. Carla, gracias por tu apoyo y por tantas llamadas que arreglaron y arreglan días torcidos A Chema, porque juntos formamos el mejor equipo (aunque eso ya se sabía). Me siento muy afortunada de haber podido trabajar contigo. A Sheila, por tu ayuda e infinita paciencia. ¡Cuánto hemos tirado la una de la otra para que hoy estés leyendo esto! To Saeedeh, for her closeness and for allowing me to see little Dani grow up. A Diego, por haber estado siempre disponible para echar una mano. A Héctor, Sara, Roci y Lorena, por tantos cafés y mañanas/tardes/findes de trabajo en vuestra compañía. Confío en que seguiréis manteniendo el bagaje científico del grupo (y el blog). Gracias, compañeros del P5 y P6 y personal del CiMUS por vuestra ayuda.

This thesis allowed me to live one of the most beautiful experiences of my life: Szeged. Thanks to my Erasmus family: to Zosia and Ana, the best roomies, to my lovelies Petros, Giannis and Antonis and my dearest Amanda and Lily. I miss you all since the day I left. Special thanks to the Institute of Pharmaceutical Technology and Regulatory Affairs, to all my colleagues who assisted me with my experiments, and especially to Mahwish, Yamini and Heba for being the best of friends. I feel so lucky to have the opportunity to meet you and keep our friendship, despite the distance.

A mi familia de Santiago: a Brenda, mi pilar desde el día que llegué, por abrirme las puertas de tu casa, casi sin conocerme, y seguir a mi lado; a Lucía, por 200 km de acantilados, experiencias gastronómicas nacionales e internacionales y por tu amistad; a Javier, Valeria y Marisol, por tantos buenos momentos. Aún nos quedan muchos logros por celebrar.
A David, por estar siempre disponible, ya sea para hacerme un pedido o para tomar una cerveza. Gracias Maca y Laura, por ser las mejores compañeras de piso, por vuestro apoyo, vuestra ayuda y por tantas y tantas risas. No imagino vivir en Santiago si no es con vosotras y con Roni.

Gracias a mis amigas, Sandra, María, Sara y Celia, por vuestros ánimos a pesar de la distancia, y por hacerme sentir, cada vez que nos reunimos, que no ha pasado el tiempo.
A Natalia y Araceli, por seguir al pie del cañón, incluso desde tierras alemanas, y a Teresa y Marga, por tantos y tan increíbles intercambios Valladolid-Santiago.
Gracias Víctor, el mejor cocinero que conozco, por cuidarme durante mi estancia en Oviedo.

Gracias a mis amigos de Llamas de la Ribera, mi pueblo del alma, por darme, desde que tengo uso de razón, los mejores veranos del mundo, que espero seguir disfrutando muchos años más.

Y, sobre todo, gracias a mi familia, mi mayor orgullo y modelo a seguir: a mis padres, Belén y Rafa y a mis hermanos Henar y Héctor, por vuestro cariño y por apoyarme, siempre, en todas las decisiones que tomo. Nada de esto hubiera sido posible sin vosotros. Gracias a mis tíos y primos, a mis abuelas Nati y Emilia, de las que tanto presumo de ser nieta, y a mi abuelo Ovi. Sé que estarías muy orgulloso de mí.

ETHICAL ISSUES

ETHICAL ISSUES

Animal and blood human-derived cells studies

The activities carried out with animals during the project, described in Chapter II, were performed after approval by the bioethics committee of the Consellería de Medio Rural e do Mar of the Xunta de Galicia (15010/2020/001, "Nova estratexia multi etapa para a liberación oral de biomacromoléculas terapéuticas), complying with the best practices standards for animal care as recommended by national authorities and/or European Union legislations. The animals were obtained from the Central Animal House of the University and other authorized commercial suppliers, and the work was conducted in the CEBEGA, registered and authorized according to Spanish and European regulations. The experiments were performed by the PhD student under the supervision of Dr. Sulay Tovar, in accordance with European and Spanish legislation.

The activities carried out with animals in the Chapter V of this thesis were performed with the colaboration of Dr. Ignacio Alcalde (Laboratory of Cellular Biology and Innervation of the Ocular Surface, Fundación de Investigación Oftalmológica (FIO) at the University of Oviedo) at the Fernández-Vega University Institute of the University of Oviedo and comply with the best practices standards for animal care (Ethics Committee for Research with Medicines of the Principality of Asturias), and authorizations PROAE 32/2018 "Test de tolerancia ocular para nanosistemas de liberación controlada y con potencial terapéutico", and PROAE 01/2021 "Ensayos de biodisponibilidad para nanosistemas de liberación controlada y para sustancias con potencial terapéutico" (ES330440003591). The human corneal epithelial cells to form the QobuR-RhCE model were collected from corneal donor rims specimens after isolation of the central corneal button for transplantation. The project with number 2020.050 was approved by the Ethics Committee for Drug Research of the Principado de Asturias.

Evaluation of nanocarriers and pollen-based platforms in human dendritic cells requiring blood collection from healthy donors (Chapter II, III and V of this thesis) were carried out after obtaining informed consent from all subjects involved in the study, following the institute's ethical standards and the national committee's guidelines on experiments involving humans, as well as the Helsinki Declaration (Ethics Committee for Clinical Research of Galicia, approval number 2014/543, "Diseño de nanovacunas terapéuticas basadas en péptidos: aplicación al tratamiento de enfermedades autoinmunes"). Evaluation was conducted at the Faculty of Pharmacy of the University of Santiago de Compostela under the supervision of Dr. Rubén Varela-Calviño.

XUNTA DE GALICIA
CONSELLERÍA DO MEDIO RURAL

Xefatura Territorial
Sº de Gandaría
Edificio administrativo Monelos, 4º andar
Rúa Vicente Ferrer, Nº 2
15008 A Coruña
Tfno.: 981 184 565, fax.: 981 184 653
Correo electrónico: servizo.gandaria.a.coruna@xunta.gal

galicia

RESOLUCIÓN DE AUTORIZACIÓN DE PROXECTO DE EXPERIMENTACIÓN ANIMAL

Expediente núm.: 15010/2020/001
Persoa interesada: Noémi Stefánia Csaba
Forma de inicio: solicitude da persoa interesada

Data de inicio: 31.1.2020
Procedemento: resolución de autorización

ANTECEDENTES

A persoa interesada presentou con data 16.12.2019 unha solicitude para a realización do proxecto de experimentación animal (entrada no Rexistro Electrónico da Xunta de Galicia 2019/2503111), cuxos datos se detallan a continuación:

Denominación do proxecto: *Nova estratexia multi-etapa para a liberación oral de biomacromoléculas terapéuticas*
Nome do centro usuario: Animalario da Facultade de Bioloxía de Santiago deCompostela
Persoa responsable do proxecto: Noémi Stefánia Csaba
Establecemento onde se realizarán os procedementos do proxecto (ou lugar xeográfico no caso de traballos de campo): Animalario do CIMUS

Clasificación do proxecto : Tipo I [ ] Tipo II [X] Tipo III [ ]

CONSIDERACIÓNS LEGAIS E TÉCNICAS

1 O Real decreto 53/2013, de 1 de febreiro (BOE 34, do 8 de febreiro), polo que se establecen as normas básicas aplicables para a protección dos animais utilizados en experimentación e outros fins científicos, incluíndo a docencias, establece no seu artigo 33 as condicións de autorizacións dos proxectos con animais de experimentación.

2 O artigo 88 da Lei 39/2015, de 1 de outubro, do procedemento administrativo común das administracións públicas (BOE 236, do 2 de outubro de 2015) establece que a resolución que poña fin o procedemento decidirá todas as cuestións expostas polos interesados e aquelas outras derivadas deste.

XUNTA DE GALICIA
CONSELLERÍA DO MEDIO RURAL

Xefatura Territorial
Sº de Gandaría
Edificio administrativo Monelos, 4º andar
Rúa Vicente Ferrer, Nº 2
15008 A Coruña
Tfno.: 981 184 565, fax.: 981 184 653
Correo electrónico: servizo.gandaria.a.coruna@xunta.gal

galicia

3 O Servizo de Gandaría da Coruña revisou a documentación achegada na solicitude e o resultado favorable da avaliación do proxecto realizada polo órgano habilitado, a Sección de Experimentación Animal do Comité de Bioética da Universidade de Santiago de Compostela.

Esta xefatura territorial é competente para ditar unha resolución, de conformidade co Decreto 149/2018, do 5 de decembro, polo que se establece a estrutura orgánica da Consellería do Medio Rural e se modifica parcialmente o Decreto 177/2016, do 15 de decembro, polo que se fixa a estrutura orgánica da Vicepresidencia e das consellerías da Xunta de Galicia (DOG 235, do 11 de novembro).

De acordo con todo o indicado, RESOLVO:

1 Autorizar o proxecto solicitado.

2 O proxecto non precisa someterase a unha avaliación retrospectiva.

3 A autorización deste proxecto terá unha duración de cinco anos e unha vez transcorrido este tempo deberá ser renovada.

A citada autorización é unicamente válida nas condicións que figuran no expediente. Ante calquera cambio significativo no proxecto que poida ter efectos negativos sobre o benestar dos animais, deberá solicitar a confirmación da autorización ao Servizo Provincial de Gandaría.

Esta autorización poderá ser suspendida, no caso de que o proxecto non se leve a cabo de acordo coas condicións de autorización e retirala, previo expediente tramitado ao que se lle dará audiencia.

Contra a presente resolución, que non lle pon fin á vía administrativa, poderá interpoñer un recurso de alzada ante o conselleiro de Medio Rural. O prazo comezará a contar dende o día seguinte ao da recepción desta resolución. Todo isto, segundo o disposto nos artigos 121 e 122 da citada Lei 39/2015.

Mediante este escrito notifícaselle a Noémi Stefánia Csaba esta resolución segundo o esixido no artigo 40.1 da antedita Lei 39/2015.

XUNTA DE GALICIA
CONSELLERÍA DE SANIDADE
Secretaría Xeral Técnica

Secretaria Técnica
Comité Autonómico de Ética da Investigación de Galicia
Secretaria Xeral. Consellería de Sanidade
Edificio Administrativo San Lázaro
15703 SANTIAGO DE COMPOSTELA
Tel: 881 546425; ceic@sergas.es

galicia

DITAME DO COMITÉ DE ÉTICA DA INVESTIGACIÓN DE SANTIAGO-LUGO

Juan Manuel Vázquez Lago, Secretario do Comité de Ética da Investigación de Santiago-Lugo

CERTIFICA:

Que este Comité avaliou na súa reunión do día 20/01/2015 o estudo:

Título: Diseño de nanovacunas terapéuticas basadas en péptidos: aplicación al tratamiento de enfermedades autoinmunes
Promotor: África González Fernández, María Josefa Alonso Fernández, Rubén Varela Calviño
Tipo de estudo: Outros
Versión:
Código do Promotor:
Código de Rexistro: 2014/543

E, tomando en consideración as seguintes cuestións:

- A pertinencia do estudo, tendo en conta o coñecemento dispoñible, así coma os requisitos legais aplicables, e en particular a Lei 14/2007, de investigación biomédica, o Real Decreto 1716/2011, de 18 de novembro, polo que se establecen os requisitos básicos de autorización e funcionamento dos biobancos con fins de investigación biomédica e do tratamento das mostras biolóxicas de orixe humana, e se regula o funcionamento e organización do Rexistro Nacional de Biobancos para investigación biomédica, a ORDE SAS/3470/2009, de 16 de decembro, pola que se publican as Directrices sobre estudos Posautorización de Tipo Observacional para medicamentos de uso humano, e a Circular nº 07/2004, investigacións clínicas con produtos sanitarios.
- A idoneidade do protocolo en relación cos obxectivos do estudo, xustificación dos riscos e molestias previsibles para o suxeito, así coma os beneficios esperados.
- Os principios éticos da Declaración de Helsinki vixente.
- Os Procedementos Normalizados de Traballo do Comité.

Emite un **INFORME FAVORABLE** para a realización do estudo **polo/a investigador/a do centro**:

Centros	Investigadores Principais
Universidade de Vigo	África González Fernández
Univerisdade de Santiago de Compostela	María Josefa Alonso Fernández
	Rubén Varela Calviño

En Santiago de Compostela, a 20 de xaneiro de 2015
O secretario

juan.manuel.vazquez.lago@sergas.es
Firmado digitalmente por juan.manuel.vazquez.lago@sergas.es
Nombre de reconocimiento (DN): cn=juan.manuel.vazquez.lago@sergas.es
Fecha: 2015.01.30 10:28:10 +01'00'

Juan M. Vázquez Lago

GOBIERNO DEL PRINCIPADO DE ASTURIAS

CONSEJERÍA DE DESARROLLO RURAL Y RECURSOS NATURALES

RESOLUCIÓN de 4 de diciembre de 2018, de la Consejería de Desarrollo Rural y Recursos Naturales, sobre autorización de proyectos de investigación que utilicen animales de experimentación.
PROAE 32/2018

Servicio de Sanidad y Producción Animal

UNIVERSIDAD DE OVIEDO
CIF: Q3318001I

RESOLUCIÓN

ANTECEDENTES DE HECHO

Primero.- Con fecha 9 de octubre de 2018, **JOSE RAMÓN OBESO SUÁREZ** en representación del **BIOTERIO DE LA UNIVERSIDAD DE OVIEDO**, presentó solicitud de autorización para la utilización de animales en el siguiente proyecto de experimentación "**TEST DE TOLERANCIA OCULAR PARA NANOSISTEMAS DE LIBERACIÓN CONTROLADA Y PARA SUSTANCIAS CON POTENCIAL TERAPÉUTICO**", constando como investigador principal D. **IGNACIO ALCALDE DOMÍNGUEZ** y como investigador responsable de los procedimientos con animales D. **IGNACIO ALCALDE DOMÍNGUEZ**.

Junto con la solicitud, aporta la propuesta del proyecto, el resumen no técnico e informe del comité ético y de evaluación del proyecto por el órgano habilitado.

Segundo.- El lugar donde se desarrollará el proyecto se encuentra autorizado como establecimiento usuario y está inscrito en el Registro de Explotaciones Ganaderas con el número **ES330440003591**.

Tercero.- Con fecha **9 de octubre de 2018**, el Comité de Ética del centro emite un informe favorable, conforme al RD 53/2013 de 1 de febrero, por el que se establecen las normas básicas aplicables para la protección de los animales utilizados en experimentación y otros fines científicos, incluyendo la docencia.

Cuarto.- Con fecha **9 de octubre de 2018**, el Comité Ético de Experimentación animal de **LA UNIVERSIDAD DE OVIEDO**, órgano habilitado, emite informe de evaluación favorable del proyecto, indicando que el proyecto cuyos datos y evaluación se proporcionan han sido evaluados con un nivel de detalle apropiados y que la evaluación ha consistido en verificar que el proyecto cumple los requisitos especificados en el artículo 34 del RD 53/2013 de 1 de febrero y que, tanto el investigador responsable del proyecto como las personas encargadas de la realización del mismo tienen capacitación para ello.

Quinto.- Una vez revisada la solicitud y la documentación presentada, la Jefa del Servicio de Sanidad y Producción Animal elevó con fecha **29 de noviembre de 2018** una propuesta de resolución de autorización de proyectos de investigación que utilicen animales de experimentación.

FUNDAMENTOS DE DERECHO

Primero.- El artículo 25 del Real Decreto 53/2013, de 1 de febrero, por el que se establecen las normas básicas aplicables para la protección de los animales utilizados en experimentación y otros fines científicos, incluyendo la docencia, dispone:

"2. Los procedimientos solo se podrán realizar si están incluidos dentro del marco de un proyecto autorizado de acuerdo con la sección 2ª de este capítulo.

)

3. Los procedimientos deberán realizarse de forma que se evite a los animales cualquier dolor, sufrimiento, angustia o daño duradero que sean innecesarios.

4. Los procedimientos se realizarán en centros usuarios autorizados, salvo autorización del órgano competente, previa justificación científica de la necesidad o conveniencia de que se realicen fuera de dichos centros.

5. Los procedimientos únicamente podrán ser realizados por personas capacitadas o autorizadas de forma temporal en las condiciones establecidas en el artículo 15.3 bajo supervisión responsable".

Asimismo, el artículo 31 del citado Real Decreto, situado en su sección 2ª, regula la tipología de proyectos con arreglo a la siguiente clasificación:

"1. Proyectos de tipo I: Aquellos proyectos en los que se den simultáneamente las tres circunstancias siguientes:

a) Implican exclusivamente procedimientos clasificados como «sin recuperación», «leves» o «moderados».
b) No utilizan primates.
c) Se realizan para cumplir requisitos legales o reglamentarios, o con fines de producción o diagnóstico por métodos establecidos.

Los proyectos tipo I podrán ser tramitados por un procedimiento simplificado y no ser sometidos a evaluación retrospectiva.

2. Proyectos de tipo II: Aquellos proyectos en los que se den simultáneamente las circunstancias siguientes:

a) Implican exclusivamente procedimientos clasificados como «sin recuperación», «leves» o «moderados».
b) No utilizan primates.

Los proyectos tipo II quedarán sujetos al procedimiento de autorización y podrán no ser sometidos a evaluación retrospectiva.

3. Proyectos de tipo III: Los proyectos diferentes de los tipos I o II. Sin perjuicio de las autorizaciones adicionales a las que puedan estar condicionados determinados proyectos, todos los proyectos tipo III quedarán sujetos al procedimiento de autorización y serán sometidos posteriormente a una evaluación retrospectiva".

Segundo.- El proyecto para el que se solicita la autorización ha de ser considerado dentro del **tipo II**, puesto que implica procedimientos clasificados como "**moderados**": **ADMINISTRACIÓN DE FÁRMACOS O PRODUCTOS EXPERIMENTALES**, y no utiliza primates.

El establecimiento donde se desarrollará tiene la correspondiente autorización.

Los informes emitidos al respecto son favorables, por lo que, cumpliendo con los requisitos previstos, ha de procederse a su autorización y **no debe someterse a evaluación retrospectiva**.

RESUELVO

Primero.- Autorizar al **BIOTERIO DE LA UNIVERSIDAD DE OVIEDO**, el proyecto denominado: "**TEST DE TOLERANCIA OCULAR PARA NANOSISTEMAS DE LIBERACIÓN CONTROLADA Y PARA SUSTANCIAS CON POTENCIAL TERAPÉUTICO**" en el que consta como investigador principal D. **IGNACIO ALCALDE DOMÍNGUEZ** y como investigador

GOBIERNO DEL PRINCIPADO DE ASTURIAS

CONSEJERÍA DE DESARROLLO RURAL Y RECURSOS NATURALES

responsable de los procedimientos con animales D. **IGNACIO ALCALDE DOMÍNGUEZ**.

Esta autorización tendrá una validez que se corresponderá con la duración prevista en su memoria, con un máximo de cinco años, siempre y cuando no se produzca una modificación relevante en dicho proyecto, en cuyo caso sería necesario efectuar una nueva solicitud de autorización a la autoridad competente.

Segundo.- Asignar el código de autorización: **PROAE 32/2018**

Tercero.- Ordenar la notificación de la presente Resolución al interesado.

Cuarto.- La presente resolución pone fin a la vía administrativa y contra ella cabe interponer recurso contencioso-administrativo ante la Sala de lo Contencioso-Administrativo del Tribunal Superior de Justicia del Principado de Asturias en el plazo de dos meses, contados desde el día siguiente al de su notificación, de acuerdo con lo establecido en los artículos 10 y 46 de la Ley 29/1998, de 13 de julio, reguladora de la Jurisdicción Contencioso–Administrativa, sin perjuicio de la posibilidad de previa interposición del recurso potestativo de reposición ante el mismo órgano que dictó el acto, en el plazo de un mes contado desde el día siguiente al de su notificación, no pudiendo simultanearse ambos recursos, conforme a lo establecido en el artículo 28 de la Ley del Principado de Asturias 2/1995, de 13 de marzo, sobre Régimen Jurídico de la Administración y en el artículo 123 de la Ley 39/2015, de 1 de octubre, del Procedimiento Administrativo Común de las Administraciones Públicas. No obstante, los interesados podrán ejercitar, en su caso, cualquier otro recurso que estimen procedente.

LA CONSEJERA

María Jesús Álvarez González

GOBIERNO DEL PRINCIPADO DE ASTURIAS

CONSEJERÍA DE MEDIO RURAL Y COHESIÓN TERRITORIAL

RESOLUCIÓN de 2 de febrero de 2021, de la Consejería de Medio Rural y Cohesión Territorial, sobre autorización de proyectos de investigación que utilicen animales de experimentación.
PROAE 01/2021

Servicio de Sanidad y Producción Animal

UNIVERSIDAD DE OVIEDO
CIF: Q3318001I

RESOLUCIÓN

ANTECEDENTES DE HECHO

Primero.- Con fecha 11 de enero de 2021, **JOSE RAMÓN OBESO SUÁREZ** en representación del **BIOTERIO DE LA UNIVERSIDAD DE OVIEDO**, presentó solicitud de autorización para la utilización de animales en el siguiente proyecto de experimentación "**ENSAYOS DE BIODISTRIBUCIÓN PARA NANOSISTEMAS DE LIBERACIÓN CONTROLADA Y PARA SUSTANCIAS CON POTENCIAL TERAPÉUTICO**", constando como investigador principal D. **IGNACIO ALCALDE DOMÍNGUEZ** y como investigador responsable de los procedimientos con animales D. **IGNACIO ALCALDE DOMÍNGUEZ**.

Junto con la solicitud, aporta la propuesta del proyecto, el resumen no técnico e informe del comité ético y de evaluación del proyecto por el órgano habilitado.

Segundo.- El lugar donde se desarrollará el proyecto se encuentra autorizado como establecimiento usuario y está inscrito en el Registro de Explotaciones Ganaderas con el número **ES330440003591**.

Tercero.- Con fecha **11 de enero de 2021**, el Comité de Ética del centro emite un informe favorable, conforme al RD 53/2013 de 1 de febrero, por el que se establecen las normas básicas aplicables para la protección de los animales utilizados en experimentación y otros fines científicos, incluyendo la docencia.

Cuarto.- Con fecha **11 de enero de 2021**, el Comité Ético de Experimentación animal de **LA UNIVERSIDAD DE OVIEDO**, órgano habilitado, emite informe de evaluación favorable del proyecto, indicando que el proyecto cuyos datos y evaluación se proporcionan han sido evaluados con un nivel de detalle apropiados y que la evaluación ha consistido en verificar que el proyecto cumple los requisitos especificados en el artículo 34 del RD 53/2013 de 1 de febrero y que, tanto el investigador responsable del proyecto como las personas encargadas de la realización del mismo tienen capacitación para ello.

Quinto.- Una vez revisada la solicitud y la documentación presentada, la Jefa del Servicio de Sanidad y Producción Animal elevó con fecha **25 de enero de 2021** una propuesta de resolución de autorización de proyectos de investigación que utilicen animales de experimentación.

FUNDAMENTOS DE DERECHO

Primero.- El artículo 25 del Real Decreto 53/2013, de 1 de febrero, por el que se establecen las normas básicas aplicables para la protección de los animales utilizados en experimentación y otros fines científicos, incluyendo la docencia, dispone:

"2. Los procedimientos solo se podrán realizar si están incluidos dentro del marco de un proyecto autorizado de acuerdo con la sección 2ª de este capítulo.

3. Los procedimientos deberán realizarse de forma que se evite a los animales cualquier dolor, sufrimiento, angustia o daño duradero que sean innecesarios.

4. Los procedimientos se realizarán en centros usuarios autorizados, salvo autorización del órgano competente, previa justificación científica de la necesidad o conveniencia de que se realicen fuera de dichos centros.

5. Los procedimientos únicamente podrán ser realizados por personas capacitadas o autorizadas de forma temporal en las condiciones establecidas en el artículo 15.3 bajo supervisión responsable".

Asimismo, el artículo 31 del citado Real Decreto, situado en su sección 2ª, regula la tipología de proyectos con arreglo a la siguiente clasificación:

"1. Proyectos de tipo I: Aquellos proyectos en los que se den simultáneamente las tres circunstancias siguientes:

a) Implican exclusivamente procedimientos clasificados como «sin recuperación», «leves» o «moderados».
b) No utilizan primates.
c) Se realizan para cumplir requisitos legales o reglamentarios, o con fines de producción o diagnóstico por métodos establecidos.

Los proyectos tipo I podrán ser tramitados por un procedimiento simplificado y no ser sometidos a evaluación retrospectiva.

2. Proyectos de tipo II: Aquellos proyectos en los que se den simultáneamente las circunstancias siguientes:

a) Implican exclusivamente procedimientos clasificados como «sin recuperación», «leves» o «moderados».
b) No utilizan primates.

Los proyectos tipo II quedarán sujetos al procedimiento de autorización y podrán no ser sometidos a evaluación retrospectiva.

3. Proyectos de tipo III: Los proyectos diferentes de los tipos I o II. Sin perjuicio de las autorizaciones adicionales a las que puedan estar condicionados determinados proyectos, todos los proyectos tipo III quedarán sujetos al procedimiento de autorización y serán sometidos posteriormente a una evaluación retrospectiva".

Segundo.- El proyecto para el que se solicita la autorización ha de ser considerado dentro del **tipo II**, puesto que implica procedimientos clasificados como "**leves**": **ADMINISTRACIÓN DE FÁRMACOS O PRODUCTOS EXPERIMENTALES y ADMINISTRACIÓN DE ANESTESIA,** y no utiliza primates.

El establecimiento donde se desarrollará tiene la correspondiente autorización.

Los informes emitidos al respecto son favorables, por lo que, cumpliendo con los requisitos previstos, ha de procederse a su autorización y **no debe someterse a evaluación retrospectiva.**

RESUELVO

Primero.- Autorizar al **BIOTERIO DE LA UNIVERSIDAD DE OVIEDO**, el proyecto denominado: "**ENSAYOS DE BIODISTRIBUCIÓN PARA NANOSISTEMAS DE LIBERACIÓN CONTROLADA Y PARA SUSTANCIAS CON POTENCIAL TERAPÉUTICO**" en el que consta como investigador principal D. **IGNACIO ALCALDE DOMÍNGUEZ** y como

GOBIERNO DEL PRINCIPADO DE ASTURIAS

CONSEJERÍA DE MEDIO RURAL Y COHESIÓN TERRITORIAL

investigador responsable de los procedimientos con animales D. **IGNACIO ALCALDE DOMÍNGUEZ.**

Esta autorización tendrá una validez que se corresponderá con la duración prevista en su memoria, con un máximo de cinco años, siempre y cuando no se produzca una modificación relevante en dicho proyecto, en cuyo caso sería necesario efectuar una nueva solicitud de autorización a la autoridad competente.

Segundo.- Asignar el código de autorización: **PROAE 01/2021**

Tercero.- Ordenar la notificación de la presente Resolución al interesado.

Cuarto.- La presente resolución pone fin a la vía administrativa y contra la misma cabe interponer recurso contencioso-administrativo ante el Juzgado Contencioso-Administrativo competente en el plazo de dos meses contados desde el día siguiente al de su notificación, sin perjuicio de la posibilidad de previa interposición del recurso potestativo de reposición ante el mismo órgano que dictó el acto en el plazo de un mes contado desde el día siguiente al de su notificación, no pudiendo simultanearse ambos recursos, conforme a lo establecido en el artículo 28 de la Ley del Principado de Asturias 2/1995, de 13 de marzo, sobre Régimen Jurídico de la Administración del Principado de Asturias, y en el artículo 123 de la Ley 39/2015, de 1 de octubre, del Procedimiento Administrativo Común de las Administraciones Públicas, y sin perjuicio de que los interesados puedan ejercitar cualquier otro que estimen oportuno.

EL CONSEJERO

Alejandro Jesús Calvo Rodríguez

GOBIERNO DEL PRINCIPADO DE ASTURIAS · CONSEJERÍA DE DESARROLLO RURAL, AGROGANADERÍA Y PESCA ·

GOBIERNO DEL PRINCIPADO DE ASTURIAS

CONSEJERÍA DE SALUD

Dirección General de Calidad, Transformación y Gestión del Conocimiento

Comité de Ética de la Investigación del Principado de Asturias

Hospital Universitario Central de Asturias

N-1, S3.19

Avda. de Roma, s/n
33011 Oviedo

Oviedo a jueves, 23 de marzo de 2020

El Comité de Ética de la Investigación con Medicamentos del Principado de Asturias ha evaluado el Proyecto nº 2020.050, titulado: "OBTENCION DE ORGANOS Y TEJIDOS HUMANOS EN EL LABORATORIO ÚTILES EN INVESTIGACION BIOMÉDICA PARA REDUCIR O ANULAR COMPLETAMENTE LA EXPERIMENTACION CON ANIMALES", Investigador Principal, Dr. ALVARO MEANA INFIESTA. Instituto Universitario Fernandez-Vega (Universidad de Oviedo .

El Comité ha tomado el acuerdo de considerar que el citado Ensayo reúne las condiciones éticas necesarias para poder realizarse y, en consecuencia, emite su autorización.

Le recuerdo que deberá guardar la máxima confidencialidad de los datos utilizados en este Proyecto; les aconsejamos que el Consentimiento Informado se firme por duplicado y que el Investigador guarde una copia en el archivo.

Le saluda atentamente.

Fdo: MAURICIO TELENTI ASENSIO

Secretario/a del Comité de Ética de la Investigación del Principado de Asturias

CONSEJERÍA DE SANIDAD
COMITÉ DE ÉTICA DE LA INVESTIGACIÓN CON MEDICAMENTOS DEL PRINCIPADO DE ASTURIAS

XUNTA DE GALICIA
CONSELLERÍA DO MEDIO RURAL

Avda. do Camiño Francés, 10, Baixo
15703 Santiago de Compostela
A Coruña

AGACAL
Axencia Galega
da Calidade Alimentaria

galicia

Certificado de capacitación en materia de protección de animais utilizados, criados ou subministrados con fins de experimentación e otros fins científicos, incluíndo a docencia conforme coa Orde ECC/566/2015 de 20 de marzo.

Certificado de capacitación en materia de protección de animales utilizados, criados o suministrados con fines de experimentación y otros fines científicos, incluyendo la docencia conforme con la Orden ECC/566/2015 de 20 de marzo.

1. IDENTIFICACIÓN

1.1. Apelidos / *Apellidos / Surname:*

ROBLA ÁLVAREZ

1.2.Nome / *Nombre / First names:*

SANDRA

DNI /*DNI / Identity card number:*

1.3. Categoría/*Categoría/Category:* **"b"**

1.4. Especies/*Especies/Species:* **ROEDORES**

1.5. Válido ata/ *válido hasta/expires:* **11/06/2028**

2. Nº DO CERTIFICADO / *Nº DEL CERTIFICADO / CERTIFICATE NUMBER*

B527

3.ORGANISMO QUE EXPIDE O CERTIFICADO / *ORGANISMO QUE EXPIDE EL CERTIFICADO / BODY ISSUING THE CERTIFICATE:*

3.1.Nome e enderezo do organismo que expide o certificado / *Nombre y dirección del organismo que expide el certificado / Name and address of the body issuing the certificate:*

CONSELLERÍA DO MEDIO RURAL – XUNTA DE GALICIA
AXENCIA GALEGA DA CALIDADE ALIMENTARIA
Avda. Do Camiño Francés, 10 baixo
15781 Santiago de Compostela
A Coruña (España)

3.2.Teléfono / *Teléfono / Telephone:*	3.3.Fax / *Fax / Fax:*	3.4.Correo electrónico / *Correo electrónico / Email:*
981 546 654	981 546 651	formacion.cmrm@xunta.es

3.5.Data / *Fecha / Date:*	3.6.Lugar / *Lugar / Place:*
22/02/2021	**Santiago de Compostela**

3.7.Nome e sinatura / Nombre y firma / Name and signature
3.8.Selo / Sello / Stamp

Asdo.: Xiana María Perales Arroyo
Xefe do Departamento de Formación
(asinado dixitalmente)

Xacobeo 2021

XUNTA DE GALICIA
CONSELLERÍA DO MEDIO RURAL

Avda. do Camiño Francés, 10. Baixo
15703 Santiago de Compostela
A Coruña

AGACAL
Axencia Galega
da Calidade Alimentaria

galicia

Certificado de capacitación en materia de protección de animais utilizados, criados ou subministrados con fins de experimentación e otros fins científicos, incluíndo a docencia conforme coa Orde ECC/566/2015 de 20 de marzo.

Certificado de capacitación en materia de protección de animales utilizados, criados o suministrados con fines de experimentación y otros fines científicos, incluyendo la docencia conforme con la Orden ECC/566/2015 de 20 de marzo.

1. IDENTIFICACIÓN		
1.1. Apelidos */ Apellidos / Surname:* **ROBLA ÁLVAREZ**		
1.2. Nome */ Nombre / First names:* **SANDRA**		DNI */DNI / Identity card number:*
1.3. Categoría/*Categoria/Category:* **"C"**	1.4. Especies/*Especies/Species:* ***ROEDORES***	1.5. Válido ata/ *válido hasta/expires:* **11/06/2028**

2. Nº DO CERTIFICADO / ***Nº DEL CERTIFICADO / CERTIFICATE NUMBER***

C564

3.ORGANISMO QUE EXPIDE O CERTIFICADO / ***ORGANISMO QUE EXPIDE EL CERTIFICADO / BODY ISSUING THE CERTIFICATE:***

3.1. Nome e enderezo do organismo que expide o certificado */ Nombre y dirección del organismo que expide el certificado / Name and address of the body issuing the certificate:*

CONSELLERÍA DO MEDIO RURAL – XUNTA DE GALICIA
AXENCIA GALEGA DA CALIDADE ALIMENTARIA
Avda. Do Camiño Francés, 10 baixo
15781 Santiago de Compostela
A Coruña (España)

3.2. Teléfono */ Teléfono / Telephone:*	3.3. Fax */ Fax / Fax:*	3.4. Correo electrónico */ Correo electrónico / Email:*
981 546 654	981 546 651	formacion.cmrm@xunta.es
3.5. Data */ Fecha / Date:* **22/02/2021**	3.6. Lugar */ Lugar / Place:* **Santiago de Compostela**	

3.7. Nome e sinatura */ Nombre y firma / Name and signature*

Asdo.: Xiana María Perales Arroyo
Xefe do Departamento de Formación
(asinado dixitalmente)

Asinado por: PERALES ARROYO, XIANA MARIA
Cargo: Xefatura Servicio
Data e hora: 22/02/2021 11:47:37

CVE: R5LtlmXws7
Verificación: https://sede.xunta.gal/cve

Xacobeo 2021

PERMISSIONS

Chapter I/ Capítulo I

Purification of hollow sporopollenin microcapsules from sunflower and chamomile pollen grains

Jose Manuel Ageitos, Sandra Robla, Lorena Valverde-Fraga, Marcos Garcia-Fuentes, and Noemi Csaba (2021). "Purification of Hollow Sporopollenin Microcapsules from Sunflower and Chamomile Pollen Grains" Polymers 13, no. 13: 2094.
DOI: *https://doi.org/10.3390/polym13132094*

ISSN: 20734360
Elsevier
Chemistry (miscellaneous) (Q1); Polymers and Plastics (Q1)
Impact score: 4.80
H- index: 89

Chapter III/ Capítulo III

A ready-to-use dry powder formulation based on protamine nanocarriers for pulmonary drug delivery

Sandra Robla, Rubén Varela Calviño, Rita Ambrus & Noemi Csaba (2023). A ready-to-use dry powder formulation based on protamine nanocarriers for pulmonary drug delivery. European Journal of Pharmaceutical Sciences; 185:106442.
DOI: *https://doi.org/10.1016/j.ejps.2023.106442*

ISSN: 18790720, 09280987
MDPI
Pharmaceutical Science (Q1)
Impact score: 4.94
H- index: 144

A ready-to-use dry powder formulation based on protamine nanocarriers for pulmonary drug delivery

Author: Sandra Robla,Rubén Varela Calviño,Rita Ambrus,Noemi Csaba

Publication: European Journal of Pharmaceutical Sciences

Publisher: Elsevier

Date: 1 June 2023

The goal of this thesis is the design of a platform that combines the benefits of nanotechnology and the capacity of pollen grains to be anchored to the mucosa, to obtain a multi-step delivery system that can be tailor-made for diverse biomedical applications, by different administration routes and for the delivery of different nanoencapsulated therapeutics.